Characterization of the single end-binding protein homologue TbEB1 in *Trypanosoma brucei*

Dissertation

Zur Erlangung des Grades

- Doktor der Naturwissenschaften (Dr. rer. nat.) -

an der Bayreuther Graduiertenschule für Mathematik und Naturwissenschaften (BayNAT)

Vorgelegt von

Gertrud Lallinger-Kube

Bayreuth, September 2016

Die vorliegende Arbeit wurde in der Zeit von Oktober 2011 bis April 2016 in Bayreuth am Lehrstuhl für Molekulare Parasitologie unter der Betreuung von Herrn Professor Dr. Klaus Ersfeld angefertigt.

Vollständiger Abdruck der von der Bayreuther Graduiertenschule für Mathematik und Naturwissenschaften (BayNAT) der Universität Bayreuth genehmigten Dissertation zur Erlangung des akademischen Grades eines Doktors der Naturwissenschaften (Dr. rer. nat.).

Dissertation eingereicht am: 29.09.2016

Zulassung durch das Leitungsgremium: 26.10.2016

Wissenschaftliches Kolloquium: 17.01.2017

Amtierender Direktor: Prof. Dr. Stephan Kümmel

Prüfungsausschuss:
Prof. Dr. Klaus Ersfeld (Erstgutachter)
PD Dr. Stefan Geimer (Zweitgutachter)
Prof. Dr. Gerrit Begemann (Vorsitz)
PD Dr. Ralf Braun

Contents

Abstract 1
Zusammenfassung 2
Acknowledgements 3

1 Introduction **4**
1.1 Trypanosoma brucei 4
1.1.1 Taxonomy 4
1.1.2 African trypanosomiasis 5
1.1.3 The developmental cycle 6
1.1.4 The cellular architecture of *T. brucei* 9
1.1.5 The cell cycle 18
1.2 Microtubules and microtubule-associated proteins (MAPs) 25
1.2.1 Microtubules 25
1.2.2 Regulation of microtubule dynamics 28
1.2.3 End-binding proteins 31
1.3 Aim of this work 40

2 Results **42**
2.1 TbEB1 is the only EB homologue in *T. brucei* and its domain architecture is similar to other EB homologues 42
2.2 Relative mRNA levels of TbEB1 in procyclic and bloodstream wild type trypanosomes 47
2.3 Localization of TbEB1 in *T. brucei* 48
2.3.1 Endogenous tagging of TbEB1 confirmed localization of TbEB1 to microtubule plus ends 48
2.3.2 A monoclonal Anti-TbEB1 antibody visualized the variation of TbEB1 labeling during the cell cycle 63
2.3.3 Electron micrographs of procyclic trypanosomes confirmed association of TbEB1 with the subpellicular microtubule array 69

2.3.4 The different detection methods for localization of TbEB1 demonstrated similar results and complemented each other in procyclic and bloodstream trypanosomes . . . 75
2.4 Functional characterization of TbEB1 . . . 76
2.4.1 Establishment of TbEB1 RNAi cell lines . . . 76
2.4.2 Depletion of TbEB1 led to severe growth defects in procyclic and bloodstream trypanosomes . . . 77
2.4.3 TbEB1 knockdown resulted in an accumulation of atypical cell cycle stages suggesting an impaired cytokinesis . . . 81
2.4.4 TbEB1 was localized near the posterior part of the division furrow similar to wild type cells but position and foci number varied . . . 90
2.4.5 The TbEB1 signal intensity at the posterior cell pole did not correlate with TbEB1 knockdown . . . 94
2.4.6 A mouse polyclonal anti-TbEB1 serum confirmed TbEB1 depletion in RNAi cell lines in immuno blots . . . 94
2.4.7 TbEB1 depleted PCF demonstrated an increase in cell rounding with a reduction of tyrosinated α-tubulin and an impediment of kinetoplast segregation . . . 106
2.4.8 In BSF, TbEB1 depleted cells demonstrated impaired kinetoplast segregation but cellular morphology was not affected . . . 111
2.4.9 TbEB1 depleted PCF and BSF demonstrated an increase in flagellar detachment but flagellar assembly was not affected . . . 111
2.4.10 TbEB1 depletion resulted in a reduced FAZ length and a reduced number of FAZ in relation to the number of nuclei in procyclic trypanosomes 115
2.4.11 Depletion of TbEB1 does not affect the overall structure of the subpellicular microtubule array . . . 123
2.4.12 Putative TbEB1 single gene knockout cell lines reflect some characteristics from RNAi phenotypes . . . 126
2.4.13 Evaluation of TbEB1 ectopic expression . . . 131
2.4.14 A heterologous system: Expression of TbEB1$^{C\text{-}GFP}$ in HeLa cells . . . 149

3 Discussion 160
3.1 Amino acid sequence and domain architecture . . . 160
3.2 TbEB1 is localized to hot spots of microtubule remodeling . . . 161
3.2.1 Posterior cell pole . . . 162
3.2.2 Subpellicular cytoskeleton . . . 163

3.2.3 The flagellar attachment zone (FAZ) . . . 165
3.3 TbEB1 labeling dynamics of the cytoskeletal components throughout the cell cycle 167
3.4 Functional analysis of TbEB1 . . . 168
3.4.1 TbEB1 is essential in procyclic and bloodstream trypanosomes . . . 168
3.4.2 TbEB1 fulfills its main function in regulation of microtubule dynamics 169
3.4.3 TbEB1 influences cytokinesis . . . 171
3.4.4 Is TbEB1 involved in proper FAZ synthesis? . . . 173
3.4.5 Individual phenotypes seem to rely on the time point when TbEB1 is depleted . . . 174
3.5 Differences and commonalities of TbEB1 to other members of the protein family 177
3.6 Conclusions . . . 178

4 Material and Methods 180
4.1 Materials . . . 180
4.1.1 Hard- and Software . . . 180
4.1.2 Bioinformatic analysis . . . 181
4.1.3 Protocols . . . 181
4.1.4 Chemicals and reagents . . . 181
4.1.5 Buffers and solution . . . 182
4.1.6 Antibodies . . . 184
4.1.7 Plasmids . . . 186
4.1.8 DNA oligonucleotides . . . 187
4.2 Microbiological methods . . . 190
4.2.1 *Escherichia coli* strains . . . 190
4.2.2 *E. coli* media, cultivation, and storage . . . 190
4.2.3 Generation of chemically competent *E. coli* . . . 190
4.2.4 Transformation of plasmid DNA in *E. coli* . . . 191
4.2.5 Recombinant protein expression in *E. coli* BL21 (DE) . . . 191
4.3 Molecular biology methods . . . 191
4.3.1 Isolation of nucleic acids . . . 191
4.3.2 PCR techniques . . . 193
4.3.3 Agarose gel electrophoresis . . . 197
4.3.4 Purification of PCR products . . . 197
4.3.5 Restriction digestion of DNA . . . 197
4.3.6 Linearization of plasmid DNA for transfection of trypanosomes . . . 197
4.3.7 DNA extraction from agarose gels . . . 198

4.3.8 Ligation of DNA fragments . . . 198
4.3.9 Site-directed mutagenesis of DNA . . . 198
4.3.10 DNA sequencing . . . 198
4.4 Protein biochemical methods . . . 199
4.4.1 Preparation of trypanosomes for SDS-PAGE . . . 199
4.4.2 Methanol-chloroform precipitation . . . 199
4.4.3 Denaturing SDS polyacrylamide gel electrophoresis (SDS-PAGE) . . . 199
4.4.4 Staining of SDS gels with Coomassie . . . 200
4.4.5 Transfer of proteins on nitrocellulose or PVDF membranes . . . 200
4.4.6 Staining of immuno blot membranes with Ponceau S . . . 200
4.4.7 Immuno blotting . . . 200
4.4.8 Immunoprecipitation (IP) using the mouse monoclonal anti-TbEB1 antibody . . . 201
4.4.9 His-tag purification of TbEB1 for mouse polyclonal antibody generation under native conditions . . . 202
4.4.10 His-tag purification of TbEB1 for mouse monoclonal antibody generation under denaturing conditions . . . 202
4.5 Cell culture . . . 203
4.5.1 Trypanosomal cell lines . . . 203
4.5.2 Mammalian cell lines . . . 210
4.6 Generation of mouse poly- and monoclonal antibodies . . . 212
4.6.1 Immunization of mice . . . 212
4.6.2 Test serum collection and analysis . . . 213
4.6.3 Enzyme-linked immunosorbent assay (ELISA) . . . 213
4.6.4 Conditioned medium derived from macrophages . . . 214
4.6.5 Harvesting myeloma cells and conditioned medium for fusion . . . 214
4.6.6 Isolation of lymphocytes derived from spleen . . . 214
4.6.7 Fusion of lymphocytes and myeloma cells . . . 215
4.6.8 Screening of hybridoma cells . . . 215
4.6.9 Sub-cloning of hybridoma cells . . . 216
4.6.10 Fractional precipitation with ammonium sulfate . . . 216
4.6.11 Determination of isotypes of hybridoma cell lines . . . 217
4.7 Microscopy . . . 217
4.7.1 Light microscopy . . . 217
4.7.2 Electron microscopy . . . 220

5 Bibliography **223**

6 Appendix **256**

6.1 Abbreviations 256

6.2 (Eidesstattliche) Versicherungen und Erklärungen 259

Abstract

Trypanosoma brucei is an early branching protist whose cytoskeleton is predominantly composed of microtubules. The cytoskeleton is the key component involved in cellular shape, organelle positioning, and cytokinesis. *T. brucei* possesses one homologue of the end-binding protein (EB) 1 family: TbEB1. EB1 proteins belong to the highly conserved family of plus-end tracking proteins (+TIPs) and are master regulators of +TIP networks, thereby coordinating microtubule dynamics. In trypanosomes, the TbEB1 labeling pattern varies throughout the cell cycle at the posterior cell pole in immunofluorescence experiments. Additionally, TbEB1 localized to the FAZ/ FAZ region and the subpellicular microtubule array. Depletion of TbEB1 resulted in a severe growth defect, accumulation of atypical cell cycle stages, and an impediment of cytokinesis. Over-expression of TbEB1 resulted in similar phenotypes, however, less severe. Ectopic expression in a mammalian cell line pointed towards an evolutionary conserved mode of action. Altogether this suggests a role of TbEB1 in microtubule polymerization and indicates its putative involvement in cytokinesis.

Zusammenfassung

Trypanosoma brucei ist ein Einzeller, dessen Zytoskelett hauptsächlich aus Mikrotubuli aufgebaut ist. Das Zytoskelett spielt in der Erhaltung der Zellform, der Organellpositionierung und der Zytokinese eine zentrale Rolle. Das Protein TbEB1 ist das einzige Homolog aus der Familie der End-binding (EB) Proteine in *T. brucei*. EB1 Proteine gehören zu einer stark konservierten Familie von Proteinen, welche an die Plusenden der Mikrotubuli (+TIPs) binden und sie sind die entscheidende Komponente in der Regulation von +TIP Netzwerken, wodurch sie die Dynamik der Mikrotubuli koordinieren. Das TbEB1 Fluoreszenzsignal variiert während des Zellzyklus am posterioren Zellende in Immunofluoreszenz-Experimenten. Außerdem war hier eine TbEB1 Lokalisation für die FAZ/ FAZ-Region und das subpellikuläre Mikrotubulizytoskelett nachzuweisen. Die Depletion von TbEB1 führte zu einem starken Wachstumsdefekt, der Akkumulation von atypischen Zellzyklusstadien und einer eingeschränkt funktionsfähigen Zytokinese. Auch eine Überexpression von TbEB1 führte zu ähnlichen, wenngleich abgeschwächten Phänotypen. Die ektopische Expression in einer Säugerzelllinie deutete zudem auf eine konservierte Wirkungsweise von TbEB1 hin. Zusammengenommen legen diese Ergebnisse nahe, dass TbEB1 eine Rolle in der Mikrotubuli-Polymerisation spielt und vermutlich auch an der Zytokinese beteiligt ist.

Acknowledgements

I would like to express my gratitude to all those who have helped me to complete my PhD thesis and without whom I would not have accomplished this task:

First of all, I would like to thank Prof. Dr. Klaus Ersfeld for the interesting projects in my favorite field, parasitology. Furthermore, I want to thank him for the continuous support and enlightening discussions during my work as well as for proof-reading the layout of this thesis. During the almost five years I have learned a lot about scientific thinking, experimental design and new methods.

My gratitude also goes to Prof. Dr. Benedikt Westermann and Dr. Stefan Heidmann for their helpful mentoring and valuable support. Their suggestions opened up new ways for experiments providing additional insights into the project.

My thanks also go to PD Dr. Stefan Geimer, Rita Grotjahn and Ann-Katrin Unger, for teaching me how to do electron microscopy and constructive discussions to improve my preparations of whole mount cytoskeletons.

Furthermore, I would like to thank Prof. Olaf Stemman for generous provision of antibodies, reagents, and cell lines, which helped me to improve the picture of TbEB1.

I would also thank Markus Spindler and Xenia Chelius for purifying TbEB1 recombinant protein.

My warmest thanks go to Evelin Urban, Kristina Seel, Philip Kahlen, Peter Wolf and Susanne Hellmuth for their continuous support and insightful discussions about experimental layouts when dealing with mammalian cell lines or protein expression.

My special thanks goes to the technical staff, notably Karin Angermann, who gave me handy hints for doing every-day laboratory tasks, creative discussions and general support whenever I needed help.

Most importantly, I would like to give my sincerest thanks to my parents, whose kind devotion and financial help supported me through all of my studies, and to my brothers for their moral support.

Sebastian, thank you for your moral and practical support during all the time, for the glimpse into bioinformatics, for your comments and corrections on this work, and - most important - for sharing your life with me.

1 Introduction

1.1 Trypanosoma brucei

1.1.1 Taxonomy

Since the identification of a haemoflagelate in amphibians by Gruby and the introduction of the genus *Trypanosoma,* a huge variety of other names was proposed for these unicellular organisms (Hoare, 1964). Using light microscopy, trypanosomes were classified morphologically due to presence or absence of a single flagellum and the varying localization of the nucleus, flagellar pocket, and kinetoplast (Maslov *et al.* , 2013; Lukeš *et al.* , 2014). Further attempts for a classification were based on the development of the parasite in tsetse flies, the presence or absence of a parasitic life style, or the route of transfection as criteria (Hoare, 1964; Lukeš *et al.* , 2014). Up to the present, the latter non-taxonomic assignment of trypanosomes to Stercoraria and Salivaria suggested by Hoare (1964) is still practiced in human and veterinary medicine. However, the existing schemes were questioned when modern molecular genetic tools, analysis of small ribosomal RNA (SSU rRNA) and glycosomal glyceraldehyde-3-phosphate dehydrogenase (gGAPDH), became available and species were regrouped (Lukes *et al.* , 1997; Hamilton *et al.* , 2004, 2007; Maslov *et al.* , 2013). In these studies, the monophyletic nature of the genus *Trypanosoma* was confirmed. The family Trypanosomatidae is situated within the order Trypanosomatida within the class Kinetoplastida in the phylum Euglenozoa. It belongs to the unranked group Excavata in the eukaryotic domain. The family Trypanosomatidae harbors the important pathogenic genus *Leishmania,* aethiologic agent of leishmaniasis, and *Trypanosoma.* The latter includes several species of medical and veterinary relevance, especially *T. cruzi*, aethiologic agent of American trypanosomiasis or Chagas disease, and *T. brucei,* which is amongst others responsible for African trypanosomiasis. *T. brucei* is further divided in *T. brucei rhodesiense, T. brucei gambiense,* and *T. brucei brucei* (Fig. 1.1) (Simpson *et al.* , 2006; Maslov *et al.* , 2013; Lukeš *et al.* , 2014).

Taxonomy of T. brucei	
Domain: Eukaryota	
Excavata	
Phylum: Euglenozoa	
Class: Kinetoplastida	
Order: Trypanosomatida	
Familiy: Trypanosomatidae	
Genus: Trypanosoma	
Species: T. brucei	
Subspecies:	T. brucei brucei
	T. brucei gambiense
	T. brucei rhodesiense

Figure 1.1: Taxonomy of *T. brucei.*

1.1.2 African trypanosomiasis

T. brucei sub-species are responsible for African trypanosomiasis, a severe fly-born disease in human and animals. With the tsetse fly only vector, the illness is restricted to the 14° north and 29° south latitude of sub-Saharan Africa, the so called tsetse fly belt (Kennedy, 2013). Reminiscent of the main symptoms, the disease is referred to "sleeping sickness" in humans and "nagana" in animals. The latter one is deduced from the Zulu language meaning listless/ powerless. Due to its affliction of both, human and animals, socio-economic effects of trypanosomiasis are dramatic resulting in poverty und underdevelopment (Connor, 1994; Steverding, 2008; Franco *et al.* , 2014). Although the clinical picture has been well-known since the ancient Egypt, the causative agent of the disease was not identified until the end of the 19th century (Steverding, 2008; Kennedy, 2013). A first step was done, when David Livingston proposed that nagana occurs after the bite of tsetse flies, which was later proven by David Bruce. The bacteriologist also identified the causative agent, *T. brucei brucei,* in cattle blood in 1895 and the parasite was named after him. A few years later, he drew conclusions about the complete transmission cycle when F. K. Kleine discovered the trypanosomal developmental cycle in the tsetse fly. At the beginning of the 20th century also the etiologic agents of human African trypanosomiasis (HAT), *T. brucei gambiense and T. brucei rhodesiense,* were discovered (Steverding, 2008). Depending on the parasite, an acute and a chronic form of the disease occur. *T. brucei gambiense,* transmitted by tsetse flies of the *Glossina palpalis* group and commonly afflicting human beings, cause the chronic progression of the disease persisting for several months up to years (Checchi *et al.* , 2008; Malvy & Chappuis, 2011; Checchi *et al.* , 2015). The acute illness is caused by *T. brucei rhodesiense* and takes only a few weeks. The parasite is transmitted by tsetse flies of the *Glossina morsitans* group and generally resides in wild and domestic animals (Brun *et al.* , 2010; Malvy & Chappuis, 2011). Both forms are characterized by a two-phase progress. During the

first or early stage, also referred to as haemolymphatic stage, the parasites only reside extracellularly in the blood and lymph system causing amongst other symptoms fever, malaise, cachexy, arthralgia, and lassitude. In the course of the disease, multiple organs are affected and finally become dysfunctional. If the parasites trespass the blood-brain-barrier, the second phase of the disease, also known as the neurological phase, starts. Due to the presence in liquor, patients develop symptoms like mental and motor-system disturbances, an abnormal sleep-wake-cycle, coma, and finally death if left untreated (Steverding, 2008; Malvy & Chappuis, 2011; Kennedy, 2013). Animals suffering from trypanosomiasis demonstrate amongst others cachexy, anemia, weakness, and are more prone to secondary infections, abortions, reduced fertility, and lactation (Connor, 1994). Infections are caused by *T. brucei brucei,* as well as other trypanosomal species like *T. evansi, T. congolense,* and *T. lewisi.* Those species were considered to be non-pathogenic for humans. However, single cases of human infections have been described with their importance to public health being still under discussion (Brun *et al.* , 2010; Lin *et al.* , 2015).

1.1.3 The developmental cycle

The developmental cycle of *T. brucei* combines three main players: the uniflagellated parasite, the tsetse fly (*Glossina* spp.) as vector, and a vertebrate reservoir including the susceptible hosts developing the illness (Fig. 1.2) (Franco *et al.* , 2014). Co-evolution of all three elements resulted in a balance whereby the same *Trypanosoma* species demonstrates a varying success to infect a certain host or to manifest in a specific vector species (Connor, 1994; Dyer *et al.* , 2013). The cyclical change between completely different environments in vector and host requires a fine-tuned adaption of the morphology, cell surface composition, gene expression, and metabolism (Brecht & Parsons, 1998; Fenn & Matthews, 2007; Rotureau *et al.* , 2011). The two main morphotypes, which occur during the *T. brucei* life cycle, have been characterized by Hoare and Wallace (1966). They are based on the positions of kinetoplast (the accumulated mitochondrial DNA) and nucleus as well as the dragging flagellum, which sets the anterior-posterior axis of the organism. Trypomastigote stages demonstrate a kinetoplast between the posterior cell pole and the nucleus. In epimastigotes, the kinetoplast is localized between the nucleus and the anterior cell pole (Rotureau *et al.* , 2011). Pre-adapted, metacyclic trypomastigote trypanosomes are transmitted to the vertebrate during a blood meal of an infected tsetse fly. They multiply subcutaneously at the site of the lesion and are further transported via the lymph system to the bloodstream (Franco *et al.* , 2014). Particularly, due to an extremely dense surface coat, composed of variant surface glycoproteins (VSGs) enabling antigenic variation, bloodstream trypanosomes are able to circumvent human immune response and thus, to sustain infection (Vickerman, 1969; Engstler *et al.* , 2004; Horn, 2014). In the mammalian host, two different forms of trypomastigote parasites with the corresponding intermediates are found:

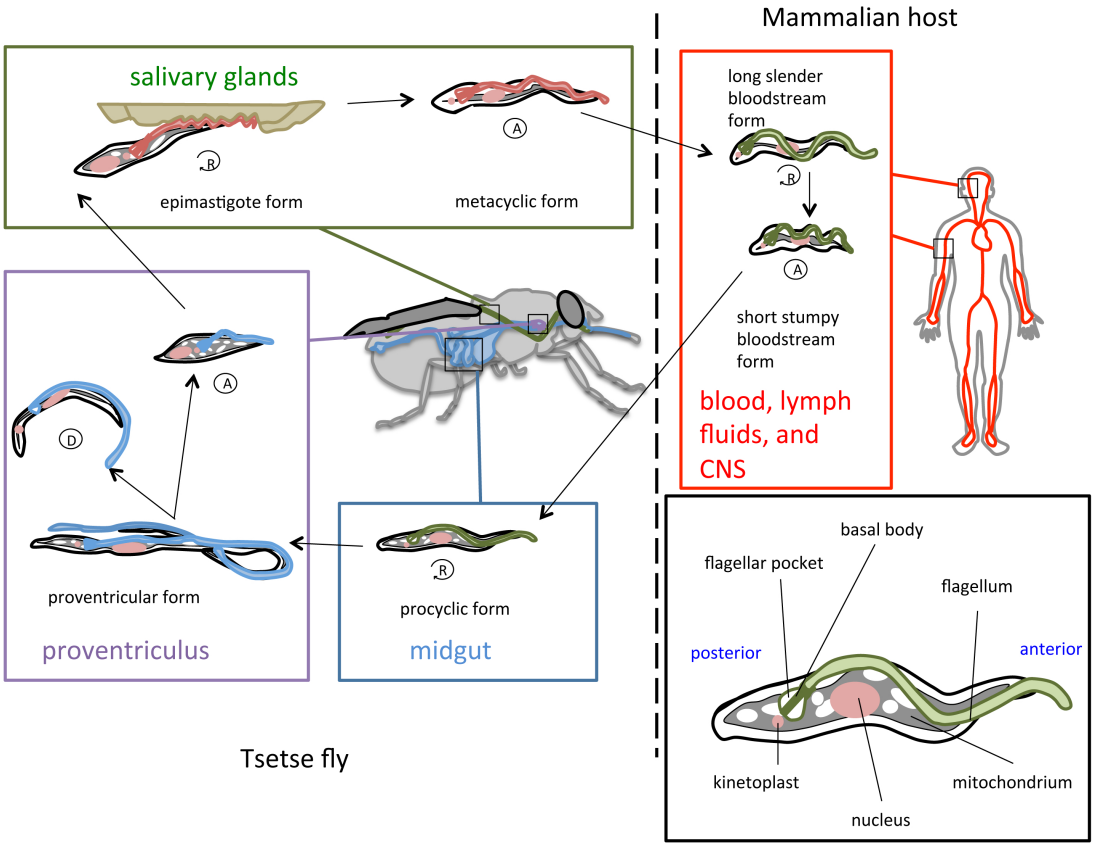


Figure 1.2: Developmental cycle of *T. brucei*. The parasite cycles between a dipteran vector, the tsetse fly, and a mammalian host. In both environments, different conditions occur forcing the parasit to adapt in morphology and metabolism by developing different life cycle stages. The black box shows a magnification of the procyclic trypomastigote form demonstrating the major organelles, which are similar in all other life cycle stages. Three life cycle stages of *T. brucei* are proliferative (R) while others are cell cycle arrested (A) or go extinct after cell division (D). Life cycle stages adapted and modified from R. Wheeler (http://www.richardwheeler.net/contentpages/image.php?gallery=Scientific_Illustration&img=Trypanosome_Life_Cycle&type=jpg), blood vessels from http://www.cocoavia.com/media/2012_Site/cms_images/cartoon_body.png.

the long, slender form and the short, stumpy form (Fig. 1.2). The first is the rapidly dividing form, prevalent during early parasitemia while the latter one is cell cycle arrested in G_1-phase, occurs at high parasite densities, and goes extinct within several hours if not ingested by the tsetse fly (Matthews & Gull, 1994; Rotureau *et al.* , 2011; Portman & Gull, 2014). Therefore, the emergence of stumpy forms prolongs host survival and facilitates colonization of the tsetse fly by synchronizing morphological transitions with the re-entry into the cell cycle (Matthews, 2005, 2015). The irreversible slender to stumpy transition is partially mediated by the so-called stumpy induction factor (SIF), which has not been characterized so far (Vassella *et al.* , 1997; Fenn & Matthews, 2007; Rico *et al.* , 2013). The transition is morphologically characterized by a shortened flagellum, the re-positioning of the kinetoplast, and a cristated mitochondrion (Vickerman, 1985; Reuner *et al.* , 1997). Examples on the molecular level are the expression of some enzymes of the Krebs cycle and respiratory chain, the change of the variant surface glycoprotein (VSG) coat to an EP/GPEET procyclin positive cell surface (Matthews & Gull, 1994; Hendriks *et al.* , 2000; Bringaud *et al.* , 2006), and expression and integration of different microtubule-associated proteins, e. g. CAP5.5/ CAP5.5V and CAP51/ CAP51V (Hertz-Fowler *et al.* , 2001; Portman & Gull, 2014). Although both forms have to be shown to be infective for the tsetse fly, successful establishment and manifestation of infection was more efficient in case of stumpy forms due to their pre-adaptions (Matthews & Gull, 1994; Hendriks *et al.* , 2000). That was already noticed by Robertson in 1912 (Fenn & Matthews, 2007).

As newborn tsetse flies have never been observed to harbor trypanosomes, the vector can only pick up the parasites when feeding on infected mammals (Brun *et al.* , 2010). In the fly midgut, the stumpy forms differentiate quickly into procyclic trypomastigotes (Fig. 1.2), which cross the peritrophic membrane. Replicating procyclics manifest the infection in the tsetse fly midgut, thereby probably providing a reservoir of infective individuals (Sharma *et al.* , 2009; Ooi & Bastin, 2013). Early procyclics are characterized by their surface coat mainly composed of GPEET procyclin, whereas that of late procyclics is composed of EP1 and EP3 procyclins. EP2 procyclin is not detectable on protein level in the cells (Fenn & Matthews, 2007). Some parasites migrate towards the proventriculus while they transform via non-proliferative meso-cyclic forms to epimastigote ones after reaching this organelle. Both forms are extremely thin and elongated and possess a long flagellum enabling increased motility. In the proventriculus, epimastigotes perform an asymmetric cell division resulting in a short and a long epimastigote configuration (Fig. 1.2) (Sharma *et al.* , 2008). The latter presumably dies (Sharma *et al.* , 2008, 2009). Therefore, persistent colonization of the proventriculus by parasites from the midgut is mandatory to sustain a trypanosomal population in this area (Ooi & Bastin, 2013). The short epimastigotes re-enter the alimentary duct and migrate towards their final destination, the salivary glands. After elongation of the flagellum, they attach immediately to the epithelium. They

represent the first developmental stage occurring at this region (Dyer *et al.* , 2013). Attached epimastigotes are coated with BARPs (brucei alanine-rich proteins) instead of procyclins (Fenn & Matthews, 2007; Urwyler *et al.* , 2007). They are proliferative and therefore, salivary gland colonization is self-sustaining (Sharma *et al.* , 2009; Rotureau *et al.* , 2012; Dyer *et al.* , 2013). Furthermore, those stages have been demonstrated to be involved in genetic exchange between different trypanosomal strains (Tait *et al.* , 2007; Peacock *et al.* , 2011). Their asymmetric division also results in pre-metacyclics. Those develop into nascent metacyclic forms, which remain attached and are arrested in G_1-phase. After release, they are infective and can be transferred as VSG-coated metacyclic trypomastigotes during the next blood meal (Sharma *et al.* , 2009).

1.1.4 The cellular architecture of *T. brucei*

1.1.4.1 Providing energy for the organism: glycosome and mitochondrion

The unicellular parasite measures about 15-20µm in length whereby the bloodstream forms - with exception of the short forms occurring in the proventriculus - are usually smaller than those emerging in the tsetse fly. Going along with the digenetic life cycle with changing environmental conditions, the parasite uses different carbon sources for its metabolism. In the mammalian host, solely glucose is metabolized (Bringaud *et al.* , 2006). The compartmentalization of glycolytic enzymes to the glycosome, a microbody near the nucleus, is a unique characteristic for kinetoplastida (Fig. 1.3) (Opperdoes & Borst, 1977). In *T. brucei*, most enzymes of the glucose conversion chain are localized to the glycosome, only the last three are cytosolic. The glycosome is an integral part for bloodstream and insect forms, although the proteome composition of the organelle is adapted to the different environments (Colasante *et al.* , 2006; Michels *et al.* , 2006). With the transition of the parasite from the host to the vector, amino acids, such as L-proline or L-threonine, become main ATP sources (Bringaud *et al.* , 2006). This is reflected by the form of the single mitochondrion, which runs through the entire cell and is highly active in insect trypanosomes (Fig. 1.3). The simple, smooth, tubular shape in bloodstream forms increases in size and forms many cristae to provide space for metabolic processes, e. g. Krebs cycle and electron transport chain (Vickerman, 1965; Matthews, 2005).

1.1.4.2 DNA-containing organelles: kinetoplast and nucleus

The kinetoplast (K) is located within the mitochondrion, at the posterior part of the cell. It is a disk-shaped organelle, which accumulates the complete mitochondrial DNA and has become eponymous for the class kinetoplastida. It is composed of two kinds of circular DNA: mini and maxi circles. The former provide genetic information of guide RNAs to decipher cryptic maxi circle transcripts by RNA editing (Fairlamb *et al.* , 1978; Corell *et al.* , 1993; Klingbeil & En-

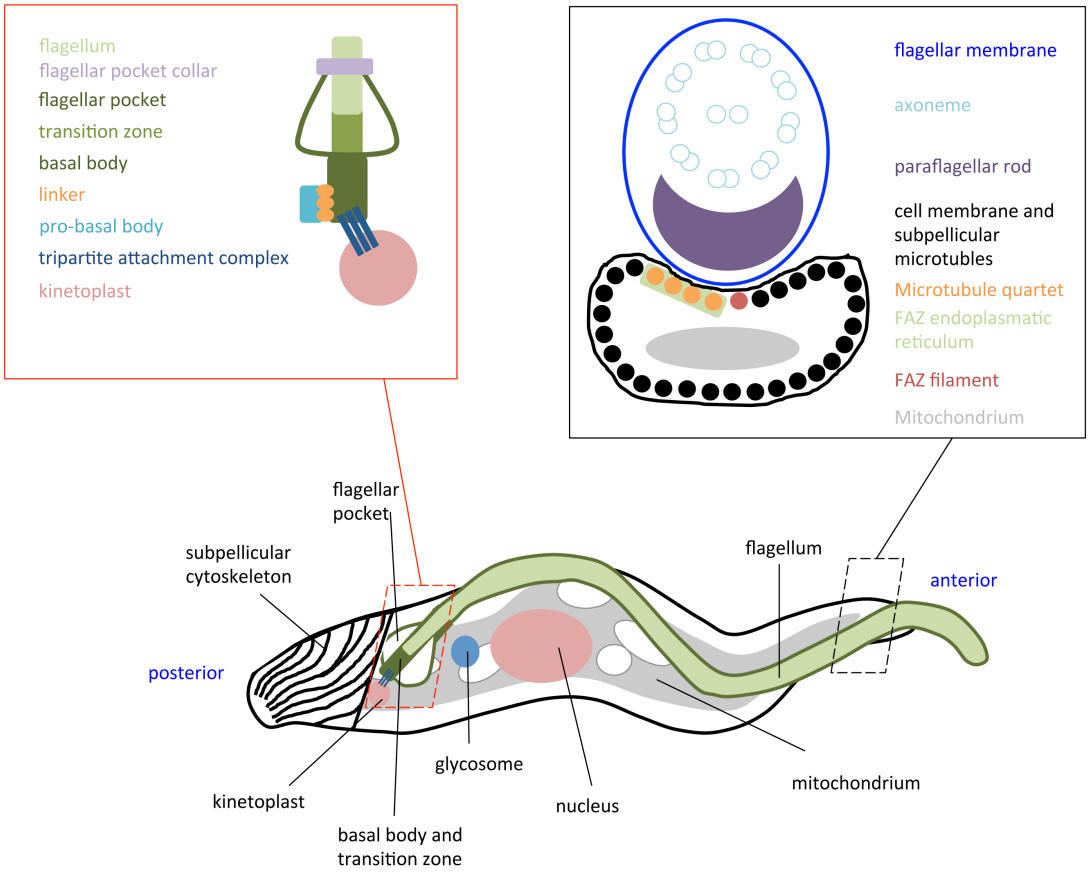


Figure 1.3: The cellular architecture of *T. brucei*. Simplified model represents the main organelles and the anterior-posterior orientation of the trypanosome. The subpellicular cytoskeleton, situated beneath the plasma membrane and covering the whole parasite, is partially shown at the posterior area of the cell. The red square depicts the kinetoplast/ basal body complex as well as the beginning of the flagellum in more detail. The black square illustrates the composition of the flagellum and adjacent components of the cytoskeleton within the cell body. The red square was adapted from Ikeda and de Graffenried (2012) and the black square from Ralston and Hill (2008).

glund, 2004). The latter encode genes for ribosomal RNAs and components of the respiratory complexes. While maxi circles (23kbp) are only several dozens per cell, the number of mini circles (~1kb) is about several thousands. The replication cycle of the kinetoplast DNA has to be tightly correlated with that of the nucleus (N), the second DNA-containing organelle of *T. brucei* (Gluenz *et al.* , 2011; Povelones, 2014). The nucleus is situated in the center of the cell, its outline is spherical in procyclic trypanosomes while it is egg-shaped in bloodstream forms. The nuclear genome is composed of 11 megabase pair chromosomes (0.9 - 5.7 Mbp), one to five intermediate chromosomes (200-900kbp), and about one hundred mini-chromosomes (30-150kbp). Genes located on megabase pair chromosomes are generally diploid and organized in polycistronic transcription units (Van der Ploeg *et al.* , 1989; Ersfeld, 2011; Alsford *et al.* , 2012a). As many early branching eukaryotes, *T. brucei* executes a closed mitosis thus, chromosomal segregation is performed within a fully assembled nuclear envelope (Ogbadoyi *et al.* , 2000; McKean, 2003; Zhou *et al.* , 2014). However, little information on spindle pole structure and components as well as kinetochore composition is available (Akiyoshi & Gull, 2014; Zhou *et al.* , 2014). Both, the nucleus and the kinetoplast, are used to assign the cell to a certain life cycle or cell cycle stage (Woodward & Gull, 1990).

1.1.4.3 From tip to base: the flagellum, flagellar pocket, basal body, and paraflagellar rod

Frequently, a third organelle, the single flagellum (F), is added for characterization because it is present throughout the whole cell and life cycle (Langousis & Hill, 2014). Its obvious function is locomotion by dragging the parasite through its liquid environment which is indispensable for survival (Kohl *et al.* , 2003; Broadhead *et al.* , 2006). Additionally, the organelle is involved in attachment to the epithelium of the salivary glands, cell morphogenesis and division, infectivity, and social motility (Ralston & Hill, 2008; Woods *et al.* , 2013a; Langousis & Hill, 2014). It is nucleated by the basal body at the posterior part of the cell (Fig. 1.3), where nine microtubule triplets form the base of the flagellum. The microtubule triplets are replaced by microtubule doublets in the transition zone and eventually form the characteristic pattern of nine microtubule doublets and a core microtubule pair, denoted as axoneme (Fig. 1.4 A, B). The transition zone is separated from the axoneme by the basal plate (Fig. 1.4 A). The axoneme is assumed to be anchored to the collarette, by which flagellum positioning is mediated. It is a fibrous structure at the base of the flagellar pocket through which the flagellum enters (Field & Carrington, 2009; Lacomble *et al.* , 2009).

The flagellum emerges to the cell surface via the flagellar pocket (Fig. 1.3), which is formed by a single gap in the dense microtubule array and an asymmetric invagination of the plasma membrane (Field & Carrington, 2009; Lacomble *et al.* , 2009). The flagellar pocket is the ex-

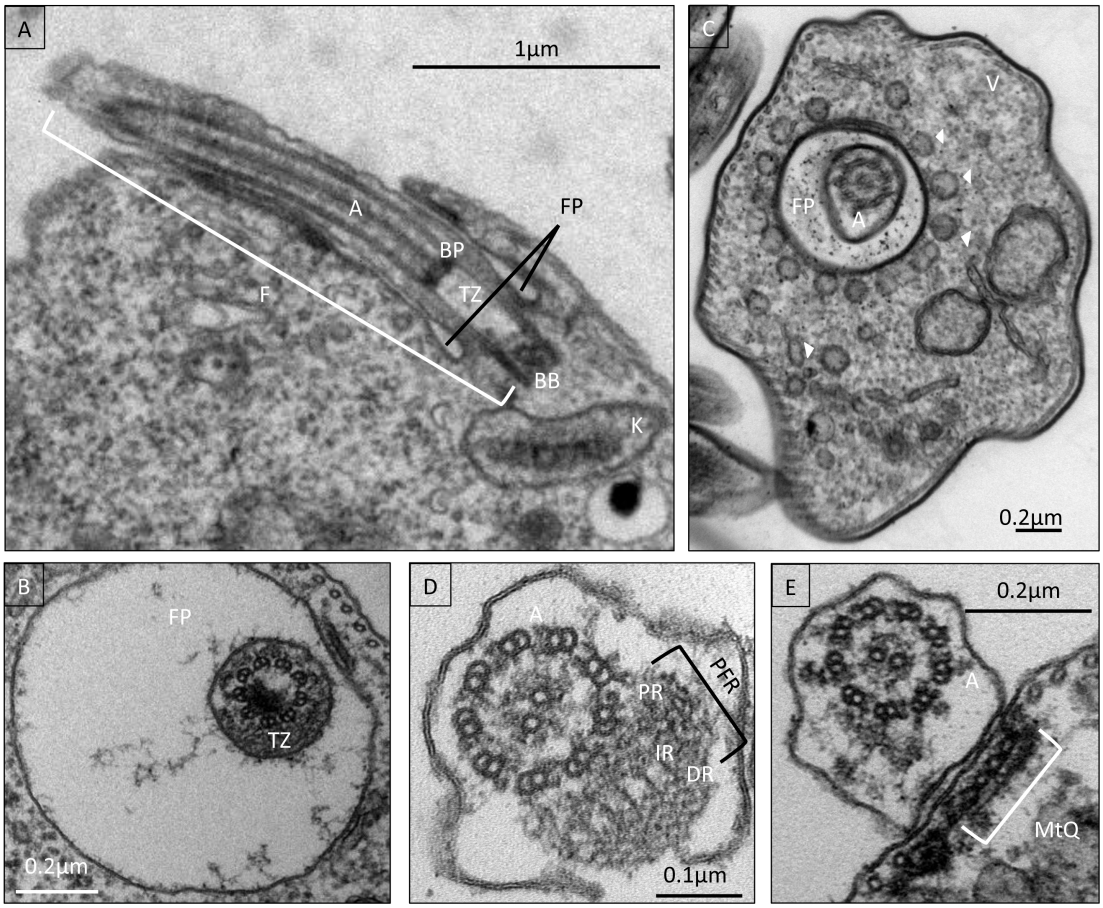


Figure 1.4: Transmission electron micrographs of the trypanosomal flagellum and adjacent structures. A) The trypanosomal flagellum (F) was cut longitudinally revealing the ultrastructural composition from base to tip: basal body (BB), transition zone (TZ), basal plate (BP), and axoneme (A). **B)** Cross-section of the transition zone of a flagellum residing in the flagellar pocket (FP). **C)** Cross-section of a flagellar pocket demonstrating the flagellar pocket as exo-/endocytotic organelle with multiple vesicles (arrowheads) either fusing with or budding of the flagellar pocket. **D)** Cross-section of a flagellum depicting the main structural components after leaving the flagellar pocket: the axoneme and the paraflagellar rod (PFR). The latter is composed of three parts: the proximal region (PR), the intermediate region (IR), and the distal region (DR) regarding the axoneme. **E)** Cross-section of the flagellum and adjacent cell body showing the microtubule quartet (MtQ), which is part of the FAZ and surrounded by smooth endoplasmic reticulum. Figures A, B, D, and E were micrographs taken from PCF preparations, figure C is taken from BSF preparations.

clusive area of endo- and exocytosis, and therefore important for nutrient supply, recycling of glycosylphosphatidylinositol (GPI-) anchored proteins from the cell surface, and immune evasion (Fig. 1.4 A-C) (Morgan *et al.* , 2002; Engstler *et al.* , 2004; Overath & Engstler, 2004). An important, electron-dense structure at the neck of the flagellar pocket is the flagellar pocket collar (Fig. 1.3 C). Up to the present, only one protein, BILBO1, has been identified to be important for flagellar pocket biogenesis, flagellar attachment zone (FAZ) formation, and calcium-binding (Bonhivers *et al.* , 2008; Florimond *et al.* , 2015; Perdomo *et al.* , 2016). Two further protein complexes are associated with the flagellar pocket collar region. The first, the 'hook complex' (formerly referred to as bilobe), contains amongst others the well-characterized protein TbMORN (Morriswood *et al.* , 2009; Morriswood & Schmidt, 2015; Morriswood, 2015) and its replication is highly coordinated with that of the Golgi apparatus (He *et al.* , 2005; Shi *et al.* , 2008). The second one is defined as 'centrin arm' due to its component TbCentrin 4 (Shi *et al.* , 2008; Morriswood, 2015). If its the same structure as the previously described 'neck microtubule', a single microtubule inside the flagellar pocket neck, remains to be investigated (Lacomble *et al.* , 2009; Morriswood, 2015; Perdomo *et al.* , 2016).

The basal body is anchored via nine transition zone fibers to the flagellar pocket membrane. The pro-basal body is physically linked to the basal body and matures during the cell cycle to a fully developed basal body with adjacent pro-basal body itself (Fig. 1.3). Due to its fibrous connections with the subpellicular cytoskeleton, the basal body is a crucial structure for organelle positioning and segregation, e. g. the kinetoplast (Robinson & Gull, 1991; Robinson *et al.* , 1995; Vaughan & Gull, 2015). Although basal bodies and animal centrioles are highly conserved structures, a striking difference exists: basal bodies are never associated with spindle poles or the nuclear envelope (Vaughan & Gull, 2015). Up to the present, several structural, e. g. γ-tubulin, TBBC, SAS-6 or SPBB1 (Scott *et al.* , 1997; Dilbeck *et al.* , 1999; Hu *et al.* , 2015a,b), and enzymatic, e. g. TbPLK and TbNRKC (Pradel *et al.* , 2006; Ikeda & de Graffenried, 2012), protein components have been identified. Furthermore, the basal body is connected to the kinetoplast via the tripartite attachment complex (TAC), which is a highly organized transmembrane structure (Fig. 1.3). It was first identified in electron micrographs by Ogbadoyi and co-workers (2003) and consists of exclusion zone filaments proximately connected to the basal body and distally to a specialized, cytosolic part of the mitochondrial bilayer. Unilateral filaments are adjacent in the mitochondrial matrix and are directly linked to the kinetoplast. Despite of the solved structural layout, only few protein components, e. g. p166, p197, and AEP-1, are described so far (Ochsenreiter *et al.* , 2008; Zhao *et al.* , 2008; Gheiratmand *et al.* , 2013).

In 1962, K. Vickerman described a large, trilaminar lattice-like structure, running alongside the axoneme, which is nowadays defined as the paraflagellar rod (PFR) (Fig. 1.3) (Vickerman, 1962; Portman & Gull, 2010). The PFR can be divided into three zones, proximal, intermediate,

and distal region, according to the orientation regarding the axoneme, to which microtubule pairs four to seven are connected via fibers (Fig. 1.4 D) (Bastin *et al.* , 1998; Ralston & Hill, 2008; Langousis & Hill, 2014). More than 55 years ago, the PFR was described to shape the membrane. Possibly, it also participates in trypanosomal motility (Vickerman, 1962). In the current literature a role in flagellar movement is favored, however, an element of uncertainty remains as a defect in PFR composition could indirectly result in defects of flagellum design and function and thereby, perturb flagellar motility (de Souza, 2010; Portman & Gull, 2010). The core proteins of the PFR are PFR 1 and PFR 2 (Schlaeppi *et al.* , 1989; Deflorin *et al.* , 1994) but a variety of new proteins have been identified assigning a subset of additional features to the PFR like transmitting external signals to the axoneme or cell body via calcium and cAMP signaling, adenine homeostasis, and regulatory functions in cell and life cycle (Portman & Gull, 2010).

1.1.4.4 Lifeline connecting flagellum and cell body: the flagellar attachment zone

When passing the flagellar pocket collar, the flagellum is immediately attached to the cell membrane over most of the cell length by the flagellar attachment zone (FAZ), a complex multicomponent element. This unique feature of trypanosomatids defines the anterior-posterior axis of the cell (Vaughan *et al.* , 2008; Langousis & Hill, 2014). Key components are the FAZ filament, the microtubule quartet (MtQ), and junctions connecting the flagellar cytoskeleton with the FAZ filament as it traverses the flagellar and cell membrane (Fig. 1.3) (Kohl & Bastin, 2005; Ralston & Hill, 2008; Lacomble *et al.* , 2009). The FAZ filament is an electron-dense structure, which starts after the flagellar pocket is inserted between two microtubules of the subpellicular microtubule array, and is directly situated beneath the flagellum (Kohl & Bastin, 2005; Lacomble *et al.* , 2009). The first structural protein that was characterized, was FAZ 1, a repetitive protein (Kohl *et al.* , 1999; Vaughan *et al.* , 2008). As the FAZ filament is only part of the cellular body, its distal end marks the anterior end of the trypanosome, too. The MtQ is a subset of four specialized microtubules first described in 1969 (Taylor & Godfrey, 1969; Vickerman, 1969). It is situated on the left of the FAZ filament as seen from the posterior. As a consequence, the FAZ represents an 'asymmetric seam' within the subpellicular microtubules (Fig. 1.4E) (Vaughan *et al.* , 2008; Lacomble *et al.* , 2009; Sunter & Gull, 2016). The MtQ is rooted between the basal body and pro-basal body, however, a clear microtubule organizing center (MTOC) has still to be revealed (Lacomble *et al.* , 2009; Vaughan & Gull, 2015). It performs a left turn around the flagellar pocket before entering into the subpellicular cytoskeleton occurs. Up to that point, these microtubules are closely associated without inter-microtubule spaces (Lacomble *et al.* , 2009). Strikingly, the polarity of the MtQ is identical to those of the

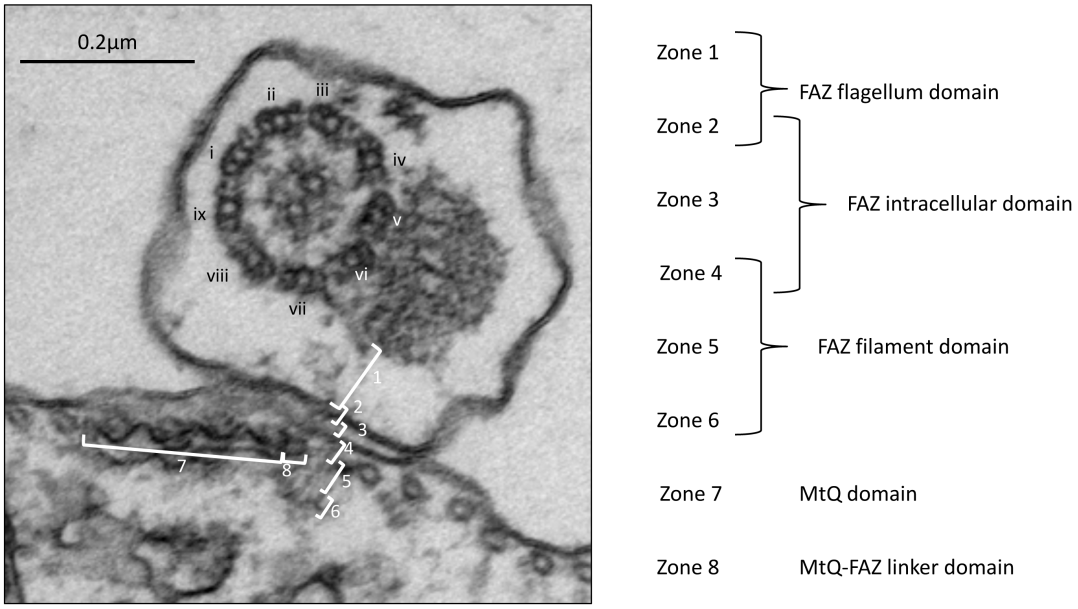


Figure 1.5: TEM image of the eight different zones of the FAZ. Procyclic trypanosome transverse section demonstrating the flagellum and adjacent cell body. FAZ zones 1 to 8 and the FAZ domains are assigned according to Sunter and Gull (2016), positions of microtubule doublets are indicated by Roman numerals according to Ralston et al. (2009).

flagellum but reverse to that of the subpellicular cytoskeleton (Lacomble *et al.* , 2009; Perdomo *et al.* , 2016). Therefore, microtubule plus ends are found at the anterior cell pole and the MtQ is considered as antiparallel (Robinson *et al.* , 1995; Kohl *et al.* , 2003; Vaughan *et al.* , 2008). In contrast to the subpellicular microtubules, the MtQ is enveloped by a part of the smooth endoplasmic reticulum, the so-called FAZ endoplasmic reticulum (FER) (Vickerman, 1962; Sherwin & Gull, 1989a; Langousis & Hill, 2014). Although the MtQ is known for more than 45 years, and a specific antibody, 1B41, is available, a function has not been assigned, yet (Gallo *et al.* , 1988; Langousis & Hill, 2014).

In more detail, eight different zones of FAZ, grouped into five domains, were defined by Sunter and Gull (2016) on electron micrographs (Fig. 1.5): the FAZ flagellum domain (zone 1 and 2), the FAZ intracellular domain (zones 2-4), the FAZ filament domain (4-6), MtQ domain (zone 7), and the MtQ-FAZ-linker domaine (zone 8). Zone 1 contains filaments connecting the flagellar membrane to the junction between the PFR and filaments linking the axoneme to the PFR. Zone 2 are the flagellar membrane junctional complexes. Zone 3 contains intermembrane staples with filaments associated to flagellar and cell membranes. Zone 4 are junctional complexes of the cell body membrane that start at the flagellar pocket and run along the attached

flagellum defining one row of evenly spaced interconnected bodies. Zone 5 consists of radiating fibers originating from the cell body membrane and ending in zone 6, where they are associated with a filamentous structure. Zone 7 is the MtQ with adjacent FER. Finally, zone 8 is composed of fibers linking the MtQ with cell body membrane junctional complexes. The complex composition also reflects the five different connection types of that structure between participating cytoskeleton elements, e. g. subpellicular microtubules to MtQ, and highlights the exquisite coordination of cytoskeleton elements during the cell cycle. Thereby, the FAZ plays a seminal role in cell morphology by determining cell length and organelle positioning, e.g flagellum and basal body, as well as cytokinesis (Vaughan & Gull, 2008; Sunter & Gull, 2016; Zhou *et al.* , 2016). The complex composition also illustrates the multiple phenotypes arising after perturbance of FAZ formation or depletion of single components. Depending on the localization of affected element, a certain type of malformation or characteristic malfunction can be assigned (Sunter & Gull, 2016). If the protein is situated in the FAZ flagellar domain, e. g. flagellar member 3 (FLAM3), depletion of the protein results predominantly in a reduced FAZ length and a kinetoplast situated in the anterior region of the trypanosome, similar to epimastigotes (Rotureau *et al.* , 2014; Sunter *et al.* , 2015b; Sunter & Gull, 2016). The described phenotype of detached flagella by Rotureau and co-workers (2014) due to FLAM3 RNAi seemed to be misinterpreted (Sunter *et al.* , 2015b). However, flagellum detachment is observed when proteins of the FAZ intracellular domain, e. g. flagellum adhesion glycoprotein (FLA1), are depleted (Nozaki *et al.* , 1996; LaCount *et al.* , 2002; Sunter *et al.* , 2015b). Depletion of proteins FAZ2 or FAZ9 leads to mispositioning of DNA containing organelles and flagellum detachment (Sunter *et al.* , 2015a; Sunter & Gull, 2016). Depletion phenotypes seemed to be less profoundly if the protein, e. g. FAZ1, was localized mainly in zone 5 (Kohl *et al.* , 1999; Vaughan *et al.* , 2008; Sunter & Gull, 2016).

1.1.4.5 Pointing the way to cell morphology: the subpellicular cytoskeleton

The subpellicular cytoskeleton is solely composed of microtubules, which enclose the whole parasite in a cage-like manner and no transcellular microtubules are present. Furthermore, in contrast to mammalian microtubules, those of trypanosomes are more resistant to cold depolymerization and anti-microtubule drugs such as cholchicines and paclitaxel (Seebeck *et al.* , 1990; Gull *et al.* , 1990; de Souza, 2008). Most likely due to cross-linking by microtubule-associated proteins (MAPs), the structure is extremely resistant to environmental influences but provides flexibility for cell motility and cytokinesis (Seebeck *et al.* , 1988, 1990). The subpellicular microtubules are evenly spaced, situated directly beneath the cell membrane, and perform a left-handed helix around the cell body (Angelopoulos, 1970; Sherwin & Gull, 1989a; Gull, 1999; Lacomble *et al.* , 2009). Depending on the cell diameter up to 100 and more microtubules could

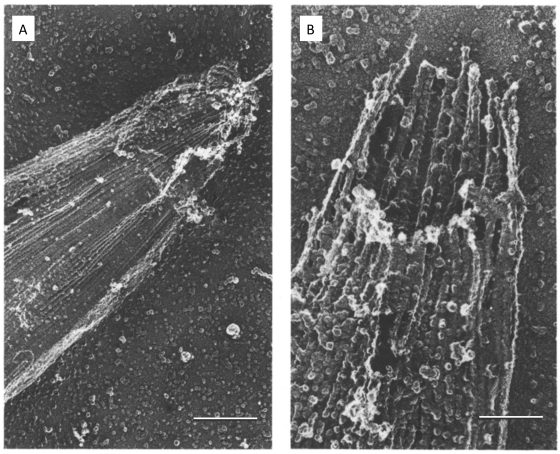


Figure 1.6: Looking at trypanosomal endings. A) The 'closed' formation of the anterior cell pole. Scale bar represents 526nm and was re-drawn in white. **B)** The 'open' formation of the posterior cell pole. Scale bar represents 220nm and was re-drawn in white. The image was taken from Seebeck et al. (1990). Samples were prepared using the quick-freezing, deep-etching, and rotary shadowing method described by Lawson in 1984 (Hemphill *et al.* , 1991a).

be counted in cross-sections of trypanosomes (Angelopoulos, 1970; Gull, 1999). Microtubules constituting the subpellicular array are of varying length and tightly connected with each other (Angelopoulos, 1970; Gull *et al.* , 1990; Hemphill *et al.* , 1991a; de Souza, 2008). Linkage to the plasma membrane is enhanced by the 'knob-carrying' surface of subpellicular microtubules while those of the flagellum are smooth and naked (Hemphill *et al.* , 1991a). Subpellicular microtubules have been shown to be linked to membranes of the endoplasmic reticulum and the endocytic pathway (de Souza, 2008). In general, those cross-links are mediated by multiple MAPs (Gull *et al.* , 1990; Hemphill *et al.* , 1991b).

Microtubules are polar structures. In *T. brucei,* microtubules, except the MtQ and axoneme, are orientated with their plus ends towards the posterior cell end. This was demonstrated by Robinson et al. (1995) with three biochemically independent approaches: hook decoration, seeding from existing ends on whole mount cytoskeletons, and finally, localization of newly assembled microtubules by immunofluorescence assay (Gull *et al.* , 1990). Resolution on ultrastructural level revealed two different formations of the *T. brucei* cell poles. While at the anterior cell pole microtubule ends are bundled to form a tight tip (Fig. 1.6 A), those of the posterior pole are ordered in an open circle (Fig. 1.6 B) (Seebeck *et al.* , 1988; Sherwin & Gull, 1989a; Seebeck *et al.* , 1990). The significance of that variation remains still enigmatic although in other kinetoplastids, e. g. *Leishmania,* an 'open' posterior formation was assumed to be associated with the preferential site of penetration into leukocytes (Seebeck *et al.* , 1990). Although there is variation in the protein content between mammalian and insect trypanosomes, no differences

at the ultrastructural level have been detected so far (Portman & Gull, 2012, 2014). Physical events taking place during the cell division cycle in *T. brucei* demonstrate the important role of cytoskeleton components, which are mainly inherited by three mechanisms. The flagellum and FAZ are inherited in a conserved pattern. Whereas a semi-conservative one was observed during the enlargement of the subpellicular microtubule array, basal body generation, and posterior end formation. Additionally, cytotaxis occurs when the new flagellum migrates along the old one supported by of the flagellar connector in PCF (procyclic form) or the groove in BSF (bloodstream form), respectively (Sherwin & Gull, 1989b; Farr & Gull, 2012; Hughes *et al.* , 2013; Wheeler *et al.* , 2013).

1.1.5 The cell cycle

As *T. brucei* possesses a set of single organelles, their distribution to each daughter cell has to be finely tuned to ensure their equal distribution to daughter cells and thus, the viability of the progeny after cytokinesis. Therefore, the duplication and segregation pathways have to be highly coordinated. Most of those processes are executed and supported by the cytoskeleton, which needs to be either dynamic or stable depending on the cell cycle stage (Gull *et al.* , 1990; McKean, 2003; Portman & Gull, 2012). During the life cycle of *T. brucei,* three replicative forms of the parasite occur: the procyclic form in the tsetse fly midgut, the epimastigote form in the salivary glands, and the long slender bloodstream form of the mammalian host (Rotureau *et al.* , 2011; Farr & Gull, 2012). Although the main sequence of cell cycle steps is similar, minor variations in the single life cycle stages exist (McKean, 2003; Rotureau *et al.* , 2011; Portman & Gull, 2012). For example, the replication cycle of the procyclic form (PCF) takes about 8.5 hours while that of the bloodstream form (BSF) takes 6 hours (Hammarton *et al.* , 2007a). Similar to mammalian cells, the trypanosomal cell cycle can be divided into G_1-, S-, G_2-, and M-phase and terminates with cell division. But in contrast to the mammalian cell cycle, a second S-phase occurs which is characterized by the duplication and segregation of the kinetoplast DNA. Evidently, most of the cell cycle stages defined by DAPI-staining and flagellum development belong to the last third of the cell cycle (Fig. 1.7) (Woodward & Gull, 1990; McKean, 2003). However, a clear assignment of trypanosomal cell morphologies to early time points in the cell cycle is still challenging. While Woodward and Gull (1990) defined the division of the kinetoplast as hallmark for the G_2-phase, similar cells were assigned to the S-phase in experiments performed by Siegel and co-workers (2008). This discrepancy was probably due to an assignment of kinetoplast division to an earlier time point combined with a prolonged nuclear $G_{0/1}$- or S-phase in the later work (Siegel *et al.* , 2008).

PCF and BSF can be easily cultivated as axenic cultures. Therefore, most data are available from these two types (Farr & Gull, 2012; Zhou *et al.* , 2014). A simplified cell cycle of PCF

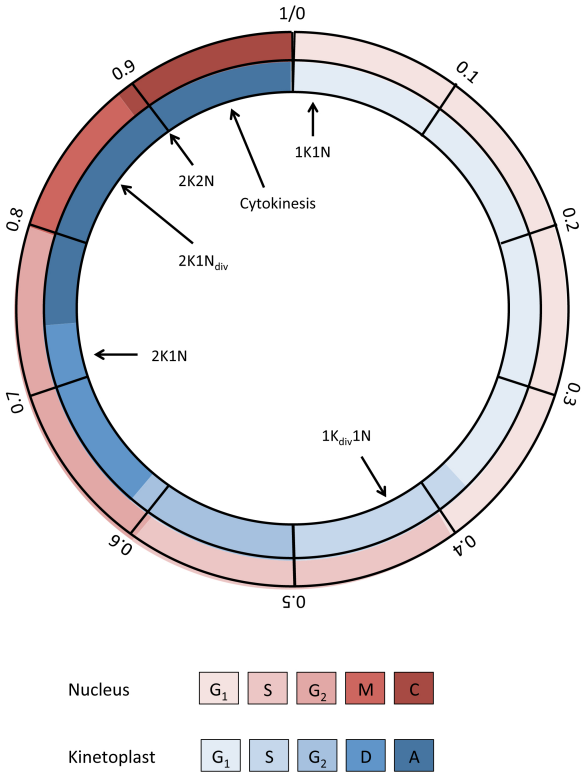


Figure 1.7: Cell cycle phases of *T. brucei*. The trypanosomal cell cycle is composed of G_1, S, G_2, M-phase, and cytokinesis (C). However, trypanosomes possess two DNA-containing organelles, nucleus (red cycle) and kinetoplast (blue cycle), which are duplicated and segregated independently. Intimate timing and correlation of events take place and both structures pass through a similar cycle. The kinetoplast S-phase (blue) starts shortly before nuclear DNA (red S-phase) is duplicated. Kinetoplast division (D) is finished before nuclear mitosis (M). The A-phase of the kineotplast cycle is characterized by the movement of segregated kinetoplasts to their final locations. As depicted, most of the cell cycle stages of *T. brucei* (1K1N, $1K_{div}1N$, 2K1N, $2K1N_{div}$, 2K2N, cytokinesis), which are distinguishable by light microscopy, are situated in the last third of the cell cycle. Temporary arrangement of cell cycle events was derived from McKean (2003).

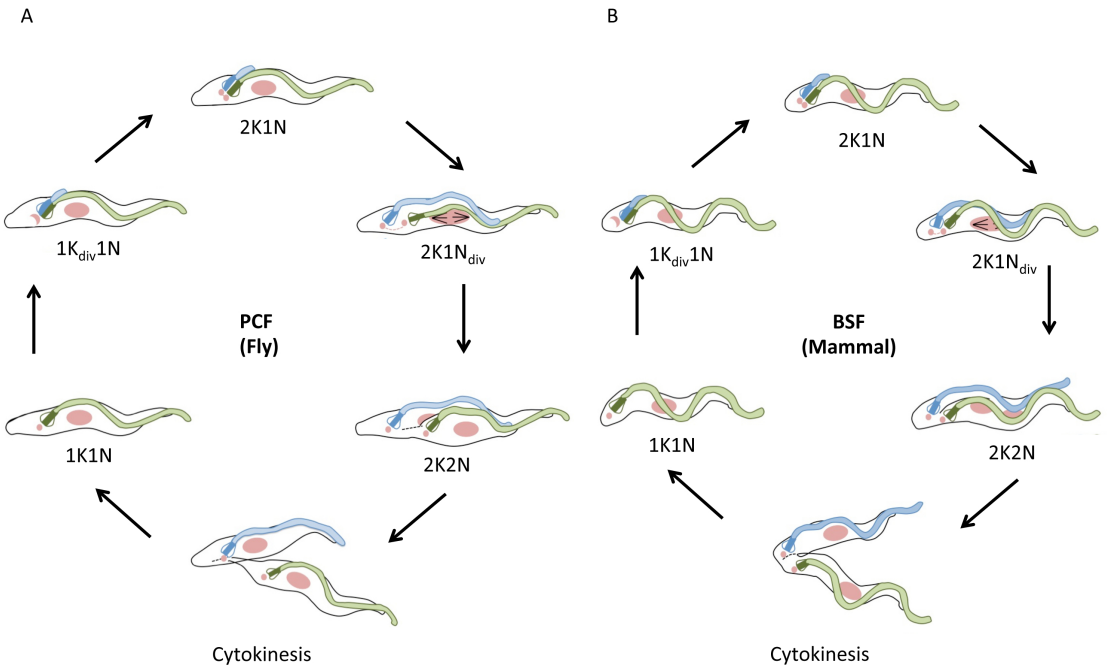


Figure 1.8: A simplified cartoon illustrating major events in the cell cycle of *T. brucei* procyclic (left circle) and bloodstream (right circle) forms. The hallmarks for positioning of trypanosomes to a certain cell cycle stage are shown: nucleus, kinetoplast, and flagellum. Trypanosomes were re-drawn from Wheeler et al. (2013).

and BSF depicting main morphological events for classification is shown in figure 1.8. As most data were derived from PCF, they are used to describe the chronology of morphological events during the cell cycle.

1.1.5.1 Pre-mitotic events

At the beginning of G_1-phase, all organelles are present as single copies and cells are referred to as 1K1N (1 kinetoplast, 1 nucleus) (Fig. 1.7, 1.8). The probasal body is located anterior to the basal body if viewed from the posterior cell end and both are parallel to each other (Lacomble *et al.* , 2010; Vaughan & Gull, 2015). However, first morphological changes indicating a new round of replication occur not until G_1/S transition (Farr & Gull, 2012). It starts with the initiation of a new microtubule quartet near the probasal body, thus anterior to the basal body. The maturing probasal body is already linked to the kinetoplast by fibers of the TAC (Ogbadoyi *et al.* , 2003; Lacomble *et al.* , 2010). Maturation of the probasal body is characterized by its elongation and connection to the flagellar pocket membrane, followed by the invasion of the flagellar pocket, and finally the formation of the basal plate (Sherwin & Gull, 1989a; Lacomble *et al.* ,

2010; Vaughan & Gull, 2015). Subsequently, the axoneme starts to grow and while still being inside the flagellar pocket, it becomes connected to the old flagellum by the flagella connector (Moreira-Leite *et al.* , 2001; Briggs *et al.* , 2004; Lacomble *et al.* , 2010). This is a dynamic, trilaminar transmembrane junction, which is only present in insect forms (Briggs *et al.* , 2004; Sharma *et al.* , 2008; Farr & Gull, 2012). Finally, two new probasal bodies were generated and are linked orthogonally to the pre-existing basal bodies with the youngest basal body still at the anterior position (Sherwin & Gull, 1989a; Lacomble *et al.* , 2009, 2010). Probasal bodies are re-oriented parallel to the mature basal bodies before the onset of mitosis (Vaughan & Gull, 2015). Additionally, microtubules of the subpellicular cytoskeleton are elongated towards the posterior cell end (Sherwin & Gull, 1989b).

The axoneme elongates and a cytoplasmic protrusion, the ridge, is formed between new and old flagellum inside the flagellar pocket, initiating the separation of the two flagellar pockets. The ridge is further elongated. The old MtQ serves as a rib for the division of the flagellar pockets together with basal body segregation. (Lacomble *et al.* , 2009, 2010; Vaughan & Gull, 2015). Subsequently, the basal body with the new flagellum rotates anti-clockwise around the older basal body and moves laterally away from it. Therefore, the newly assembled flagellum is always localized at the posterior position (Sherwin & Gull, 1989a; Lacomble *et al.* , 2010). The kinetoplast simultaneously rotates as it is linked to the proximal part of the basal body via the TAC. However, the underlying mechanisms enabling the rotation remain to be elucidated (Gluenz *et al.* , 2011). Concomitant with basal body rotation, kinetoplast S-phase occurs ($1K_{div}1N$ cells, Fig. 1.7, 1.8), which is slightly initiated before the onset of nuclear S-phase (Gluenz *et al.* , 2011). Both S-phases require about the same time and hence, nuclear S-phase is finished after that of the kinetoplast (Fig. 1.7) (Sherwin & Gull, 1989a; McKean, 2003; Farr & Gull, 2012).

Simultaneously to axonemal extension, the FAZ filament elongates while it is linked to the old FAZ at the distal end (Absalon *et al.* , 2007; Farr & Gull, 2012). The FAZ origin aside the flagellar pocket is marked by the protein TbLRRP1 (leucin-rich repeat protein). The protein is a component of the hook complex, which partially overlaps with the FAZ filament and probably supports formation of the so-called FAZ root (Morriswood *et al.* , 2013; Zhou *et al.* , 2015). Although the FAZ root is built before PFR assembly, FAZ elongation later lags behind both, flagellum and PFR assembly (Kohl *et al.* , 1999, 2003; Rotureau *et al.* , 2014). Therefore, the length of the flagellum determines the length of FAZ and flagellar assembly continues even in the absence of the FAZ (Davidge *et al.* , 2006; Absalon *et al.* , 2008; Vaughan *et al.* , 2008). FAZ formation is executed near the flagellar pocket collar while flagellum assembly starts from the distal tip of the flagellum (Davidge *et al.* , 2006; Absalon *et al.* , 2008; Sunter *et al.* , 2015b; Zhou *et al.* , 2015). During that time, new microtubules are also inserted between existing ones

of the microtubule cage as the subpellicular cytoskeleton was not depolymerized during the cell cycle (Sherwin & Gull, 1989b; Wheeler *et al.* , 2013; Sheriff *et al.* , 2014).

When the flagellum emerges from the flagellar pocket, PFR assembly is initiated, mainly from the distal tip, and immediately attached to the cell membrane via the FAZ (Sherwin & Gull, 1989a; Bastin *et al.* , 1999; Zhou *et al.* , 2014). In insect stage trypanosomes, the flagellum elongates until a predefined stop point anterior of the nucleus is reached, which is about 0.6 of the length of the mature flagellum (Absalon *et al.* , 2007; Vaughan & Gull, 2008; Farr & Gull, 2012). At the same time, basal body segregation takes place, which is a two step process. First, basal bodies divide slowly until a distance of 2µm is reached (Robinson *et al.* , 1995; Absalon *et al.* , 2007). Due to linkage by the TAC complex, kinetoplast division follows, which has duplicated (Robinson & Gull, 1991; Robinson *et al.* , 1995; Vaughan & Gull, 2008). Cells are referred to as 2K1N cells and at the beginning of G_2-phase (Fig. 1.7, 1.8) . The second segregation step includes the fast migration of the new basal body-flagellum complex to the posterior cell end (Robinson *et al.* , 1995; Absalon *et al.* , 2007). However, if that movement is solely driven by forces produced from the fixated but still growing new flagellum, is still under discussion as some RNAi phenotypes cannot be fully explained by that model (Farr & Gull, 2012; Zhou *et al.* , 2014).

1.1.5.2 Mitotic and post-mitotic events

Starting with flagella segregation and early mitosis, the latter characterized by an elongating nucleus, integration of new microtubules between new and old FAZ continuous. They are oriented like the majority of subpellicular microtubules. Incorporation of new microtubules seems to be asymmetric with a core area at the side of the new FAZ (Sheriff *et al.* , 2014). The assembled spindle is parallel to the old flagellum and cells are referred to as $2K1N_{div}$ (Fig. 1.7, 1.8) (Sherwin & Gull, 1989a; Wheeler *et al.* , 2013; Sheriff *et al.* , 2014). Terminating mitosis, two single nuclei are identified with the most posterior one being positioned between the two kinetoplasts resulting in the typical KNKN pattern of PCF (Fig. 1.7, 1.8 A) (Sherwin & Gull, 1989a; Vaughan & Gull, 2008; Farr & Gull, 2012). Post-mitotic cells are referred to as 2K2N (Fig. 1.7, 1.8). These cells also demonstrate a high number of short microtubules interwoven in the subpellicular microtubule array. Their occurrence is speculation on lateral nucleation of microtubules and severing mechanisms (Sherwin & Gull, 1989b; Gull, 1999).

In contrast to mammalian cytokinesis, there is no contractile actin-myosin ring in the center but cells divide along the longitudinal axis (Fig. 1.8). Even more, trypanosomes lack myosin II and actin plays a more important role in endocytosis than in cytokinesis (García-Salcedo *et al.* , 2004; Zhou *et al.* , 2014). The newly assembled FAZ is proposed to define the cleavage plane (Robinson *et al.* , 1995; Kohl *et al.* , 2003; Zhou *et al.* , 2011). During mitosis, the chromosomal

passenger complex (CPC) is localized to the nucleus but shortly before cytokinesis starts, the CPC migrates towards the distal end of the new FAZ, the starting point of the ingression furrow (Li *et al.* , 2008; Zhou *et al.* , 2014). Distinct from mammals, it only contains three elements: TbAUK1 (an aurora B kinase ortholog in *T. brucei*), TbCPC1, and TbCPC2. Together with co-located TbPLK (Polo-like kinase) and CIF1 (Cytokinesis initiation factor 1), it regulates the start of the cell division process and later moves alongside the progressing cleavage furrow (Hammarton *et al.* , 2007b; Li *et al.* , 2008; Zhou *et al.* , 2014, 2016).

A hallmark for the beginning of cytokinesis is the invagination of the cell membrane. Thereby, a fold between new and old FAZ is established, which did not reach the posterior cell pole. In the first of four phases of cytokinesis, the division fold generation, the two future daughter cells can be distinguished: the new-flagellum daughter cell and the old-flagellum daughter cell. Although the fold is asymmetric, the nascent daughter cells have a similar cell volume after cell division but most of the newly assembled microtubules are inherited by the new-flagellum daughter cell (Farr & Gull, 2012; Wheeler *et al.* , 2013; Sheriff *et al.* , 2014). During the second phase, the division furrow ingression, the two anterior ends are separated but the new flagellum is still connected to the old one. Subsequently, in the pre-abscission phase, only the two posterior ends are still linked laterally by a small cytoplasmic bridge whereas the new flagellum has been liberated from the old one (Fig. 1.8). Finally, the two daughter cells are completely separated in the abscission phase. During the last phases of cytokinesis, the two posterior ends are re-organized, e. g. microtubules in the old-flagellum daughter cell are bundled (Wheeler *et al.* , 2013; Sheriff *et al.* , 2014). Strikingly, if the anterior to posterior cytokinesis pathway is blocked, a TbAUK1 independent back-up mechanism starting from the opposite direction is activated (Zhou *et al.* , 2016; Zhou & Li, 2016).

After cytokinesis, the old-flagellum daughter cell possesses a 'pointed' posterior end while that of the new-flagellum daughter cell is more round. Therefore, remodeling processes take place to form a rounded posterior ending in the old-flagellum daughter cell while flagellum is elongated in the new-flagellum daughter cell until it overlaps the anterior cell pole (Wheeler *et al.* , 2013).

1.1.5.3 Some differences between procyclic and bloodstream trypomastigotes

Although no variation at the ultrastructural level is discernible and main cell division processes are similar, several differences between the procyclic and bloodstream trypomastigotes at the morphological and molecular level can be noted. The kinetoplast of bloodstream trypanosomes is localized closer to the posterior end than that of procyclic ones. This implies that segregation of basal bodies, and therefore also of kinetoplasts, is less stretched out than in PCF (Fig. 1.8) (Portman & Gull, 2010; Wheeler *et al.* , 2013). A structure similar to the flagellar connector oc-

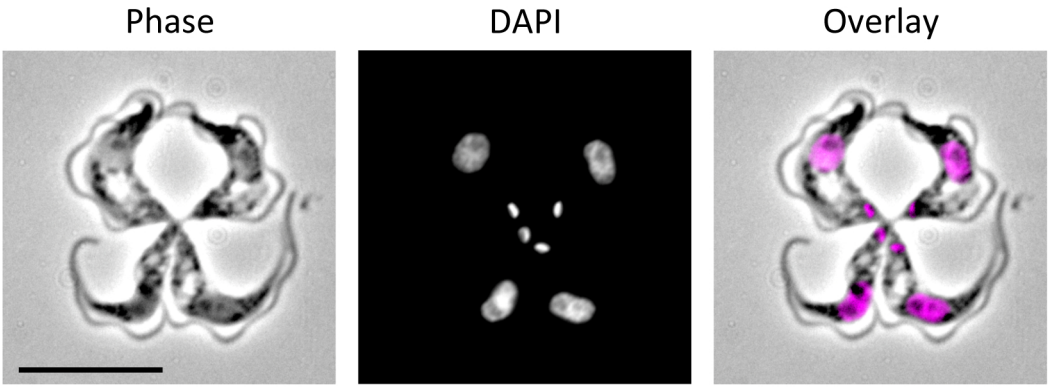


Figure 1.9: Tetrad (4K4N) occurring in bloodstream trypomastigotes and its division into four times 1K1N cells. Scale bar represents 10µm.

curring in PCF has not been found so far but flagellar growth is guided by the so-called groove in BSF. Here, the tip of the flagellum is inserted in the cell body near the microtubule quartet and considerable remodeling during the migration of the growing flagellum is performed (Hughes *et al.* , 2013). After mitosis, procyclic trypanosomes possess the characteristic KNKN arrangement while it is KKNN in BSF indicating the anterior position of both post-mitotic nuclei (Fig. 1.8) (Sharma *et al.* , 2009; Portman & Gull, 2012; Wheeler *et al.* , 2013). Furthermore, only katanins are involved in the cytokinesis of procyclic trypanosomes whereas spastins additionally participate in that of BSF (Casanova *et al.* , 2009; Benz *et al.* , 2012). The fold terminates closer to the posterior cell pole in BSF and thus, abscission is more polar compared to the lateral orientation of posterior ends in PCF (Wheeler *et al.* , 2013). In general, a 2K2N cell results in two 1K1N in procyclic and bloodstream trypanosomes. With a higher frequency in BSF, also 'tetrads' or 'quadriflagellated doubled cells', 4K4N cells, occur but their contribution and significance to the parasite population remains to be investigated. Their division is speculated to be four times 1K1N or two times 2K2N (Fig. 1.9) (Wheeler *et al.* , 2013).

Life cycle stages also differ in their cell cycle check points with cytokinesis inhibition being the most prominent one. Progression to cytokinesis depends on basal body segregation in PCF while successful mitosis is the requirement for cytokinesis in BSF (Ploubidou *et al.* , 1999; Hammarton *et al.* , 2007a; Zhou *et al.* , 2014). Furthermore, the kinetoplast cycle is uncoupled from the nuclear one only in bloodstream parasites (Hammarton *et al.* , 2003; Tu & Wang, 2005). Although often the same cyclines and CRKs (cdc2-related kinases) regulate the cell cycle, variation in RNAi phenotypes between both life cycle stages exist indicating a different role or site of action of the same molecule. For example, CRK1 knockdown resulted in both forms in an accumulation of 1K1N cells but only procyclic G_1-phase cells demonstrated

also an elongated, sometimes branched posterior end if CRK2 was down regulated at the same time (Tu & Wang, 2004, 2005; Hammarton, 2007). Therefore, protein characterization should involve both life cycle stages to discover not only cell cycle but also life cycle specific effects and differences.

1.2 Microtubules and microtubule-associated proteins (MAPs)

1.2.1 Microtubules

During the cell cycle, the cytoskeleton contributes to cell morphology and polarity, cell division, anchoring and segregation of organelles as well as cellular motility and cargo transport (Fletcher & Mullins, 2010; Galjart, 2010). In *T. brucei,* the microtubule-based cytoskeleton plays the major role in these processes and the importance of this organelle is illustrated by the large number of kinesins present in this organism (Gull *et al.* , 1990; Wickstead & Gull, 2006; Chan *et al.* , 2010). Three microtubule-based structures can be distinguished in the trypanosomal cell: the subpellicular microtubule array (see 1.1.4.5), the flagellum originating from the basal body (see 1.1.4.3), and the mitotic spindle (Fig. 1.10). While the first two structures remain assembled over the whole cell cycle, the latter is only temporarily (Kohl & Gull, 1998; Gull, 1999).

As for other organisms, trypanosomal microtubules generally consist of α- and β-tubulin encoded by a gene array of α- and β-tubulin tandem repeats (Kinunel *et al.* , 1985; Imboden *et al.* , 1987; Seebeck *et al.* , 1988). Both molecules can be extensively post-translational modified by acetylation, glutamylation, and tyrosination (Sasse & Gull, 1988; Schneider *et al.* , 1997; Kohl & Gull, 1998). While acetylation and glutamylation are frequently considered to stabilize microtubules, tyrosination of α-tubulin is a hallmark for newly assembled microtubules (Sherwin & Gull, 1989b; Gull, 1999).

Generally, α/β-tubulin dimers assemble longitudinally in a head-to-tail fashion to protofilaments. 13 of them form the intrinsically polar microtubule with a diameter of about 25nm. The overall microtubule symmetry is helical with an additional seam. α-tubulin is always situated at the minus end of the cylinder, which is *in vivo* stabilized by the MTOC (microtubule-organizing center) but can grow slowly *in vitro* (Fig. 1.11). The β-tubulin subunits point towards the microtubule plus end, the unique place for assembly *in vivo* and the fast growing end under *in vitro* conditions (Howard & Hyman, 2003; Akhmanova & Hoogenraad, 2005; Galjart, 2010). At the plus ends, microtubules are dynamically unstable. They alternate between phases of growth and shrinkage which are separated by metastable intermediate states (pause) *in vivo* (Mitchison & Kirschner, 1984; Howard & Hyman, 2003). However, dynamic instability has not been shown

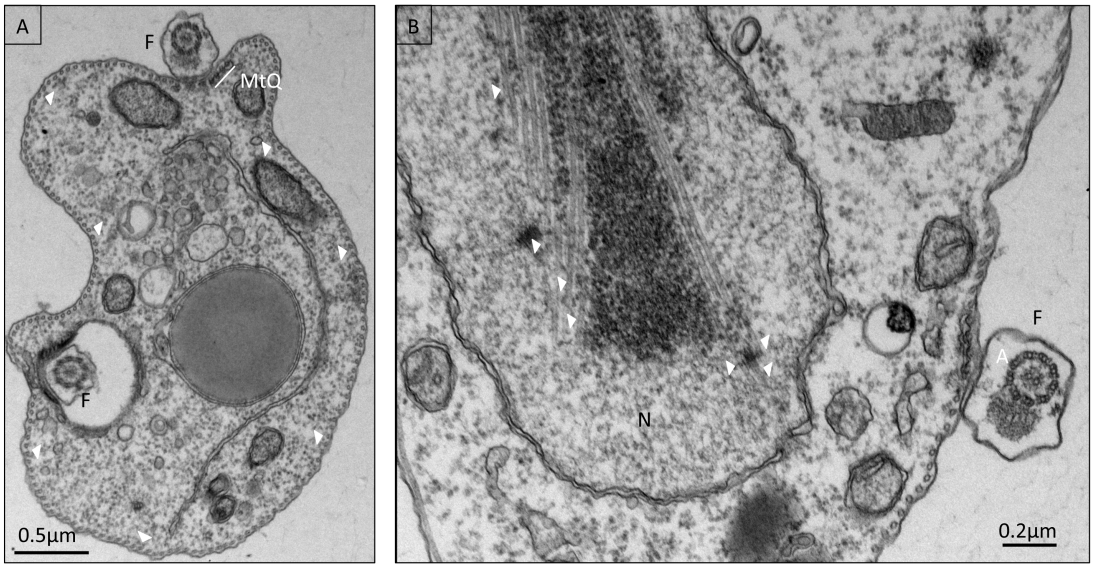


Figure 1.10: *T. brucei* possesses 3 types of microtubules: subpellicular, flagellar, and spindle microtubules. TEM cross-sections of procyclic trypanosomes. **A)** Cross-section of the evenly-spaced subpellicular microtubule array (arrowheads) directly beneath the cell membrane with integrated microtubule quartet (MtQ), which is adjacent to the flagellum (F) and associated with smooth endoplasmic reticulum. Two traverse sections of the flagellum (F) are shown. **B)** Cross-section of the closed mitosis of trypanosomes. While the nucleus (N) is still enveloped by the nuclear membrane, spindle microtubules (arrowheads) segregate the DNA. Additionally, axonemal (A) microtubules with their characteristic 9+2 pattern are shown.

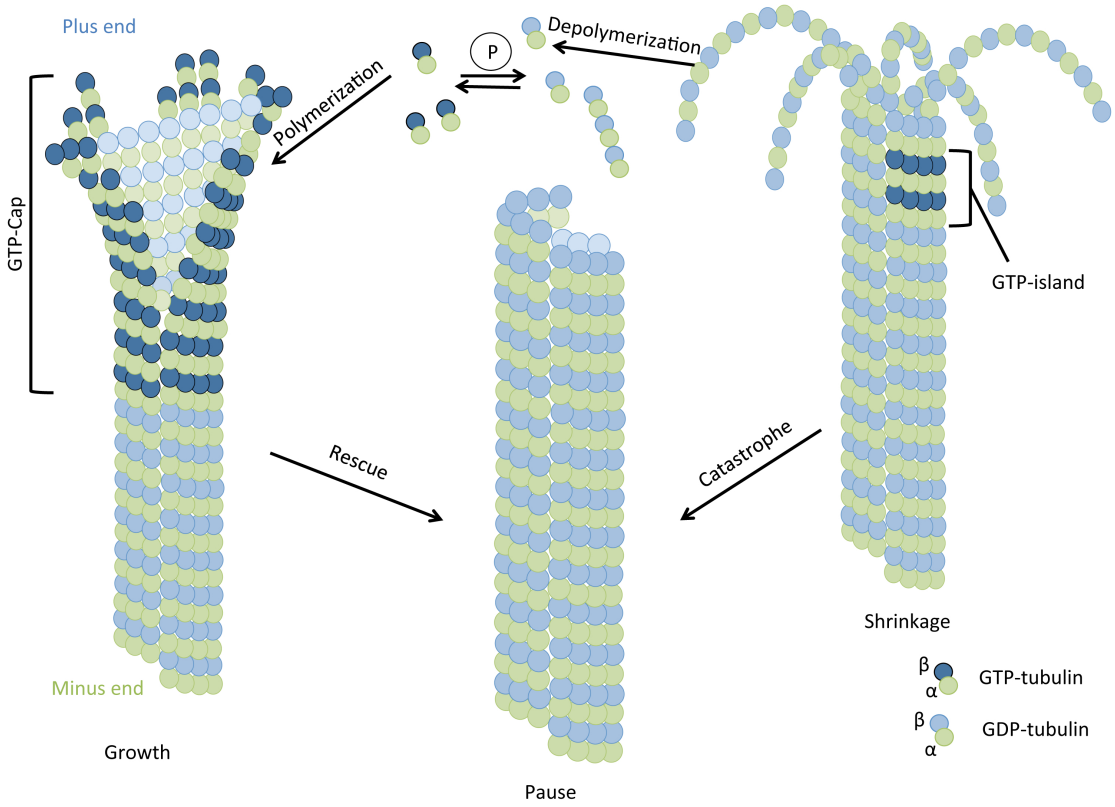


Figure 1.11: The assembly/ disassembly cycle of microtubules. During polymerization, α/β-tubulin dimers bound to GTP (GTP-tubulin) are incorporated head-to-tail resulting in a GTP-cap and a straight conformation of the tube which both prevent depolymerization. Hydrolysis of the nucleotide to GDP (GDP-tubulin) enables a curved conformation and favors microtubule depolymerization. GTP-islands promote rescue events. Re-drawn and modified after Akhmanova and Steinmetz (2008; 2015).

for the subpellicular microtubules of *T. brucei*, yet (K. Ersfeld, personal communication).

In vitro, microtubule growth (polymerization) depends predominantly on the concentrations of tubulin and GTP (guanosine-5´-triphosphate), which is bound to both subunits (Horio & Hotani, 1986). Only the GTP of β-tubulin is prone to hydrolysis. GTP-hydrolysis is one of the key factors of microtubule dynamics and triggers the switch from polymerization to depolymerization. Furthermore, GTP-hydrolysis is generally slower than microtubule synthesis. This results in an accumulation of tubulin-bound GTP at the microtubule tip, the so-called GTP cap. The cap is the second key factor and proposed to mediate stability (Howard & Hyman, 2003; Galjart, 2010). Depolymerization is prevented due to the slightly bent conformation of GTP-tubulin resulting in a stable, flattened sheet-like structure of neighboring protofilaments. Phosphate release leads to a conformational change in the interface between α- and β-tubulin. As a consequence, tubulin protofilaments bent outwards and depolymerization is facilitated (Mandelkow *et al.* , 1991; Chrétien *et al.* , 1995; Akhmanova & Steinmetz, 2015). Although the microtubule shaft is characterized by the presence of GDP-tubulin, multiple bonds between adjacent tubulin dimers mediate the straight conformation. Single GTP-tubulin islands are localized within the shaft and putatively initiate rescues by mimicking the GTP cap (Galjart, 2010; Akhmanova & Steinmetz, 2015). Taken together, microtubule growth depends on four factors: speed of microtubule polymerization or depolymerization and the frequency of catastrophe and rescue events (van der Vaart *et al.* , 2009).

1.2.2 Regulation of microtubule dynamics

Besides intra-molecular events, such as GTP-islands, microtubule dynamics are extensively governed by external factors, mainly microtubule-associated proteins (MAPs) (de Forges *et al.* , 2012).

1.2.2.1 Regulation at microtubule minus ends

Compared to the slow spontaneous microtubule polymerization occurring *in vitro* as a consequence of kinetic barriers, initial polymerization occurs much faster *in vivo* at microtubule nucleation sites (Desai & Mitchison, 1997; Kollman *et al.* , 2011; Wieczorek *et al.* , 2015). Those nucleation sites are commonly associated with MTOCs and marked by the presence of γ-tubulin in animal, fungi, and plants. Together with a varying number of other proteins, γ-tubulin is part of a ring complex. It is termed γ-tubulin small complex (γ-TuSC) in primal organisms and γ-tubulin ring complex (γ-TuRC) in higher eukaryotes (Kollman *et al.* , 2011; Petry & Vale, 2015). In contrast to plant cells, these complexes also cap the minus ends of microtubules in yeast and animals, thereby preventing minus end growth and increasing stability (Wiese & Zheng, 2000;

Wasteneys & Ambrose, 2009).

Recently, it was shown that the *T. brucei* γ-TuSC consists of γ-tubulin and the Gamma-tubulin complex proteins (GCP) 2 to 4. While the GCP were newly identified (Zhou & Li, 2015), γ-tubulin is a well-studied component and its localization has been already described in earlier studies (Scott *et al.* , 1997; He *et al.* , 2005). The most prominent localization is aside the basal bodies, where the γ-TuSC provides the MTOC for the central pair of microtubules of the axoneme (McKean, 2003; Zhou & Li, 2015). The localization to the spindle poles was not confirmed by Zhou et al. (2015). However, all components of the γ-TuSC have been described as punctate pattern on the subpellicular cytoskeleton in immunofluorescence experiments. It remains still enigmatic wether γ-TuSC components provide nucleation sites for new subpellicular microtubules in *T. brucei* as depletion of GCP 2 and 3 had only minor effects on the subpellicular microtubule array (Zhou & Li, 2015). Yet, there is speculation that subpellicular microtubules are nucleated by acentrosomal MTOCs and γ-tubulin in trypanosomes (K. Ersfeld, personal communication). Those have been described for cortical microtubules in plants, fission yeast, and differentiated animal cells like neurons (Bartolini & Gundersen, 2006; Nakamura *et al.* , 2010). They are generated either by release from the centrosome, breakage of older microtubules by microtubule severing mechanisms, branching from pre-existing microtubules (microtubule-dependent microtubule nucleation) or *de novo* synthesis in areas without microtubules (Murata *et al.* , 2005; Bartolini & Gundersen, 2006; Fishel & Dixit, 2013; Petry & Vale, 2015). Similar to acentrosomal-based microtubules, trypanosomal microtubules of the subpellicular array are linear, quite stable, and polarized (Seebeck *et al.* , 1990). Additionally, a lateral nucleation from pre-existing microtubules followed by microtubule severing was already proposed to explain the semi-conservative inheritance pattern of the microtubule array and its stability throughout the cell cycle in *T. brucei* (Sherwin & Gull, 1989b).

Recently, a new protein family CAMSAP/Patronin/Nezha, specifically targeting to the minus ends of microtubules has been described. An intriguing function is the stabilization of non-centrosomal microtubules. Additionally, the family-assigning CKK domain (C-terminal domain common to CAMSAP1, KIAA1078 and KIAA1543) is also encoded by several protists (Yau *et al.* , 2014; Akhmanova & Hoogenraad, 2015). If members of the protein family also occur in trypanosomes has still to be revealed.

1.2.2.2 Binding along the microtubule wall

Most 'classic' MAPs bind to tubulin subunits of the microtubule wall (Halpain & Dehmelt, 2006). Those structural MAPs frequently contain repetitive sequences enabling binding to more than one microtubule. They mediate cross-links and microtubule bundling, thereby enhancing microtubule stability. They are often substrates of microtubule-affinity-regulating kinases

(MARKs), and therefore integrated in signaling pathways that control microtubule dynamics (Drewes *et al.* , 1998; Amos & Schlieper, 2005). Several MAPs of *T. brucei*, e. g. WCB210, and microtubule-associated repetitive protein (MARP) 1 and 2, have been identified and associated with the cross-links of the subpellicular microtubule array and its increased stability (Gull, 1999).

A class of ATPases associated with diverse cellular activities (AAA) proteins, that severe microtubules, also localizes preferentially to the lattice. Three families are known so far: katanin, spastin, and fidgetin. All interfere with microtubule dynamics by 'cutting' microtubules, thereby influencing microtubule length and number as well as providing additional microtubule nucleation sites and structural re-organization (Eckert *et al.* , 2012; Sharp & Ross, 2012). Although all three protein families are encoded by *T. brucei,* only katanin and spastin play a role in trypanosomal cytokinesis (see 1.1.5.3) (Casanova *et al.* , 2009; Benz *et al.* , 2012).

1.2.2.3 Regulation at microtubule plus ends

A huge variety of proteins consisting of multiple domains or subunits accumulate at the plus ends of microtubules and are termed plus-end-tracking proteins (+TIPs). Here, they appear as comets at growing tips and vanish if microtubules shrink (Tamura & Draviam, 2012). They attach at the distal tips by various mechanisms: recognition of a structural feature of the growing end, lateral diffusion along the microtubule, co-polymerization with tubulin subunits, kinesin-based transport or association with microtubule-binding proteins, termed hitchhiking. Some factors undergo tread-milling thus, accumulation at microtubule plus ends is due to fixation and molecules detach if the conformation of the growing tip changes (Schuyler & Pellman, 2001; Akhmanova & Hoogenraad, 2005; Lansbergen & Akhmanova, 2006). At growing microtubule tips, they regulate microtubule dynamics, mediate interaction with diverse cellular components, e. g. cell and organelle membranes, kinetochores, guide growing microtubules along pre-existing ones, generate pushing and pulling forces, and introduce signaling pathways (Dogterom *et al.* , 2005; Akhmanova & Steinmetz, 2015). Several +TIPs, e. g. EB1 and XMAP215, also co-localize with MTOCs and microtubule minus-ends and heavily influence nucleation and elongation (Chan *et al.* , 2003; Akhmanova & Steinmetz, 2015; Wieczorek *et al.* , 2015).

+TIPs are roughly divided in two groups: kinesin motor proteins and plus-end-binding proteins (Howard & Hyman, 2003). The kinesin families 8, 13, and 14 accumulate at microtubule plus ends and exhibit ATP-dependent microtubule depolymerizing capacities (Wu *et al.* , 2006; Akhmanova & Steinmetz, 2015). No members of the kinesin-8 family are encoded by *T. brucei* but there are two kinesin-14 family members (Chan *et al.* , 2010; Wickstead *et al.* , 2010). Those are minus-end directed kinesins hence, with a C-terminal motor domain (Marx *et al.* , 2009). However, one plays a role in acidocalcisome maintenance and the function of the second

remains to be elucidated (Dutoya *et al.* , 2001; Chan *et al.* , 2010). In contrast, family-13 kinesins have a motor domain in the middle of the molecule and lost the ability of directional motility (Marx *et al.* , 2009; Su *et al.* , 2012). Seven members are known in trypanosomes and six have been characterized in more detail. The best characterized are kinesin 13-1 and 13-2. The first is the only mitotic kinesin of the family, which is involved in spindle assembly (Chan *et al.* , 2010; Wickstead *et al.* , 2010). The second localizes to the flagellar tip. However, flagellar length was only modestly affected upon gene deletion (Chan & Ersfeld, 2010). The others are localized to the cell body, the flagellum or the mitochondrion. However, their function at those areas still needs to be elucidated (Chan, 2008; Chan *et al.* , 2010; Wickstead *et al.* , 2010).

The second cluster is more diverse in structure and function and includes also membrane proteins. The XMAP215 family members are processive microtubule polymerizers enabling microtubule growth (Akhmanova & Steinmetz, 2008). The trypanosomal TbXMAP215 was used to reveal microtubule dynamics in PCF and BSF (Wheeler *et al.* , 2013). Further important regulators in mammals and yeast are cytoplasmic linker proteins (CLIPS), e. g. CLIP170, which induce rescue events, and CLIP-associating proteins (CLASPS), which recruit tubulin dimers, stabilize microtubules, and influence their number (Galjart, 2005; Akhmanova & Steinmetz, 2008). *T. brucei* seems to encode at least one putative CLIP homologue (Fern, 2012).

However, the most prominent members of the +TIP group are end-binding (EB) proteins which are encoded by almost all eukaryotes investigated so far (Akhmanova & Steinmetz, 2015). Originally identified as binding partner to APC (adenomatous polyposis coli) (Su *et al.* , 1995), the family turned out to be the 'master' regulator of molecular networks at the plus end (Vaughan, 2005; Slep, 2010; Akhmanova & Steinmetz, 2015). Their ability to track autonomously to growing microtubule ends, and hence their interaction with the diversity of other +TIPs, contribute to that role (Lansbergen & Akhmanova, 2006; Bieling *et al.* , 2007; Komarova *et al.* , 2009).

1.2.3 End-binding proteins

1.2.3.1 EB protein domain architecture

Interaction with the tubulin cytoskeleton and other +TIPs is mediated by the highly conserved domains of the protein family: the calponin-homology (CH) domain at the N-terminus, a variable linker region, and the C-terminal domain. The latter contains a coiled-coil region, a four helix bundle, and the disordered tail frequently terminating with the EEY/F motif (Fig. 1.12) (Bu & Su, 2003; Akhmanova & Steinmetz, 2015). The globular CH domain interacts with microtubules (Hayashi & Ikura, 2003; Huang *et al.* , 2015) and is followed by a variable, unstructured linker region which connects N- and C-terminal domains. Both, CH domain and linker region are necessary to maintain binding to microtubules (Akhmanova & Steinmetz, 2015). The coiled-

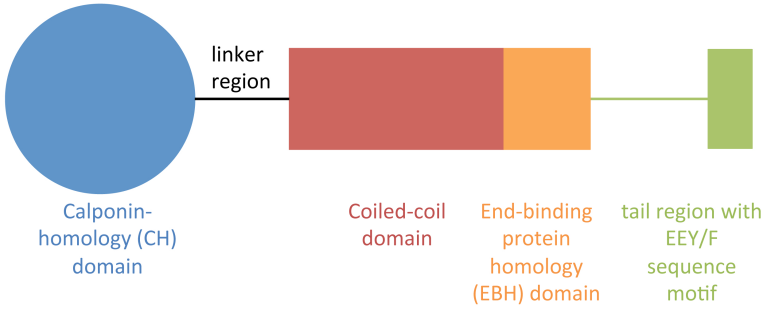


Figure 1.12: Schematic representation of conserved domains in end-binding proteins. EB proteins consist of the highly conserved N-terminal calponin-homology (CH) domain, a variable linker region, and the C-terminal domain. The latter includes a coiled-coil domain, the end-binding homology (EBH) domain, and a tail region with the EEY/F sequence motif.

coil region at the beginning of the C-terminus is responsible for dimerization which is required for cavity formation of two adjacent EBH domains and indispensable for proper functioning (Honnappa *et al.* , 2009; De Groot *et al.* , 2010; Sen *et al.* , 2013). The end-binding homology (EBH) domain lies within the C-terminus and refers to the four-helix bundle and the beginning of the tail region (Hüls *et al.* , 2012; Akhmanova & Steinmetz, 2015). EBH domains are required for interaction with SxIP motifs, which are common in many +TIPs (Honnappa *et al.* , 2009; Kumar & Wittmann, 2012). Additionally, the EEY/F sequence motif enables binding with CAP-Gly domain proteins, e. g. CLIP170 (Galjart, 2005; Komarova *et al.* , 2005; Weisbrich *et al.* , 2007). It is also involved in auto inhibition of EB proteins (Hayashi *et al.* , 2005; Manna *et al.* , 2008; Kanaba *et al.* , 2013). However, auto-inhibition is EEY/F independent in plants (Komaki *et al.* , 2010). Finally, the C-terminal domains of EB proteins are frequently negatively charged, regulating the interplay of intrinsic CH domains with microtubules and providing binding capacity to basic regions of other +TIP network members like APC or CLASPs (Galjart, 2005; Akhmanova & Steinmetz, 2015).

1.2.3.2 Localization of EB1 on the microtubule level and mode of action

Albeit the C-terminal domain is not necessary for microtubule plus-end tracking it supports CH- and linker domain binding to microtubules (Zanic *et al.* , 2009; Akhmanova & Steinmetz, 2015; Lopez & Valentine, 2016). Here, one EB molecule interacts with four adjacent tubulin subunits of two neighboring protofilaments (Fig. 1.13). While the *Schizosaccharomyces pombe* homologue Mal3 was initially suggested to localize to the microtubule seam pointing towards a role in stabilization of this weak region (Sandblad *et al.* , 2006), more recent data from yeast and mammalian EB homologues indicate a localization to the microtubule sheet except the seam

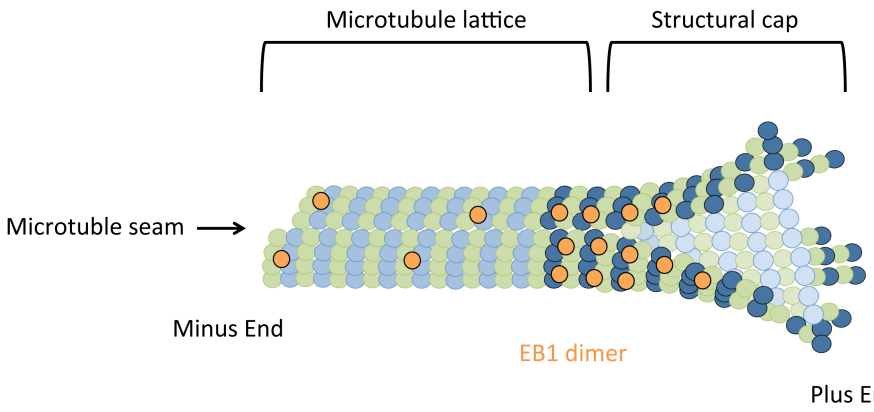


Figure 1.13: Localization of EB1 on the microtubule. EB1 connects four adjacent tublin subunits. It localizes predominantly to the plus tip albeit a modest decoration of EB1 along the microtubule wall and the minus end is found, too.

(Maurer *et al.* , 2012; Alberico *et al.* , 2013; Zhang *et al.* , 2015). EB proteins are targeted to microtubule ends by recognition of the structural cap at plus tips, more precisely, the post-hydrolysis state of GTP-tubulin (Maurer *et al.* , 2012; Zhang *et al.* , 2015). This is corroborated by the fact that EB proteins do not bind to the outermost tip of growing microtubules but to the region underneath (Maurer *et al.* , 2014; Akhmanova & Steinmetz, 2015; Zhang *et al.* , 2015). Additionally to the comet-like appearance at plus tips, EB proteins modestly decorate the microtubule lattice in a punctate pattern due to diffusion of bound EB protein. That behavior also explains the mismatch between GTP cap size (3 to 5 tubulin dimers) and size of EB1 comet (about 40 to 70 tubulin dimers) (Lopez & Valentine, 2016). Furthermore, the role of EB1 at microtubule ends was discussed quite conversely as different experimental set ups or model organism favored both, a role in promoting microtubule growth and contradictorily, an increase in catastrophe events (Vitre *et al.* , 2008; Alberico *et al.* , 2013; Zhang *et al.* , 2015). This was partially resolved by the suggestion of Vitre et al. (2008) that EB1 protein both support microtubule growth by binding laterally to the growing sheet but at the same time relief stress at microtubule lattice mismatches in a catastrophic event. In the end, association with the GDP-microtubule lattice then favor rescue events.

1.2.3.3 Cellular localization of EB protein homologues

The ambivalent role of EB1 in microtubule dynamics explains the different functions of EB1 during the cell cycle and thus the localization of EB1 to certain cellular compartments and structures. Homologues of EB1 have been identified and characterized in a plethora of eukaryotes ranging from protists and fungi to animals and plants () (Tirnauer & Bierer, 2000; Komaki *et al.*

, 2010; Mouriño-Pérez *et al.* , 2013).

EB homologues are localized to microtubules throughout the cell cycle (Tirnauer & Bierer, 2000). Using fusion proteins or specific antibodies on interphase cells, EB1 homologues were found on distal tips of cytoplasmic microtubules in fungi *Saccharomyces cerevisiae* (Bim1) (Schwartz *et al.* , 1997; Tirnauer *et al.* , 1999), *S. pombe* (Mal3) (Beinhauer *et al.* , 1997), *Dictyostelium dentriticum* (DdEB1) (Rehberg & Gräf, 2002), *Neurospora crassa* (MTB-3) (Mouriño-Pérez *et al.* , 2013), *Cryptococcus neoformans* (Bim1) (Staudt *et al.* , 2010) and the green algae *Chlamydomonas rheinhardtii* (CrEB1) (Pedersen *et al.* , 2003). Metazoa often harbor several members of EB proteins, e.g. mammalia possess three end-binding proteins (EB1, EB2, EB3) (Berrueta *et al.* , 1998; Morrison *et al.* , 1998; Su & Qi, 2001). A similar staining pattern was described for EB1 homologues in insects (*Drosophila melanogaster* EB1) (Rogers *et al.* , 2002), mammalians (EB1 and EB3) (Berrueta *et al.* , 1998; Morrison *et al.* , 1998; Komarova *et al.* , 2009), and plants (*Arabidopsis thaliana* EB1a and EB1b) (Chan *et al.* , 2003; Mathur *et al.* , 2003; Komaki *et al.* , 2010). Frequently, the typical comet-like distribution pattern of +TIPs on growing microtubule ends was observed reflecting a conserved mode of action (Chan *et al.* , 2003). Few EB members preferentially localize to the microtubule lattice, e. g. human EB2 (Komarova *et al.* , 2009) or *Xenopus laevis* EB1. The latter demonstrated a plus-tip localization only in mitotic extracts (Tirnauer *et al.* , 2002a).

Many eukaryotic EB homologues (*S. cerevisiae, S. pombe, D. dentriticum, N. crassa, C. rheinhardtii, D. melanogaster,* mammalian EB) were additionally associated with mitotic structures such as spindle, kinetochore, and astral microtubules or microtubule nucleation sites, e. g. centrosomes, spindle pole bodies, or basal bodies (Tab. 1.2.3.4). In *A. thaliana,* one of the three EB1 members, EB1c, is exclusively situated within the interphase nucleus and is associated with the spindle during mitosis (Komaki *et al.* , 2010). Such a distinct and specific localization have also been demonstrated for protists which generally contain one EB1 family member. Similar to AtEB1c, TgEB1 of *Toxoplasma gondii* resides in the nucleus in interphase cells and attaches to the mitotic spindle. However, for a well-coordinated period, just before terminating nuclear division, TgEB1 is also found on the subpellicular microtubules of growing daughter buds (Chen *et al.* , 2015). In *Giardia lamblia,* the GlEB1 localization pattern covers the spindle, the nuclear membrane, the median bodies, axoneme, and flagellar tips. (Kim *et al.* , 2014). Localization to cilial and flagellar tips was also described for CrEB1 and mammalian EB1 and EB3 (Pedersen *et al.* , 2003; Schrøder *et al.* , 2011).

Noteworthy, in organisms with multiple EB1 homologues, the members frequently associate with different microtubule subtypes. Those different microtubule populations, e. g. spindle or subpellicular microtubules, are characterized by different stabilization and polymerization abilities which are mediated by a corresponding subset of MAPs (Chen *et al.* , 2015). In

mammals, EB1 and EB3 share more commonalities with each other than with EB2, which is illustrated by EB1-EB3 dimerization capacity and a synergistic effect upon depletion. (Komarova *et al.* , 2009). It is even more pronounced in *A. thaliana.* Although AtEB1a and b both localize to subpellicular microtubules, both proteins associate with other structures. In case of AtEB1a, the protein is localized to minus-ends of cortical microtubules indicating putative nucleation sites while AtEB1b is additionally found at intracellular membranes, e. g. mitochondria, chloroplast, or ER (Chan *et al.* , 2003; Mathur *et al.* , 2003; Bisgrove *et al.* , 2004). Therefore, on the one hand, different EB homologues seem to possess a varying affinity for the diverse subtypes of microtubules within cells (Chen *et al.* , 2014a). While on the other hand, differences in +TIP network composition also create a diverse subset of microtubule populations (Ligon *et al.* , 2003).

1.2.3.4 EB1 homologues perform diverse functions during the cell cycle

In many eukaryotes, EB1 proteins are localized on interphase and mitotic microtubules (Tab. 1.2.3.4), thereby promoting microtubule growth and dynamics (Akhmanova & Steinmetz, 2010; Liu & Han, 2015). Their partial or complete loss affects microtubule stability and dynamics. EB1 function is determined by its localization, especially EB1 homologues with a restricted site of localization. AtEB1c, GlEB1, and TgEB1 are associated with mitotic structures. Partial or complete loss interferes with the proper formation of spindles or kinetochores, the proper progression of mitotic events, and chromosome segregation. (Komaki *et al.* , 2010; Chen *et al.* , 2014a; Kim *et al.* , 2014). Similar effects upon loss of EB1 were noted in many eukaryotes as localization to mitotic elements is a widespread phenomenon (Tab. 1.2.3.4). In *Drosophila,* mitosis is heavily affected by loss of EB1 but no clear phenotype was observed during interphase (Rogers *et al.* , 2002). In contrast, *S. cerevisiae* Bim1 is important during G_1-phase (Tirnauer *et al.* , 1999). Additionally, if EB homologues act at similar sides, the local deletion or depletion phenotypes may vary. While no or only modest perturbations of the cytoplasmic microtubule network were observed in *Dictyostelium* (Rehberg & Gräf, 2002), *Drosophila* (Rogers *et al.* , 2002), and *Arabidopsis* (Bisgrove *et al.* , 2008), considerable perturbation was described for fission yeast (Beinhauer *et al.* , 1997), *Neurospora* (Mouriño-Pérez *et al.* , 2013), *Cryptococcus* (Staudt *et al.* , 2010), and mammalia (Yan *et al.* , 2006). Structural integrity of sub-cellular microtubule networks is important for organelle positioning (Beinhauer *et al.* , 1997; Schwartz *et al.* , 1997; Staudt *et al.* , 2010) and maintaining cellular shape and polarity (Beinhauer *et al.* , 1997; Staudt *et al.* , 2010). Furthermore, both depletion and over-expression of EB1 homologues may result in bundled microtubules, thereby creating more stable microtubule populations and hindering microtubule re-organization (Bu & Su, 2001; Rogers *et al.* , 2002; Ligon *et al.* , 2003; Goldspink *et al.* , 2013).

EB1 proteins also participate in guided microtubule growth either by interaction with motor proteins, e. g. kinesin-14 family members, or by spectraplakin-mediated cooperation with actin (Prokop *et al.* , 2013; Akhmanova & Steinmetz, 2015). Although EB1 proteins predominantly bind to microtubules, a recent study demonstrated their affinity to F-actin suggesting a competitive binding between the two cytoskeletal elements. This could explain F-actin induced microtubule destabilization, e. g. near the cell cortex (Alberico *et al.* , 2016). However, if F-actin concentrations are low at those sites, growing microtubules are stabilized by anchorage to the cell cortex (Akhmanova & Steinmetz, 2008). Aside from the cell cortex, EB1 proteins mediate linkage of microtubule ends to a variety of other cellular structures such as kinetochores or intracellular membranes. Their concerted interplay with other +TIPs at those locations enables dynamic microtubules which create pushing and pulling forces for chromosome segregation or elongation of ER membranes (Cheeseman & Desai, 2008; Grigoriev *et al.* , 2008; Akhmanova & Steinmetz, 2008).

Finally, at microtubule nucleation sites such as centrosomes or spindle pole bodies, EB1 homologues interact with microtubule minus ends by putatively anchoring microtubules or providing a reservoir of newly assembled microtubules (Rehberg & Gräf, 2002; Bisgrove *et al.* , 2004; Louie *et al.* , 2004). Recently, Wieczorek et al. (2015) described their promoting role in spatiotemporal microtubule outgrowth from γ-TURCs (Akhmanova & Steinmetz, 2015).

Although EB proteins perform crucial roles in many microtubule-mediated processes during the cell cycle and development, depletion and deletion phenotypes are frequently compatible with survival of affected organisms. Null mutants of *S. cerevisiae (Schwartz* et al. *, 1997), S. pombe (Beinhauer* et al. *, 1997), N. crassa (Mouriño-Pérez* et al. *, 2013),* and *T. gondii* (Chen *et al.* , 2015) are viable. Similar findings were observed for the multicellular organisms *A. thaliana (Bisgrove* et al. *, 2008), D. dentriticum (Rehberg & Gräf, 2002)* and *D. melonagaster.* The latter also successfully progressed through all developmental stages but adults demonstrated neuromuscular defects (Elliott *et al.* , 2005). In contrast, only the complete and simultaneous knockdown of all three mammalian EB proteins was lethal (Komarova *et al.* , 2009).

Localization and depletion/deletion phenotypes of EB1 homologues in various organisms. CSF = cytostatic factor, MT = microtubule, n/a = not available

Organism	EB1 homologue	Localization	Depletion/ Deletion phenotype	Literature
		Fungi		
S. cerevisiae	Bim1	cytoplasmic MT, spindle MT and spindle poles	short and less dynamic cytoplasmic MTs, strong bilateral karygamy defects, nuclear positioning defect, spindle is short and mispositioned, retarded growth	Schwartz *et al.* (1997)
S. pombe	Mal3	cytoplasmic MT, spindle MT, and septum	short MTs, altered sub-cellular MT array, altered cell morphology and polarity, nuclear positioning defect, increased chromosome condensation index indicates delay during mitosis, loss of mini-chromosome	Beinhauer *et al.* (1997)
D. dentriticum	DdEB1	cytoplasmic MT, centrosomes, protruding pseudopodes, spindle MT and spindle poles, kinetochores	retardation of prometaphase progression,	Rehberg & Gräf (2002)
N. crassa	MTB-3	cytoplasmic MT, septal rings	fewer, less bundled and organized MTs, decreased MT polymerization and depolymerization rates, less compact mitotic spindle	Mouriño-Pérez *et al.* (2013)

Organism	EB1 homologue	Localization	Depletion/ Deletion phenotype	Literature
C. neoformans	Bim1	n/a	altered sub-cellular MT array, abnormal filament formation during sexual development, defects in diploid formation and diploid filamentation, defects in α frutation	Staudt *et al.* (2010)
		Insects		
D. melanogaster	DmEB1	cytoplasmic MT, centrosomes, astral MT, spindle MT and spindle poles	minimal perturbation of cytoplasmic MT array, increased pausing time of MTs, short and unattached astral MTs, aberrant spindle morphology and position, increased mitotic index, chromosomal segregation defects	Rogers *et al.* (2002)
DmEB1 mutants		ubiquitous, subset of chordotonal organ cells, (cap cells, scolopale cells, ligment cells)	neuromuscular defects , (flightlessness, uncoordinated movement), functional and organisatory defects in chordotonal sensory organs	Elliott *et al.* (2005)

Organism	EB1 homologue	Localization	Depletion/ Deletion phenotype	Literature
		Vertebrates		
X. laevis extract		cytoplasmic MT, spindle MT and spindle poles	reduced length of astral MTs in CSF extract, increase of catastrophe and pausing events; decrease in rescue events, short spindle MTs and reduced density, tri- and multipolar spindles, impeded chromosome segregation	Tirnauer *et al.* (2002a); Kronja *et al.* (2009)
Mammalia	EB1-3	cytoplasmic MT, centrosomes, spindle MT and spindle poles, cilia and flagellar tips	aberrant MT network, loss of MT anchoring, impeded cilia formation, accumulation of vesicles at the ciliar base, aberrant spindle morphology	Berrueta *et al.* (1998); Morrison *et al.* (1998); Yan *et al.* (2006); Brüning-Richardson *et al.* (2011); Schrøder *et al.* (2011)
		Plants		
C. rheinhardtii	CrEB1	flagellar tips, basal body	n/a	Pedersen *et al.* (2003)

Organism	EB1 homologue	Localization	Depletion/ Deletion phenotype	Literature
A. thaliana	AtEB1a-c	cortical MT, cortical MT nucleation sites, spindle MT and spindle poles, intracellular membranes (mitochondria, chloroplast), phragmoplast	impeded root growth, delayed response to gravity, aberrant spindle morphology, impeded chromosome segregation, defect phragmoplast	Chan *et al.* (2003); Mathur *et al.* (2003); Bisgrove *et al.* (2008); Komaki *et al.* (2010)
		Protozoa		
G. lamblia	GlEB1	axoneme and flagellar tips, median bodies, nuclear membrane, mitotic spindle	increased mitotic index, reduced median body size	Kim *et al.* (2014)
T. gondii	TgEB1	nucleoplasm, spindle MT and spindle poles, temporary associated with subpellicular MT of growing daughter buds	aberrant kinetochore structure, modest growth defect, minor defect in cytokinesis	Chen *et al.* (2015)

1.3 Aim of this work

Genes coding for proteins of the EB1 protein family have been discovered in a myriad of eukaryotic organisms (Tirnauer & Bierer, 2000; Komaki *et al.* , 2010; Mouriño-Pérez *et al.* , 2013). Several of those EB1 homologues have been characterized so far. Their localization to the distal tips of interphase and mitotic microtubules is well documented in literature and coherent with their ability to regulate microtubule dynamics (Tirnauer & Bierer, 2000; Mimori-Kiyosue & Tsukita, 2003; Tamura & Draviam, 2012). However, number, localization and key functions of EB1 homologues vary (see 1.2.3.3 and 1.2.3.4). Thus, studies of EB1 homologues in a distinct set of organisms are important to understand the role EB1 proteins perform on microtubule dynamics itself but also in complex +TIP networks. Furthermore, deregulation of EB1 proteins is also found in certain cancer types and basic research will also offers opportunities to challenge them (Dong *et al.* , 2010; Stypula-Cyrus *et al.* , 2014; Kumar *et al.* , 2016). Additionally, due to the pivotal role of the cytoskeleton throughout the cell cycle EB1 proteins may also be a tar-

get of future drug development against pathogens, particularly if they are becoming resistant to conventional medication (Matovu *et al.* , 2001).

One such pathogen is the parasite *T. brucei* whose cytoskeleton is predominantly composed of microtubules. Numerous studies helped to reveal the underlying architecture and to discover the differences in the cytoskeletal composition between the proliferative procyclic and bloodstream form (Sherwin & Gull, 1989b; Robinson *et al.* , 1995; He *et al.* , 2004; Wheeler *et al.* , 2013). Although the knowledge about the composition and structure of the cytoskeletal components and the execution and timing of cytoskeleton-mediated processes increased over the last years, less is known about the basic underlying molecular mechanisms controlling microtubule arrangements and thereby leading to the observed remodeling processes during the parasite´s cell and life cycle (Farr & Gull, 2012). Quite early, an antibody recognizing tyrosinated α-tubulin was available, which enabled the visualization of the inheritance pattern of subpellicular microtubules (Sherwin & Gull, 1989b; Stephan *et al.* , 2007) as well as remodeling processes at the posterior cell body (Wheeler *et al.* , 2013). Moreover, several trypanosomal kinesins are known to interfere with microtubule dynamics supporting growth, shrinkage or pausing (Chan & Ersfeld, 2010; Hu *et al.* , 2012b,a; Vicente & Wordeman, 2015). Recent publications described microtubule-associated proteins which indicated regulatory functions on microtubule fibers due to homologues known in other eukaryotic organisms: TbXMAP215 (Wheeler *et al.* , 2013) and TbEB1 (Sheriff *et al.* , 2014).

The latter one was investigated in more detail in this work. TbEB1 was localized by endogenous tagging or with the help of specific antibodies and sera. TbEB1 function was investigated by comparing wild-type and knockdown cell lines of bloodstream and insect forms of the parasite in immunofluorescence experiments and proliferation assays. The results were further corroborated by the morphological analysis of single gene knockout and over-expression cell lines. TbEB1 localization dynamics were recorded over the cell cycle and abberant mitosis products classified. A conserved mode of action was investigated by ectopic expression in mammalian cells.

2 Results

2.1 TbEB1 is the only EB homologue in *T. brucei* and its domain architecture is similar to other EB homologues

The *genedb* database contains a single EB1 homologue in *T. brucei brucei:* Tb927.9.2760 (former Tb09.160.1440) (Logan-Klumpler *et al.* , 2012; Sheriff *et al.* , 2014). The protein consists of 536 amino acids and possesses a calculated molecular weight of 57kDa. It is further referred to as TbEB1.

The protein sequence of TbEB1 was compared to 21 EB1 proteins of 14 species described in literature ranging from single-cell to multi-cellular organisms. The closely related family *Leishmania* and the parasite *Theileria annulata*, which is able to recruit host EB1 proteins, did not possess an EB1-homologue, and were therefore not integrated into the analysis (Berriman *et al.* , 2005; Woods *et al.* , 2013b). TbEB1 shared the highest sequence identity of 58% with its homologue in *T. cruzi* in the BLAST analysis, whereas the sequence identity drops to about one third and below when compared to EB1 homologues in other organisms from yeast to human. As the complete protein sequences were blasted, the weakly conserved linker sequence between the N- and C-terminal domains contributes mostly to that effect. It is unusually long in the *Trypanosoma* species. The sequence diversity is also illustrated by the phylogenetic tree (Fig. 2.1), where the more ancient organisms, single-celled organisms, and plants, share more commonalities with TbEB1, than homologues in animals. The nearest neighbor-joining tree was produced with ClustalW2 phylogenetic tree (McWilliam *et al.* , 2013), after sequence alignment in MAFFT (Katoh *et al.* , 2002; Katoh & Standley, 2013).

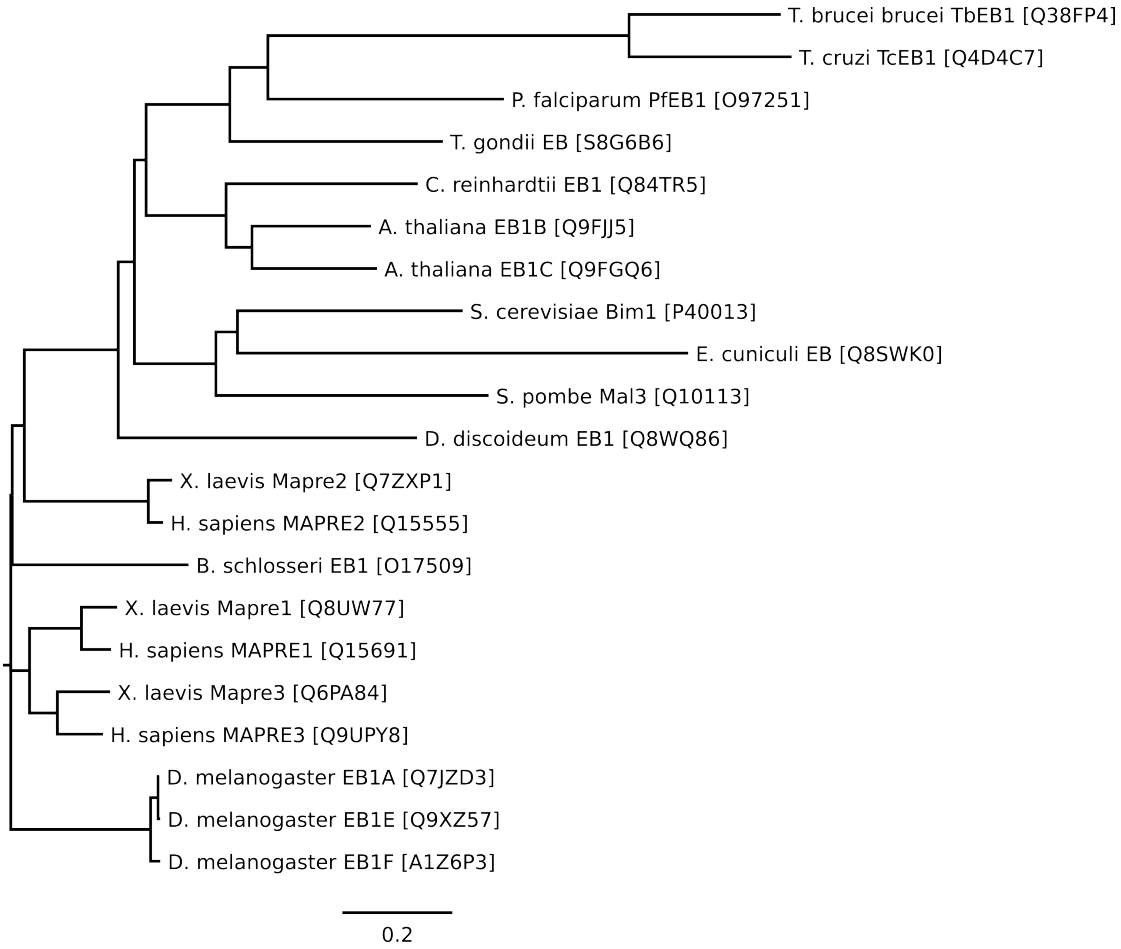


Figure 2.1: Phylogenetic tree of selected EB1 homologues. The protein sequence of the TbEB1 homologue was aligned to 21 EB1 homologues of 14 species using MAFFT. The proteins are indicated by their UniProt accession number. The phylogenetic tree was produced using ClustalW with the nearest neighbor end joining method and excluded gaps. The scale bar represents the amino acid substitions per site.

Multiple sequence alignment of selected EB1 sequences using MAFFT revealed the predicted N-terminal calponin homology (CH) domain and the C-terminal end-binding homology (EBH) domain (Fig. 2.2 A). Both are characteristic for EB1 proteins (Bu & Su, 2003). The highest conservation was found within the CH domain, which is common in EB proteins (Fig. 2.2 B). In contrast to many other members of the CH domain family, e. g. calponin, EB proteins mediate association to microtubules instead of actin as CH domains normally bind to F-actin (Korenbaum & Rivero, 2002; Slep, 2010). Compared to other EB1 N-terminal domains, the TbEB1 N-terminal domain contains an additional unstructured insertion and several small insertions between the conserved regions, which were also found in the close relative *T. cruzi.* The

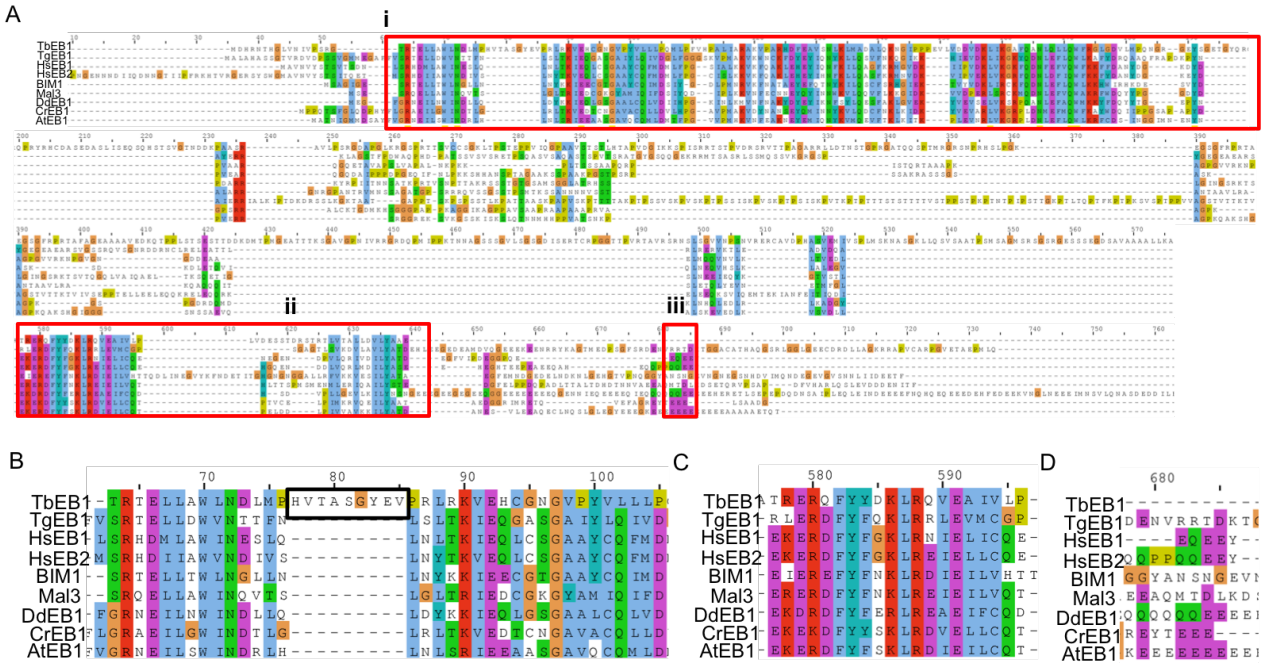


Figure 2.2: TbEB1 is a large protein with highly conserved N- and C-terminal domains but it lacks the EEY/F motif. A) Multiple alignment of EB amino acid sequences from *T. brucei brucei* (TbEB1, Q38FP4), *T. gondii* (TgEB1, S8G6B6), *H. sapiens* EB1 (MAPRE1, Q15691), *H. sapiens* EB2 (MAPRE2, Q15555), *S. cerevisiae* (BIM1, P40013), *S. pombe* (Mal3, Q10113), *D. discoideum* (DdEB1, Q8WQ86), *C. reinhardtii* (CrEB1, Q84TR5), and *A. thaliana* (AtEB1, Q9FJJ5). The highly conserved N- (i) and C- (ii)-terminal domains, as well as the EEY/F sequence (iii) are marked by red boxes. The multiple sequence alignment was performed with MAFFT. **B**) Sequence alignment of a part of the highly conserved N-terminal domains, which contain an additional unstructured insertion in *T. brucei* (black box). **C**) Alignment of the N-terminal part of the conserved C-terminal coiled-coil domain. **D**) The EEY/F motif is localized after the C-terminal coiled-coil sequence but is missing in trypanosomes.

short N-terminal amino acid sequence at the conserved CH domain is not as long as in EB2 homologues of higher organisms, like in *Xenopus* or mammalians.

The C-terminal coiled-coil domain is less conserved than the N-terminal domain (Fig. 2.2 C). That region also contains the EBH domain, which is necessary for dimerization (Sen *et al.* , 2013) and is relatively short compared to the other EB1 proteins with the coiled-coil structure similar in length to that of mammalian EB1 proteins. However, the following possibly disordered sequence at the end is missing. Notably, that part contains frequently conserved basic residues adjoining after the EBH domain as well as the EEY/F motif (Fig. 2.2 D; BA Fern). The latter mediates interaction with CAP-Gly (cytoskeleton-associated protein-glycine-rich) proteins (Weisbrich *et al.* , 2007). Up to the presence, only one CAP-Gly protein, tubulin-binding cofactor (TBC) B, is known in *T. brucei* (Fleming *et al.* , 2013), thus evolution of a specialized motif was probably not necessary. Interestingly, that motif is also missing in *T. cruzi, S. cerevisiae* and the AtEB1c variant of *A. thaliana.* The sequence motif is poorly conserved in other single-cell organisms like *S. pombe, P. falciparum, and T. gondii.* Other EBs, like AtEB1a and CrEB1, exhibit an accumulation of acidic residues at that position. In contrast, multicellular organisms, which often also possess more than one variant of EB proteins, seem to contain the EEY/F motif in general. It does not only mediate interaction with other proteins but is also involved in autoinhibition (Hayashi *et al.* , 2005; Manna *et al.* , 2008). Probably, the evolutionary emergence of the motif coincided with an increased complexity in the organisms and hence, the need for further regulatory mechanisms. The linker region between the conserved amino- and carboxy termini is highly variable in the EB1 family (Bu & Su, 2003; Akhmanova & Steinmetz, 2008). In *Trypanosoma,* it contributes decisively to the high molecular weight of TbEB1 compared to other proteins of the EB1 family.

Due to the conservation found for N- and C-terminal domains for TbEB1, both domains were modeled based to the published structure of human EB1 and yeast Bim1p, respectively (Fig. 2.3 A, B) (Hüls *et al.* , 2012; Huang *et al.* , 2015). The additional unstructured insertion of *Trypanosoma* species in the amino-terminal region is shown in green and demonstrated no interaction with the tubulin subunits of the microtubule polymer in a model based on pdb 3JAR (Fig. 2.3 C) (Zhang *et al.* , 2015). The short length of the sequence turns it also unlikely that it is the target of modifications or an interacting platform with further molecules. Hence, the short sequence was putatively lost in evolutionary younger organisms. EB proteins have been demonstrated to be obligate dimers (Sen *et al.* , 2013). A putative TbEB1 dimer is shown as ribbon model and characteristic domains are highlighted (Fig. 2.3 D).

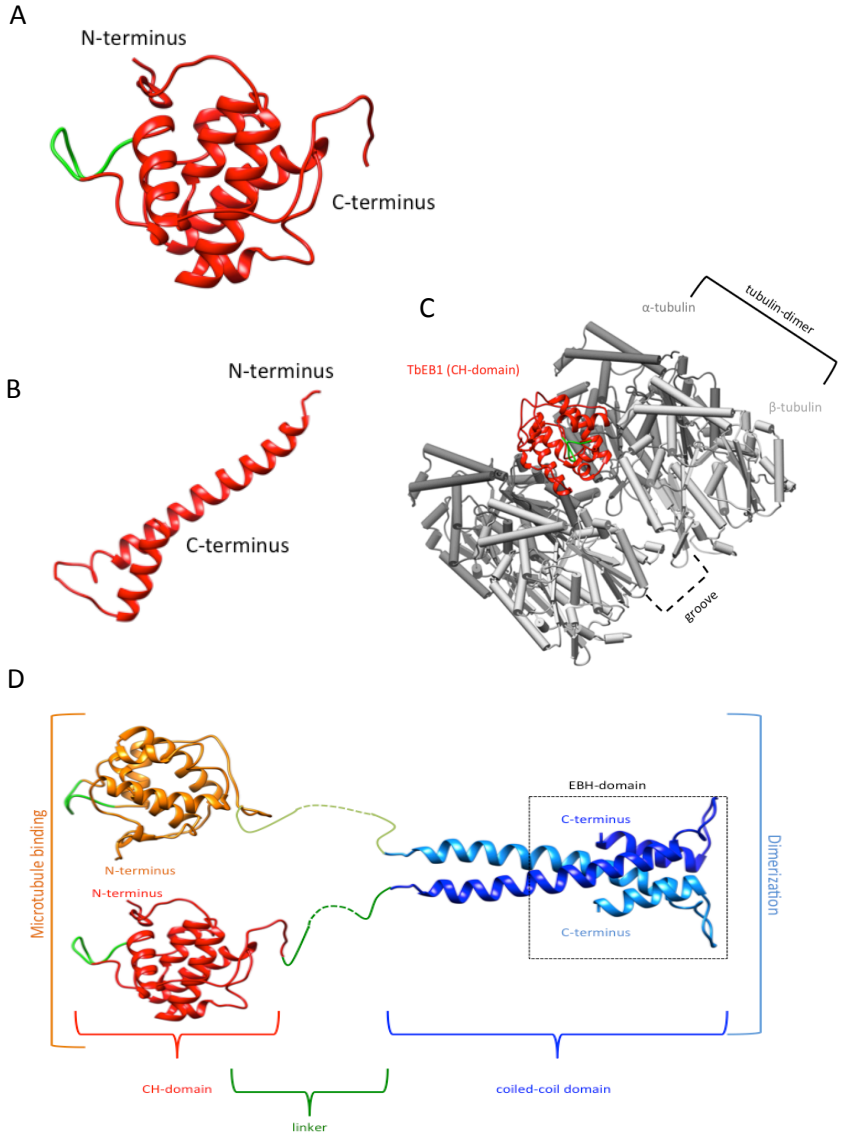


Figure 2.3: Homology models of the highly conserved N- and C-terminal domains of TbEB1. A) The N-terminal Calponin-homology (CH) domain was modeled based on the known structure of the CH domain of human EB1 [2R8U] (Huang *et al.* , 2015). Compared to other EB-proteins, the CH domain of TbEB1-sequence contains an extra short insertion (green). **B**) The conserved C-terminal region shows the typical coiled-coil motif predicted for this domain. Structures were modeled based on sequence homology to yeast Bim1p [4E61] (Hüls *et al.* , 2012). **C**) Model of TbEB1 association with four tubulin molecules in a microtubule according to literature. Structure model of TbEB1 N-terminal domain is based on human EB1. The model of alpha/beta tubulin is derived from Zhang *et al.* (2015). **D**) Putative TbEB1-dimer with conserved N- and C-terminal domains. The poorly conserved linker domain could not be modeled and is represented as a line.

2.2 Relative mRNA levels of TbEB1 in procyclic and bloodstream wild type trypanosomes

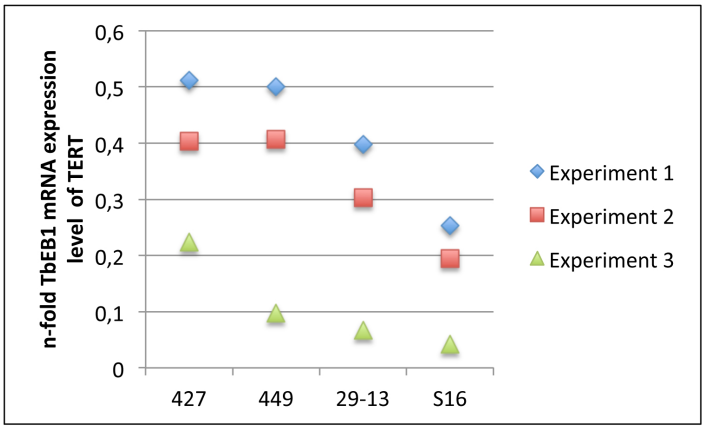


Figure 2.4: Relative mRNA levels of TbEB1 determined in wild type trypanosomes were higher in procyclic than in bloodstream trypanosomes. Three independent cell culture samples of three procyclic (427, 449, 29-13) and one bloodstream (S16) cell lines were compared in three independent qPCR runs. n-fold relative expression levels of TbEB1 were calculated with the ΔC_T-method using TERT as reference gene.

T. brucei undergoes a complex life cycle, alternating between a mammalian host and the dipteran vector combined with different developmental stages in each environment. The changes from one stage to the other frequently comprise a series of morphological re-structuring, e. g. cell size and shape as well as kinetoplast positioning. These processes involve cytoskeletal remodeling. End-binding proteins are known as master regulators of microtubule networks (Akhmanova & Steinmetz, 2008). Therefore, it is quite likely that TbEB1 would be expressed in both life cycle stages although the trypanosomal cytoskeleton can differ in its composition (Hertz-Fowler *et al.* , 2001; Portman & Gull, 2014).

TbEB1 mRNA levels were evaluated in individual life cycle stages. Total RNA of three procyclic (427, 449, 29-13) and one bloodstream (S16) cell line was isolated from three independent cell culture samples. The RNA was transcribed into cDNA, which was used as template in qPCR approaches. Relative mRNA levels were calculated with the ΔC_T-method, which delivers the n-fold gene expression after normalization to an endogenous reference gene (Livak & Schmittgen, 2001; Schmittgen & Livak, 2008). The telomerase reverse transcriptase (TERT) was used as reference (Brenndörfer & Boshart, 2010). The n-fold expression of TbEB1 of PCF and BSF cell lines of three independent qPCR runs are demonstrated in figure 2.4. TbEB1 mRNA was transcribed in both life cycle stages as the positive n-fold expression values demonstrate.

In each run, the mRNA levels of TbEB1 were higher in all procyclic cell lines compared to the bloodstream one. A similar tendency was found by Vasquez et al. (2014).

2.3 Localization of TbEB1 in *T. brucei*

Subcellular localization of a target protein, is one major step of protein characterization. Varying detection methods as well as different treatment and fixation of cells allow the assignment of the protein to sub-cellular compartments, e. g. flagellum, nucleus or cell body, and thereby providing indications for a possible function of the protein as well.

2.3.1 Endogenous tagging of TbEB1 confirmed localization of TbEB1 to microtubule plus ends

To investigate if the trypanosomal candidate protein demonstrates a distribution in vivo under physiological conditions as described in literature for other eukaryotic species (Schwartz *et al.* , 1997; Berrueta *et al.* , 1998) the endogenous TbEB1 was targeted by either endogenous tagging of one allele or a TbEB1-specific monoclonal antibody.

2.3.1.1 N-terminal tagging of TbEB1 pointed towards a cell cycle dependent localization of TbEB1 in whole cell preparations of bloodstream forms

In a first experiment, one allele of the endogenous protein was N-terminally tagged with a 6x-c-myc epitope using the pNAT vector in procyclic and bloodstream trypanosomes. Proper genomic insertion of the construct was verified by immuno blot analysis demonstrating a band of approximately 70kDa corresponding to a calculated molecular mass of 64.2 kDa. Obtained clones are referred to as 29-13 EB1pNAT$^{N\text{-}6xmyc}$for PCF and S16 EB1 pNAT$^{N\text{-}6xmyc}$for BSF, respectively (Fig. 2.5). Whole cell immuno fluorescence analysis demonstrated only a strong staining of the posterior two thirds of the cell body but no enrichment at the expected morphological structures, e. g. posterior cell pole - in the procyclic form (Fig. 2.6). An intense spot occurred sometimes at the posterior part of the cell body, close to the nucleus. Position and shape suggest a lysosomal localization indicating that the N-terminal tagged version of TbEB1 probably was more prone to degradation.

In contrast, BSF cells demonstrated an intensive, spot-like staining at the posterior cell pole additionally to the cell body staining indicative for the concentrated microtubule plus ends at that cell pole (Sherwin & Gull, 1989b; Robinson *et al.* , 1995). Variations in the TbEB1 labeling were found at the posterior cell pole, e. g. 1K1N/ 2K1N cells with one or two spots at the posterior end or a linear pattern in 2K2N cells (Fig. 2.7). However, only a part of cells

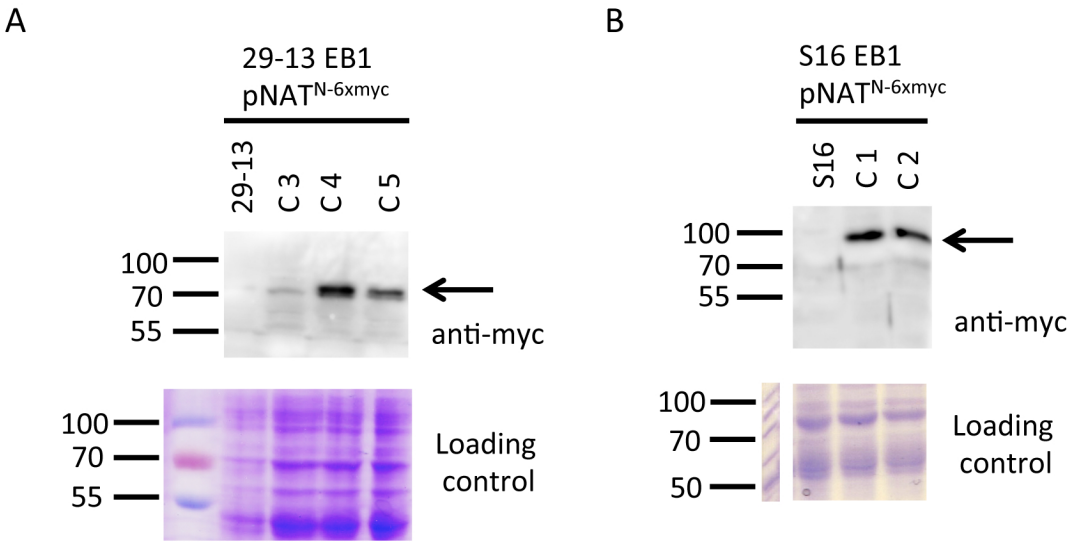


Figure 2.5: Detection of endogenously tagged TbEB1$^{N\text{-}6xmyc}$ demonstrated proper genomic insertion. A prominent band of approximately 70kDa (arrow) was detected in (**A**) clones of PCF cell line 29-13 and (**B**) clones of BSF cell line S16 by the monoclonal anti-c-myc antibody and an appropriate HRP-labeled secondary antibody. Coomassie-stained SDS-gels were used as loading control.

demonstrated a clear relationship between labeling and a certain cell cycle stage. Due to the microtubule-binding domain, the protein should be associated with the subpellicular microtubule array and be traceable by cytoskeletal preparation (CSK). However, in both life cycle stages no fluorescence signal was detected. This is possibly due to the N-terminal tag, which can interfere with proper localization of end-binding proteins and minimize microtubule binding behavior (Zhu *et al.* , 2009; Skube *et al.* , 2010). However, growth dynamics were similar to untagged wild type. The posterior spot-like staining in BSF might be explained by the fact, that the protein is transported to its target area but a stable binding to microtubule plus ends is prohibited by the tag, and therefore the interaction is not strong enough to remain microtubule-associated during the CSK procedure.

Summing up, only BSF pointed towards an expression pattern of TbEB1 that varied over the cell cycle at the posterior cell pole. The labeling pattern for PCF was similar for each cell cycle stage and evenly distributed over the posterior two third of the cell body. An accumulation of TbEB1$^{N\text{-}6xmyc}$ at the posterior cell pole in this life cycle stage is probably masked by the more intense cell body labeling.

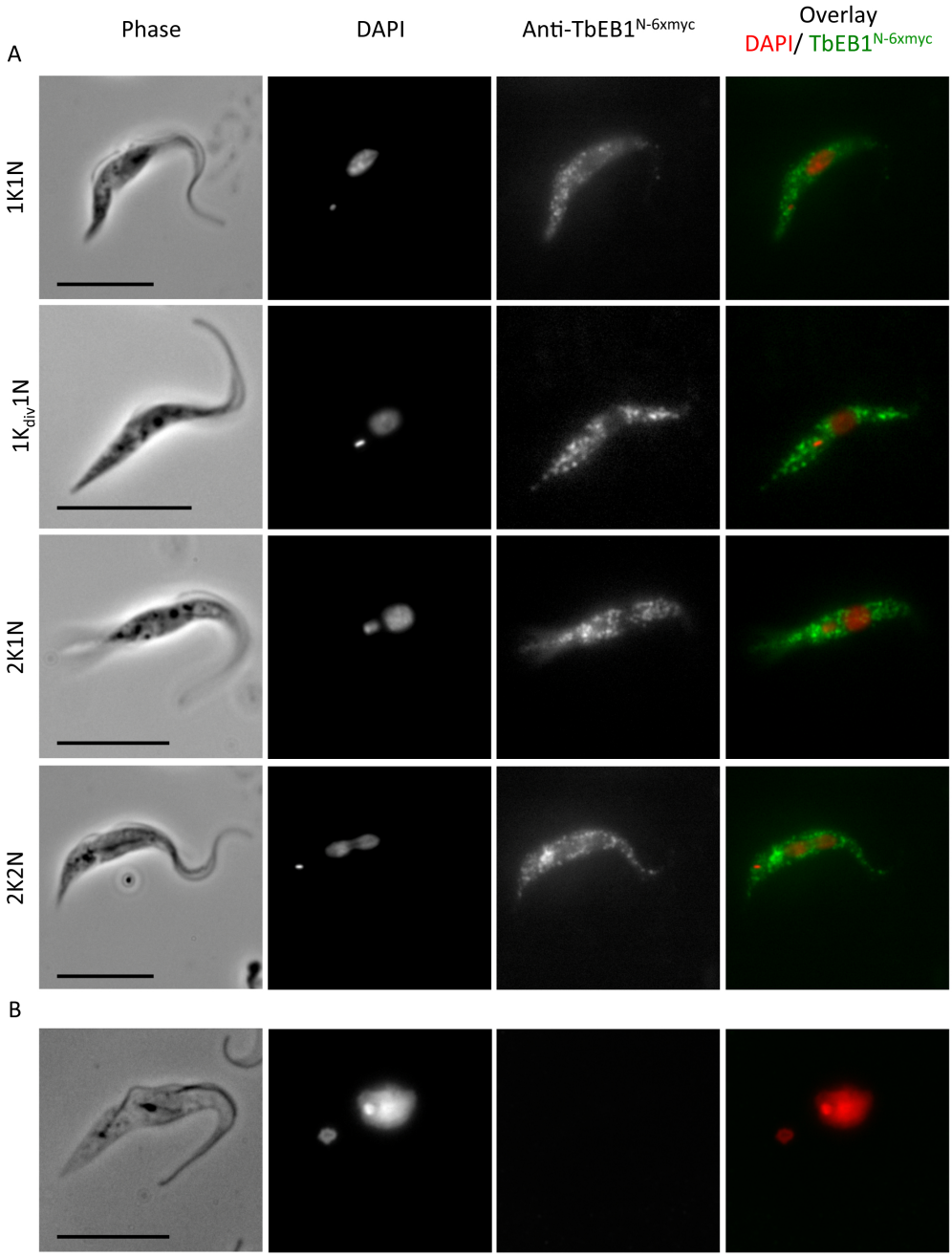


Figure 2.6: Localization of TbEB1 by endogenous tagging with the N-terminal pNAT-system on whole cell preparations and detergent-extracted cytoskeletons of procyclic trypanosomes did not hint a varying protein distribution during the cell cycle. A) The anterior third of the cell body showed a reduced TbEB1$^{N\text{-}6xmyc}$-labeling in whole cell preparations. A variation of protein distribution during the cell cycle was not detectable. Cells were fixed with 3.7% FA. **B**) The N-terminal tag of TbEB1$^{N\text{-}6xmyc}$ was not detected in detergent-extracted cytoskeletons. Samples were fixed in ice-cold methanol. Scale bars represent 10µm.

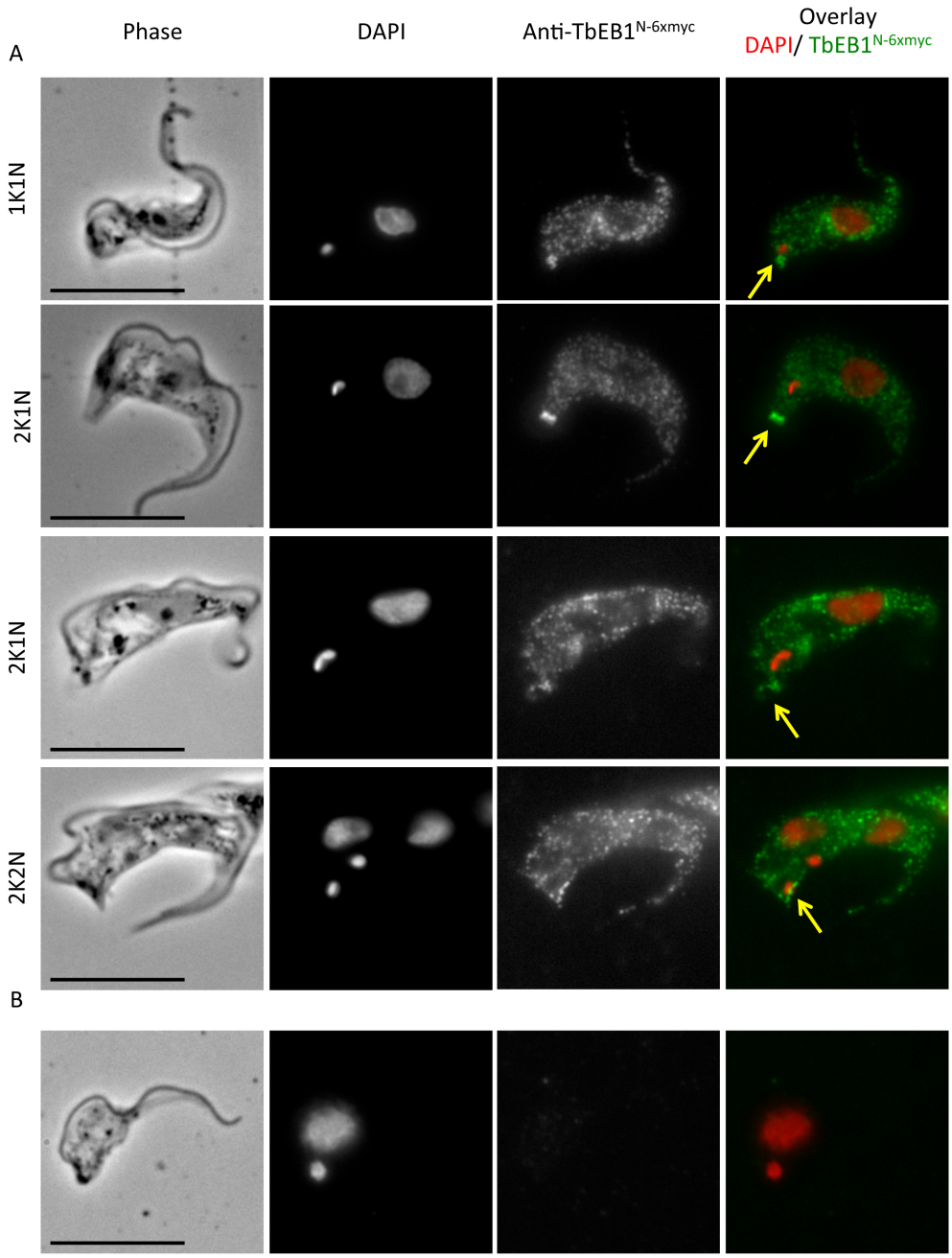


Figure 2.7: Localization of TbEB1 by endogenous tagging with the N-terminal pNAT-system on whole cell preparations and detergent-extracted cytoskeletons of bloodstream trypanosomes pointed towards a difference in protein distribution during the cell cycle. A) The anterior third of the cell body showed a reduced TbEB1$^{N\text{-}6xmyc}$-labeling, but the posterior end of the trypanosomes often demonstrated a strong labeling indicative for the concentrated microtubule plus ends at that cell pole in whole cell preparations. A variation in labeling patterns throughout the cell cycle as indicated in this image sequence by arrows was found only in a part of the cells. Cells were fixed with 3.7% FA. **B**) The N-terminal tag of TbEB1$^{N\text{-}6xmyc}$ was not detected in cytoskeletal preparations. Samples were fixed in ice-cold methanol. Scale bars represent 10µm.

2.3.1.2 C-terminally tagged TbEB1 was detectable at the cytoskeleton

As TbEB1 did not localize to the cytoskeleton with the help of the N-terminal tag, the protein was also tagged on its C-terminus. However, C-terminal tags are reported to impede interplay with EB1 interacting partners and might skew system dynamics (Skube *et al.* , 2010).

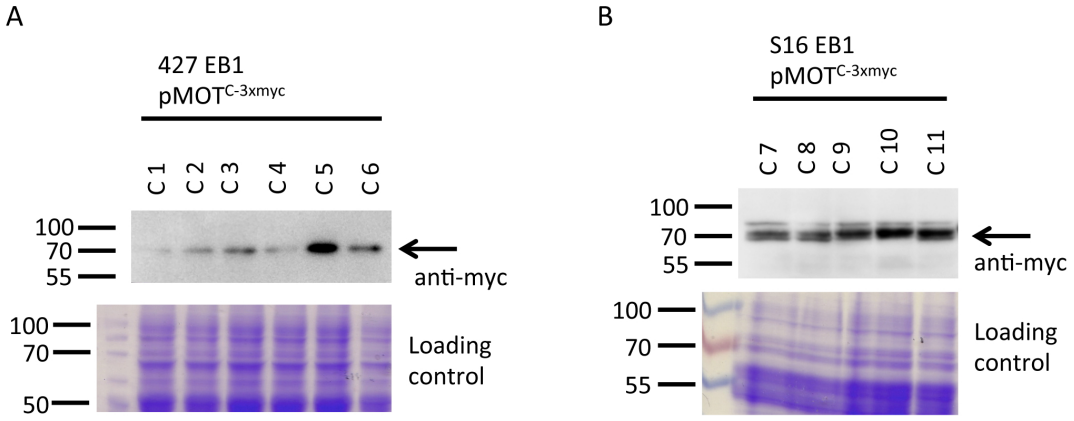


Figure 2.8: Detection of endogenously tagged TbEB1$^{C\text{-}3xmyc}$ demonstrated proper genomic insertion. A prominent band of approximately 70kDa (arrow) was detected in **A**) clones of PCF cell line 427 and **B**) clones of BSF cell line S16. The tagged proteins were detected by the monoclonal anti-c-myc antibody and an appropriate HRP-labeled secondary antibody. Coomassie stained SDS-gels were used as loading control.

The pMOT vector system: provides evidence for a localization on the subpellicular cytoskeleton To minimize the disturbance by the tag, initially only three repeats of the c-myc epitope were used together with a short linker sequence between tag and target gene sequence (Skube *et al.* , 2010). Therefore, appropriate gene and 3´UTR sequences of TbEB1 were cloned into the pMOT43M vector enabling homologous recombination. Procyclic (427) and bloodstream (S16) trypanosomes were transfected and obtained clones are referred to as 427 EB1pMOT$^{C\text{-}3xmyc}$ and
S16 EB1pMOT$^{C\text{-}3xmyc}$. Proper genomic insertion of the construct was tested by immuno blot analysis resulting in a 70kDa band as shown for N-terminally tagged cell lines (Fig. 2.8). During cultivation, cellular growth was not visibly affected by introduction of the tagged EB1 allele. C-terminal endogenous tagging revealed a disperse punctate pattern in PCF as observed for the N-terminal tagged cell lines as well as the diminished labeling at the anterior cell part. Again, no enhancement of the signal was detected at the posterior cell pole. However, analysis of CSK preparations demonstrated a staining of the posterior cell pole consisting of one or two spots (Fig. 2.9). The remaining cell body demonstrated a weak punctate staining. Again, as in the

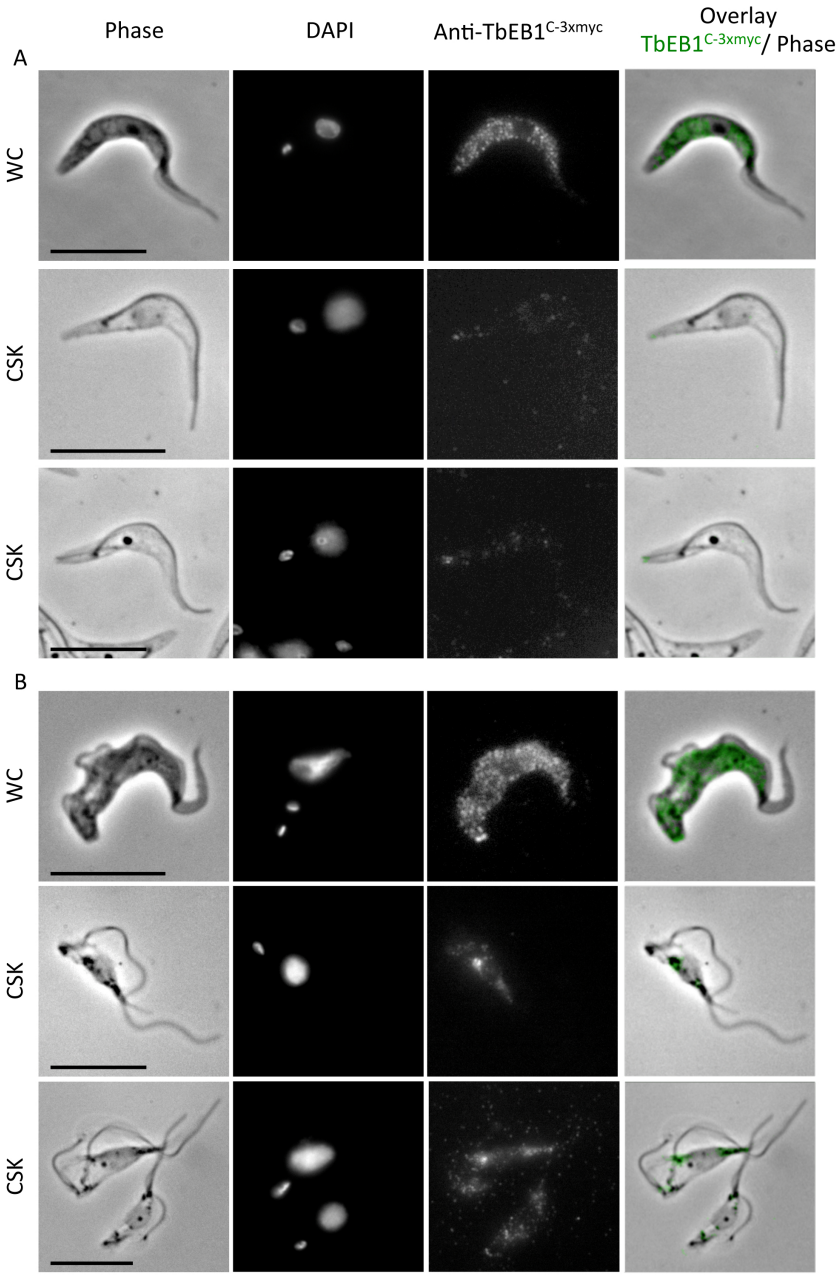


Figure 2.9: C-terminally tagged TbEB1 was detected on cytoskeletons in procyclic and bloodstream trypanosomes. Whole cell preparations (upper panels) demonstrated the same labeling as for N-terminal tagging. However, C-terminal tagging is indispensable for tracking the fusion protein in detergent-extracted cells (middle and lower panels). Procyclic trypanosomes (**A**) often demonstrated one or two spots at the posterior cell pole while in bloodstream cells (**B**) a posterior staining was only rarely detected. Stars indicate posterior cell poles. WC = whole cell preparation; CSK = cytoskeletal preparation. Whole cells were fixed with 3.7% FA, cytoskeletal preparations in ice-cold methanol. Scale bars represent 10µm.

N-terminally tagged versions, the BSF cell lines frequently demonstrated a strong spot-like fluorescence signal at the posterior cell pole, which was rarely traceable in CSK specimen (Fig. 2.9). Here, the staining was at best faint, sometimes more intense near the kinetoplast or at a linear structure reminiscent of the FAZ (flagellar attachment zone). Interestingly, when switching from formaldehyde to methanol fixation, the posterior cell pole labeling was lost in bloodstream CSK preparations. This observation is probably explained by the different modes of fixation of both reagents. While methanol fixates by dehydration of proteins, formaldehyde fixates proteins by cross-linking. The latter fixation method is more stable to mechanical and chemical forces. A staining of the mitotic spindle was neither detected in PCF nor in BSF. In both forms, the intensity of tagged TbEB1 was strongest in whole cells compared to cytoskeletal preparations, suggesting that most parts of the fusion protein were cytoplasmic. Additionally, in PCF the posterior cell pole labeling on cytoskeletal preparations was more intense at the subpellicular microtubule array while it was the other way round in BSF.

The pNATC vector system: showed a more intense labeling on whole cell and cytoskeletal preparations As selection markers were not compatible with culture conditions of procyclic cell line 29-13, the pMOT system could not be used to create a c-myc-traceable system in these RNAi cell lines. As the specific monoclonal antibody did not work in immuno blots and TbEB1 at the posterior cell pole was frequently not diminished in immuno fluorescence experiments after TbEB1 depletion, a second C-terminal tagging system, pNAT$^{\text{C-12xmyc}}$, was used to confirm RNAi specificity although the huge tag probably interferes with TbEB1 C-terminal interaction partners. Thus, the construct was introduced into TbEB1 RNAi cell lines 449 and 29-13 as well as into the corresponding procyclic wild type cell lines to evaluate the effect of the tag. Obtained clones were referred to as 449 TbEB1i pNAT$^{\text{C-12xmyc}}$ and 29-13 TbEB1i pNAT$^{\text{C-12xmyc}}$ for RNAi lines with the endogenously tagged allele and 449 pNAT$^{\text{C-12xmyc}}$ and 29-13 pNAT$^{\text{C-12xmyc}}$ for endogenously tagged wild type cell lines. The tag was also introduced in S16 bloodstream cell line, resulting in S16 pNAT$^{\text{C-12xmyc}}$. All selected clones demonstrated a clear band of 100kDa in immuno blots, which was higher than the calculated mass of about 72kDa. Some weak bands of lower size were detected, too, probably degradation products of the tagged protein (Fig. 2.10). The difference between real and calculated size is putatively caused by the large c-myc-tag. It is negatively charged molecule and those are known to migrate anomalously in SDS PAGE (Casarégola *et al.* , 1992; Armstrong & Roman, 1993).

Endogenous tagging influenced growth dynamics in procyclic forms while the bloodstream clone was not affected (Fig. 2.11). Although cellular growth was affected in PCF, only single atypical cell cycle stages were found. However, as those cell lines were not maintained for an extended period, an accumulation of atypical stages over time is possible.

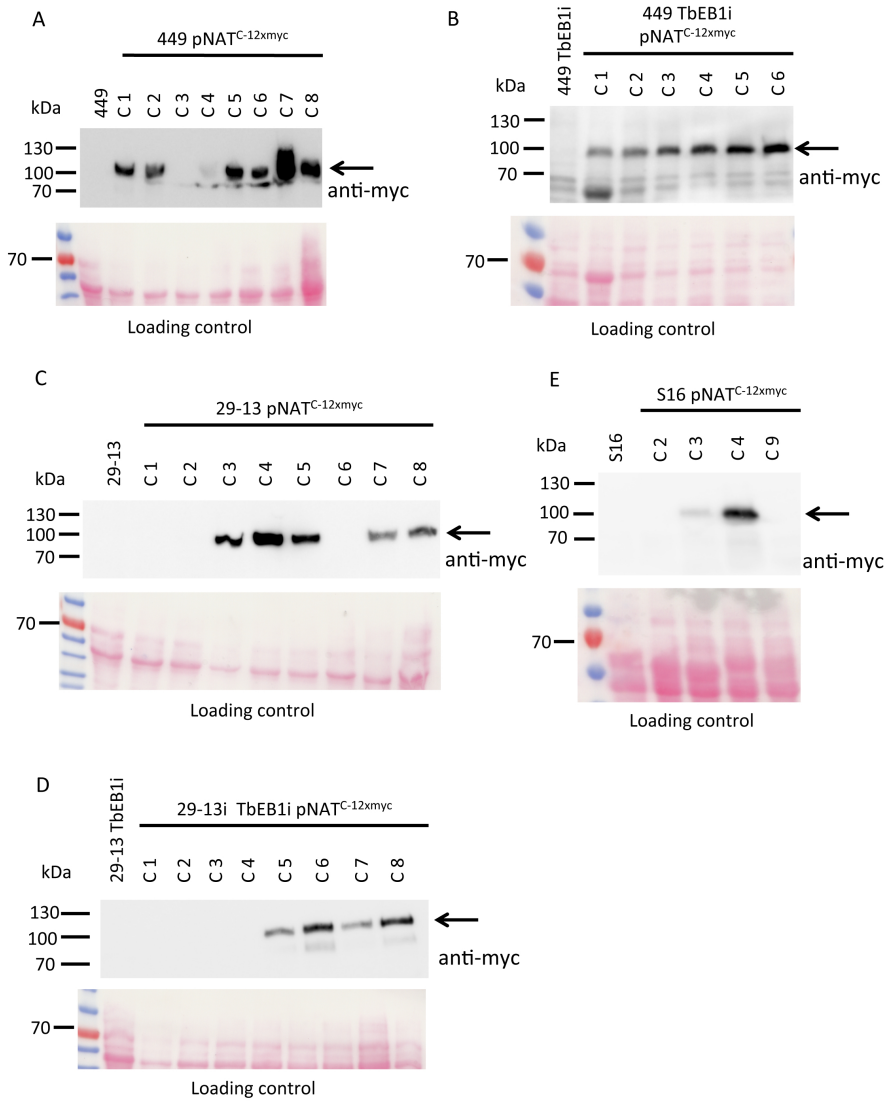


Figure 2.10: Detection of endogenously tagged TbEB1$^{C\text{-}12xmyc}$ demonstrated proper genomic insertion. A prominent band of approximately 100kDa (arrow) was detected in (**A**-**D**) clones of procyclic cell lines 449 and 29-13 and their corresponding TbEB1 RNAi cell lines and **E**) clones of bloodstream cell line S16. In cell lines 449 pNAT$^{C\text{-}12xmyc}$, 29-13 pNAT$^{C\text{-}12xmyc}$, and S16 pNAT$^{C\text{-}12xmyc}$, the endogenously tagged TbEB1$^{C\text{-}12xmyc}$ was introduced into corresponding cell lines 449, 29-13, and S16. In cell lines 449 TbEB1i pNAT$^{C\text{-}12xmyc}$ and 29-13 TbEB1i pNAT$^{C\text{-}12xmyc}$, the endogenously tagged TbEB1 was introduced into cell lines 449 TbEB1i and 29-13 TbEB1, which contain the inducible TbEB1 RNAi system. The tagged proteins were detected by the monoclonal anti-c-myc antibody and an appropriate HRP-labeled secondary antibody. Ponceau-stained immuno blot membranes were used as loading control.

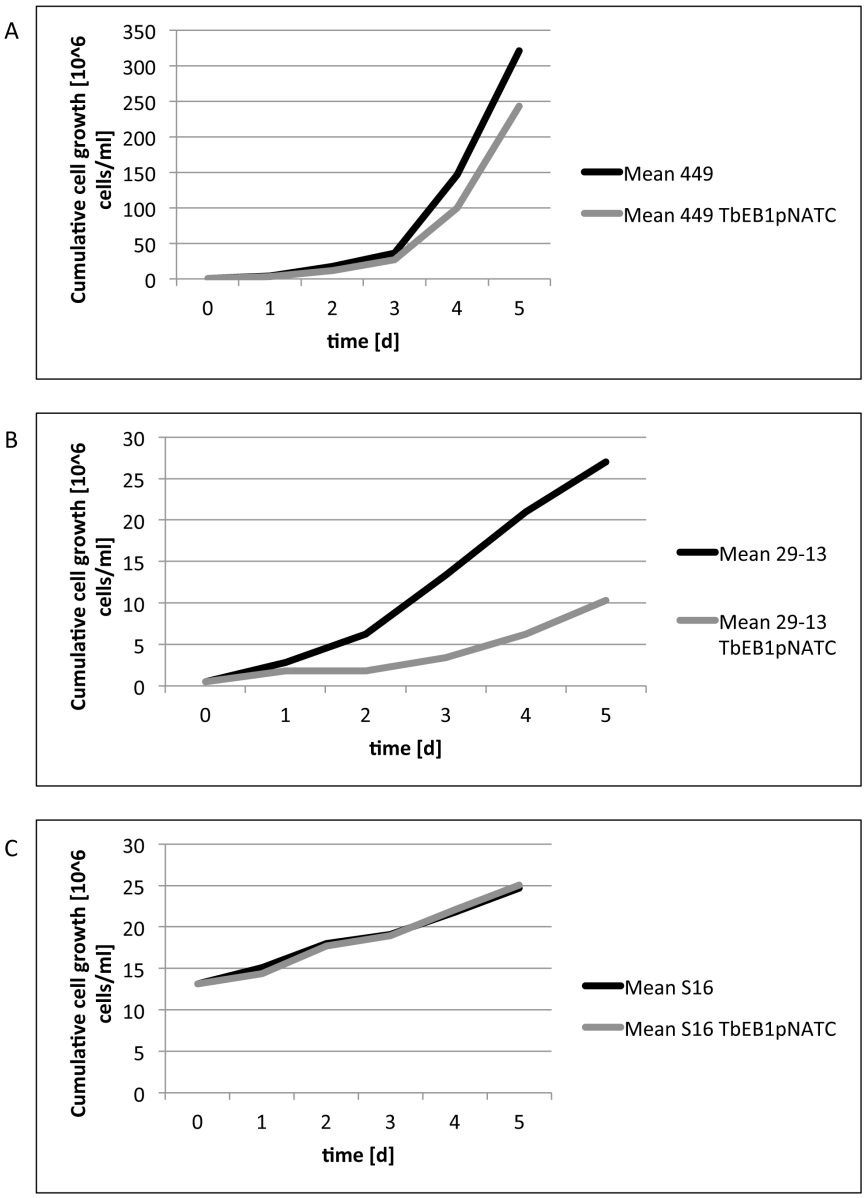


Figure 2.11: Growth curves of procyclic and bloodstream trypanosomes with C-terminally tagged TbEB1 (pNAT$^{C\text{-}12xmyc}$). **A-B)** Procyclic trypanosomes demonstrated a growth inhibition due to the modified TbEB1 allele while in **C)** bloodstream ones no effect was detectable. All approaches started with $5*10^5$ cells per ml. Cultures were diluted at several time points to maintain a steadily growing culture. Dilution factors were taken into account and cumulative cell numbers were plotted.

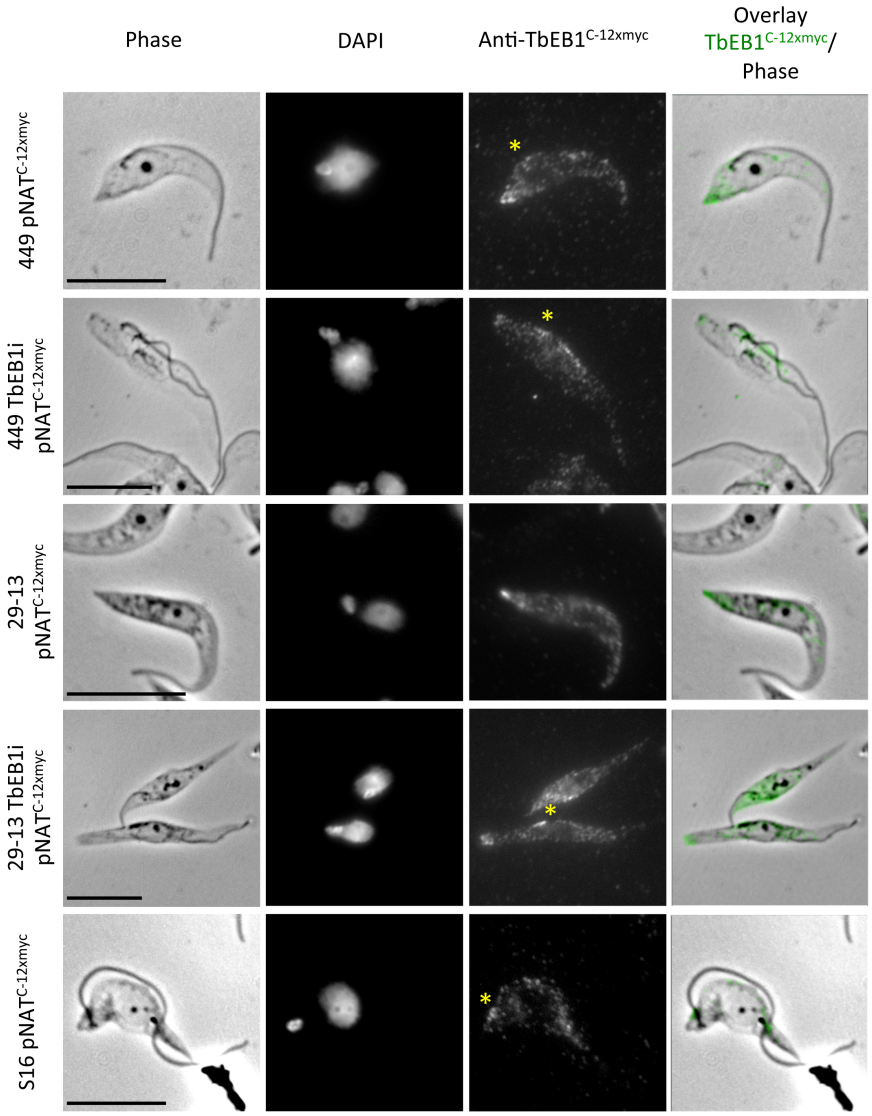


Figure 2.12: Anti-TbEB1$^{C\text{-}12xmyc}$ labeling on procyclic (449, 29-13) and bloodstream (S16) cell lines with the endogenously tagged TbEB1 allele. The staining pattern was similar to anti-TbEB1$^{C\text{-}3xmyc}$ labeling using the pMOT system, except that here a spot near the kinetoplast was labeled, too (star). Compared to whole cell preparations the posterior cell pole was frequently not stained in BSF detergent-extracted cytoskeletons. Cells were detergent-extracted with either 1% NP-40 for 5 minutes on ice (PCF) or 0.5% NP-40 for 1 minute at room temperature (BSF). Cells were fixed in ice-cold methanol for PCF and in 3.7% FA for BSF. Scale bars represent 10µm.

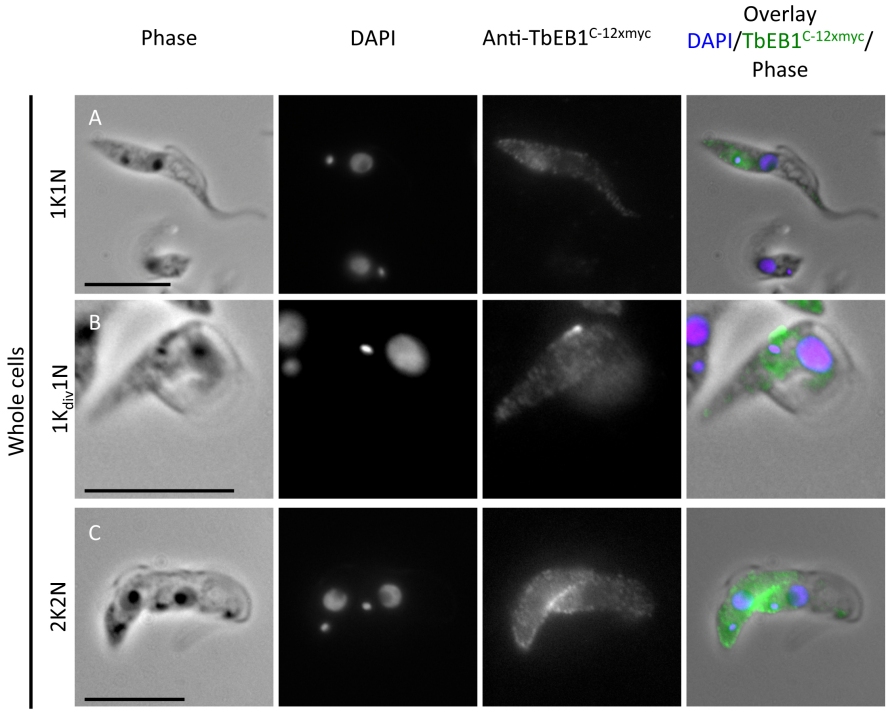


Figure 2.13: Amplification of signals due to the 12xmyc tag supported localization of TbEB1 und demonstrated a different labeling pattern of TbEB1 in PCF during the cell cycle. A) The fusion protein was distributed in a gradient starting from the posterior cell pole. **B**) TbEB1$^{C\text{-}12xmyc}$ was now detectable at the posterior cell pole in whole cell preparations as well as near the kinetoplast. **C**) TbEB1$^{C\text{-}12xmyc}$ often highlighted remodeling of posterior cell poles in dividing cells. Cells were fixed with 3.7% FA. Scale bars represent 10µm.

Compared to procyclic trypanosomes, immunofluorescence assays demonstrated that less fusion protein was associated with cytoskeletal elements in BSF than for PCF (compare Fig. 2.12). As the huge tag could interfere with interaction partners of TbEB1 and skew cytoskeleton dynamics (Skube *et al.* , 2010), the growth delay of PCF could be possibly traced back to the higher amount of dysfunctional fusion protein linked to the cytoskeleton.

The labeling pattern of cytoskeletons was comparable to that of the corresponding pMOT system for all PCF and BSF cell lines (Fig. 2.12). In contrast to the pMOT-system, a strong labeling was frequently found near the kinetoplast of S- and G_2-phase trypanosomes. That labeling pattern often intensified and elongated with progressing assembly of the new flagellum. However, the signal was restricted to the cell body. Therefore, the labeled organelle is probably the FAZ or microtubules adjacent to that region. Similar to the pMOT-system, cytoskeletal preparations of BSF trypanosomes resulted in low levels of TbEB1 labeling at the posterior cell pole and subpellicular cytoskeleton. Here, the highest labeling intensities were obtained for the region near the kinetoplast and the FAZ. Whole cell preparations of BSF for all cell cycle stages frequently demonstrated an intensified labeling of the posterior cell pole. It did not vary to a great extent during the various cell cycle stages as it was observed for the S16 pNAT$^{\text{N-6xmyc}}$ cell line.

The pNATC-system allowed tracking of the variation of the TbEB1 distribution throughout the cell cycle also in procyclic trypanosomes, which was best detectable in whole cell preparations (Fig. 2.13). Samples of G_1-phase, 1K1N cells, demonstrated no intensified spot-like signal of TbEB1$^{\text{C-12xmyc}}$ at the posterior cell pole, but the typical gradient distribution along the cell body was observed (Fig. 2.13A). Starting with S-phase ($1K_{\text{div}}$-cells) a signal occurred next to the kinetoplast and the signal elongated during cell cycle progression (Fig. 2.13B). Labeling of the subpellicular microtubule array also intensified with approaching 2K2N phase, occurring more homogeneously in intensity at the whole cell body (Fig. 2.13C). The TbEB1 fluorescence signal was highest at the newly defined posterior end indicating a high activity of microtubule modulation. Labeling of new and old FAZ is less strong, probably due to termination of remodeling processes in this region. Notably for cytoskeletons, the amount of TbEB1$^{\text{C-12xmyc}}$ linked to cytoskeletal elements varied in different cells. Therefore, different labeling intensities for organelles within similar cell cycle stages occurred and information about labeling intensity should be treated with care. That phenomenon retained after a further round of clone selection, thereby indicating that different amounts of the fusion protein were associated with the cytoskeleton in individual cells. However, cell cycle specific labeling was detectable in cytoskeleton samples in many cells (Fig. 2.14). The characteristic accumulation of TbEB1 at the posterior cell pole and the disperse pattern of the subpellicular microtubule array was well established. Corresponding to cell cycle progression, labeling of the newly synthesized FAZ occurred (Fig. 2.14B). Posi-

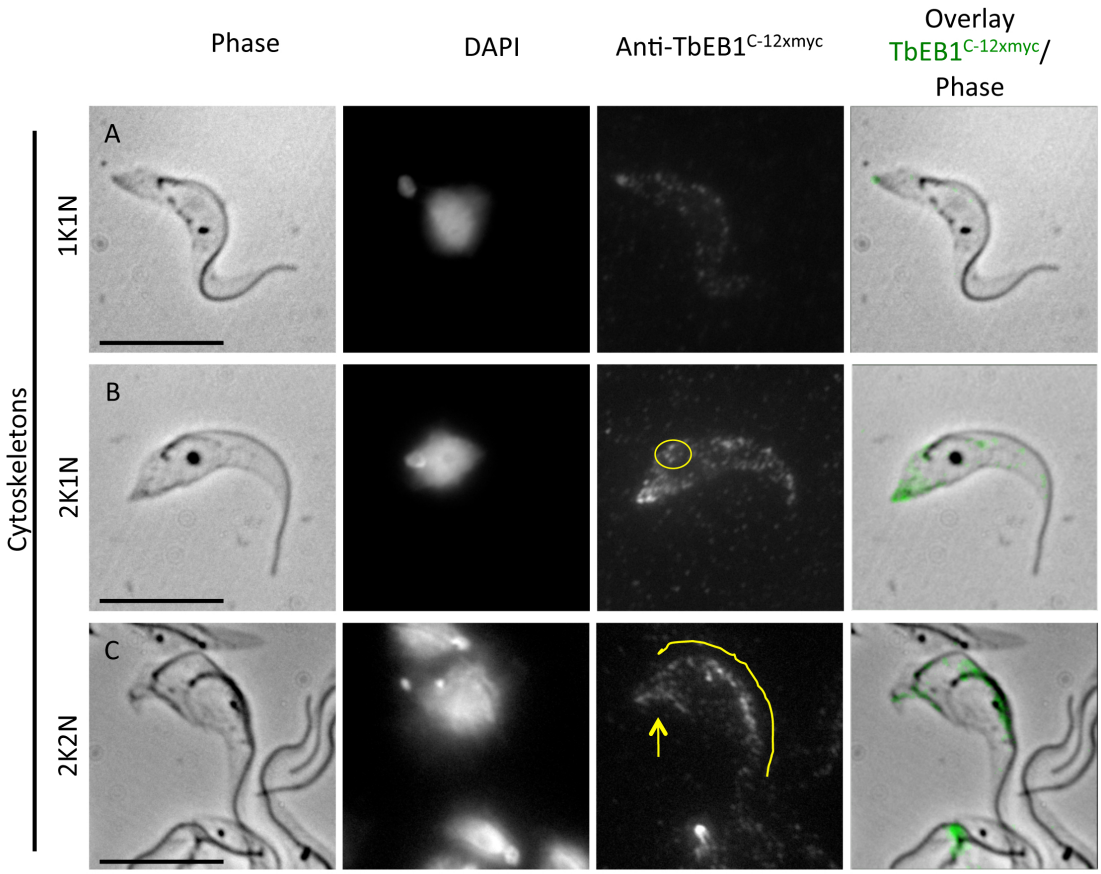


Figure 2.14: Variation in labeling patterns of TbEB1$^{C\text{-}12xmyc}$throughout the cell cycle after detergent-extraction in procyclic trypanosomes. The amount of TbEB1$^{C\text{-}12xmyc}$ linked to cytoskeletal elements varied in different cells but variations in protein localization during the cell cycle were still detectable. **A**) The posterior cell pole, FAZ and a dispersed labeling pattern of the subpellicular microtubule array was detected. **B**) The same organelles as for 1K1N cells were labeled as well as the putative beginning assembly of the new FAZ (circle). **C**) Cytoskeletal preparations revealed a TbEB1 localization at the remodeling posterior cell pole (arrow) and at the new and old FAZ (line). Cells were detergent-extracted with 1% NP-40. Scale bars represent 10µm.

tions near new and old FAZ were labeled due to cytoskeletal reorganization in this area (Fig. 2.14C). In general, the labeling of the new FAZ tended to be more intense than for the mature one. Similar to TbEB1 detection by the monoclonal antibody, a distribution along the posterior part of the division furrow was detected. Compared to the pMOT staining of PCF, an accumulation of the protein at the posterior cell pole was also detectable in many whole cell preparations. Additionally the area close by the kinetoplast and new and old FAZ were labeled. Quite likely, the signal is far more enhanced by the 12x-c-myc tag of pNATC than the 3x-c-myc of pMOT and especially for whole cell preparations above background signal of cytoplasmic fusion protein. In some cells, the gradient distribution of TbEB1 was also emphasized and remodeling processes at the posterior cell poles of dividing 2K2N cells were also visible. Neither in cytoskeletal nor whole cell preparations staining of the spindle was observed. The labeling of the posterior cell pole frequently demonstrated a higher intensity than that of subpellicular microtubules and FAZ in cytoskeletal preparations.

Summing up, C-terminal tagging of endogenous TbEB1 enabled a localization of TbEB1 to the subpellicular cytoskeleton in PCF and BSF. A variation of the TbEB1 labeling throughout the cell cycle was best detectable using the 12x-c-myc tag in PCF.

2.3.1.3 Detergent-extracted TbEB1$^{C\text{-}myc}$ was shown to localize to the cytoskeleton

TbEB1$^{C\text{-}myc}$ was shown to localize to microtubules in IFA. To confirm microtubule association *in vivo,* detergent-extractions with NP-40 were analyzed as proteins linked to the subpellicular microtubule corset generally co-precipitate with microtutubles (Vedrenne *et al.* , 2002). Treatment of cells with 1% NP-40 results in an insoluble fraction containing chromatin, microtubules and associated proteins and a soluble fraction containing cytoplasmic components. A characteristic band pattern is visible on Coomassie-stained SDS gels and Ponceau S-stained immuno blot membranes, which were also used as loading controls. As expected, TbEB1 was found in the pellet after detergent treatment for pMOT and pNATC-derived cell lines (Fig. 2.15). It is worth noting that a high amount of TbEB1 seemed to be degraded during the extraction process when comparing input and fractionated samples in their signal intensities. The discrepancy between cytoskeleton-associated and free TbEB1 is even more pronounced in IFA. Here, the most intense signals where obtained for whole cells while only little labeling occurred on the cytoskeleton (Fig. 2.9). But the low signal intensity obtained in Western blot for the cytoskeleton associated TbEB1 fits to the low signal intensities in IFA. Therefore, soluble TbEB1 in the cytoplasm seems to be more prone to degradation which would explain that TbEB1 was below the detection level in those fractions. Detergent treatment of pNATC cell lines, demonstrated an approximately equal distribution of tagged protein in both fractions for 449- and 29-13- TbEB1$^{C\text{-}12xmyc}$ and

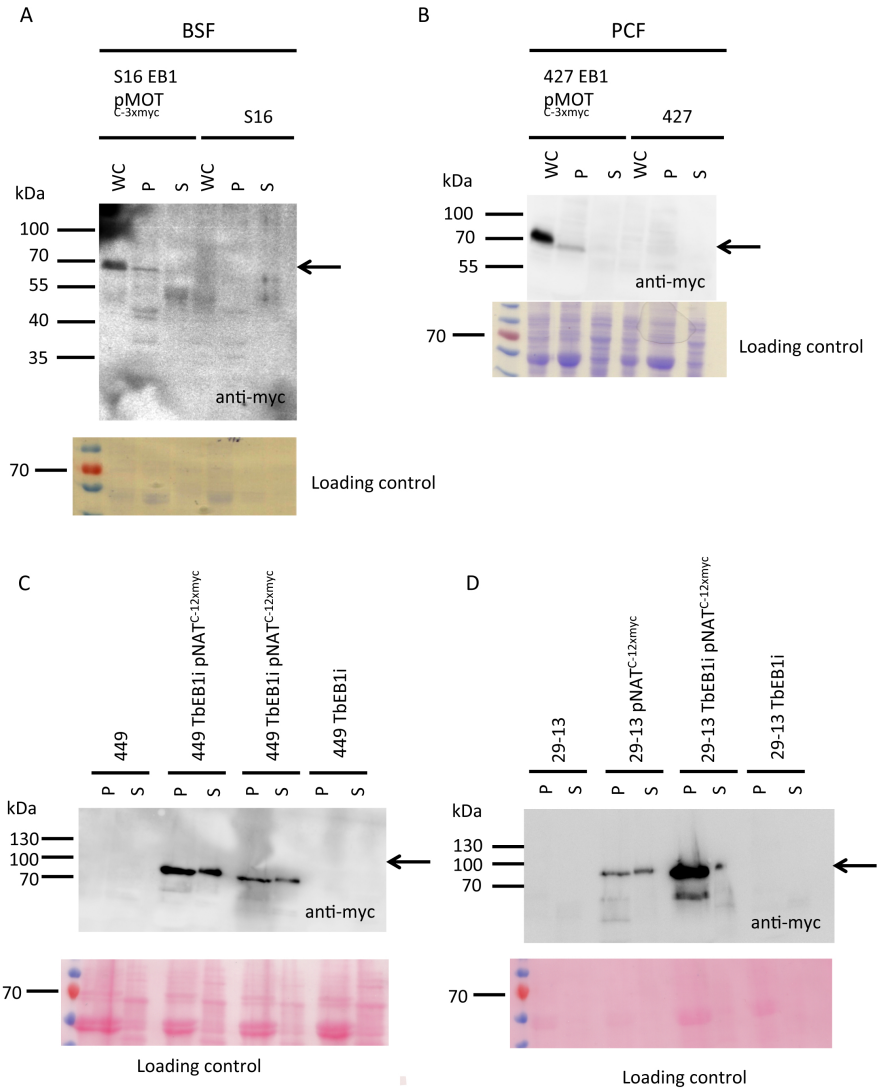


Figure 2.15: Detergent-extracted cell lines with an endogenously tagged TbEB1$^{C\text{-}myc}$ in bloodstream and procyclic cell lines confirmed association with microtubules. C-3xmyc –tagged procyclic (**A**) and bloodstream (**B**) trypanosomes were detected by immuno blot in whole cell lysates (WC), NP-40 insoluble cytoskeleton (P) and soluble (S) fractions. TbEB1$^{C\text{-}3xmyc}$ was detectable only in the microtubule-containing fraction. Notably, most TbEB1$^{C\text{-}3xmyc}$ was degraded during the extraction process although protease inhibitors had been added. 449 TbEB1$^{C\text{-}12xmyc}$ (**C**) and 29-13 TbEB1$^{C\text{-}12xmyc}$ (**D**), and their correspondent RNAi cell lines were tested, too. Here, an approximately equal amount of tagged TbEB1 was detectable in NP-40 insoluble and soluble fractions in three cell lines, except for the 29-13 TbEB1i pNAT$^{C\text{-}12xmyc}$ cell line. Quite likely, background induction reduced the amount of tagged TbEB1 in the supernatant fraction. Coomassie-stained SDS gels or Ponceau S-stained membranes demonstrated comparable protein loading.

449 TbEB1i pNAT$^{C\text{-}12xmyc}$. TbEB1 was detectable in the soluble fractions by the 12xmyc tag. The lower signal obtained for 29-13 TbEB1i pNAT$^{C\text{-}12xmyc}$ in the soluble fraction can be explained by background induction of the RNAi system, which was analogously found in IFA samples. Extraction of cells ectopically expressing TbEB1$^{C\text{-}2xmyc}$ with 300mM NaCl added to the extraction buffer as well as extraction of trypanosomes in RIPA buffer with and without 1% SDS (Fig. 2.16) confirmed that most of the fusion protein is localized to the cytoplasm and only a minor, probably fine-tuned part is associated with the cytoskeleton.

Corroborant to IFA, TbEB1$^{C\text{-}myc}$ was detectable in the insoluble NP-40 fraction indicating that TbEB1 is a microtubule-associated protein.

2.3.2 A monoclonal Anti-TbEB1 antibody visualized the variation of TbEB1 labeling during the cell cycle

Modification of proteins by tagging can interfere with proper localization and effects of tagging had been described for mammalian EB1 (Skube *et al.* , 2010). Furthermore, as demonstrated above, N-terminal tagging of the TbEB1 adversely affected binding to microtubules while the large C-terminal tag interfered with growth dynamics in trypanosomes. To verify localization of TbEB1 revealed by endogenous tagging, a mouse monoclonal antibody was raised against the purified His-tagged protein in a master´s thesis project (MA, Spindler). Localization studies in procyclics confirmed the results obtained by Sheriff *et al.* (2014) and demonstrated a varying labeling pattern of TbEB1 in BSF during the cell cycle, too (Spindler, 2014). However, monoclonal hybridoma cell lines were not stable and stopped antibody production.

Therefore, two further mice were immunized and mouse 2 demonstrated the best immune response and the corresponding immune serum was tested in IFA and Western blot analysis (Fig. 2.17). In whole cell preparations the complete cell body was labeled as well as the nucleus (Fig. 2.17A). Preparations of cytoskeletons (Fig. 2.17B) revealed a staining of the subpellicular microtubules, the FAZ, and the nucleus. The signal at the posterior cell pole was only slightly enhanced compared to the cytoskeleton. A spot-like signal occurred frequently at the end of FAZ near the anterior cell pole. A variation of TbEB1 labeling at the posterior cell pole was not detected probably due to the too low concentration of the antibody in the immune serum. Mouse anti-serum 2 recognized the TbEB1 protein with a mass of about 70kDa and putative degradation products or truncated proteins due to pre-mature translation termination. The ectopically expressed TbEB1$^{C\text{-}2xmyc}$has a similar mass, for which a faint band was stained. However, a protein with a similar mass was found in the wild type cell line. Together with the weak expression in TbEB1$^{C\text{-}2xmyc}$ the reaction was considered as unspecific. Antibody binding to the His-Sumo-tag used for antigen purification seemed unlikely as no signal was detected for the His-Sumo-SMC3 fragment 2 with an expected mass of about 30kDa, which was purified under

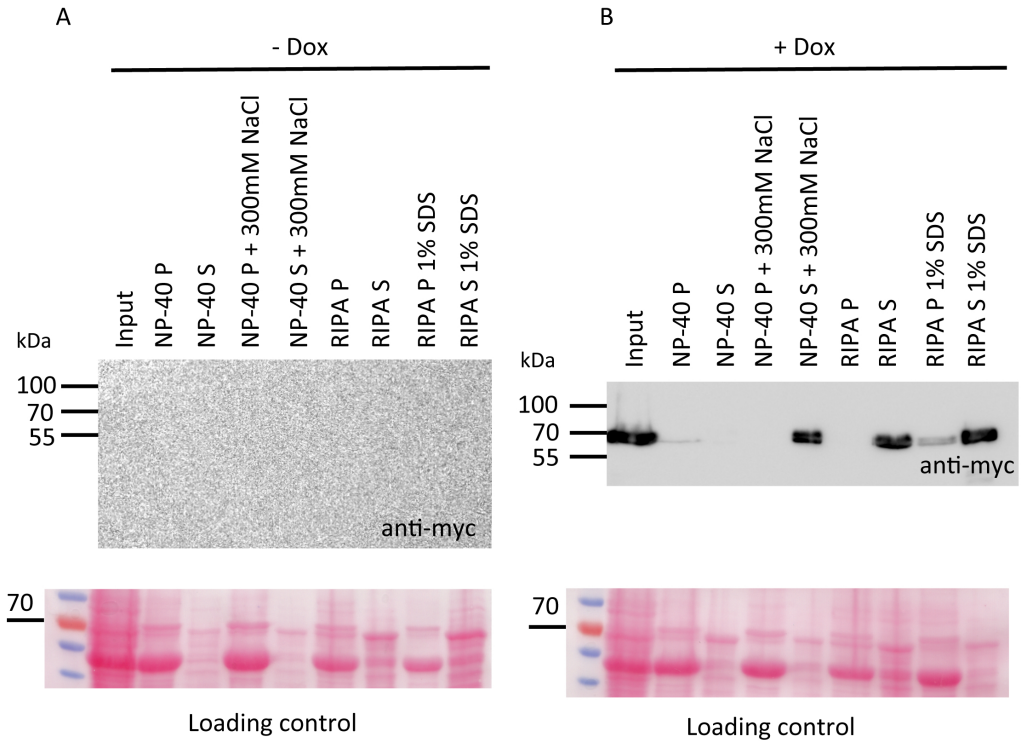


Figure 2.16: Pre-test to evaluate conditions for IP of TbEB1$^{C\text{-}2xmyc}$ by the mouse monoclonal antibody. TbEB1$^{C\text{-}2xmyc}$ was expressed over night by addition of 1µg/ml doxycycline to elevate levels of cytoplasmic TbEB1$^{C\text{-}2xmyc}$. **A**) Non-induced (-Dox) and **B**) induced (+Dox) samples were treated with 1% NP-40, 1% NP-40 with 300mM NaCl, RIPA buffer, and RIPA buffer with 1% SDS. Although protease inhibitors were added, most TbEB1 was degraded in the supernatant fraction and beyond detection limits. Immuno blot membranes were probed with anti-c-myc antibody and the appropriate secondary antibody. The exposure time was the same for both membranes and comparable amounts of input, and treated samples were loaded onto the gel. Ponceau S-stained immuno blot membranes were used as loading control.

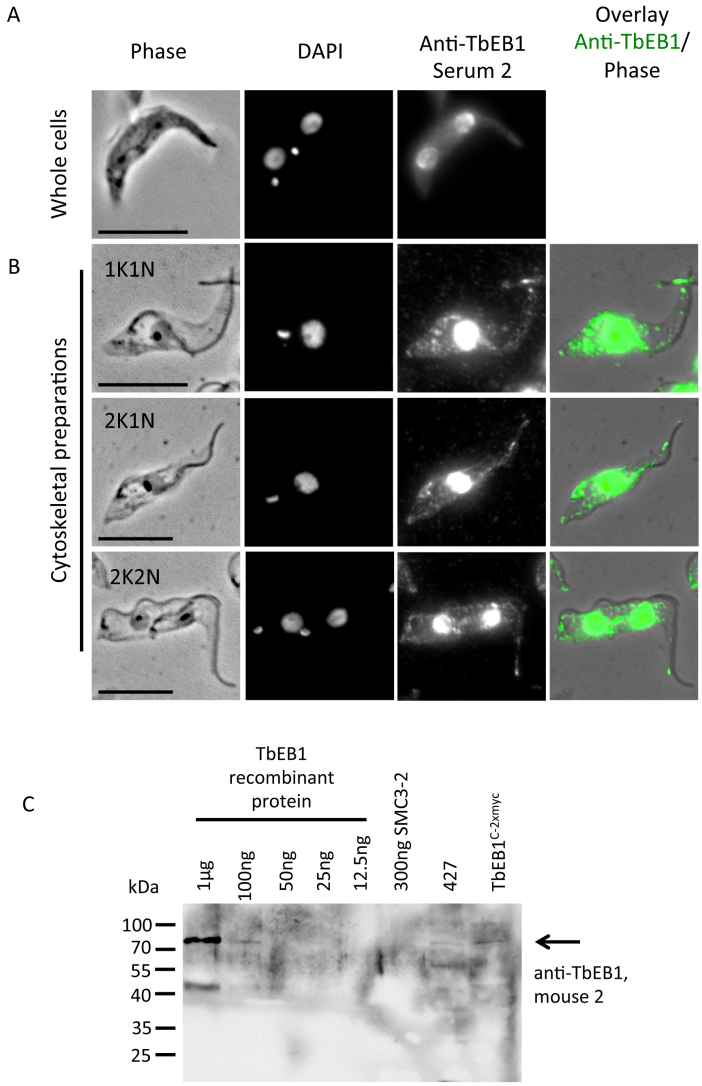


Figure 2.17: Mouse immune response after inoculation of TbEB1 peptide only recognized the peptide. **A**) IFA of procyclic, whole cells demonstrated an intensive staining of the cell body and nuclei with exception of the flagellum. **B**) In cytoskeletal preparations, the posterior cell pole, the nucleus, FAZ and cytoskeleton were detected by the immune serum. Only mouse 2 demonstrated a positive result. Scale bars represent 10µm. **C**) Immuno blot using TbEB1 recombinant protein in several concentrations, a further recombinant protein with a calculated mass of 30kDa (SMC3-2, 300ng, negative control), wild type procyclic cells (427), the inducible ectopic expression cell line TbEB1$^{C\text{-}2xmyc}$ (1µg/ml doxycyclin, overnight) as antigens. The blot was probed with 1:200 diluted immune serum of mouse 2 and an anti-mouse-HRP-conjugated secondary antibody. Endogenous TbEB1 possesses a molecular weight of 57kDa and the ectopically expressed version of about 70kDa. The calculated protein molecular weight is about 70kDa.

similar conditions (Spindler, 2014). A band of about 57kDa, the expected mass of wild type TbEB1, was only detected in the cell line 427 but not in the procyclic cell line ectopically expressing TbEB1. Establishment of hybridoma cells resulted in two monoclonal cell lines, whose antibodies recognized TbEB1 in immuno fluorescence analysis quite well but did not in immuno blots. Hence, the produced antibodies can only bind to native, non-denatured TbEB1. To verify the specificity of anti-TbEB1(mouse monoclonal IgM, $\varkappa$), immuno precipitation was performed using the ectopically expressed TbEB1$^{\text{C-2xmyc}}$ as bait. TbEB1 was ectopically expressed to increase TbEB1 levels within the cell, as the protein is normally tightly associated with the cytoskeleton and the main part found in the pellet fraction after NP-40 treatment. Furthermore, cytoplasmic TbEB1 seemed to be degraded fast even in the presence of protease inhibitors. At first, conditions were tested to elevate TbEB1$^{\text{C-2xmyc}}$ amounts in the supernatant after treatment as this part would be used for immuno precipitations. TbEB1$^{\text{C-2xmyc}}$ was only detectable in samples after addition of doxycycline (compare Fig. 2.16). Treatment with either NP-40 and 300mM NaCl or RIPA-buffer gave the best results. The immune precipitation was performed with the latter conditions. The supernatant containing ectopically expressed TbEB1$^{\text{C-2xmyc}}$ was first incubated with anti-TbEB1 antibody then with protein L beads (kindly provided by M. Hermann). Anti-c-myc antibody was used to detect TbEB1$^{\text{C-2xmyc}}$ in the immuno blot assay. Clearly, a band was detectable in the pellet fraction beyond the thick white band representing protein L with a similar molecular mass of 70kDa (Fig. 2.18). Thereby, at least ectopically expressed TbEB1$^{\text{C-2xmyc}}$ was recognized and precipitated by anti-TbEB1.

IFAs with the obtained antibody resulted in a strong signal of the posterior cell pole, where bundled microtubule plus ends are expected (Sherwin & Gull, 1989b; Robinson *et al.* , 1995). Compared to the posterior staining, the overall cytoskeleton was very weakly labeled. Rarely, the FAZ was stained. Only in PCF, a quite weak staining of the spindle was sometimes observed in immuno fluorescence images but this might be artificial as it coincided with a stronger background. Due to form-specific cell division, the anti-TbEB1 labeling manifested slightly different staining patterns in procyclic and bloodstream trypanosomes. Despite a weak increase in signal intensity, no variation in the labeling pattern had been observed for the cytoskeleton. Therefore, the focus was laid on the posterior cell pole. In cytoskeletal preparations of PCF (Fig. 2.19), TbEB1 was visible as a spot-like staining at the posterior end in 1K1N cells. With progressing in the cell cycle, the intensity at the posterior cell pole increased until two spots were visible. They were often connected with each other by weaker bands forming a ring-like structure, which fits to the 'open' end formation of microtubules at the posterior cell pole of trypanosomes (Seebeck *et al.* , 1988). The 'point'-like appearance in G_1-phase is probably due to restrictions of light microscopic resolution. With entering late G_2-phase and starting mitosis, the TbEB1 signal was elongated, often coinciding with nuclear division. Frequently a more intensely labeled

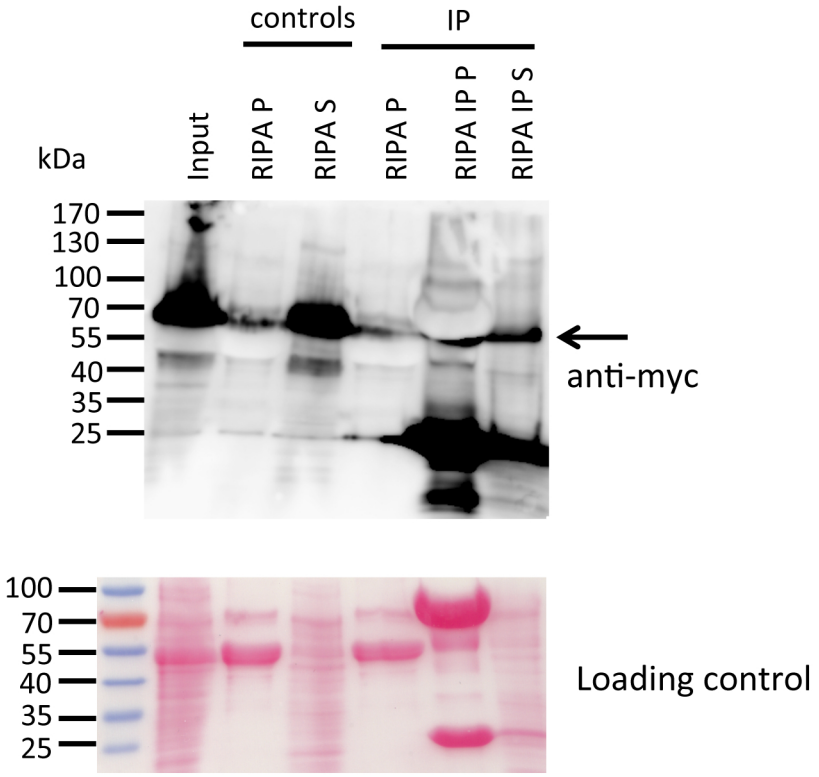


Figure 2.18: Ectopically expressed TbEB1$^{C\text{-}2xmyc}$ was successfully immunoprecipitated with the mouse monoclonal anti-TbEB1 antibody. Samples were induced (+Dox 1µg/ml) overnight to elevate levels of TbEB1$^{C\text{-}2xmyc}$ and treated with RIPA-buffer to release TbEB1 from the subpellicular cytoskeleton. Input refers to whole cells after induction. RIPA P and S samples were taken to demonstrate successful release of TbEB1$^{C\text{-}2xmyc}$ from the cytoskeleton. The RIPA S sample was used for the IP with anti-TbEB1 antibody. The immuno blot membrane was probed with anti-c-myc antibody and an appropriate secondary antibody conjugated to HRP. The TbEB1 signal is partially masked by Protein L, which has a molecular mass of 70kDa.

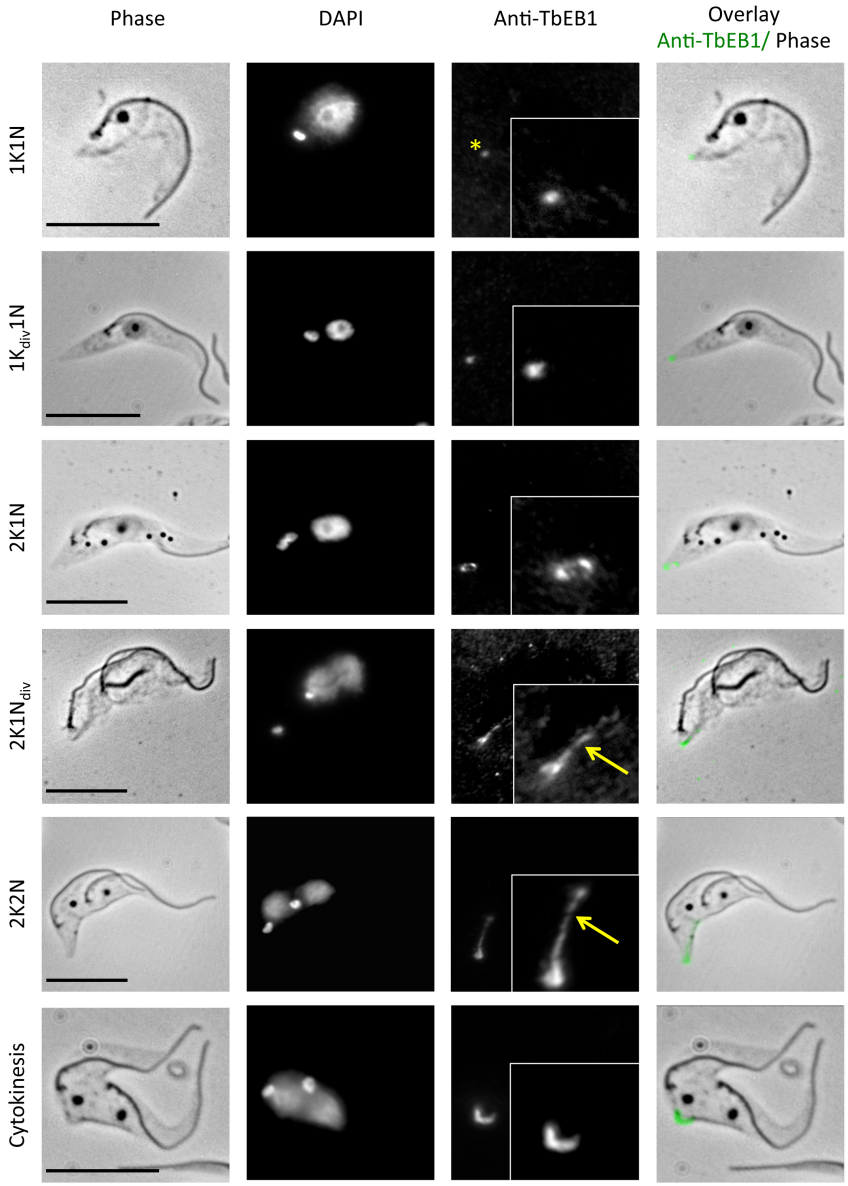


Figure 2.19: Localization of TbEB1 at the posterior cell pole during the cell cycle of procyclic trypanosomes visualized by the mouse monoclonal anti-TbEB1 antibody on cytoskeletal preparations. The weak posterior signal (star) of TbEB1 in 1K1N cells intensified over the cell cell cycle, divided into two spots in 2K1N cells, and elongated, thereby marking the progression of the division furrow and the newly forming, second posterior cell pole (arrows). Inserts show magnifications of the developing TbEB1 signal at the posterior cell pole. Scale bars indicate 10µm.

part within the line was observed, the newly forming posterior end of the old flagellum daughter cell. The elongation reached a maximum in early 2K2N cells and quite possibly marked the posterior end of division furrow. Late 2K2N cells, when cytokinesis is almost finished, demonstrated a shorter, but intense signal at the two newly formed posterior cell poles, where daughter cells still stuck together. Like in PCF, TbEB1 was localized as spot-like accumulation at the posterior cell pole in BSF (Fig. 2.20). Similarly, the intensity increased over cell cycle and as soon as the kinetoplast started division, often 2 posterior spots were identified. An elongation of the signal was visible but did not reach the dimensions of procyclic ones and stayed quite the same from 2K1N stage on. Again, the posterior staining often appeared as ring-like structure. The signal decreased with progressing cytokinesis to a single, but intense spot again due to the posterior-to-posterior position of dividing bloodstream trypanosomes. The variation in the TbEB1 distribution during the cell cycle was observed best in cytoskeletal preparations. Whole cell preparations only demonstrated the posterior staining in procyclics and sometimes an additional weak labeling of the cell body in bloodstream trypanosomes. In most procyclic trypanosomes observed, the intensity of TbEB1 posterior cell pole labeling was weaker in 1K1N and 2K2N cells than for the other cell cycle stages (Fig. 2.21). Bloodstream trypanosomes frequently demonstrated a lower posterior labeling intensity of 1K1N cells while for the remaining cell cycle stages the labeling intensity was similar (Fig. 2.22).

Thereby, the described remodeling of the posterior cell pole was similar to published data in PCF (Sheriff *et al.* , 2014) and to the observations obtained for PCF and BSF during a master´s thesis (Spindler, 2014).

2.3.3 Electron micrographs of procyclic trypanosomes confirmed association of TbEB1 with the subpellicular microtubule array

To study the localization of TbEB1 in more detail, whole mount cytoskeletons were prepared for electron microscopy. The obtained cytoskeletons were probed with the mouse monoclonal anti-TbEB1 antibody and a corresponding secondary antibody conjugated to 10nm gold. Due to mechanic forces during the extraction process some trypanosomes were destroyed leaving remnants of the cytoskeleton. Here, the subpellicular microtubule array is spread out and single microtubules can be distinguished. An association of TbEB1 to microtubules was detected (Fig. 2.23A) but a clear evidence for localization at microtubule branching points was not found because of method restrictions. However, the distribution of γ-tubulin occurred in a similar pattern (Scott *et al.* , 1997) indicating further spots of microtubule activity. Intact whole mount cytoskeletons often possessed a quite electron dense posterior cell pole hindering visualization of TbEB1 by immuno electron microscopy at this position. Nonetheless, in some cells TbEB1 was detectable at the posterior cell pole. Here, the TbEB1 labeling was sometimes arranged in

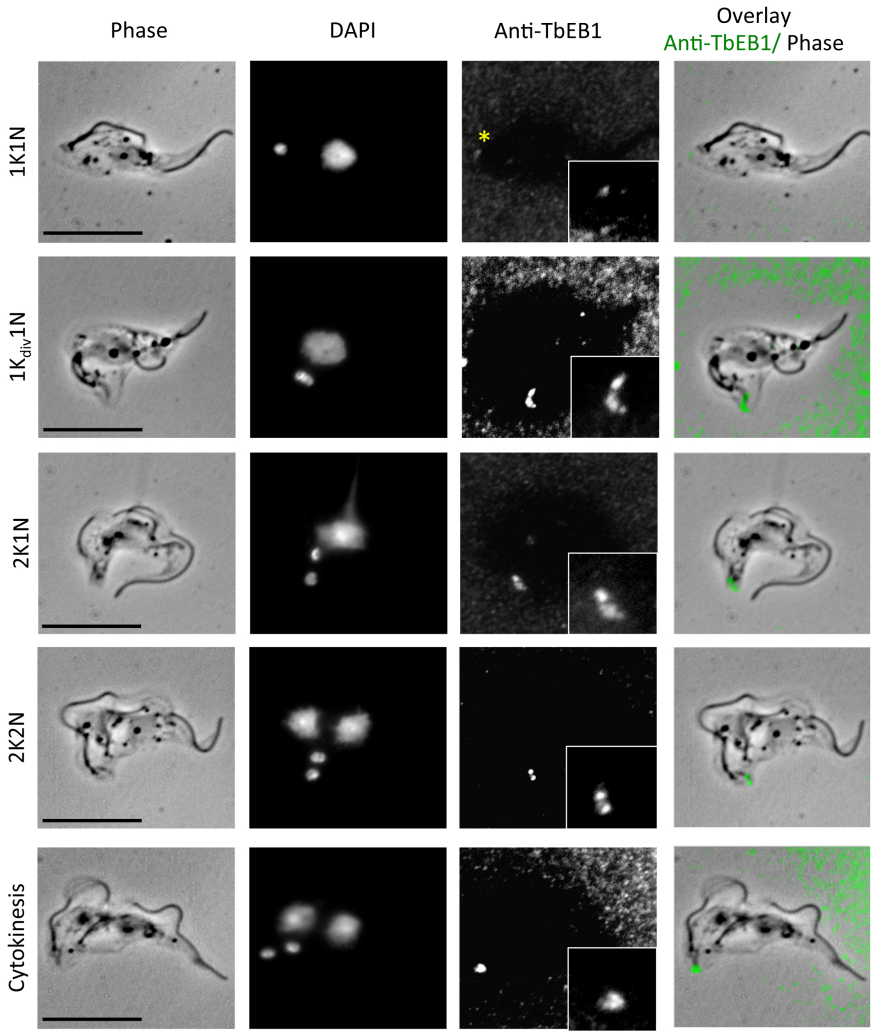


Figure 2.20: Localization of TbEB1 at the posterior cell pole during the cell cycle of bloodstream trypanosomes visualized by the mouse monoclonal anti-TbEB1 antibody on cytoskeletal preparations. The weak posterior signal (star) of TbEB1 in 1K1N cells intensified over the cell cycle, elongated, and finally divided into two distinct spots indicating the posterior ends of separating daughter cells. Inserts show magnifications of the developing TbEB1 signal at the posterior cell pole. Scale bars indicate 10µm.

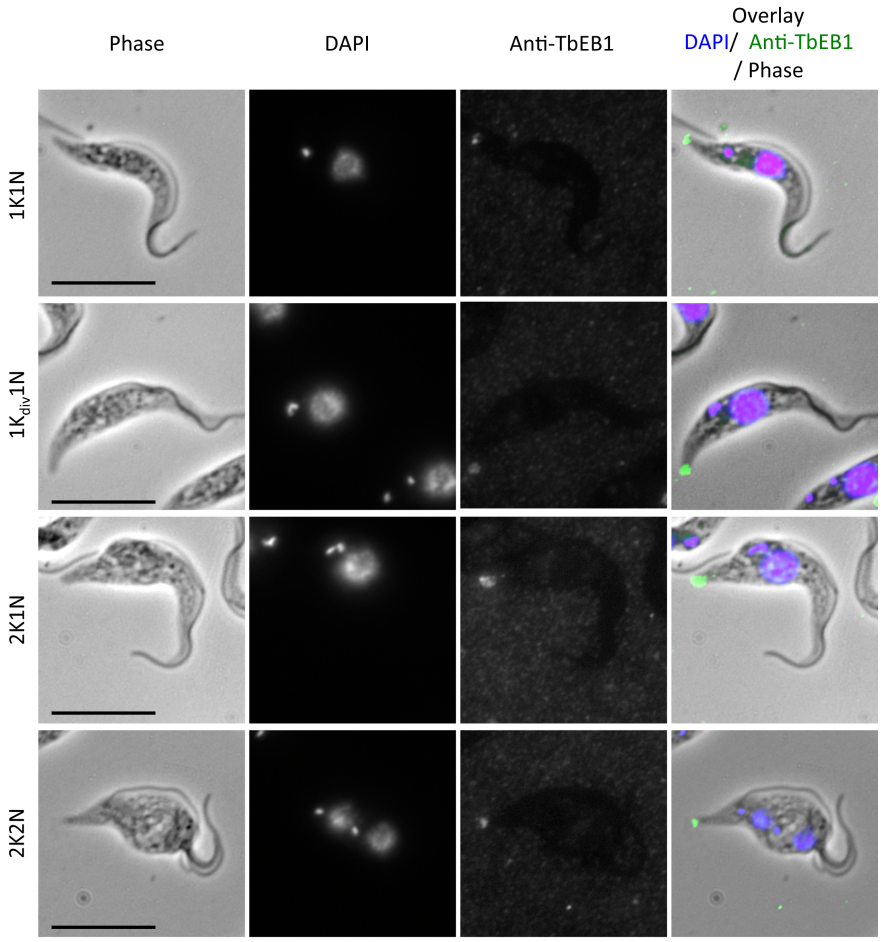


Figure 2.21: Localization of TbEB1 at the posterior cell pole during the cell cycle of procyclic trypanosomes visualized by the mouse monoclonal anti-TbEB1 antibody in whole cell preparations. The weak posterior signal of TbEB1 in 1K1N cells intensified frequently in 1K$_{div}$1N and 2K1N cells while it decreased again in 2K2N cells. Compared to CSK, the posterior part of the division furrow is not marked. Procyclic trypanosomes were fixed in ice-cold methanol. Scale bars indicate 10µm.

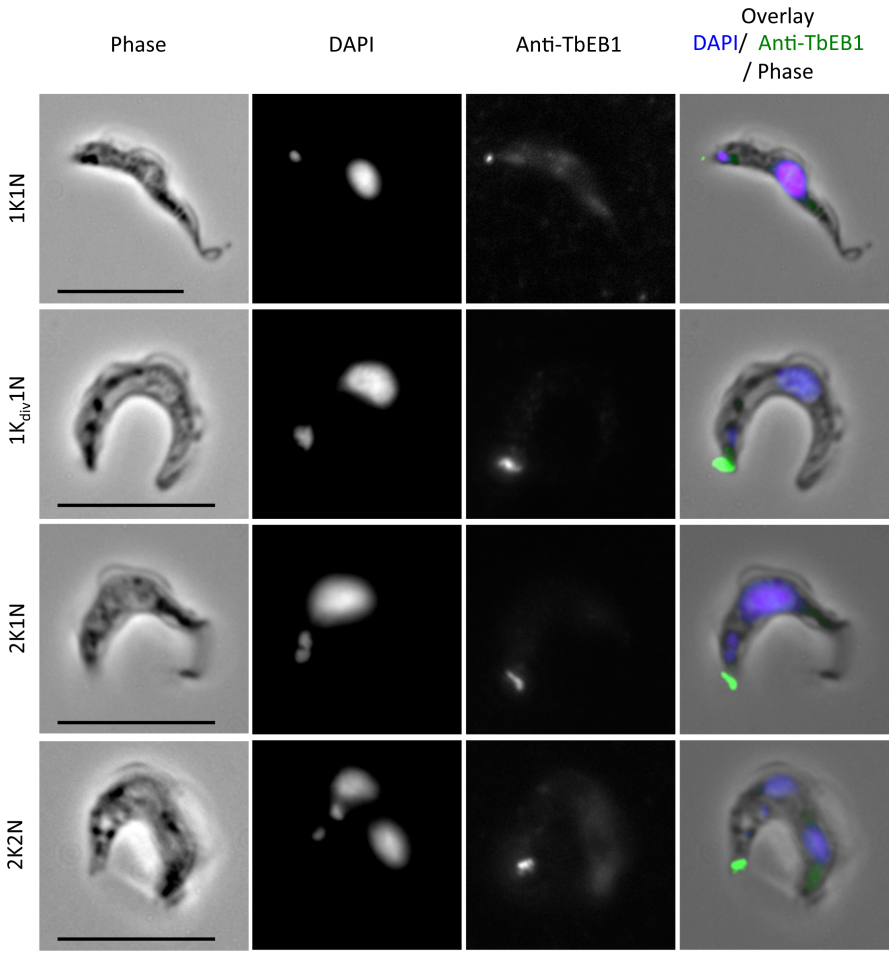


Figure 2.22: Localization of TbEB1 at the posterior cell pole during cell cycle of bloodstream trypanosomes visualized by the mouse monoclonal anti-TbEB1 antibody in whole cell preparations. The weakest signal for TbEB1 was obtained in 1K1N cells while the other cell cycle stages demonstrated an equivalent intensity. Bloodstream trypanosomes were fixed in ice-cold methanol. Scale bars indicate 10µm.

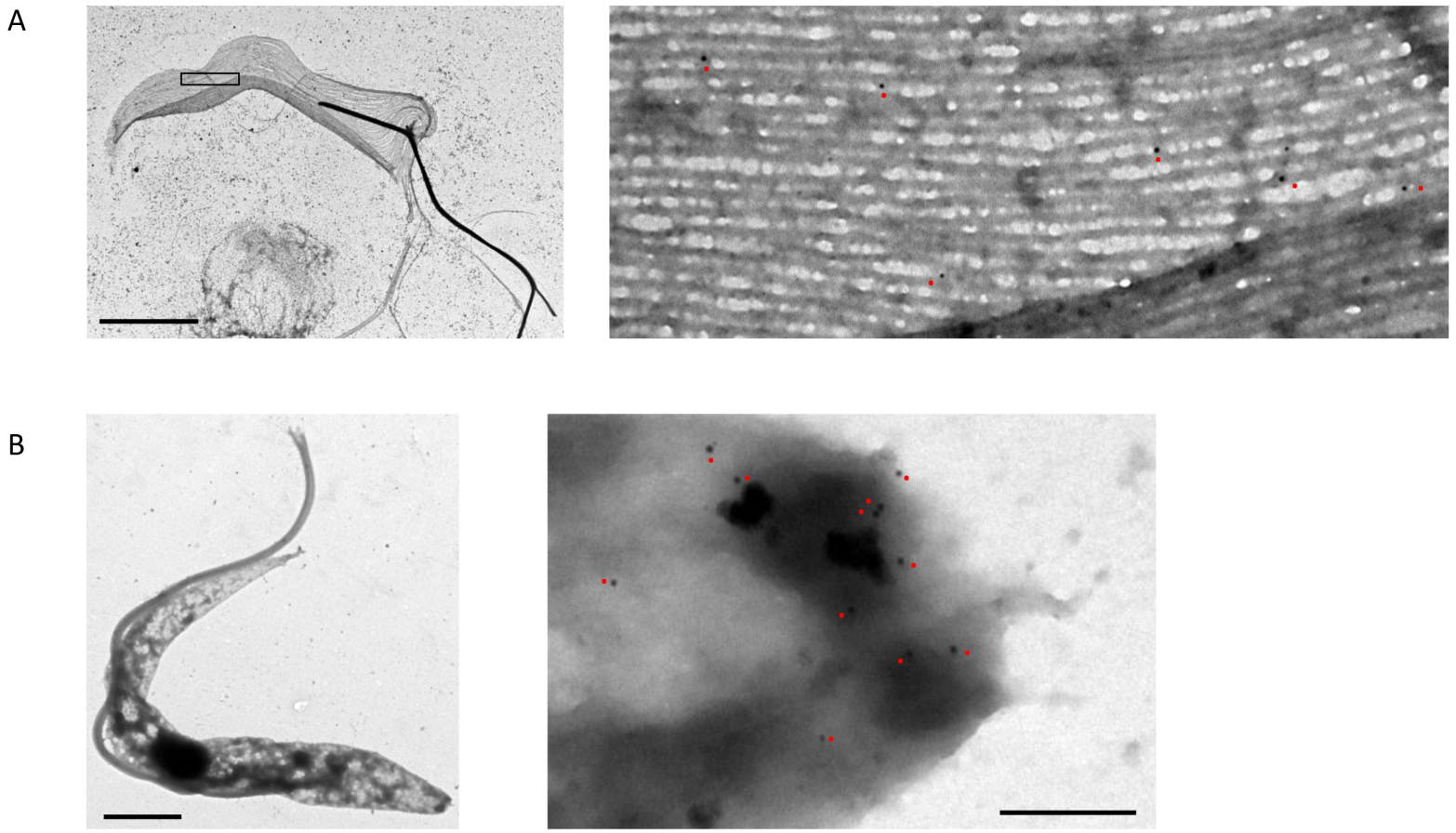


Figure 2.23: TbEB1 localizes to subpellicular microtubules in procyclic trypanosomes. Whole mount cytoskeletons were produced by detergent-extraction of trypanosomes and visualized by transmission electron microscopy. TbEB1 was detected by the anti-TbEB1 mouse monoclonal antibody and an anti-mouse antibody labeled with 10nm gold. **A**) TbEB1 is localized to microtubules of the cell body. Left electron micrograph magnification 4,400-fold, right electron micrograph 50,000-fold magnification. Scale bar left image 5µm, right image 0.2µm. **B**) TbEB1 defines the open ring-like structure of trypanosoma´s posterior end. Left electron micrograph magnification 7,000, right 50,000. Scale bar left image 2µm, right image 0.2µm.

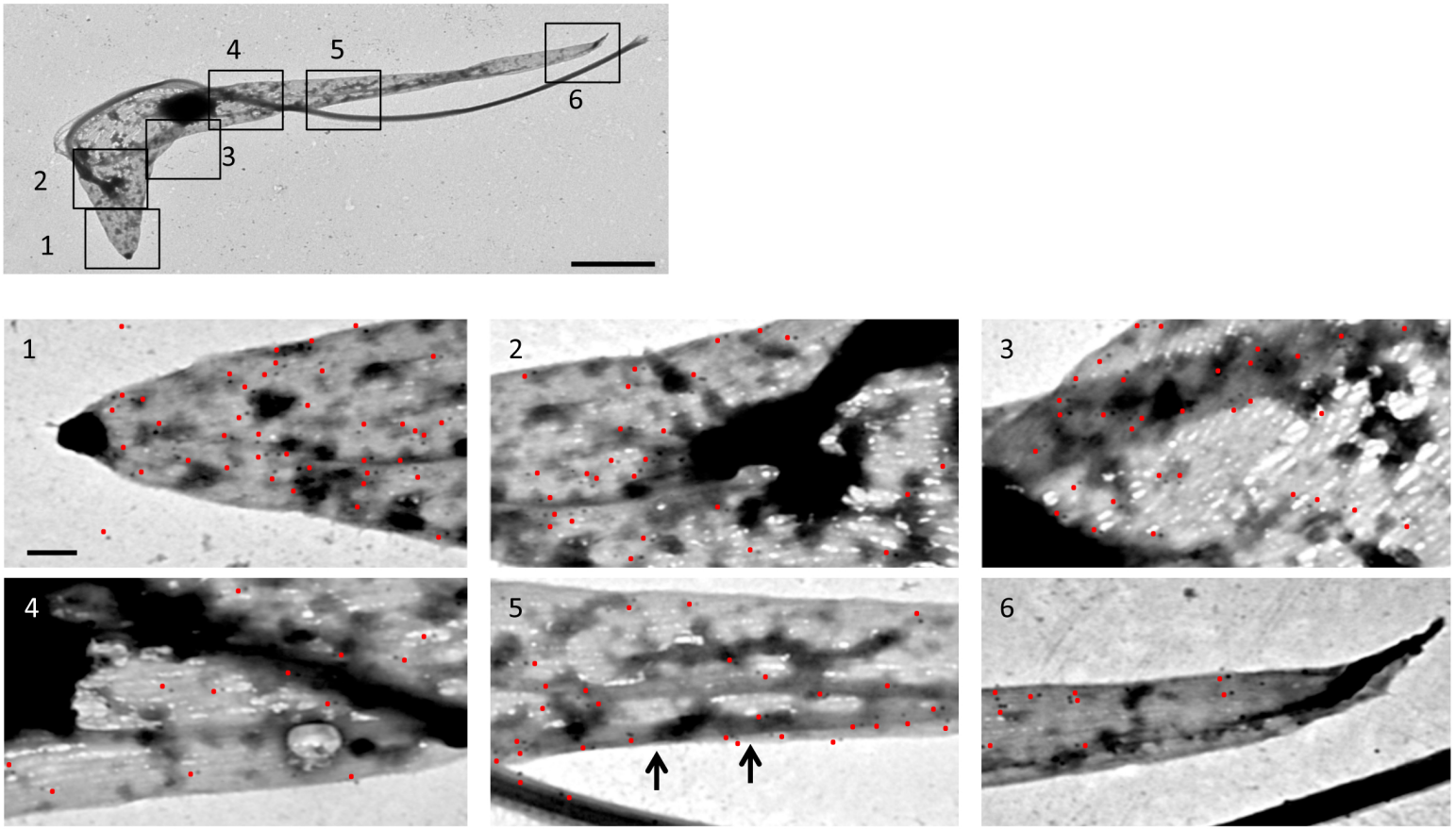


Figure 2.24: Gradient distribution of TbEB1 along the cell body. As the series demonstrates, the highest labeling density was found at the posterior cell pole. Labeling frequency diminished towards the anterior cell end. Compared to the subpellicular cytoskeleton, intense labeling of the FAZ region occurred, too (image 5, arrows). The electron micrograph series are magnifications at indicated locations of the upper image. Scale bar upper image 2µm, image series 0.2µm.

a circle (Fig. 2.23B) reflecting the open structure of the posterior microtubule bundle (Seebeck *et al.* , 1988). A series of electron micrographs along the posterior anterior axis emphasizes the gradient distribution of the protein in wild type trypanosomes starting at the posterior cell pole (Fig. 2.23C). Consistent with the FAZ labeling in IFA, a slightly higher density of TbEB1 was detected in that region compared to the density of the middle trypanosomal cell body. Only sporadic antibody labeling occurred at the flagellum. In general, immune labeling of TbEB1 at sub-micrometer resolution confirmed localization hot spots of immuno fluorescence assays.

2.3.4 The different detection methods for localization of TbEB1 demonstrated similar results and complemented each other in procyclic and bloodstream trypanosomes

Table 2.1: Summary of TbEB1 localization in procyclic (PCF) and bloodstream (BSF) trypanosomes according to the various detection methods. TbEB1 localization was investigated at the posterior cell pole (posterior), the subpellicular microtubule array (cytoskeleton), the flagellar attachment zone (FAZ), the spindle (spindle), and the cytoplasm (cytoplasm). N- (pNATN) and C- (pMOT, pNATC) terminal tagging of a TbEB1 allele as well as a specific monoclonal antibody anti-TbEB1 (Ab) identified endogenous TbEB1. OE states the localization of TbEB1 after over-expression of an ectopic copy of the protein. If evidence of TbEB1 localization was found on either whole cell preparations or detergent-extracted cytoskeletons, the localization was stated as positive (+), otherwise as negative (-). Negative/ positive (-/+) is referred to ambiguous results.

	PCF					BSF				
Localization	pNAT N	pMOT	pNAT C	Ab	OE	pNAT N	pMOT	pNAT C	Ab	OE
posterior	-	+	+	+	+	+	+	+	+	+
CSK	-	+	+	+	+	-	+	+	+	+
FAZ	-	-	+	+	+	-	+	+	+	+
spindle	-	-	-	-/+	+	-	-	-	-	-
cytoplasm	+	+	+	-	+	+	+	+	-	+

The variation of TbEB1 labeling pattern of the posterior cell pole in trypanosomes during the cell cycle was already described in literature using specific antibodies and N-terminal tagging of the

protein (Sheriff *et al.* , 2014; Spindler, 2014). Consistent with those data, TbEB1 was identified at the posterior cell pole in all approaches evaluating the protein distribution throughout the cell cycle. Additionally, evidence is given to a further localization in a punctate pattern at the cell body possibly in a posterior-to-anterior gradient, and to the FAZ region. A localization to the spindle is not likely in the light of current data. A summary of results for localization corresponding to the different detection approaches is given in table 2.1. TbEB1 localization results obtained by ectopic expression of the protein were included for a better comparison and complementary results obtained for endogenous TbEB1.

The localization was stated as positive (+) if evidence of TbEB1 localization was found on either whole cell preparations or detergent-extracted cytoskeletons. Negative (-) stated that neither in whole sample preparations nor on detergent-extracted cell lines TbEB1 was detectable.

2.4 Functional characterization of TbEB1

To investigate the function of TbEB1 on cell morphology and cytoskeleton dynamics, multiple approaches were used: RNA interference (RNAi) and gene deletion, ectopic over-expression, and transgenic expression in a mammalian cell line to analyze wether the localization or mode of action are conserved.

2.4.1 Establishment of TbEB1 RNAi cell lines

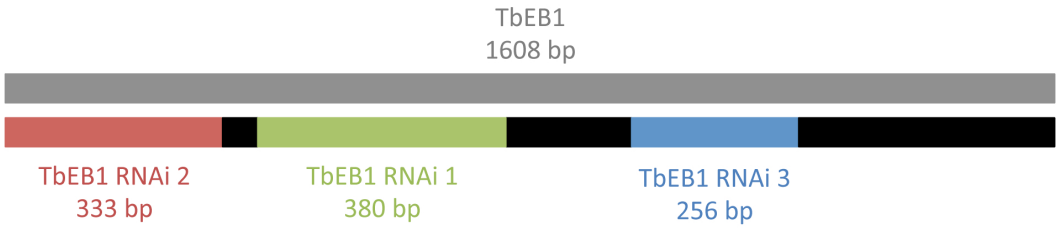


Figure 2.25: TbEB1 RNAi sequences within the TbEB1 gene used for generation of constructs. For the first construct, the sequence of TbEB1 RNAi 1 (green) was used. Afterwards, TbEB1 RNAi 2 (red) and 3 (blue) were created to cover the whole gene sequence of TbEB1. RNAi sequences 1-3 of TbEB1 were identified by trypanoFAN (Redmond *et al.* , 2003).

The function of TbEB1 was investigated using inducible RNAi knockdown constructs. The suggested part of the gene was confirmed to be specific for TbEB1 by BLAST analysis. It was cloned into the pALC14 plasmid resulting in a stem-loop mRNA construct when transcribed (Bochud-Allemann & Schneider, 2002). Stable integration of the plasmid into the trypanosomal genome is achieved after linearization of the construct within an rDNA homologous section

of the vector. siRNA transcription was controlled by a doxycycline-inducible TETrepressor-operator system (Wirtz *et al.* , 1999).

Three constructs directed against different regions of TbEB1 mRNA were tested (Fig. 2.25). However, only usage of construct 1 resulted in two procyclic RNAi cell lines with an obvious phenotype in cellular growth and morphology after the selection conditions had been slightly adapted. The fetal calf serum used for medium preparation had been exposed to sunlight for several days to reduce the levels of residual tetracyclin and the amount of preconditioned medium in the selection medium was increased from 20% to 50%. The cell lines are referred to as 29-13 TbEB1i and 449 TbEB1i.

A strong negative selection was observed in BSF S16 RNAi cell lines as only few clones with a low knockdown efficiency determined by qPCR were obtained. These clones quickly became refractive. The bloodstream cell line used for further RNAi experiments is referred to as S16 TbEB1i.

2.4.2 Depletion of TbEB1 led to severe growth defects in procyclic and bloodstream trypanosomes

Successful depletion of TbEB1 was investigated by qPCR and relative mRNA expression levels calculated by the $\Delta\Delta C_T$- method. The TERT gene was used as a reference gene transcript. Relative expression levels of induced cell lines were compared to non-induced counterparts and their corresponding native 449, 29-13, and S16 cell lines.

After 4 days of induction, qPCR revealed a considerable knockdown in 449 and 29-13 RNAi cell lines of about 90% and 80% (Fig. 2.26 A and B), respectively, compared to the parental wild type cell lines. However, both RNAi cell lines already demonstrated a reduced TbEB1 mRNA level of about 50% (449) and 25% (29-13) under non-induced conditions probably due to leakiness of the system. In addition, both cell lines demonstrated a severe growth defect after RNAi induction already after 48 hours. The growth deficiency of non-induced procyclic TbEB1 RNAi cell lines was more pronounced in the 449 TbEB1 RNAi cell line, which fits to the lower mRNA transcript levels determined by qPCR (Fig. 2.26 C and D).

Successful depletion of TbEB1 in procyclic cell lines was also confirmed by additionally introducing an endogenous c-myc tag at the C-terminus of one TbEB1 allele via homologous recombination into the RNAi cell lines 449 TbEB1i and 29-13 TbEB1i. The obtained cell lines are referred to as 449 TbEB1i pNAT$^{\text{C-12xmyc}}$ and 29-13 TbEB1i pNAT$^{\text{C-12xmyc}}$, respectively. The decrease of the c-myc-signal would allow to track the degradation of the tagged TbEB1 on protein level and to demonstrate that RNAi is working efficiently. IFA and Western blot analysis confirmed successful depletion of TbEB1$^{\text{C-12xmyc}}$ (Fig. 2.27, 2.28). Occasionally, the reduction of the myc-tag labeling was also observed in control samples, which had not been induced. This

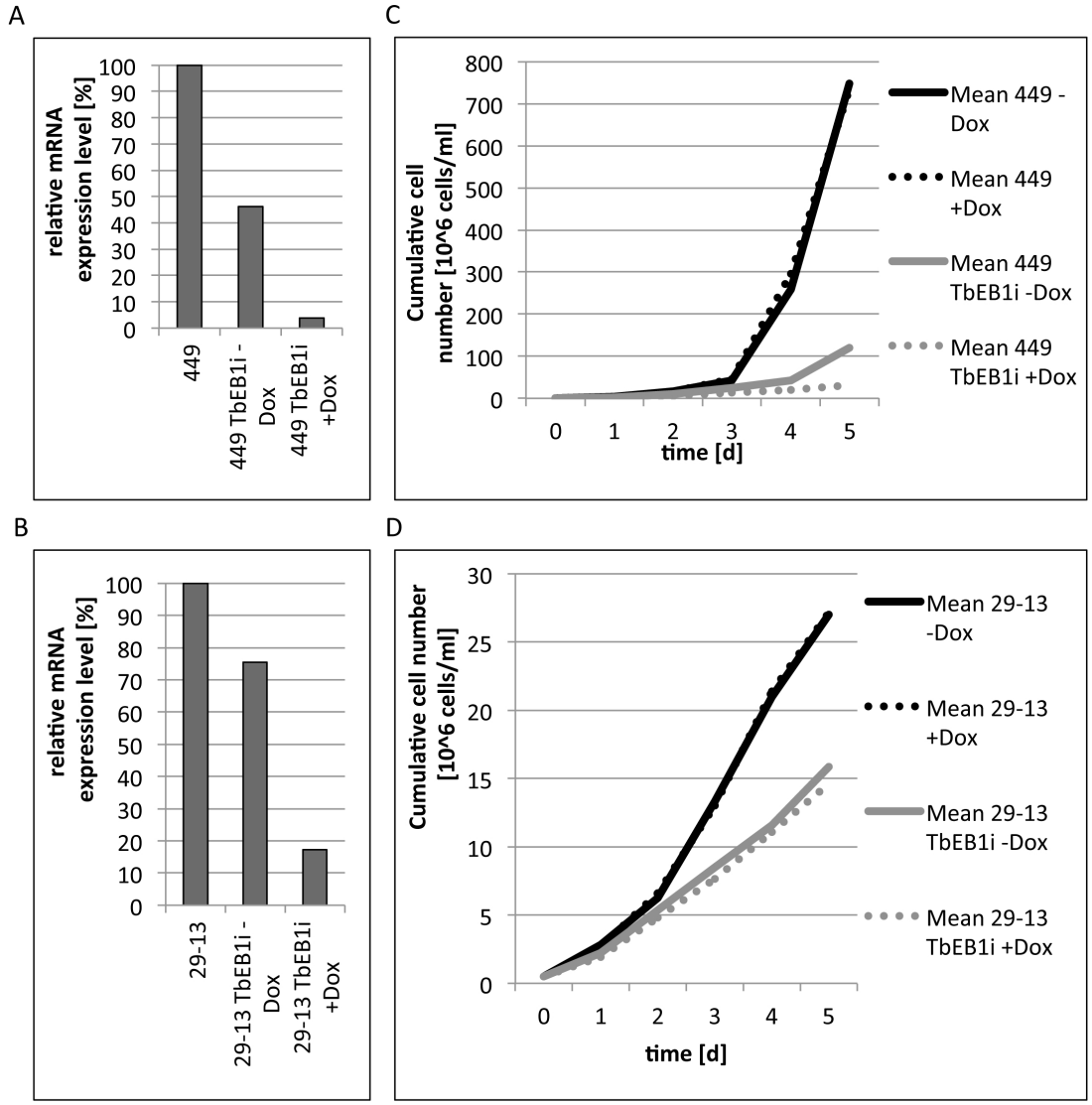


Figure 2.26: Relative mRNA expression levels in procyclic (449, 29-13) trypanosomes after TbEB1 knockdown and growth curves. **A**) Non-induced (-Dox) TbEB1 procyclic cell line 449 demonstrated a decreased TbEB1 level of about 46%, whereas knockdown (+Dox) reduced mRNA levels to about 3% after 4 days. **B**) Non-induced (- Dox) TbEB1i procyclic cell line 29-13 demonstrated already a reduced TbEB1 mRNA level of 75% compared to wild type 29-13 due to the leaky vector system. After RNAi onset (29-13 TbEB1i +Dox), mRNA levels are further reduced to about 17% on day 4. Growth curve in the absence (-Dox) and presence (+Dox) of doxycycline of a representative TbEB1 RNAi knockdown cell line and the corresponding wild type 449 (**C**) or 29-13 (**D**) for procyclic RNAi cell lines. Both approaches started with $5*10^5$ cells per ml. Cultures were diluted at several time points to maintain a steadily growing culture. Dilution factors were taken into account and cumulative cell numbers are reported.

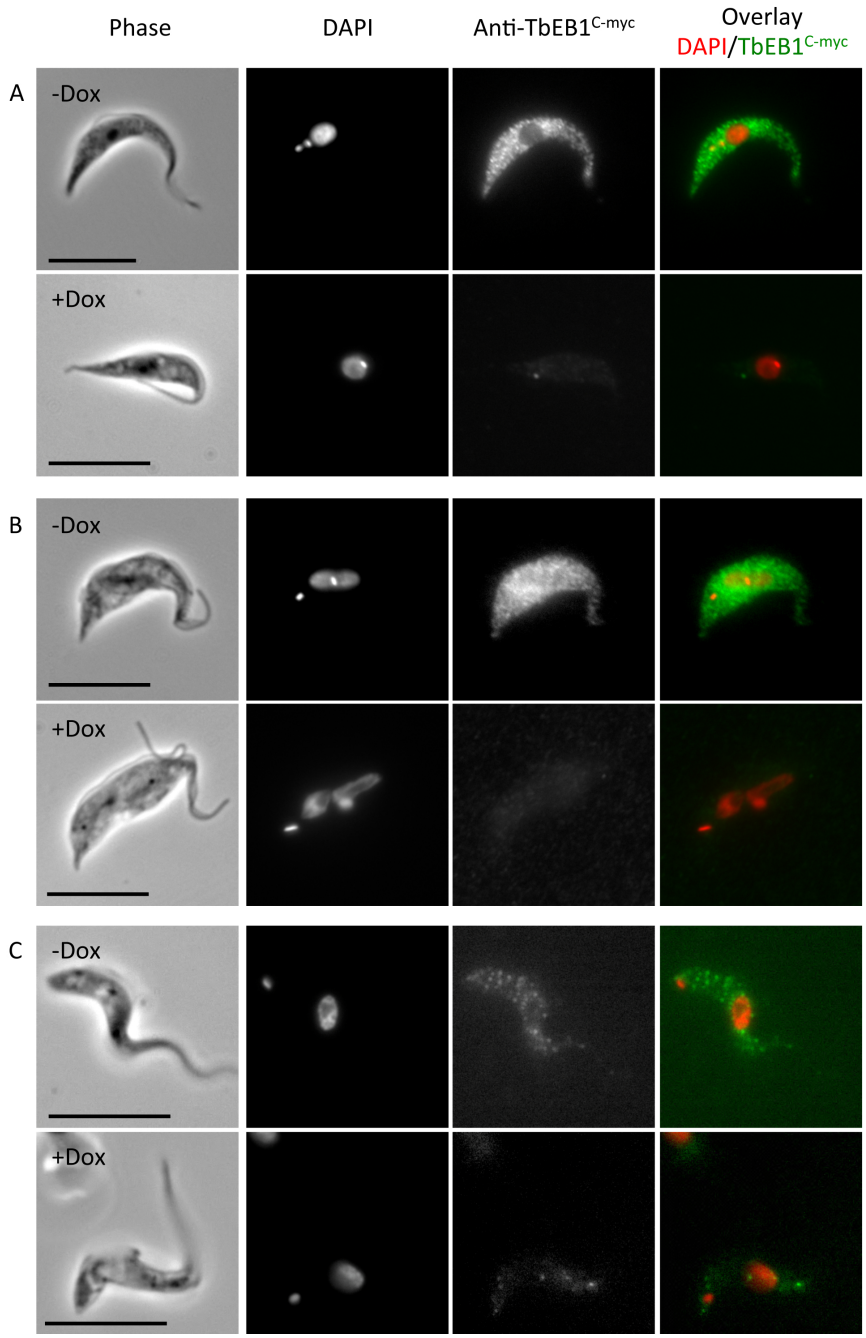


Figure 2.27: Confirmation of successful depletion of TbEB1 by RNAi in the procyclic RNAi-cell lines 449 TbEB1i pNAT$^{C\text{-}12xmyc}$ (A), 29-13 TbEB1 RNAi pNAT$^{C\text{-}12xmyc}$ (B), and the bloodstream cell line S16 TbEB1i pMOT$^{C\text{-}3xmyc}$ (C) on whole cells. After three (449, S16) or four (29-13) days of TbEB1 knockdown, a decreased signal intensity of the endogenously tagged protein was observed in many cells. Scale bars represent 10µm.

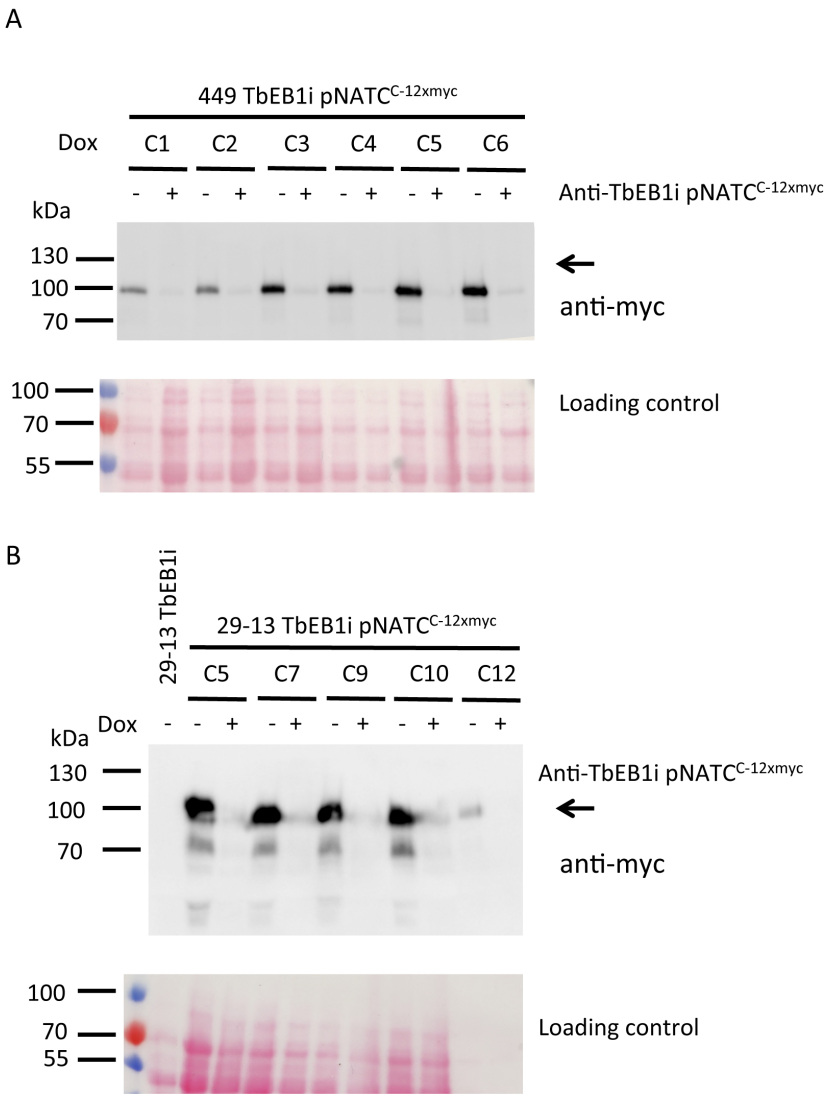


Figure 2.28: Western blot based confirmation of successful TbEB1 RNAi-mediated knock-down in procyclic trypanosomes using cell lines combining RNAi and an endogenously C-terminally c-myc-tagged allele of TbEB1 gene. $6*10^6$ cells were loaded per lane for all cell lines (except the samples of 29-13 TbEB1i pNAT$^{C\text{-}12xmyc}$ Clone 12). Tagged proteins were detected primarily by mouse monoclonal anti-c-myc antibody (9E10), followed by an anti-mouse antibody conjugated with HRP. Ponceau S-stained immuno blot membranes were used as loading control. siRNA expression was induced by media supplementation with 1µg/ml doxycycline for 3 days in 449 derived cell lines (**A**) and for 4 days in of 29-13 derived cell lines (**B**). All procyclic cell lines demonstrated a strong reduction of TbEB1$^{C\text{-}myc}$ signal after the respective incubation period (+Dox) compared to non-treated (-Dox) samples (A, B).

was attributed to the leakiness of the RNAi system. Similarly, atypical cell cycle stages due to the tag itself as described earlier (see 2.3.1.2) had also been found in these samples.

Only few TbEB1 RNAi-clones were obtained in bloodstream trypanosomes. The clones had been induced for 4 days and examined by light microscopy. That one demonstrating the strongest phenotype was further evaluated. Growth curve suggested a fast escape from RNAi (Fig 2.29 A, B). qPCR analysis confirmed that the highest knockdown rate was obtained on day 3 of TbEB1 depletion (Fig. 2.29 C). Compared to wild type and non-induced cells, TbEB1 levels were reduced about 66%. That reduction is normally considered too low when screening for an effective RNAi cell line (Klaster, 2013). Nonetheless, that modest reduction had already severe effects on growth and K/ N ratios of trypanosomes (Fig2.29 A, B) supporting the hypothesis that TbEB1 knockdown clones undergo negative selection. qPCR results further demonstrated that cellular TbEB1 levels already increased on day 4 indicating an escape from RNAi (Fig. 2.29 C). qPCR analysis was confirmed by immuno blot analysis of RNAi clones containing an endogenously c-myc-tagged TbEB1 allele. For this, an endogenous TbEB1 allele was additionally C-terminally c-myc-tagged in the RNAi cell line. One clone was further investigated and is referred to as S16 TbEB1i pMOT$^{\text{C-3xmyc}}$. After three days of induction, the signal intensity of TbEB1$^{\text{C-3xmyc}}$ in S16 TbEB1i pMOT$^{\text{C-3xmyc}}$ cells decreased efficiently compared to the non-induced sample (Fig. 2.27). Consistent with qPCR results (Fig. 2.30), levels of tagged TbEB1 fall beyond detection limit on day 2 of TbEB1 knockdown but again on day 4, tagged TbEB1 was traced in induced samples of most clones. Microscopic analysis of those samples also lacked the atypical cell cycle stages. Hence, for following experiments, only samples up to day 3 were evaluated when no RNAi escape had taken place, yet.

Summing up, TbEB1 was successfully depleted in PCF and BSF but only the 449 TbEB1i RNAi cell line demonstrated an effective knockdown. The low number of obtained clones and the fast escape from RNAi suggest TbEB1 as an essential protein.

2.4.3 TbEB1 knockdown resulted in an accumulation of atypical cell cycle stages suggesting an impaired cytokinesis

To further investigate the delay in cell growth, the morphology and cell cycle dynamics of trypanosomes were examined on day 1 to 5 post induction for PCF and on day 1 to 3 for BSF. The arrangement of the trypanosomal DNA in nucleus and kinetoplast can be used for a categorization of cells cycle stages and determination of their abundance (Woodward & Gull, 1990). A cell was classified as multi-nucleated if the number of nuclei or kinetoplasts exceeded two. 100 cells were counted for each time point.

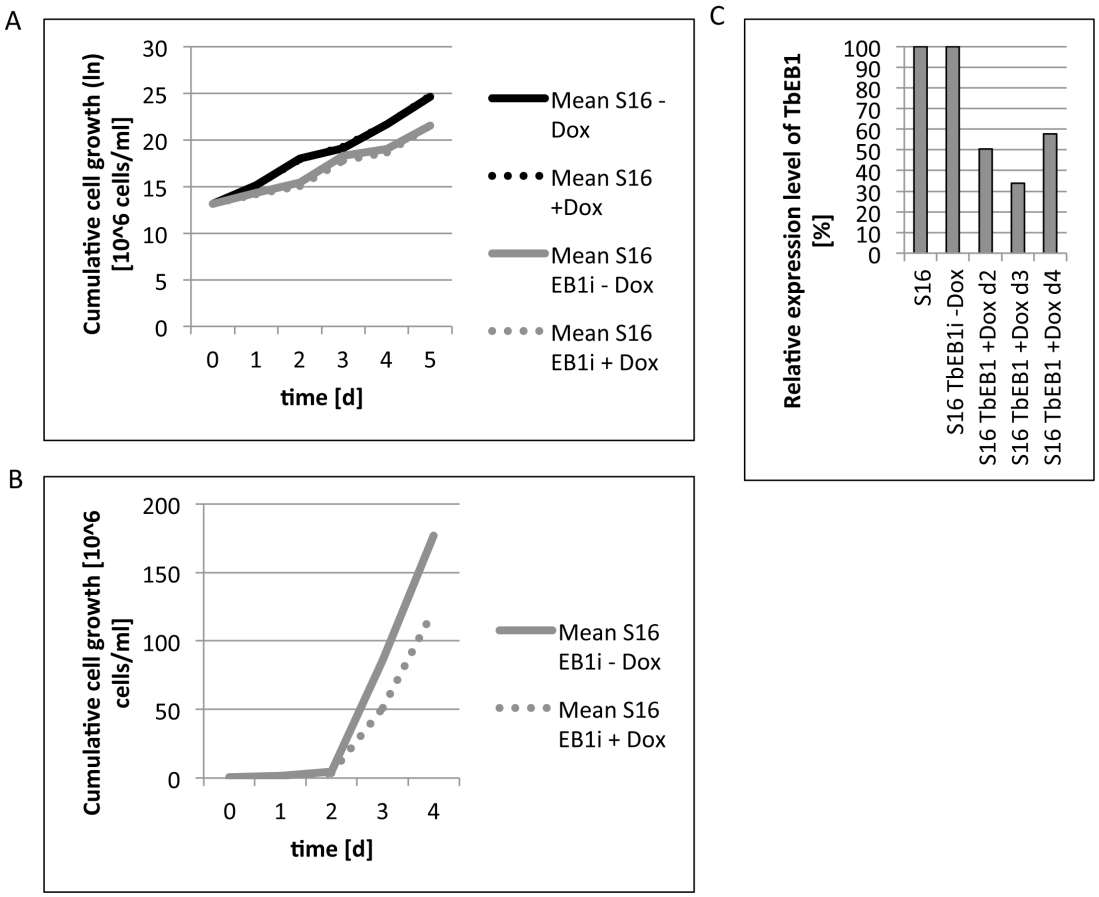


Figure 2.29: Cell growth and TbEB1 expression levels of RNAi and wild type cell line in bloodstream trypanosomes. **A**) Growth curve in the absence (-Dox) and presence (+Dox) of doxycycline of a representative TbEB1 RNAi knockdown cell line and the corresponding wild type S16. Starting cell density was $5*10^5$ cells per ml. Cultures were diluted at several time points to maintain a steadily growing culture. Dilution factors were taken into account and cumulative cell numbers were reported. **B**) Non-induced and induced TbEB1 RNAi cell lines of A) are plotted separately to demonstrate the growth retardation between both samples. **C**) Relative mRNA expression levels in bloodstream (S16) trypanosomes after TbEB1 knockdown for four days. The non-induced (-Dox) bloodstream TbEB1i showed no significant reduction compared to wild type S16. In treated samples TbEB1 mRNA levels decreased to a minimum of about 33% on day 3. TbEB1 expression increased again on day 4 indicating an escape from RNAi.

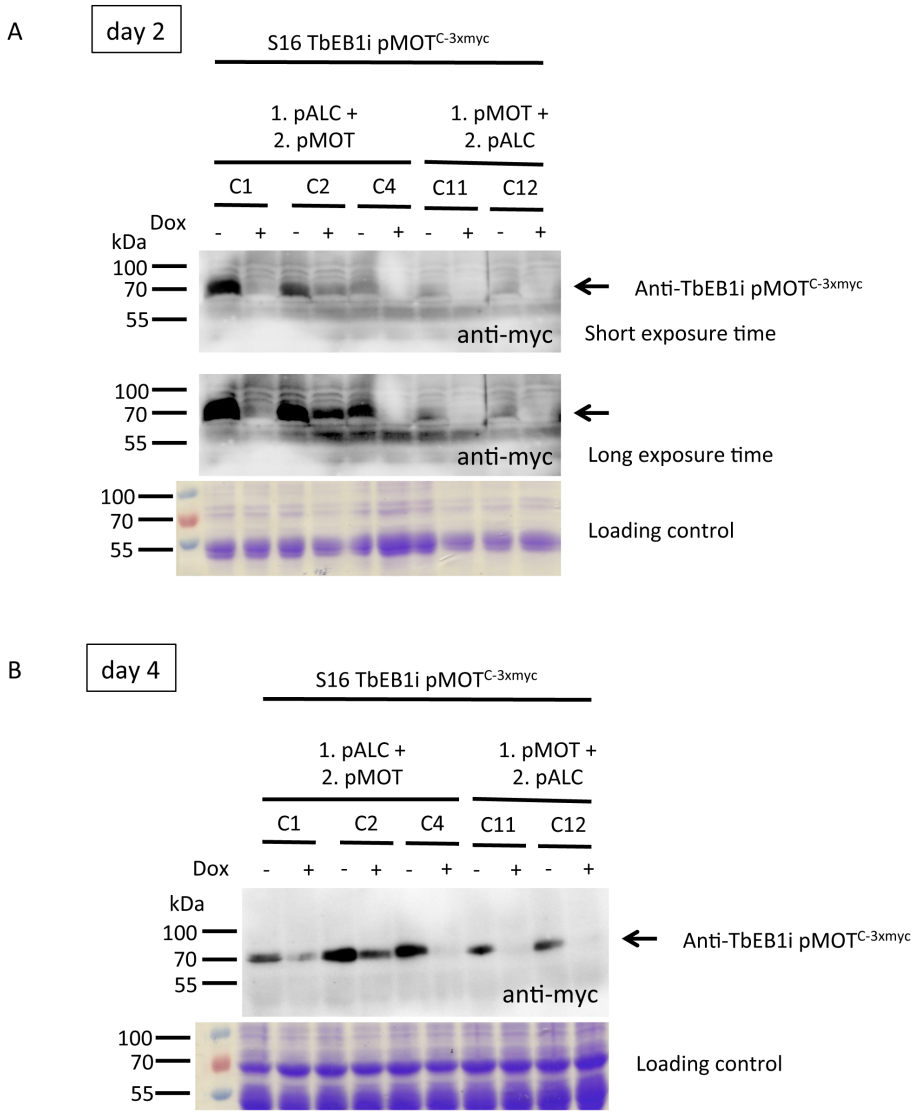


Figure 2.30: Western blot based confirmation of successful TbEB1 RNAi-mediated knock-down in bloodstream trypanosomes using cell lines combining RNAi and an endogenously C-terminally c-myc-tagged allele of TbEB1 gene. $6*10^6$ cells were loaded per lane. Tagged proteins were detected primarily by mouse monoclonal anti-c-myc antibody, followed by an anti-mouse antibody conjugated with HRP. Coomassie-stained SDS-gels were used as loading controls. RNAi expression was induced by media supplementation with 1µg/ml doxycycline for 2 (**A**) or 4 (**B**) days. Bloodstream cell lines demonstrated a decreased TbEB$^{C\text{-}3xmyc}$ level already on day 2 (A). Clone 1 and 2 started to grow resistant to RNAi on day 4 (B).

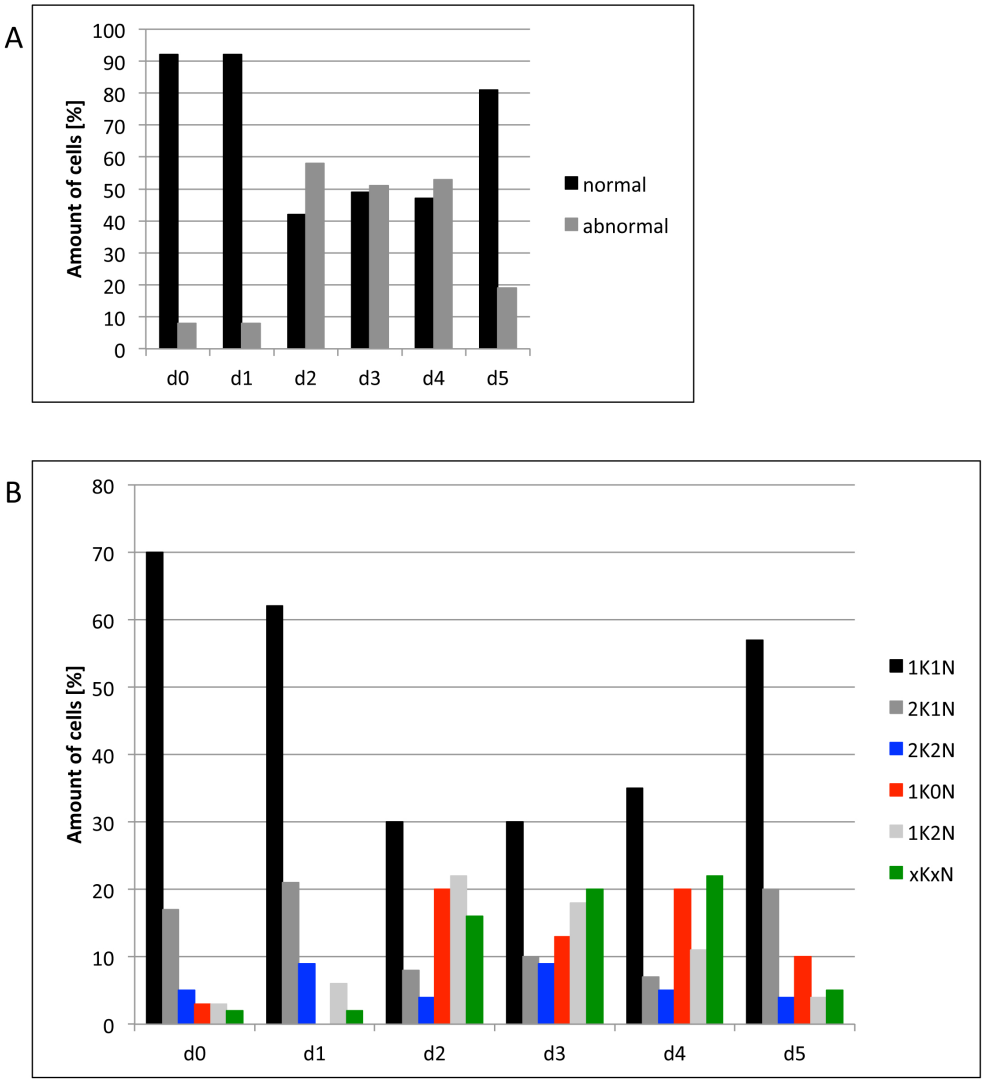


Figure 2.31: RNAi-mediated knockdown of TbEB1 in 449 TbEB1i resulted in an accumulation of zoids (1K0N), 1K2N, and multi-nucleated cells indicating an impeded cytokinesis. **A**) Summary and **B**) detailed mapping of cell cycle stages occurring in 449-derived TbEB1 RNAi cell line. Cell cycle stages were counted during TbEB1 knockdown for 5 days. Cells were categorized by DAPI-stained trypanosomal DNA and counted as multinuclear if the cell possessed more than two nuclei. 100 cells were counted per time point.

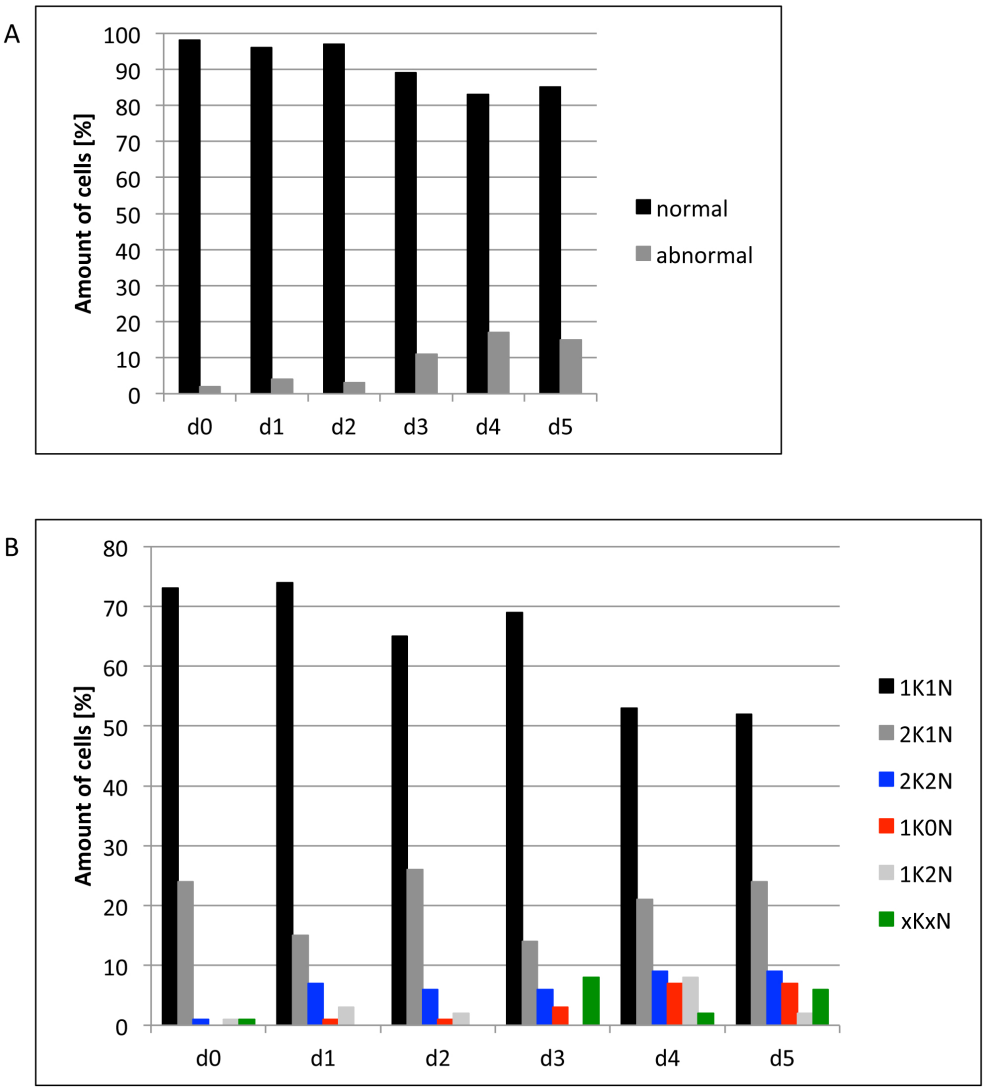


Figure 2.32: RNAi-mediated knockdown of TbEB1 in 29-13 TbEB1 RNAi cells resulted in an accumulation of zoids (1K0N), 1K2N, and multi-nucleated cells indicating an impeded cytokinesis. **A**) Summary and **B**) detailed mapping of cell cycle stages occurring in 29-13-derived TbEB1 RNAi cell line. Cell cycle stages were counted during TbEB1 knockdown for 5 days. Cells were categorized by DAPI-stained trypanosomal DNA and counted as multinuclear if the cell possessed more than two nuclei. 100 cells were counted per time point.

1K2N and multi-nucleated cells were already detectable in low frequencies after 24 hours of induction in both procyclic RNAi cell lines and values were quite similar to those of the non-induced populations, indicating background induction (Fig. 2.31 and Fig. 2.32). 2 days p. i., the amount of anuclear (zoids, 1K0N), 1K2N, and multi-nucleated cells increased dramatically to about 60% in the 449-derived TbEB1 RNAi cell line with 1K2N cells being the prevalent abnormal stage on day 2, which switched to the multi-nucleated type from day 3 on (Fig. 2.31A, B). Occurrence of abnormal cell cycle stages decreased to 20% in that cell line on day 5. The amount of unusual cell types was less pronounced in the 29-13-derived cell line during all days and rose to a steady level of 30% (Fig. 2.32A). The amount of anuclear cells is mostly equivalent to the amount of either 1K2N cells or multi-nucleated ones suggesting an impaired cytokinesis (Fig. 2.31B, 2.32B). Figure 2.33 and 2.34 show typical phenotypes of PCF evolving during progress of TbEB1 depletion. At the beginning, frequently 1K2N or 2K4N cells can be detected (Fig. 2.33B, E). Especially in the case of 1K2N cells, the time point during which TbEB1 depletion effectively started seemed to affect basal body segregation processes and dynamics as 2N cells with a mispositioned kinetoplast possessed either 1K, $1K_{div}$ or 2K. Thus after mitosis, this resulted in a localization of the kinetoplast/s between the two nuclei (Fig. 2.33C). The mispositioning of basal body/ kinetoplast system was more obvious in the 29-13 derived TbEB1 RNAi cell line. For the early depletion period, the detached flagellum was attributed to the newly generated daughter flagellum in all cases as it was positioned closer to the posterior end (Fig. 2.33 C-E). Mitosis was still on-going in TbEB1 depleted cells until cells were heavily crowded with nuclei. Nuclei entered mitotic processes often simultaneously (Fig. 2.33D). However, duplication of the kinetoplast/ basal body complex seemed to be hampered because in densely packed cells the number of nuclei was higher than those of kinetoplasts (Fig. 2.34B-D). Initially, the overall cell morphology was not altered, but after a few days several trypanosomes became rounded (Fig. 2.34C-E). Especially during the first days of TbEB1 knockdown, cells with an extremely elongated posterior cell end and aberrant K/ N ratio were observed. The high numbers of zoids, 1K2N, and multi-nucleated cells point towards a deregulation of the cell cycle (Fig. 2.35). 1K2N cells and zoids were division products of multi-nucleated cells. The 1K2N were the preferred split product for both 2K2N and 2K4N cells while 1K0N were frequently detected in dividing 2K2N cells and those with more than four nuclei (Fig. 2.35 A, B). That multi-nucleated cell class gave also rise to other abnormal K/ N ratios (Fig. 2.35 C, D). Particularly after day 4 of TbEB1 depletion, single cases of dividing cells densely packed with nuclei also raised the impression that more than one division occurred at once (Fig. 2.35 E, F) resulting in daughter cells with varying K/ N ratios. Frequently, abnormal cell division also seemed to be connected with the observed anterior/intermediate localization of the kinetoplast relative to the nucleus/ nuclei. Furthermore, obtained zoids were extremely slim indicating that possibly no or

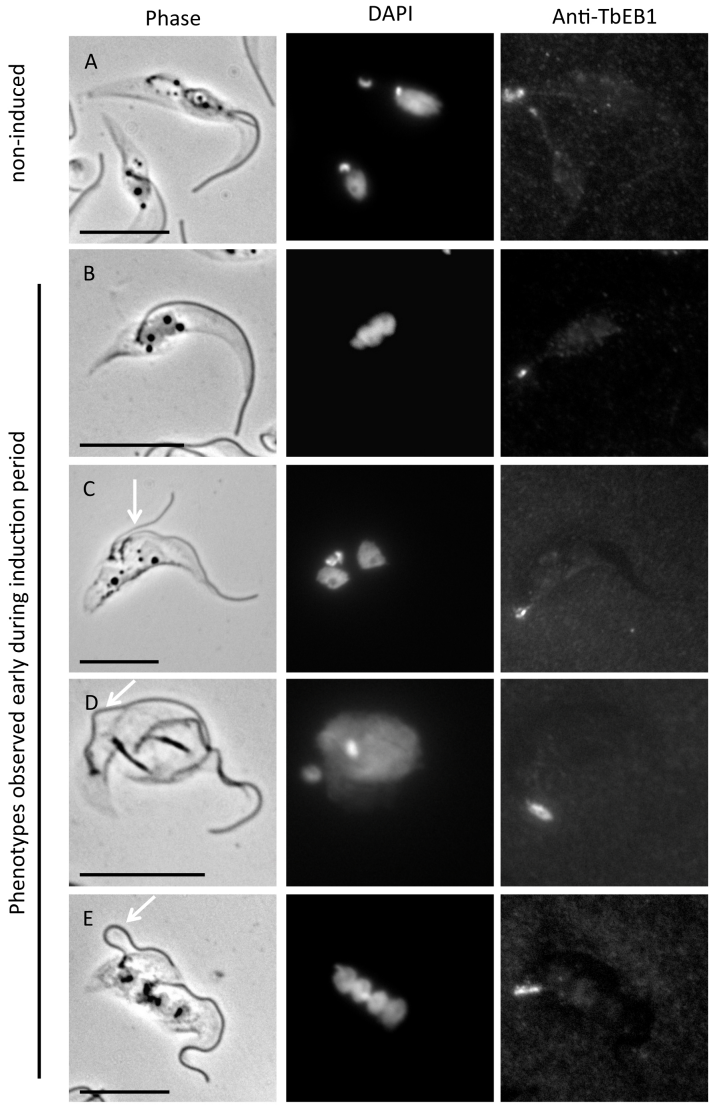


Figure 2.33: Examples of observed phenotypes during early TbEB1 depletion (up to day 3). TbEB1 was depleted for up to 5 days in procyclic cells. The RNAi mechanism was induced by addition of 1µg/ml doxycycline to cell culture media and samples taken every 24h for up to 5 days. **A)** Non-induced cells with 1K1N and 2K1N demonstrating the typical TbEB1 staining at the posterior cell pole were taken as reference for labeling intensity. **B-E)** During the first days (up to d3), knockdown of TbEB1 resulted in an accumulation of 1K2N (B) and multi-nucleated cells (D, E) as well as zoids (1K0N) indicating an impeded cytokinesis. In some cases, a segregation of the kinetoplast/ basal body complex seemed to be still possible (C), however, this was often delayed finally resulting in a surplus of nuclei. A decrease of TbEB1 signal at the posterior was rarely observed. The morphology of affected cells still resembled those of wild type cells except the high frequency of detached flagella (arrow). Scale bars represent 10µm.

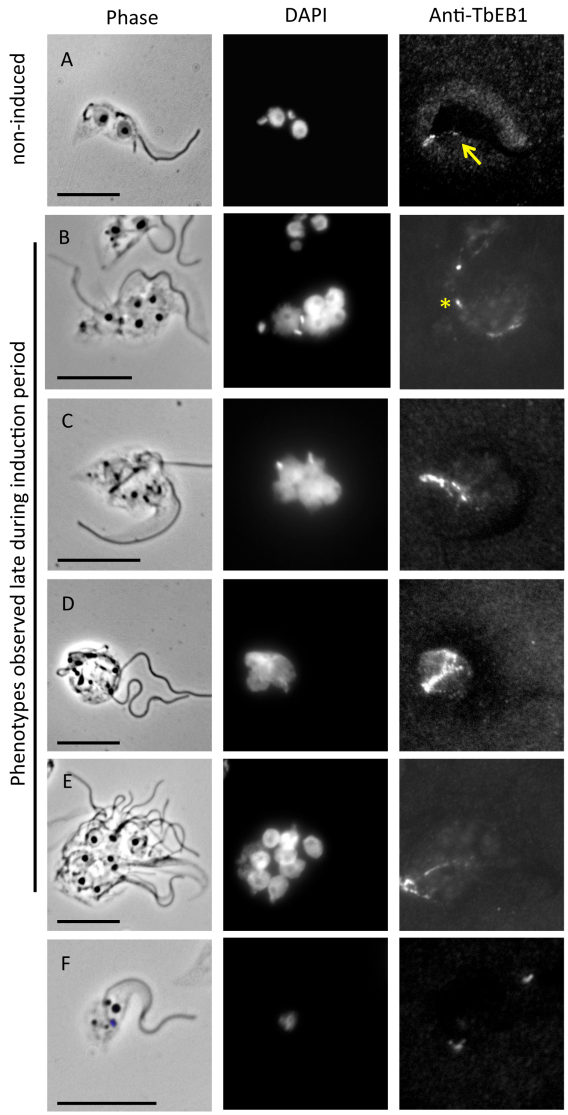


Figure 2.34: Examples of observed phenotypes during late TbEB1 depletion (after day 3). TbEB1 was depleted for up to 5 days in procyclic cells. The RNAi mechanism was induced by addition of 1µg/ml doxycycline to cell culture media and samples taken every 24h for up to 5 days. **A)** Non-induced cells with 2K2N demonstrating the typical TbEB1 staining at the posterior cell pole were taken as reference for labeling intensity. **B-F)** With progressing TbEB1 knockdown (after d3), only some cells demonstrated a reduced TbEB1 signal at the posterior cell pole (B). In most cells, TbEB1 still localized to the posterior cell pole as well as along the ingression furrow with an increased signal intensity (C-E). Though, many affected cells lost the typical trypanosomal morphology and gained a round shape (D, E). These cells often possessed a shifted TbEB1 signal to the middle of the cell body which indicates where the former posterior end now was located. Furthermore, the number of nuclei within one cell had increased producing cells completely crowded with the organelle (E). The resulting tension on the cytoskeleton may lead to an atypical cell division resulting in zoids (F). The arrow indicates the posterior end of the old flagellum daughter cells. The star marks the possible division of a zoid from the multi-nucleated cell. Scale bars indicate 10µm.

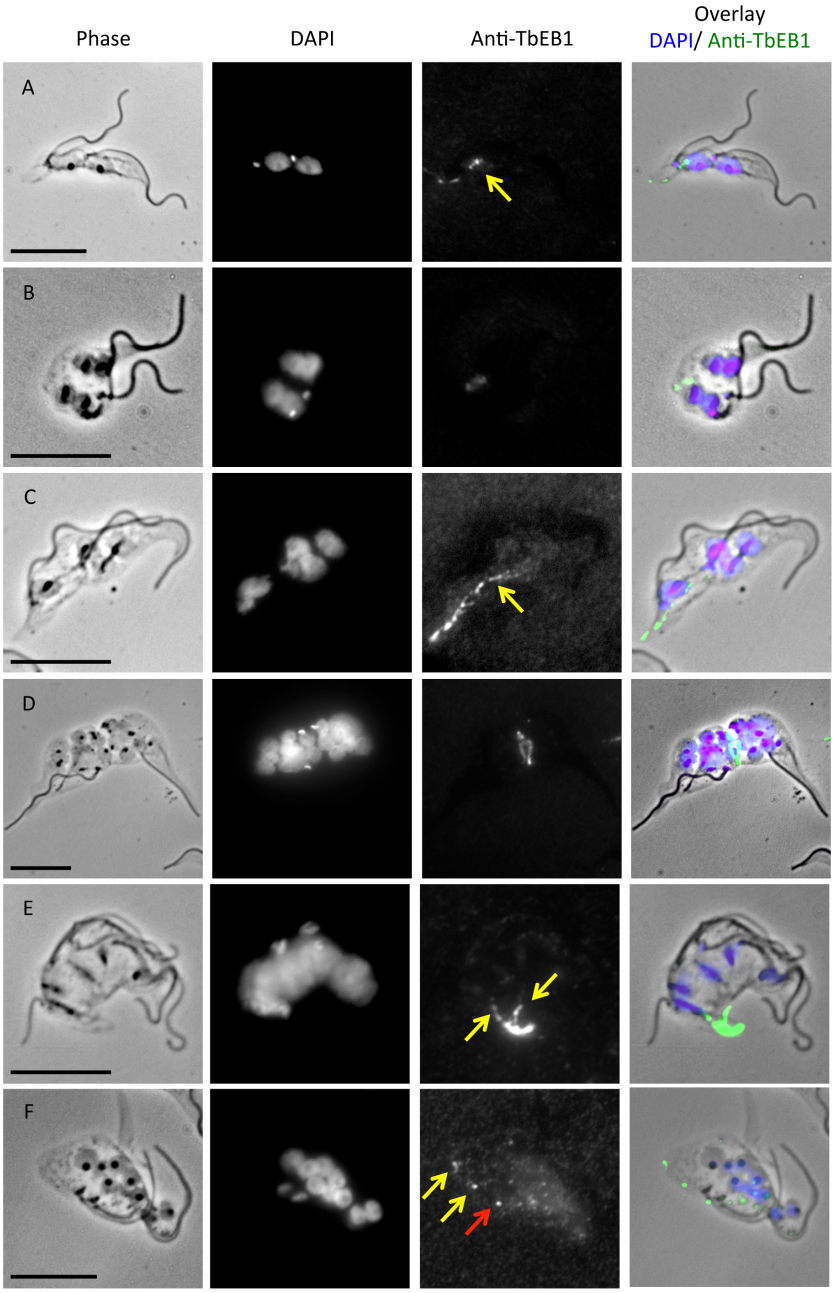


Figure 2.35: Different events of an impeded cytokinesis observed in procyclic TbEB1 RNAi cell lines. A) Cell division of a 2K2N cell with 1K0N and 1K2N (mispositioned kinetoplast) as possible end products. **B**) Example of a 2K4N cell probably resulting in two 1K2Ns, again with a mispositioned kinetoplast. **C-D**) Dividing multi-nucleated cells resulting in xKxN daughter cells. **E-F**) More than one division furrow seemed to occur at the posterior cell pole while mitosis still occurred. Yellow arrows point towards posterior ends, the red one indicated the beginning separation of a zoid from the xKxN cell. The line indicates the putative division furrow.

low amplification of microtubules occurred before cell division. A fact, which was supported by 1K1N cells with reduced size and/ or shortened flagella arising particularly during the last days of the 5-days induction period. Although TbEB1 was depleted, cytokinesis still occurred in the described anterior-to-posterior direction. Therefore, depletion of TbEB1 seems not to prevent cytokinesis completely.

Due to the low knockdown efficiency of TbEB1 in bloodstream forms, the effects were less pronounced than in procyclic forms. Abnormal cell cycle stages reached a maximum of 14% on day 2, with zoids (1K0N) being the most common atypical form (Fig. 2.36). Small numbers of 1K2N or xKxN cells were detected, too. Again, those abnormal stages give evidence for a hampered cell division. Compared to PCF, high amounts of dead and lysed cells were found, too, confirming the high lethality observed in growth assays due to TbEB1 depletion. The observed phenotypes were similar to PCF: abnormal K/ N-ratios, zoids, and a misguided cytokinesis (Fig. 2.37). The number of kinetoplasts was not mandatorily lower than those of nuclei as it was the case in procyclics. Additionally, in bloodstream trypanosomes mostly a maximum of only four nuclei was counted. Compared to procyclics, the most evident morphological change had been detached flagella. In BSF, the high number of zoids arising in TbEB1 depleted bloodstream cultures, also hinted to a deregulation of cytokinesis. Most zoids were descendants of 2K2N cells (Fig. 2.38 A). However, tetrads (4K4N) also pointed towards a misguided cytokinesis. Those 4K4N are suggested to divide either as 2 times 2K2N or 4 times 1K1N (Wheeler *et al.* , 2013). In figure 2.38 B, the tetrad divides in a 1K2N and a 3K2N cell. 2K4N or 3K4N cells were compared to tetrads due to the number of nuclei. Again, depending on cleavage furrow positioning and number of kinetoplasts/ nuclei, those descendants varied in K/ N ratio and demonstrated a mislocalized kinetoplast as observed for PCF.

For both life cycle stages, the amount of atypical cell cycle stages increased after TbEB1 depletion. The impeded cytokinesis was observed for PCF and BSF in IFAs.

2.4.4 TbEB1 was localized near the posterior part of the division furrow similar to wild type cells but position and foci number varied

As long as the cell sustained an elongated morphology (Fig. 2.35 A, C), the distribution of TbEB1 along the posterior part of the division furrow resembled that of the wild type even though multi-nucleated cells had a longer one, often going along with an increased intensity of TbEB1 staining. If the cell shape was rounded (Fig. 2.35 B, D), the extended TbEB1 signal of dividing cells was gradually repositioned in the middle of the cell compared to the "bottom" position in wild type cells. Finally with approaching abscission, those round, multi-nucleated procyclics demonstrated a dividing configuration generally observed for bloodstream trypanosomes. During the complete knockdown period, single cases of multi-nucleated cells

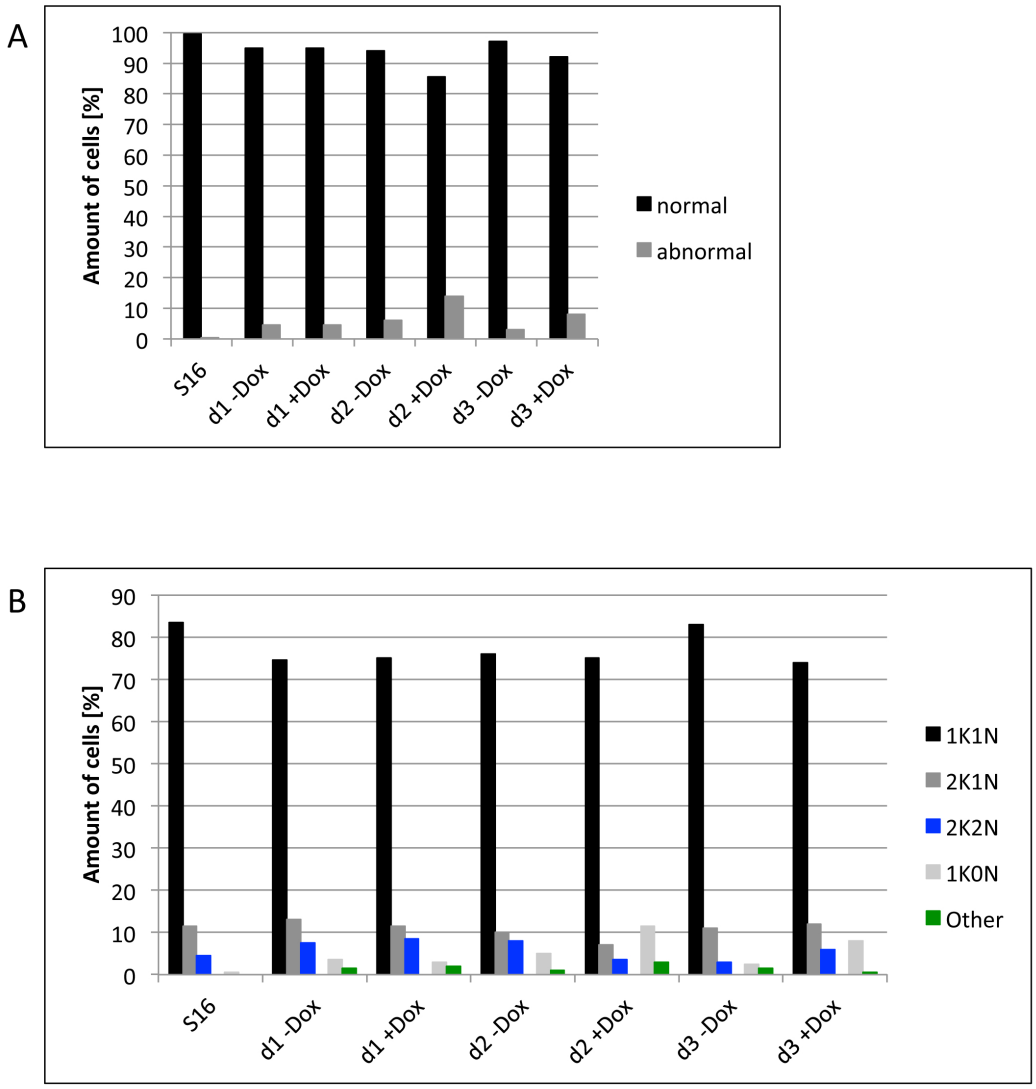


Figure 2.36: RNAi-mediated knockdown of TbEB1 results in an accumulation of zoids (1K0N) and multi-nucleated cells indicating an impeded cytokinesis in S16 derived RNAi cell lines. Cells were categorized by DAPI-stained trypanosomal DNA and counted as multinuclear if the cell possessed more than two nuclei or kinetoplasts. 100 cells were counted per time point. S16-derived TbEB1 RNAi cell lines demonstrated atypical K/ N ratios during the induction time with up to about 15% affected cells. The difference to procyclic cell lines is probably due to the higher mortality of affected bloodstream trypanosomes.

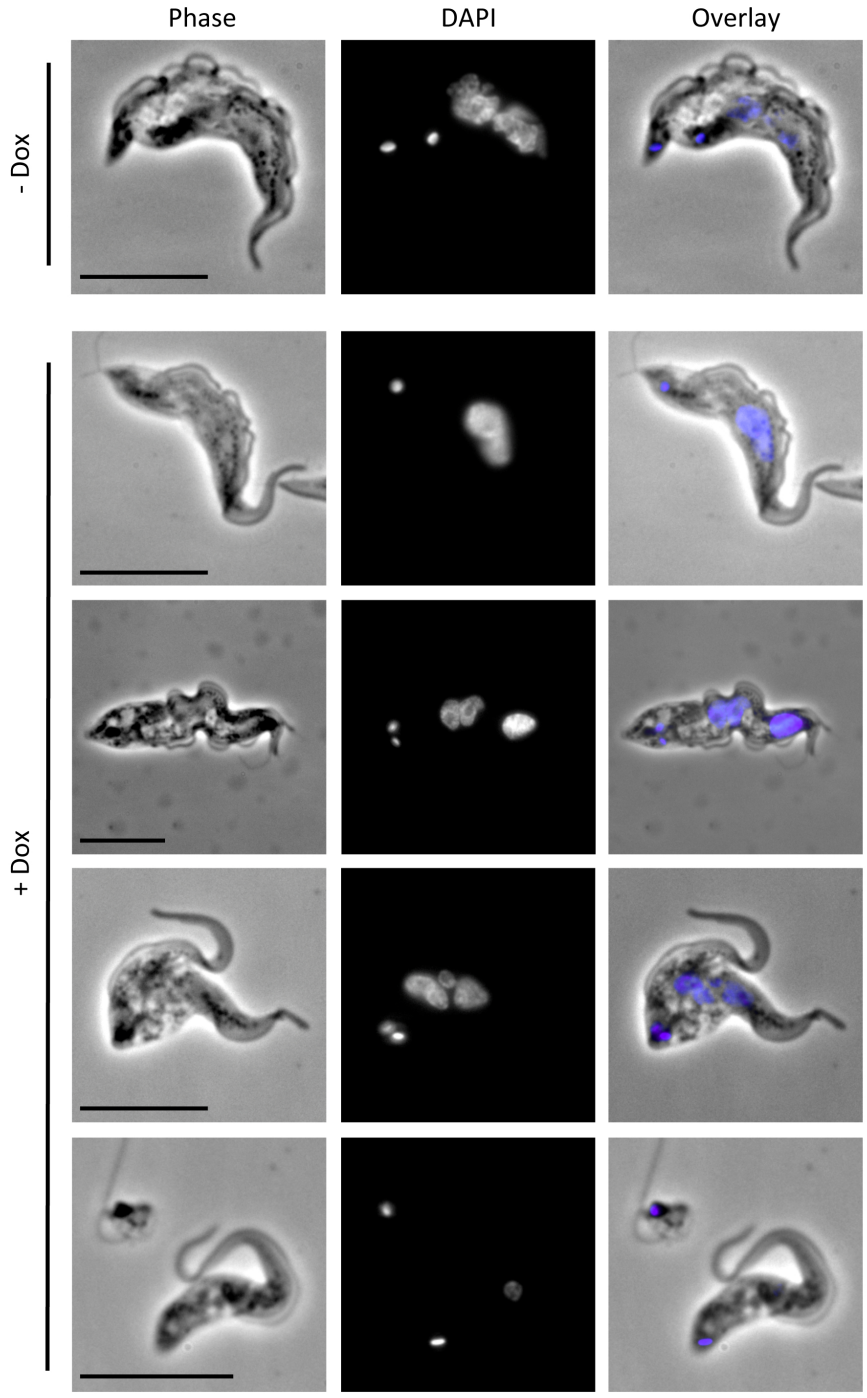


Figure 2.37: TbEB1 depletion results in abnormal K/ N ratios in the S16 derived RNAi cell line. The bloodstream TbEB1 RNAi cell line was cultivated in the absence (-Dox) and presence (+Dox) of 1µg/ml doxycycline for 3 days. Accumulation of 1K2N, xKxN, and zoids was detectable as indicators of an impeded cytokinesis. Single cells with a small nucleus were detected occasionally. Whole cell preparations were fixed with 3.7% FA. Trypanosomal DNA was stained with DAPI. Scale bars represent 10µm.

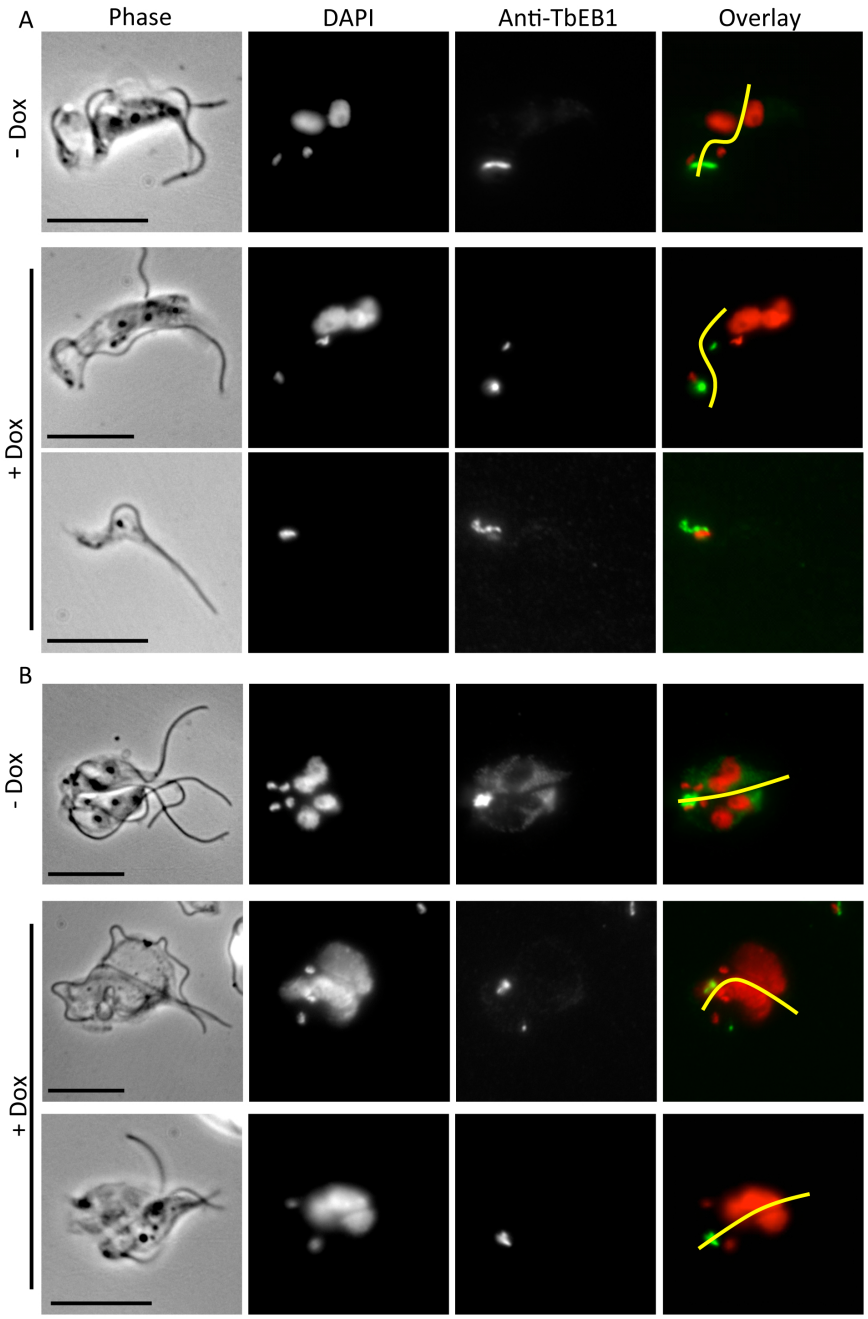


Figure 2.38: Similar to PCF, depletion of TbEB1 caused an impeded cytokinesis in BSF RNAi cell lines. A) Example of an abnormal cytokinesis in 2K2N cells. The upper panel demonstrates the cell division of a normal 2K2N cell. The middle panel demonstrates an impeded cell division with a zoid daughter cell (lower panel). **B**) Examples of an abnormal cytokinesis in cells resembling the tetrad form. The upper panel demonstrates a typical division of a tetrade (4K4N) while the other two panels demonstrate a malfunctioning cytokinesis of this cell type. The putative division furrow is indicated by a yellow line. Cells were detergent-extracted with 0.5% NP-40 for 1 minute at room temperature. Scale bars represent 10µm.

with up to two elongated TbEB1 staining patterns were detected, both arising from the same posterior end (Fig. 2.35 E) as well as cells with more TbEB1 spots at the posterior cell body suggesting a surplus of posterior ends (Fig. 2.35 F). This could be the origin for the additional cleavage furrows. In BSF trypanosomes the labeling of TbEB1 near the cleavage furrow was less pronounced than in procyclics due to a different mode of cell division (Wheeler *et al.* , 2013).

In PCF, the distribution of TbEB1 along the posterior part of the division furrow was elongated and the division furrow repositioned while no effects were detected for BSF.

2.4.5 The TbEB1 signal intensity at the posterior cell pole did not correlate with TbEB1 knockdown

For both life cycle stages, it was observed that cells with K/ N ratios adequate to the corresponding life cycle stage rarely demonstrated a reduced level of TbEB1 at the posterior cell pole. The signal intensity of abnormal K/ N ratios was compared to that of 1K1N cells in case of zoids and 1K2N or 2K2N cells in case of multi-nucleated ones. A deviation from the normal K/ N distributions resulted in about 50% of cases in a diminished intensity of the posterior TbEB1 signal. However, frequently the signal did not vanish completely. Sometimes, the signal even intensified in zoids and multi-nucleated cells (Fig. 2.39 and 2.40).BSF trypanosomes demonstrated in about 80% of cells a reduced labeling at the posterior cell pole compared to PCF although the determined knockdown rate was lower in that life cycle stage. However, the overall signal intensity of TbEB1 at the posterior cell pole was lower in cytoskeletal preparations.

In general, a reduction of TbEB1 labeling at the posterior cell pole was more frequent in BSF trypanosomes.

2.4.6 A mouse polyclonal anti-TbEB1 serum confirmed TbEB1 depletion in RNAi cell lines in immuno blots

As the monoclonal anti-TbEB1 antibody only recognized native TbEB1 and the TbEB1 labeling intensity in depleted cell lines was sometimes even increased at the posterior cell pole, a mouse polyclonal anti-TbEB1 antiserum was generated to obtain antibodies, which recognizes native TbEB1 in both immunofluorescence assays and immuno blots. Four mice were immunized with bacterially expressed TbEB1. Two mice were immunized with a His-tagged version of the full length protein (mouse 1 and 2), the remaining two (mouse 3 and 4) with a His-tagged truncated version of the protein consisting of the highly conserved N-terminal domain and a part of the linker region. Pre-serum was taken prior to first immunization and used in identical dilutions in immunofluorescence and immuno blot assays. Only one mouse pre-serum (mouse 3) already demonstrated a labeling of the posterior cell pole in immunofluorescence assays and

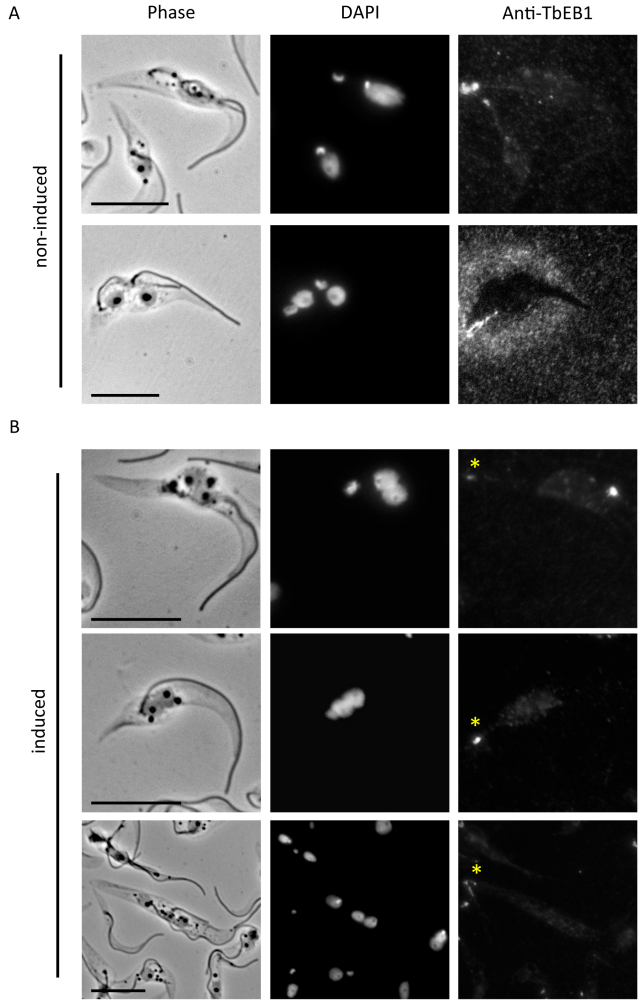


Figure 2.39: Depletion of TbEB1 did not obligatorily decrease the signal at the posterior cell pole in TbEB1 depleted procyclic cell lines. A) Three different cell cycle stages of non-induced procyclic trypanosomes. In the upper row, a 1K1N and a 2K1N cell demonstrate an increase in TbEB1 signal at the posterior cell pole during cell cycle progression. The lower row shows a 2K2N cell with the typical elongated TbEB1 signal along the division furrow. **B**) Three cells affected by TbEB1 depletion via doxycycline-induced RNAi on-set after 48 hours. While the upper panel shows a reduced TbEB1 signal at the posterior cell pole, the signal intensity of the middle one is comparable to the wild type signal. The signal of multi-nucleated cells was compared to that of 1K2N or 2K2N cells but again a decrease (lower panel) as well as an increase of signal intensity was observed. Scale bars represent 10µm.

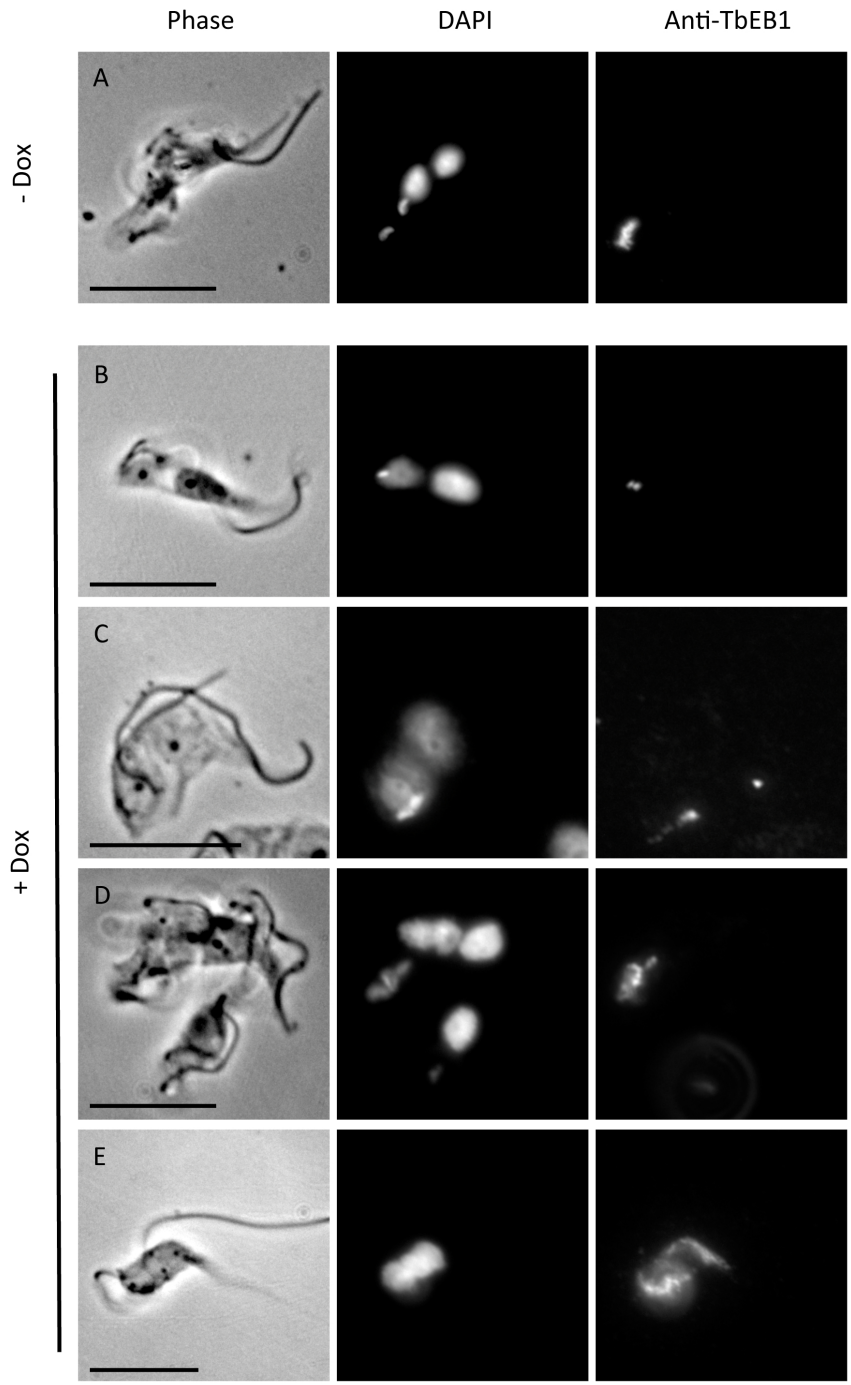


Figure 2.40: TbEB1 depletion resulted in a reduced labeling at the posterior cell pole, a mis-positioned kinetoplast and abnormal K/ N-ratios in TbEB1 depleted bloodstream cell lines. Compared to the non-induced 2K2N cell (**A**), the labeling at the posterior cell pole of trypanosomes in **B**) and **C**) is diminished in addition to a mis-positioned kinetoplast. **D**) and **E**) demonstrate an aberrant number of nuclei while the posterior signal is unchanged (D) or even more intense (E). Scale bars represent 10µm.

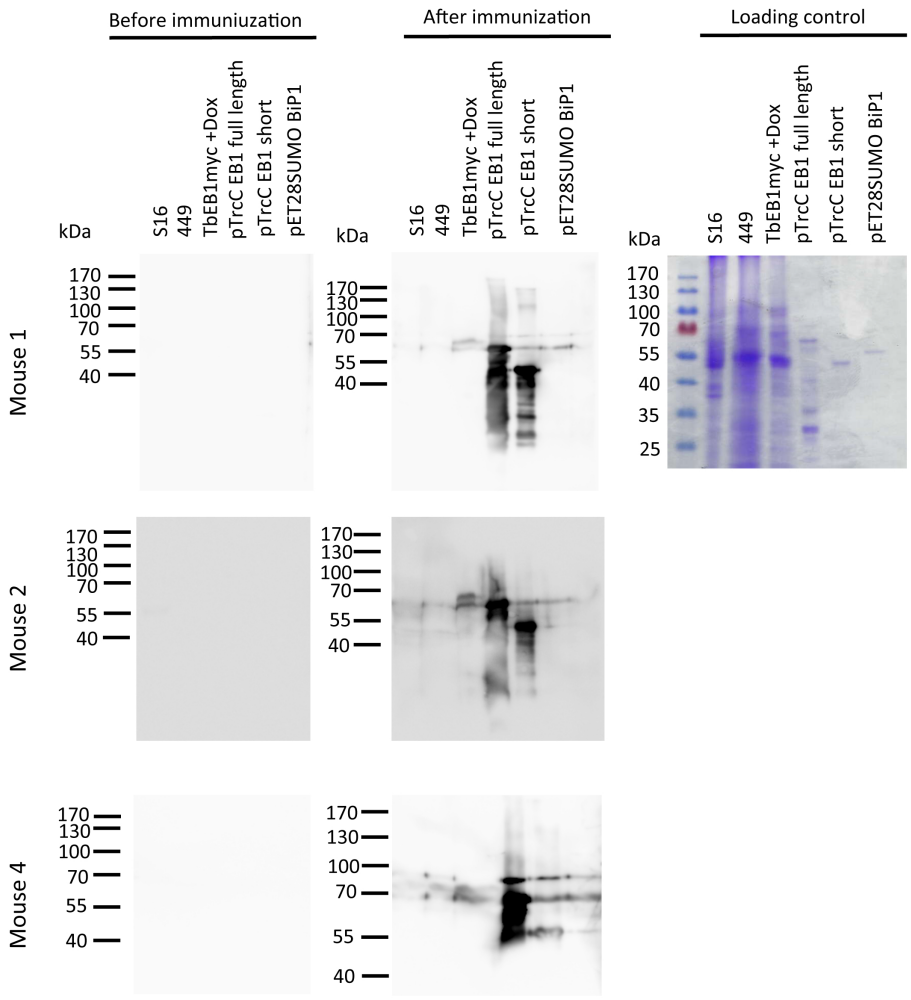


Figure 2.41: Immune reactions of mice pre-sera and anti-TbEB1 sera detected by immuno blot analysis. Whole cell extracts of bloodstream (S16) and procyclic trypanosomes (449, TbEB1myc +Dox) were loaded with 10^6 cells per lane. To increase the amount of available antigen, TbEB1myc was cultivated in the presence of 1µg/ml doxycycline for ectopic expression of TbEB1$^{C\text{-}2xmyc}$(TbEB1myc +Dox). 100ng of bacterially expressed His-tagged TbEB1 full length, His-tagged TbEB1 short, and His-Sumo-tagged BiP 1 proteins were loaded, too. Pre-sera (before immunization) and mice sera (after immunization) were diluted 1:200. Immune reactions were visualized by an anti-mouse HRP conjugated antibody. Bands corresponding to wild type TbEB1 (57kDa), ectopically expressed TbEB1$^{C\text{-}2xmyc}$ (70kDa), TbEB1 full length (64kDa), and TbEB1 short (45kDa) were detected with all three sera after immunization. No signal for BiP 1 protein (52kDa) was detectable with anti-TbEB1 sera. For all sera taken before immunization, no bands were detectable. The Coomassie-stained SDS-gel was used as loading control.

was excluded from further analysis.

A detection of wild type TbEB1 (57kDa) in BSF and PCF was possible with all three anti-sera (Fig. 2.41). Immuno blots also demonstrated a band corresponding to the ectopically expressed TbEB1$^{C\text{-}2xmyc}$ at about 70kDa. Furthermore, both antigens, TbEB1 and TbEB1$^{C\text{-}2xmyc}$, were identified while no reaction was detectable against the expressed Sumo-tag in bacteria transformed with pET28-SUMO-BiP 1. The corresponding mice pre-sera did not demonstrate a signal in immuno blots. Additionally, wild type and ectopically expressed TbEB1 were detected in pellet fractions of detergent-extracted procyclic trypanosomes on immuno blots treated with the anti-sera (Fig. 2.42)

Obtained mouse sera were also tested in immuno fluorescence assays. Similar to immuno blot results only a faint labeling of the cell body on whole cell preparations and detergent-extracted cells was detectable with pre-sera (Fig. 2.43 and Fig. 2.44). Frequently, a more intense labeling of the flagellum and the nucleus was observed, which is a common phenomenon for polyclonal anti-trypanosomal antisera (K. Ersfeld, personal communication). Only the serum of mouse 2 did not recognize the nucleus on cytoskeletal preparations, and therefore was used in later analysis. On whole cell preparations, the complete cell body, except flagellum and nucleus, was intensively stained (Fig. 2.43). On detergent-extracted cells, the subpellicular cytoskeleton, the basal body or associated structures, and the FAZ were labeled (Fig. 2.44). The characteristic intense labeling of the posterior cell pole was only occasionally detectable. Additionally, a variation in TbEB1 labeling at the posterior cell pole throughout the cell cycle as demonstrated for the mouse monoclonal anti-TbEB1 antibody or tagged TbEB1 was never observed. In contrast, labeling of the subpellicular cytoskeleton was more intense. This could presumably mask the labeling of the posterior cell pole.

Using anti-TbEB1 mouse antiserum 1, a clear reduction of the endogenous TbEB1 was detectable for both procyclic and the bloodstream TbEB1 RNAi cell lines in immuno blots (Fig. 2.45). In immunofluorescence assays, a reduction of the subpellicular cytoskeleton labeling and less frequently also labeling at the posterior cell part was observed in most procyclic trypanosomes (Fig. 2.46 and Fig. 2.47). In contrast to immuno blots, the signal intensity of the bloodstream RNAi cell line after siRNA expression was similar to non-induced and wild type trypanosomes (Fig. 4.18). Only single cells demonstrated a reduced labeling of the subpellicular cytoskeleton (Fig. 4.18E and G).

Summing up, successful depletion of endogenous TbEB1 was demonstrated on the protein level by immunoblots detecting endogenously tagged (Ch. 2.4.2) or wild type TbEB1 in PCF and BSF. Furthermore, immunofluorescence assays of endogenously tagged (Ch. 2.4.2) and wild type TbEB1 demonstrated also a reduced labeling intensity for procyclic trypanosomes. Immunofluorescence assays of bloodstream trypanosomes only demonstrated a decreased signal

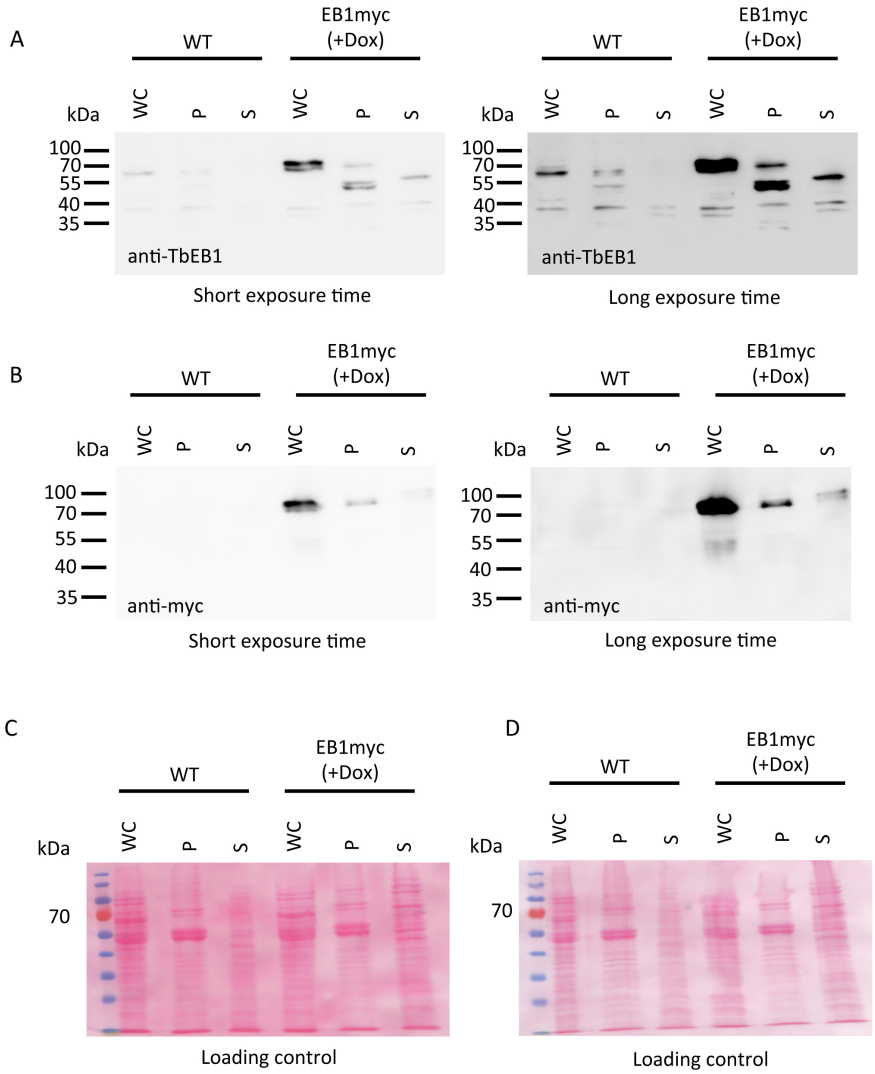


Figure 2.42: Detection of endogenous or ectopically expressed TbEB1 in NP-40 detergent-extracted fractions by the mouse polyclonal anti-TbEB1 serum. Whole cell extracts (WC), NP-40 insoluble cytoskeleton (P) and soluble (S) fractions of procyclic 449 (WT) and TbEB1myc (EB1myc +Dox) were loaded. The latter cell line was cultivated in the presence of doxycycline (1µg/ml) for 24h. Immuno blots probed with mouse polyclonal anti-TbEB1 **(A)** and anti-c-myc antibody **(B)**. Ponceau S-stained immuno blot membranes as loading control for the anti-TbEB1 immuno blot **(C)** or the anti-c-myc immuno blot **(D)**.

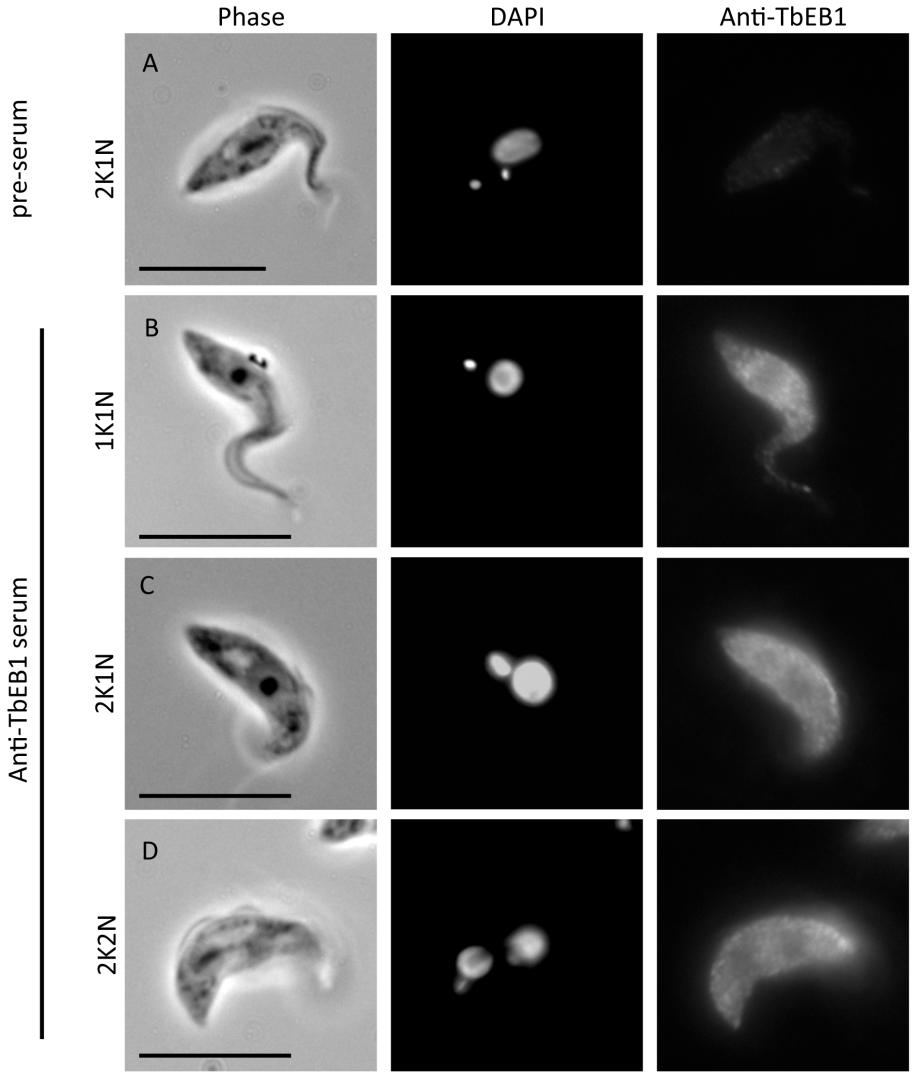


Figure 2.43: Immunoreactivity of mouse serum 2 before and after immunization with bacterially expressed TbEB1 protein shown on whole cell preparations of PCF. After immunization, an intense labeling of the whole cell body was found, which was similar for all cell cycle stages. Whole cell preparations were incubated with 1:200 diluted pre-serum and anti-TbEB1 serum followed by incubation with an appropriate fluorescence conjugated secondary antibody. **A)** Representative example for cells incubated with mouse pre-serum. **B-D)** Example of 1K1N, 2K1N, and 2K2N cells treated with anti-TbEB1 polyclonal serum. Scale bars represent 10µm.

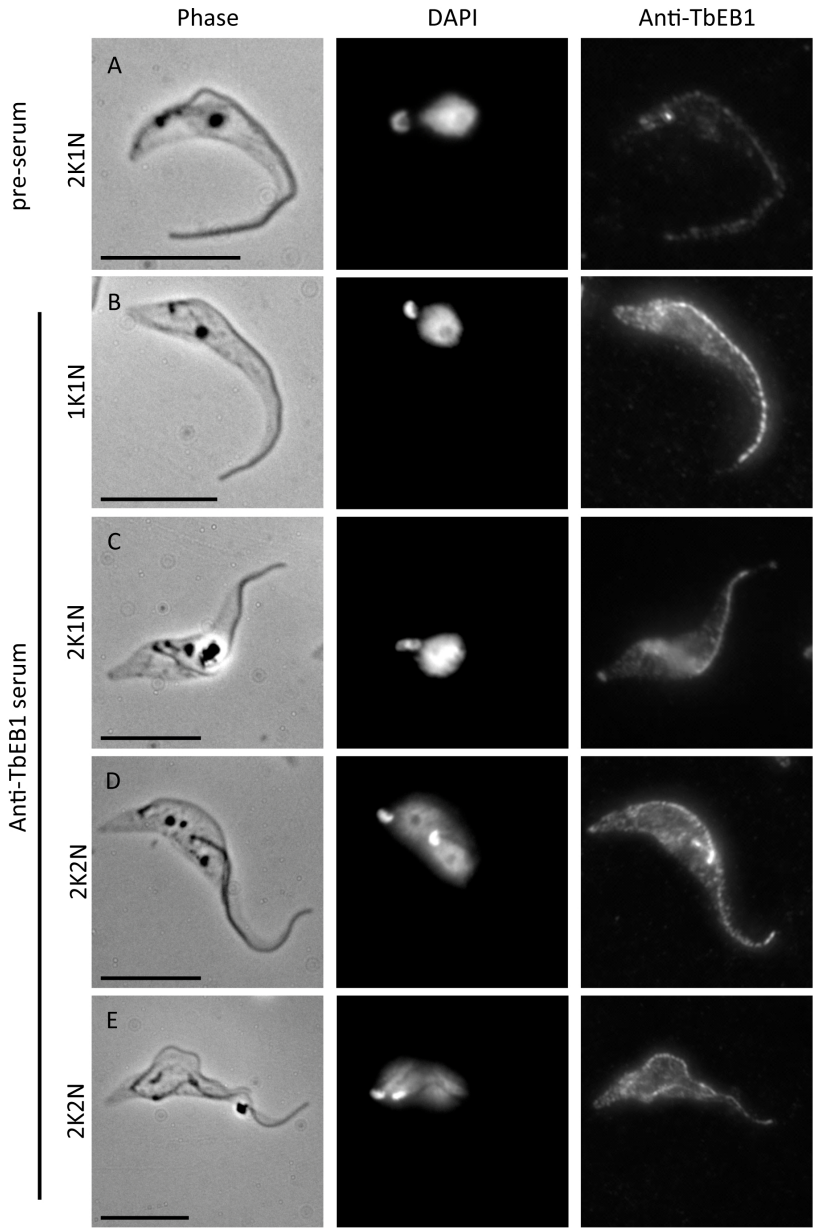


Figure 2.44: Immunoreactivity of mouse serum 2 before and after immunization with bacterially expressed TbEB1 protein shown on detergent-extracted cytoskeletons of PCF. After immunization, an intense labeling of the subpellicular cytoskeleton was detected, which was similar for all cell cycle stages. The posterior cell pole labeling was frequently detectable. However, a cell cycle specific labeling pattern was not found. Cytoskeletal preparations were incubated with 1:200 diluted pre-serum and anti-TbEB1 serum followed by incubation with an appropriate fluorescence conjugated secondary antibody. **A)** Representative example for cells incubated with mouse pre-serum. **B-E)** Example of 1K1N, 2K1N, and 2K2N cells treated with anti-TbEB1 polyclonal serum. However, an intensified labeling of the posterior cell pole was not mandatorily. Scale bars represent 10µm.

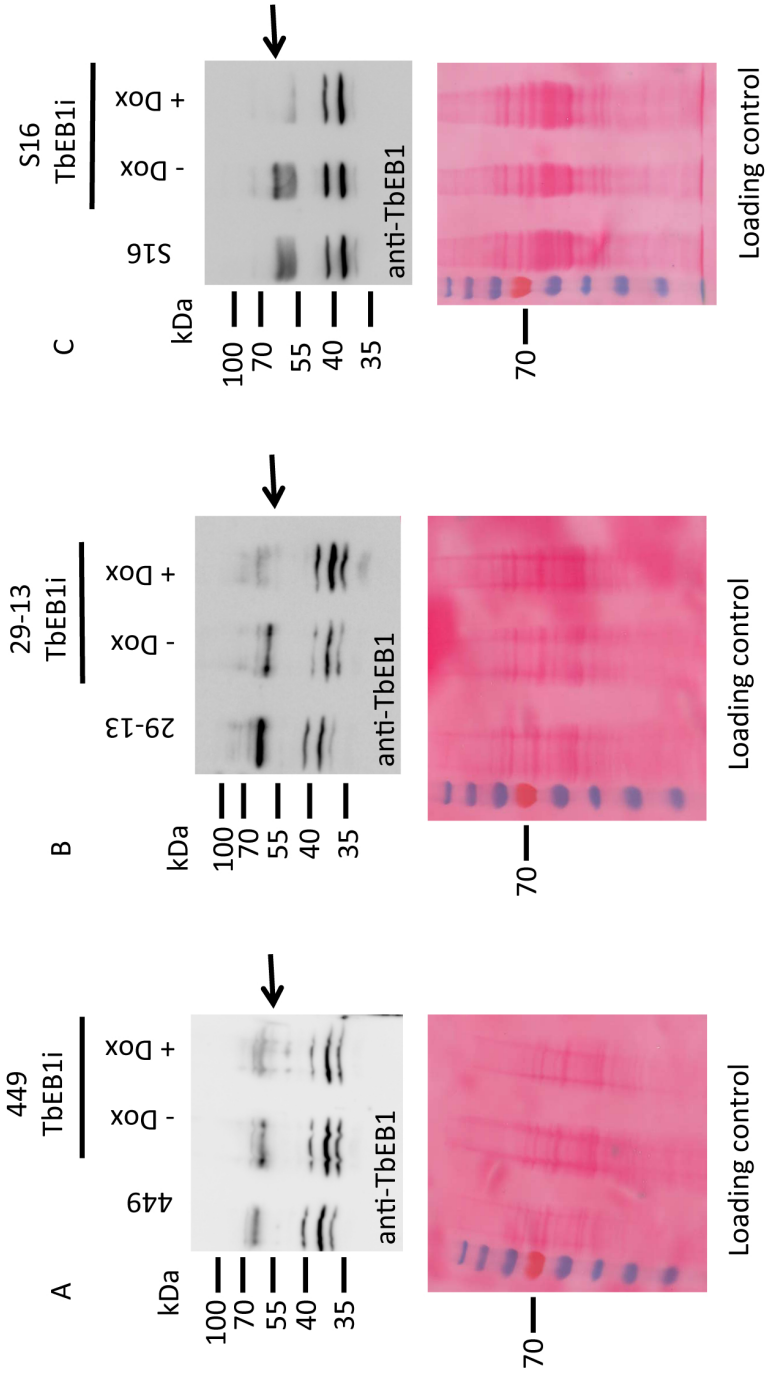


Figure 2.45: Treatment of immuno blots with mouse polyclonal anti-TbEB1 antiserum confirmed successful TbEB1 knockdown in procyclic and bloodstream TbEB1 RNAi cell lines. Procyclic 449 **(A)** and 29-13 **(B)** TbEB1 RNAi cell lines were cultivated in the absence (-Dox) or presence (+Dox) for 4 days, the bloodstream S16 TbEB1 RNAi cell line **(C)** for 3 days. Additionally the corresponding wild type cell lines were loaded. If TbEB1 siRNA expression was induced a strong decrease of TbEB1 signal (arrow) was found in all three cell lines. Ponceau S-stained immuno blot membranes were used as loading control.

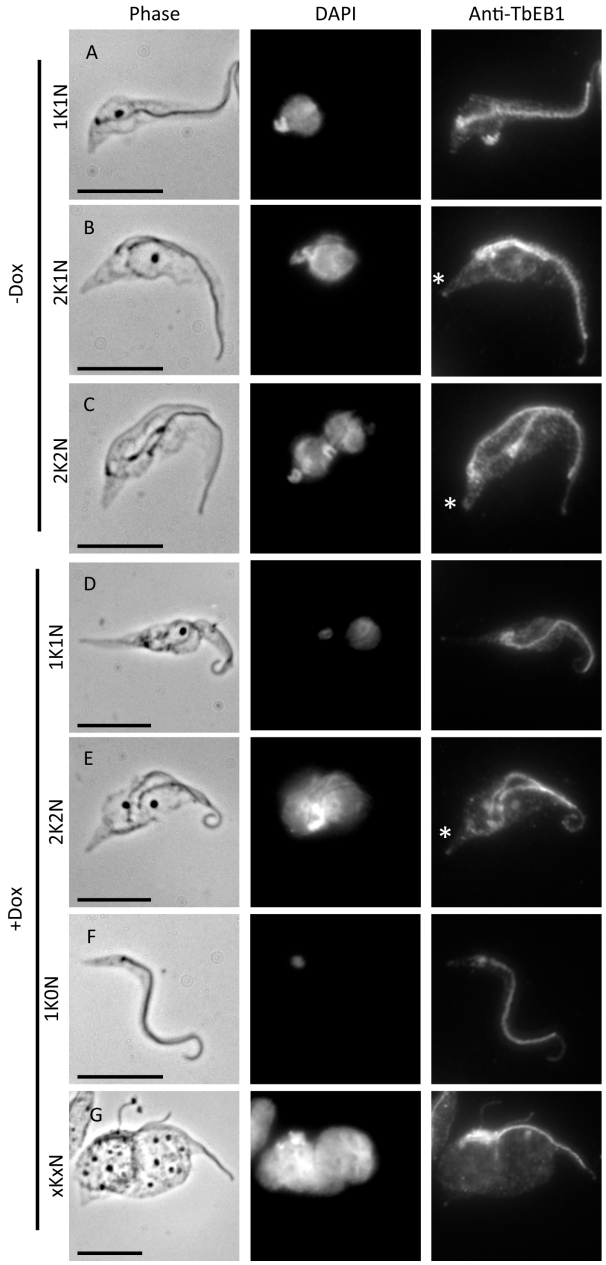


Figure 2.46: Procyclic cell line 449 TbEB1i demonstrated a reduced TbEB1 signal at the subpellicular cytoskeleton after siRNA expression. 449 TbEB1i was cultivated in **A-C)** the absence (-Dox) or **D-G)** presence (+Dox) of 1µg/ml doxycycline for 4 days. Detergent-extracted cytoskeletal preparations were labeled by the mouse anti-TbEB1 antiserum followed by incubation with an appropriate secondary antibody. A-C) Example of 1K1N, 2K1N, and 2K2N cells of non-induced 449 TbEB1i sample. A strong labeling at the subpellicular cytoskeleton occurred while the posterior cell pole was only sometimes labeled. D-G) Example of 1K1N, a 2K2N with mis-positioned kinetoplast, a zoid (1K0N), and a xKxN cell of induced 449 TbEB1i sample. A clear reduction of the labeling intensity at the subpellicular cytoskeleton was visible in the induced sample images while posterior cell pole labeling (star) was sometimes still detectable. Scale bars represent 10µm.

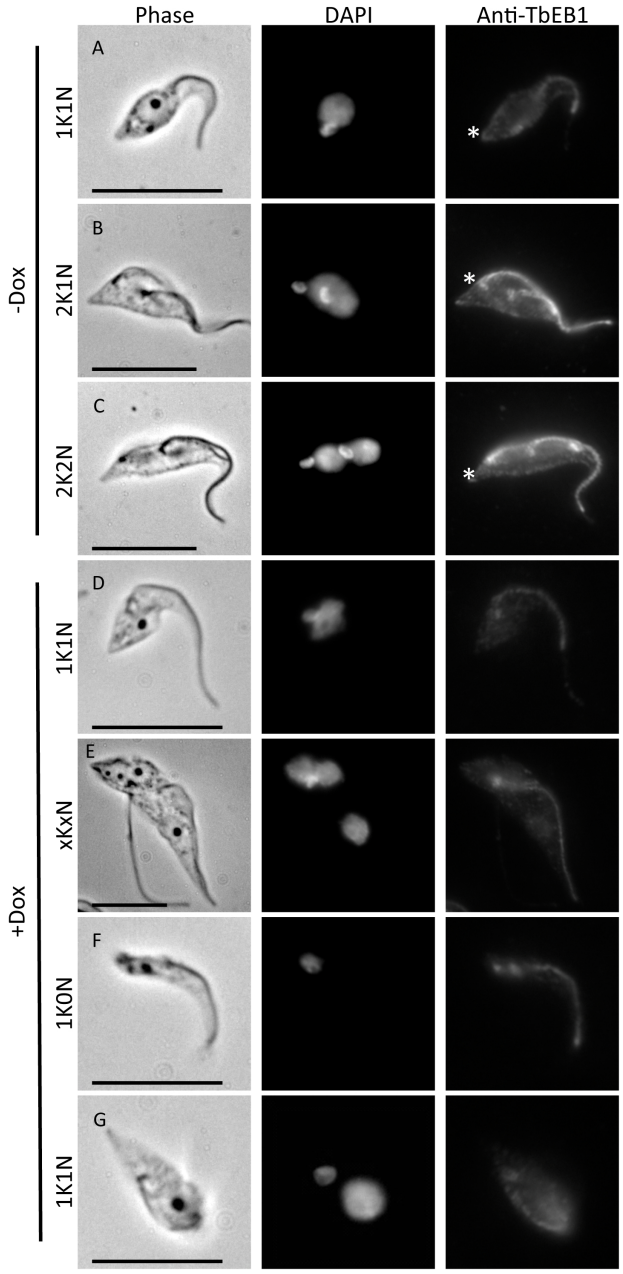


Figure 2.47: Procyclic cell line 29-13 TbEB1i demonstrated a reduced TbEB1 signal at the subpellicular cytoskeleton after siRNA expression. 29-13 TbEB1i was cultivated in **A-C)** the absence (-Dox) or **D-G)** presence (+Dox) of 1µg/ml doxycycline for 4 days. Detergent-extracted cytoskeletal preparations were labeled by the mouse anti-TbEB1 antiserum followed by incubation with an appropriate secondary antibody. A-C) Example of 1K1N, 2K1N, and 2K2N cells of non-induced 29-13 TbEB1i culture. A strong labeling of the subpellicular cytoskeleton occurred while the posterior cell pole was only occasionally labeled (star). D-G) Example of a 1K1N, a xKxN with mis-positioned kinetoplast, a zoid (1K0N), and a small 1K1N cell of induced 29-13 TbEB1i culture. A clear reduction of the labeling intensity of the subpellicular cytoskeleton was visible in the induced sample images. Scale bars represent 10µm.

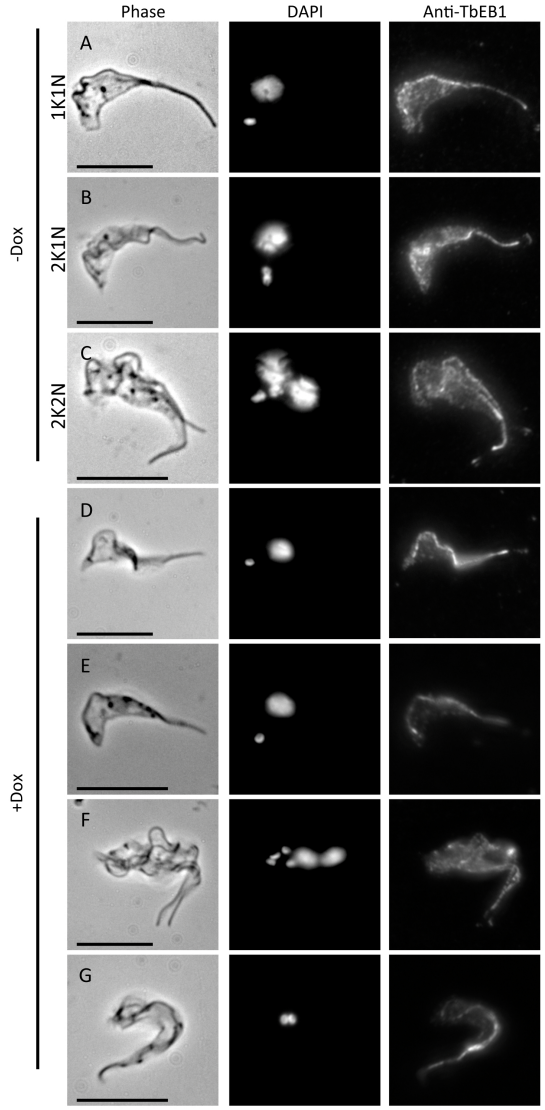


Figure 2.48: Bloodstream cell line S16 TbEB1i demonstrated only rarely a reduced TbEB1 signal at the subpellicular cytoskeleton after siRNA expression. S16 TbEB1i was cultivated in **A-C)** the absence (-Dox) or **D-G)** presence (+Dox) of 1µg/ml doxycycline for 2.5 days. Detergent-extracted cytoskeletal preparations were labeled by the mouse anti-TbEB1 antiserum followed by incubation with an appropriate secondary antibody. A-C) Example of a 1K1N cell, a 2K1N cell, and a 2K2N cells of non-induced S16 TbEB1i culture. The subpellicular cytoskeleton demonstrated labeling. D-G) Example of a 1K1N cell with TbEB1 labeling similar to the non-induced sample, a 1K1N cell with a decreased labeling intensity compared to non-induced cells, a xKxN cell, and a zoid (1K0N) from an induced S16 TbEB1i culture. A clear reduction of the labeling intensity of the subpellicular cytoskeleton was only rarely visible in the induced sample images. Scale bars represent 10µm.

intensity for the endogenously tagged TbEB1 while only few cells demonstrated a diminished signal intensity using the polyclonal antiserum. Immunofluorescence and blot results fit well to qPCR results, which demonstrated reduced TbEB1 levels based on relative mRNA levels.

2.4.7 TbEB1 depleted PCF demonstrated an increase in cell rounding with a reduction of tyrosinated α-tubulin and an impediment of kinetoplast segregation

Before a trypanosome undergoes cytokinesis and creates daughter cells of almost identical size it is necessary to replicate not only cell organelles but also the surrounding plasma membrane and cytoskeleton. The enlargement of the subpellicular microtubule array of trypanosomes proceeds in a semi-conservative manner as new microtubules are integrated between the already existing ones, which are extended themselves, too (Sherwin & Gull, 1989b). The process occurs mainly at the posterior third of the cell, as here the majority of microtubules plus ends exist. Those assembly processes are characterized by the presence of C-terminally tyrosinated α-tubulin, which is recognized by the YL1/2 antibody (Sherwin *et al.* , 1987; Stephan *et al.* , 2007). As EB1 is intrinsically tied to microtubule dynamics across all eukaryotes (Vaughan, 2005; Lansbergen & Akhmanova, 2006), the use of the YL1/2 antibody on TbEB1 depleted cells would reveal some aspects of microtubule dynamics in the absence of that protein. As already described in literature (Sherwin *et al.* , 1987; Stephan *et al.* , 2007; Wheeler *et al.* , 2013), the YL1/2 labeling in wild type cells is localized at the posterior cell body over the whole cell cycle with increasing intensity during progression in the posterior third of the trypanosome indicating remodeling processes of that area (Fig. 2.49 and Fig. 2.50). But the most prominent label is situated aside the basal body. Two spots appear during S-phase when both basal bodies are fully developed and segregated. The recently assembled axoneme of the arising flagellum is also stained.

Depletion of TbEB1 often led to cells with a rounded posterior combined with abnormal K/ N ratios, and their number increased coincidently with the onset of RNAi. Those cells demonstrated a reduced level of YL1/2 labeling at the posterior cell body after 48 hours. If cells demonstrated a posterior morphology resembling the wild type, the typical graduated YL1/2 staining was visible even if K/ N ratios were anomalous and cells derived from the same time point of the trial (Fig. 2.51 A, B). Many zoids (1K0N) had decreased levels of tyrosinated α-tubulin, too (Fig. 2.51 C, D). The reduction of YL1/2 labeling was only detectable at the subpellicular cytoskeleton, but not at the basal body. Kinetoplasts or the emerging point of a flagellum were used as a marker for localization of a basal body complex. Up to day 3 of TbEB1 depletion, up to two kinetoplasts accompanied by one or two mature basal bodies were found. Their number did not correlate with the number of nuclei (Fig. 2.51 E, F). This process culminated in enlarged kinetoplasts, probably due to several rounds of mitochondrial DNA replication without follow-

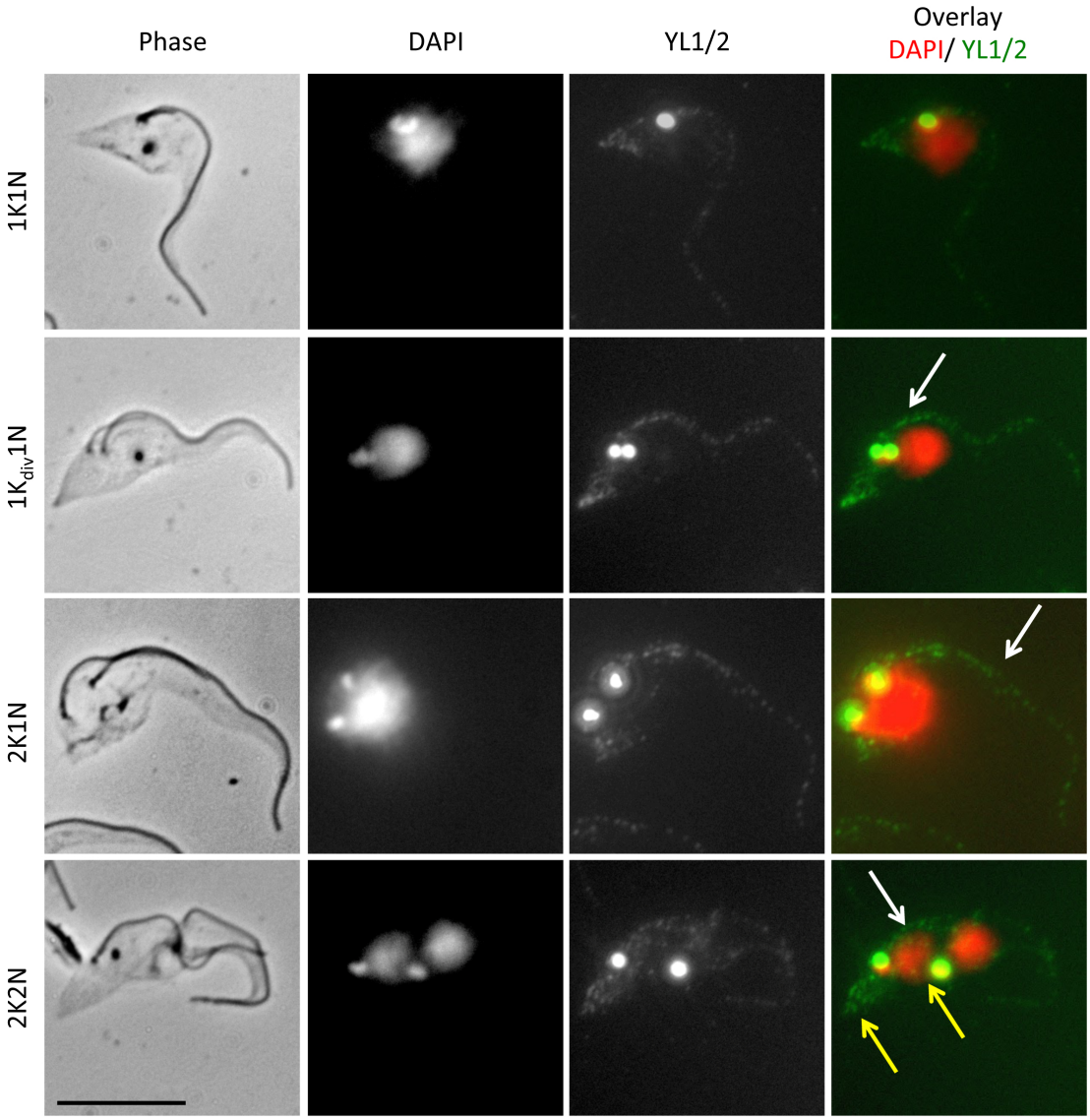


Figure 2.49: Staining pattern of the marker for tyrosinated α-tubulin (YL1/2) varies during the cell cycle on detergent-extracted cytoskeletons of procyclic trypanosomes. Tyrosinated α-tubulin is primarily localized at the posterior cell body and at the base of mature basal bodies. Through cell cycle progression, it also associates with the axoneme of the new flagellum (white arrow) as well as the generating old and new posterior ends of dividing daughter cells (yellow arrows). Scale bar represents 10µm.

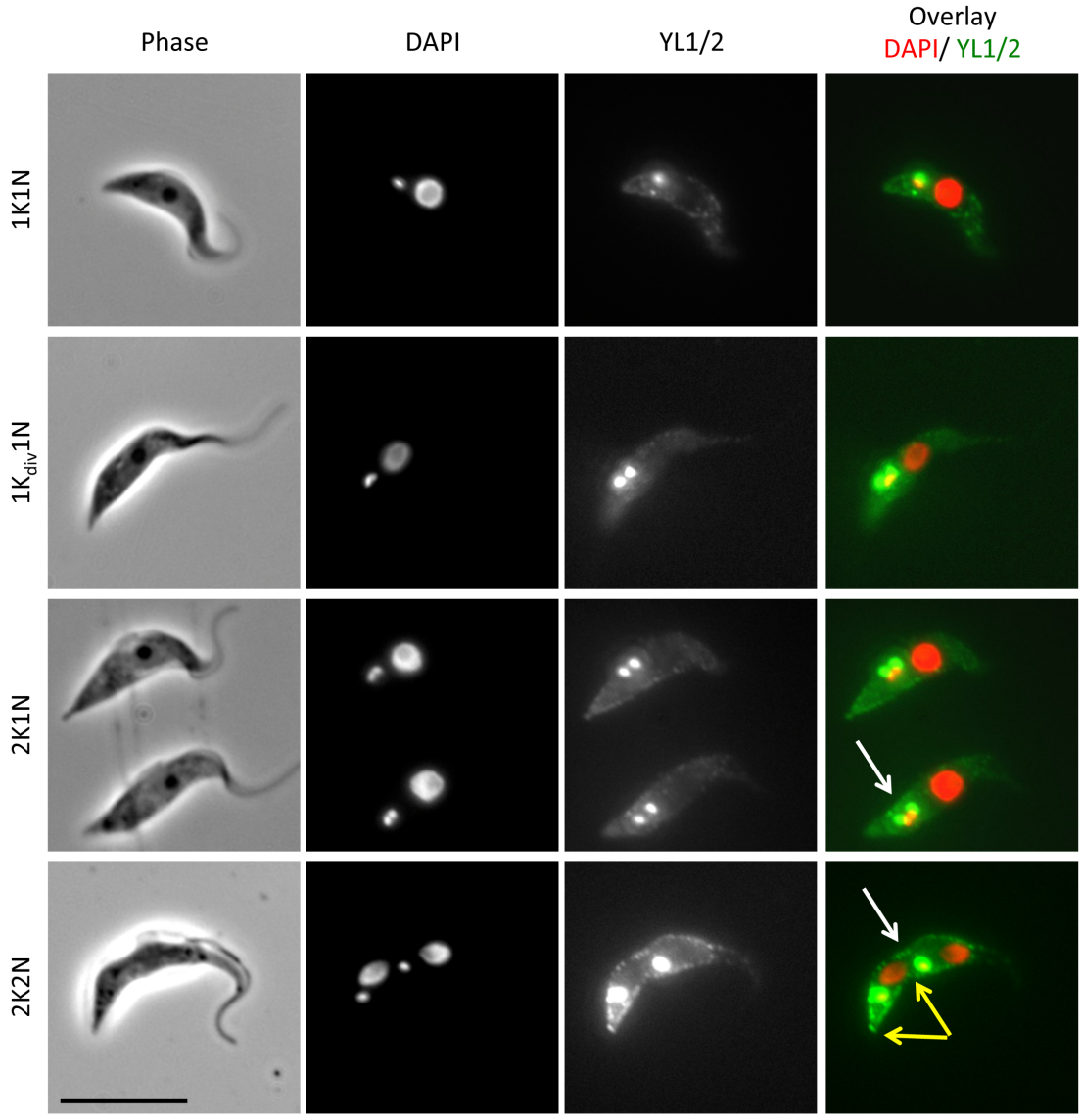


Figure 2.50: Staining pattern of the marker for tyrosinated α-tubulin (YL1/2) varies during the cell cycle on whole cell preparations of procyclic trypanosomes. Tyrosinated α-tubulin is primarily localized at the posterior cell body and at the base of mature basal bodies. Through cell cycle progression, it also associates with the axoneme of the new flagellum (white arrow) as well as the generating old and new posterior ends of dividing daughter cells (yellow arrows). Scale bar represents 10µm.

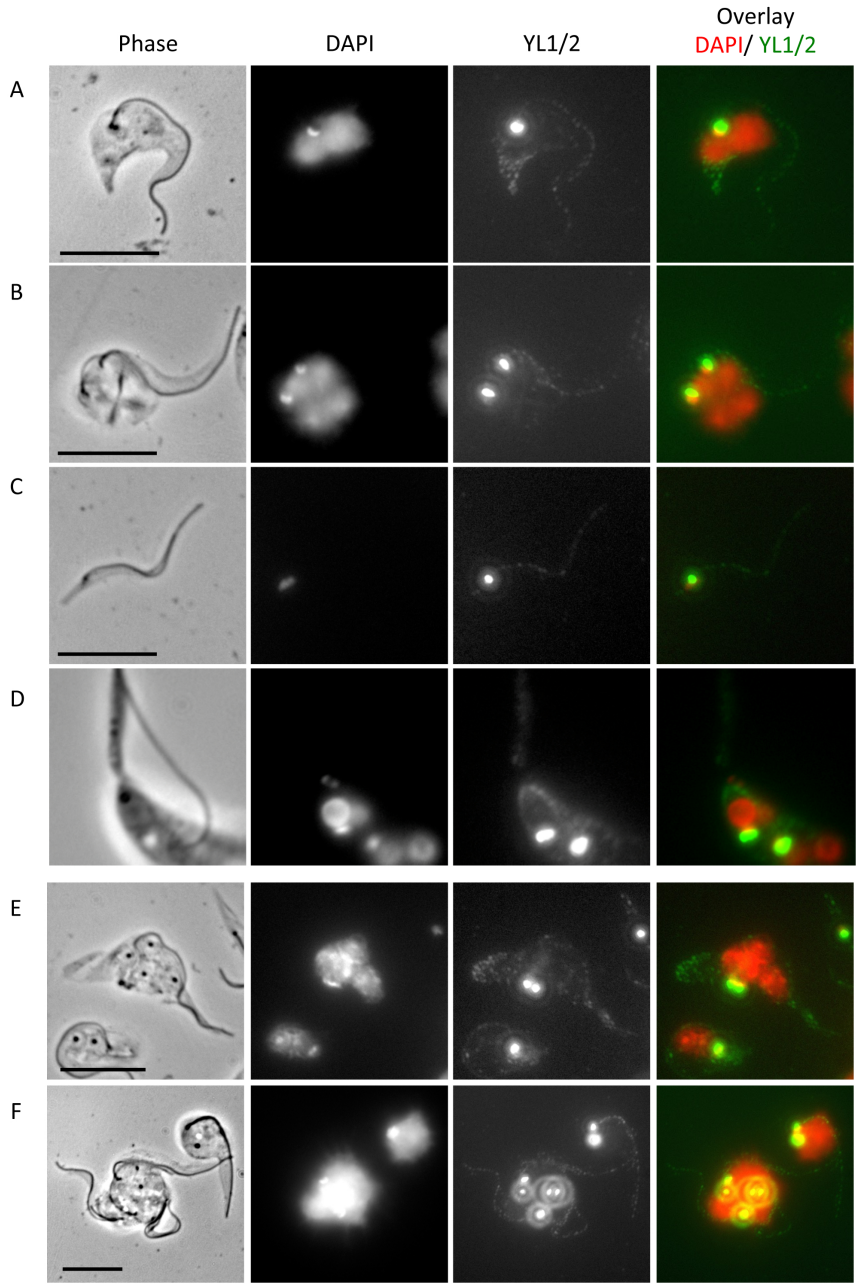


Figure 2.51: Depletion of TbEB1 resulted in round cells going along with a reduction of YL1/2 labeling as well as an impediment of kinetoplast segregation. **A**) After 4 days of TbEB1 depletion, some cells still maintained an elongated posterior cell pole while in **B**) the typical shape was lost and accompanied by a loss of YL1/2 labeling. **C**) Zoids deriving from a malfunctioning cytokinesis often lack a YL1/2 labeling of the subpellicular cytoskeleton. **D**) Magnification of a whole cell preparation of a dividing cell giving rise to a zoid with diminished YL1/2 labeling. **E**) During early TbEB1 depletion mainly up to two kinetoplasts were detected regardless of the number of nuclei. **F**) Later, when cell bodies were heavily crowded with nuclei, the number of kinetoplasts increased. Cells were detergent-extracted and fixed in ice-cold methanol (except D: whole cell preparation, FA fixation). Scale bars represent 10µm.

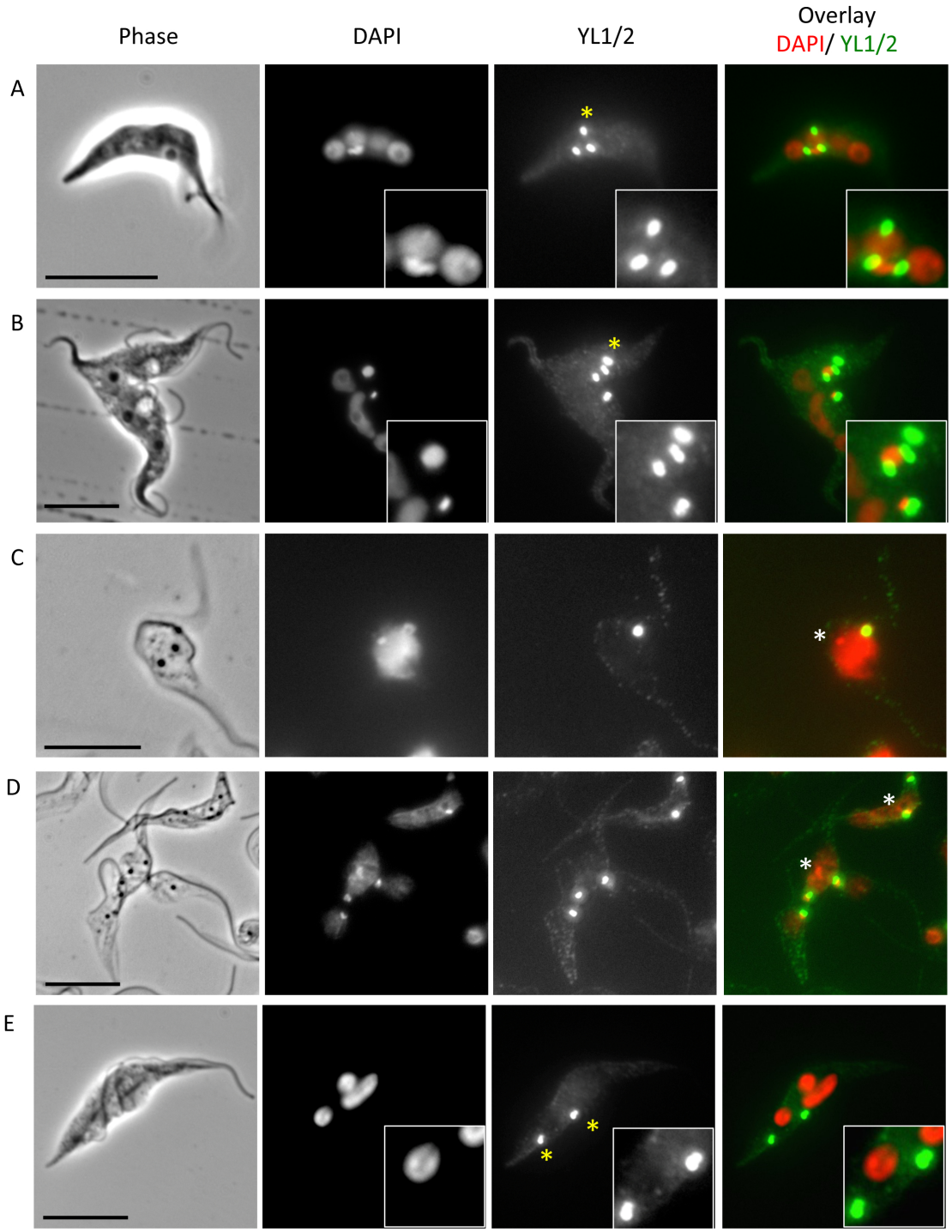


Figure 2.52: Abnormal YL1/2 labeling nearby the kinetoplast upon TbEB1 depletion in PCF. Depletion of TbEB1 rarely resulted in additional YL1/2 labeling nearby kinetoplasts, reduced labeling aside kinetoplasts or absent kinetoplasts in multi-nucleated cells although flagella and basal bodies existed. Additional spots or lines are marked with a yellow star, missing ones with a white star. **A-B**) Whole cell preparations, **C-E)** detergent-extracted cytoskeletons. Scale bars represent 10µm.

ing segregation, accompanied by several YL1/2 spots (Fig. 2.52 A, B). However, several cells demonstrated no YL1/2 labeling in the vicinity of a kinetoplast (Fig. 2.52 C, D). Occasionally, a kinetoplast was missing although a basal body with an extending daughter flagella existed (Fig. 2.52 E). These findings suggest that the stability of the TAC (tripartite attachment complex), which links basal body and kinetoplast, might be destabilized.

After TbEB1 depletion in PCF, the tyrosinated α-tubulin labeling was diminished on the posterior subpellicular cytoskeleton indicating reduced microtubule dynamics. Furthermore, a surplus of basal bodies was found indicative for an impeded kinetoplast segregation.

2.4.8 In BSF, TbEB1 depleted cells demonstrated impaired kinetoplast segregation but cellular morphology was not affected

Cytoskeletal preparations of wild type BSF demonstrated a labeling of tyrosinated α-tubulin (YL1/2 antibody) similar to procyclics (Fig. 2.53). Depletion of TbEB1 resulted in abnormal K/ N ratios and those cells normally possessed an adequate ratio of kinetoplasts and basal bodies (Fig. 2.54A). As in PCF, exceptions were found: cells with additional basal basal bodies (Fig. 2.54 B, C), a weak labeling of basal bodies and the posterior cell pole (Fig. 2.54D) or that the basal body was separated from the corresponding kinetoplast (Fig. 2.54E). These are indications for a disturbed kinetoplast - basal body connection and an impeded kinetoplast segregation.

Summing up, the effects of TbEB1 depletion detected by investigation of tyrosinated α-tubulin in trypanosomes were similar concerning the kinetoplast/ basal body system but different at the morphological level.

2.4.9 TbEB1 depleted PCF and BSF demonstrated an increase in flagellar detachment but flagellar assembly was not affected

Microscopic analysis of the TbEB1 RNAi cell lines revealed many detached flagella. Flagella were categorized as detached if any part of the flagellum missed association with the plasma membrane. 100 cells were observed and partial and complete detached flagella counted (Fig. 2.55 A). In BSF, 60% of TbEB1 knockdown cells had a detached flagellum on day 3 compared to 33% in non-induced cells and 23% in wild type cells (Fig. 2.55 B). The high amount of detached flagella in BSF trypanosomes was most likely caused by the preparation of the cytoskeletons. However, the number of detached flagella in induced cells was still 37% higher than the in wild type. This is similar to 29-13 TbRNAi cell lines on day 3 with 35% (Fig 2.55 C). Values of the remaining days ranged between 16 and 24%. 449 RNAi cell lines were less affected and percentage of detached flagella ranged between 4 and 12% (Fig. 2.55 D).

Studies of mammalian and chlamydomonal end-binding proteins notified their presence at

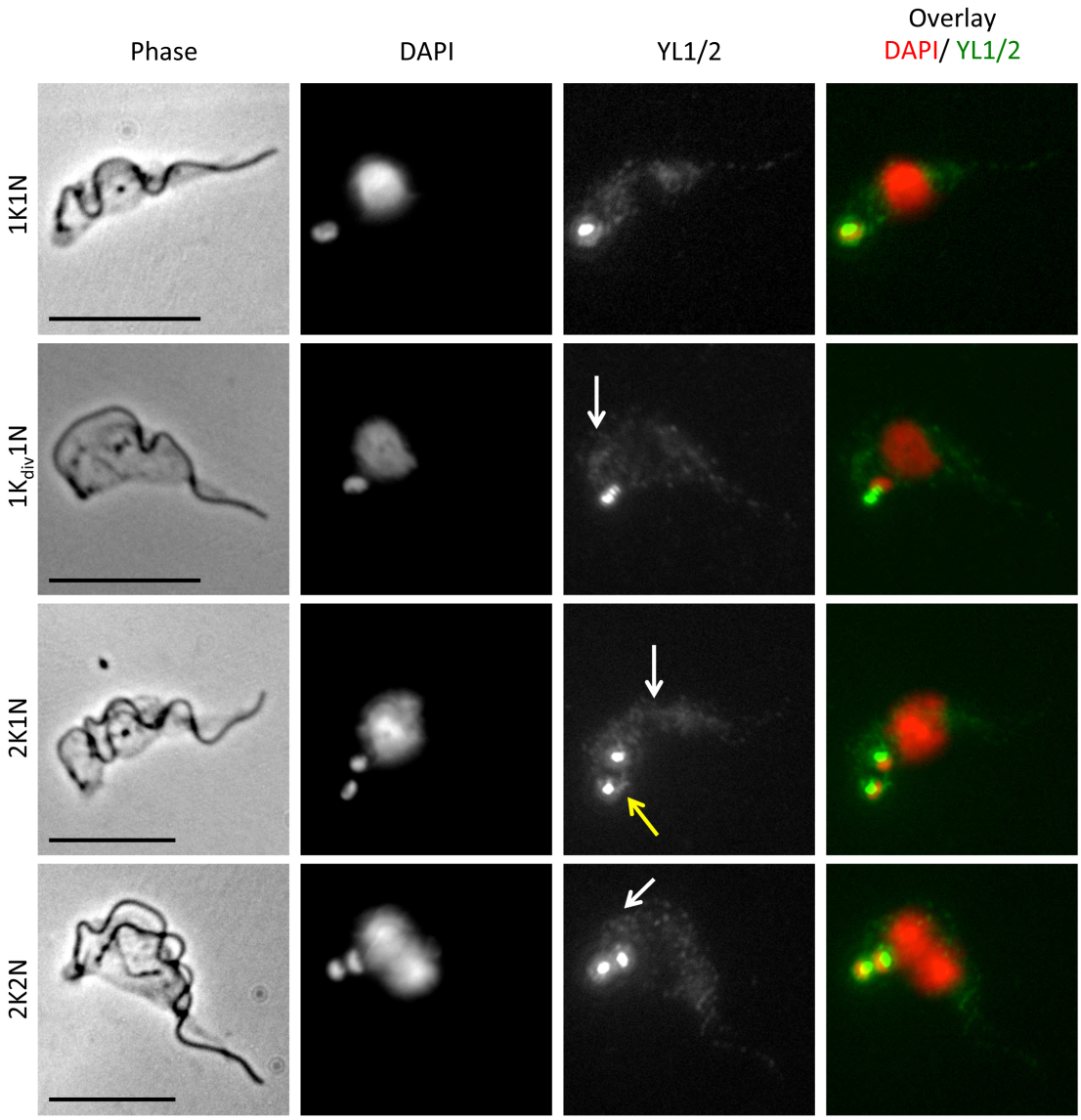


Figure 2.53: Staining pattern of the marker for tyrosinated α-tubulin (YL1/2) varies during the cell cycle on detergent-extracted cytoskeletons of bloodstream trypanosomes. Through cell cycle progression, it also appears at the axoneme of the new flagellum (white arrows) as well as the generating old and new posterior ends of dividing daughter cells (yellow arrow). Scale bars represent 10µm.

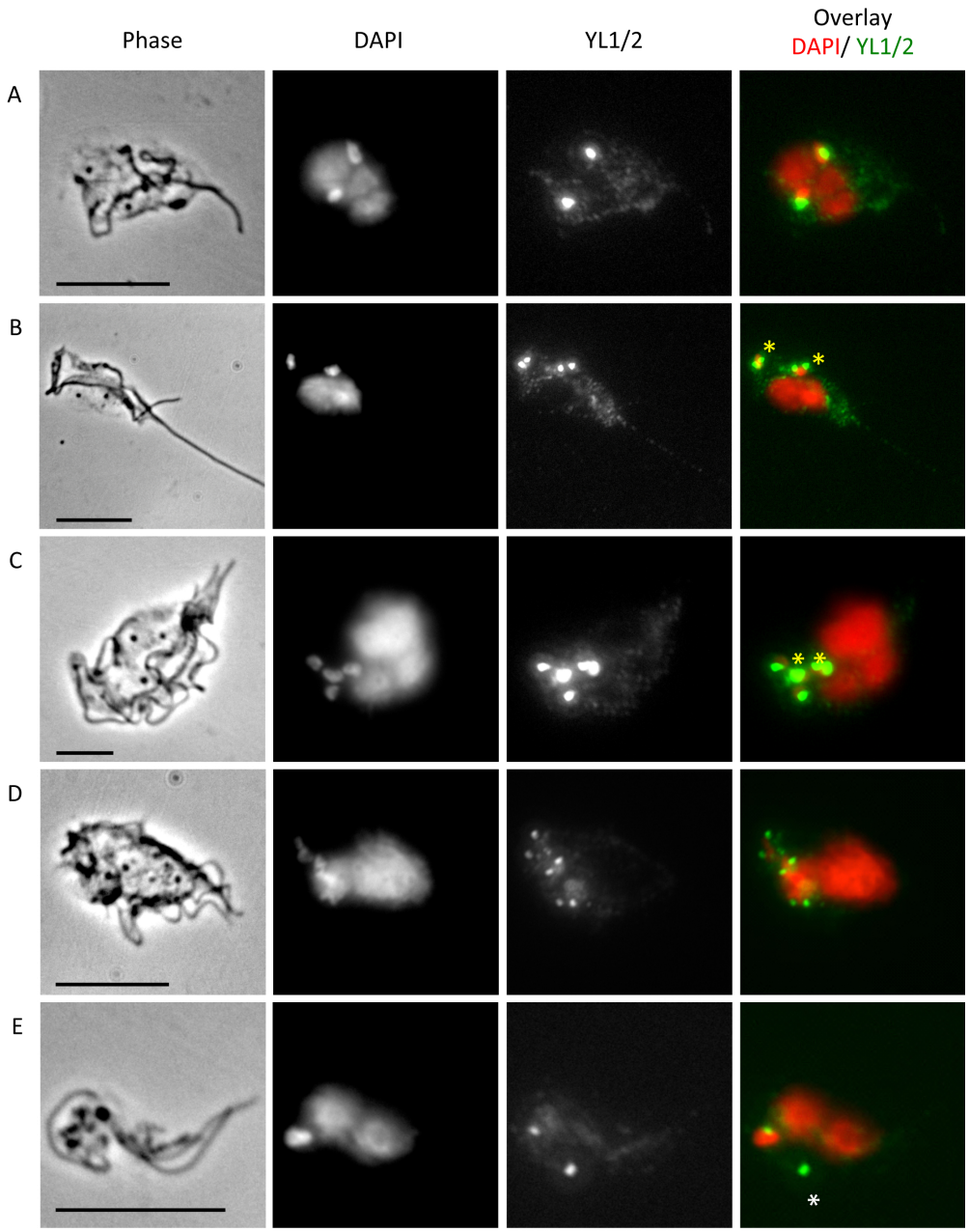


Figure 2.54: Phenotypes of TbEB1 depletion revealed by YL1/2 staining in BSF. A) Despite abnormal K/ N ratios, basal body and kinetoplast numbers were equal in most cells. In some cases a higher number of basal bodies per cell was counted (**B**, **C**; yellow star), the YL1/2 signal was reduced (**D**) or one basal body separated from the adjacent kinetoplast (**E**, white star). Scale bars represent 10µm.

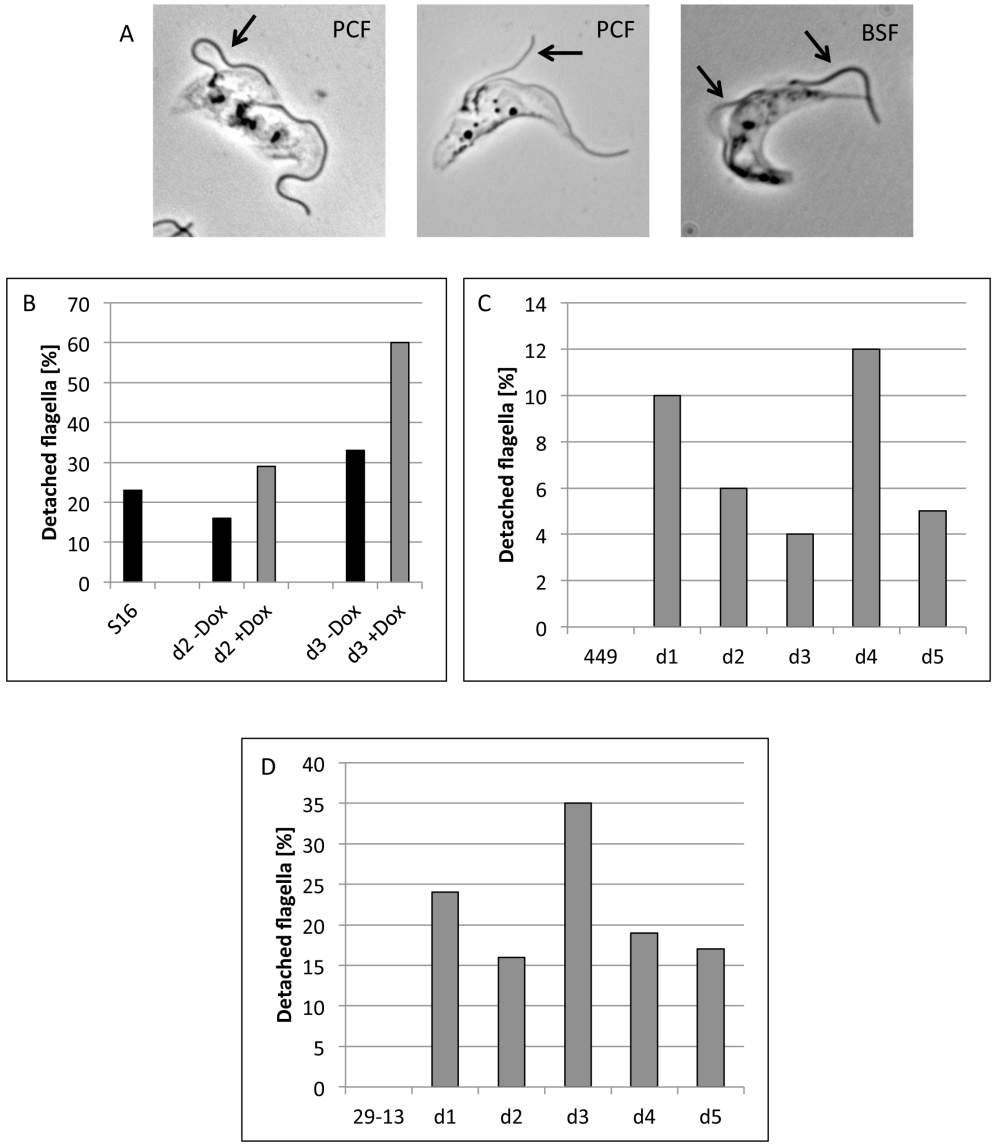


Figure 2.55: TbEB1 depletion resulted in detached flagella in bloodstream and procyclic trypanosomes. **A**) Exemplary phase images of trypanosomes demonstrate different grades of flagellar detachment in trypanosomes. 100 cells were evaluated per condition. **B**) After TbEB1 depletion the amount of detached flagella increased up to 60% in induced (+Dox) cells compared to wild type (S16) and non-induced (-Dox) cells. Due to restrictions of the preparation, wild type cells already demonstrated about 20% detached flagella. **C**) The amount of detached flagella counted in 449 TbEB1 RNAi cultivated in the presence of doxycycline up to 5 days compared to 449 (wild type) increased up to 12% under TbEB1 depletion. **D**) 29-13 TbEB1 cell line cultivated in the presence of doxycycline for up to 5 days demonstrated up to 35% of cells with detached flagella.

the basal body and a role in ciliagenesis (Pedersen *et al.* , 2003; Leterrier *et al.* , 2011; Larsen *et al.* , 2013). Together with the localization of C-terminal tagged TbEB1$^{\text{C-12xmyc}}$ near the basal body complex in $1K_{div}1N$ and early 2K1N cells, depletion of TbEB1 might have effects on flagellar assembly and structure in trypanosomes. The trypanosomal flagellum can be visualized by the monoclonal Mab25 antibody. It binds to a prolin-rich protein situated along the axoneme of old and new flagellum (Fig. 2.56) (Pradel *et al.* , 2006; Dacheux *et al.* , 2012). The flagellar length is about 17 - 21µm in 29-13 procyclic cells (Zhou *et al.* , 2011) and about 19 - 21µm in the 449 procyclic cell line (Chan & Ersfeld, 2010).

Flagella of multi-nucleated cells were comparable in length to wild type cells during the whole depletion period indicating that synthesis and maturation of flagella still occurred (Fig. 2.57, A-C). The overall anterior-posterior-polarity was not adversely affected even though a posterior cell pole could not be distinguished unambiguously anymore. Measurements of Mab25 stained flagella of tiny cells arising late during TbEB1 depletion, in general a 1K1N or a 1K0N cell, resulted in two groups: one contained flagella with a length comparable to the wild type (Fig 2.57 D, E), whilst others demonstrated a reduced length up to half of the wild type. Both groups seemed to be division products of multi-nucleated cells. Although cytokinesis was badly affected by the loss of TbEB1, the majority of cells had flagella of wild type length but aflagellated cells were found, too, indicating that the cleavage furrow was mispositioned (Fig. 2.57 F) (Vaughan *et al.* , 2008). According to YL1/2 labeling on TbEB1 depleted cells single kinetoplasts or basal bodies were observed which was confirmed by Mab25 labeling (Fig. 2.58 A, B).

After TbEB1 depletion in PCF and BSF, the number of detached flagella was increased but cellular polarity and flagellar assembly were not disturbed.

2.4.10 TbEB1 depletion resulted in a reduced FAZ length and a reduced number of FAZ in relation to the number of nuclei in procyclic trypanosomes

Microscopic analysis of TbEB1 depleted cells revealed the presence of dwarf and multi-nucleated cells and raised the question about FAZ length and formation. Moreover, in all cell types, flagella became detached, many already shortly after exiting the flagellar pocket. Detached flagella are a well-known source of a hampered FAZ synthesis as flagellar growth starts before elongation of the new FAZ, which uses the simultaneously growing daughter flagellum as track (Kohl *et al.* , 1999; Vaughan *et al.* , 2008; Zhou *et al.* , 2011). Therefore, daughter flagellum length is crucial for FAZ length. Furthermore, the FAZ defines the cleavage furrow and its length correlates with the size of the cell body after cell division (Langousis & Hill, 2014; Rotureau *et al.* , 2014). A mouse monoclonal antibody, named L3B2, was used to identify the trypanosomal FAZ. The antibody detects FAZ1, a component of the FAZ filament (Kohl *et al.* , 1999; Vaughan

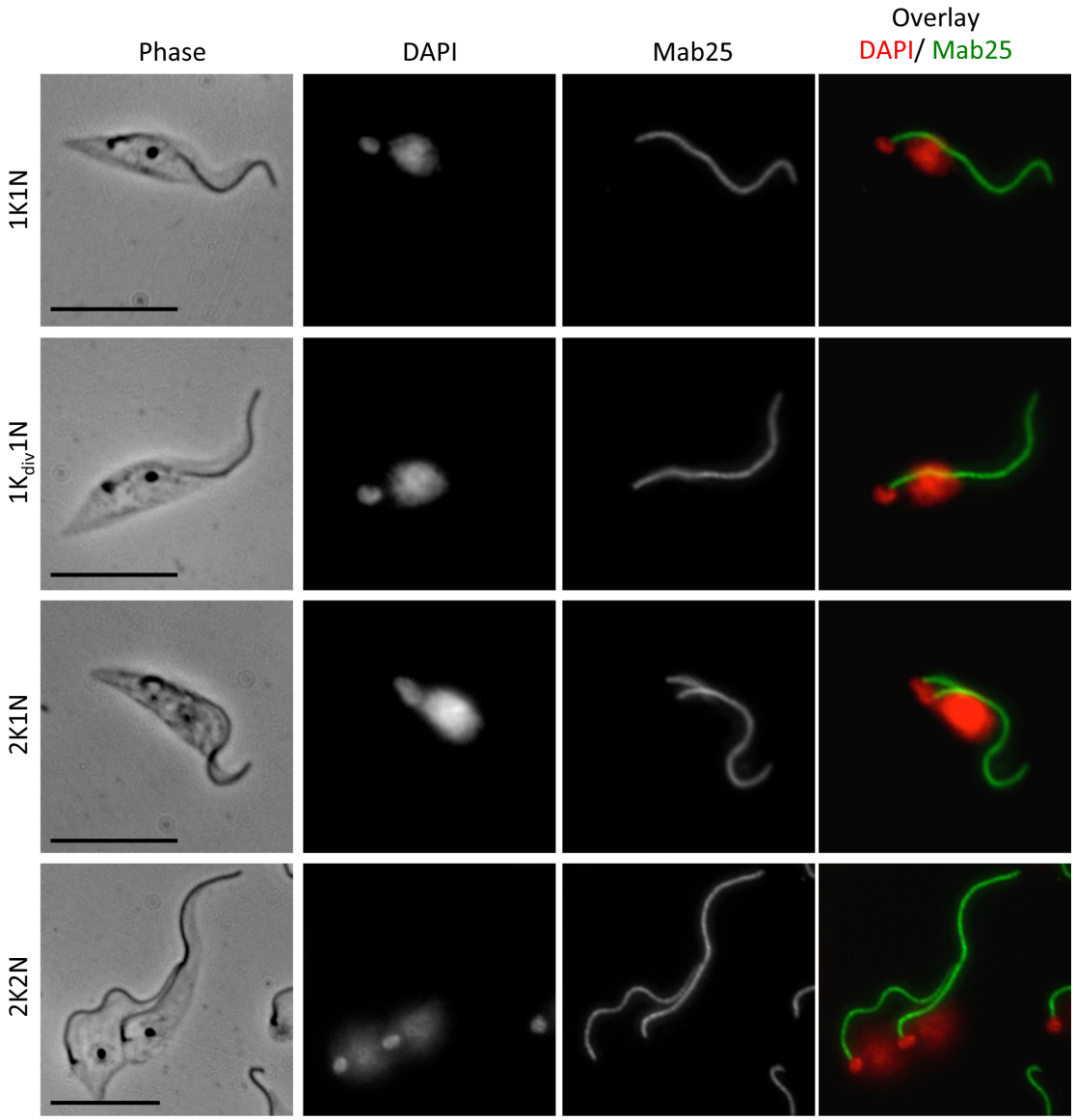


Figure 2.56: Progression of Mab25 (axonemal marker) labeling during the cell cycle in PCF. The antibody detects a prolin-rich protein of new and old flagellum. Cells were detergent-extracted with 1%NP-40 and fixed in ice-cold methanol. Scale bars represent 10µm.

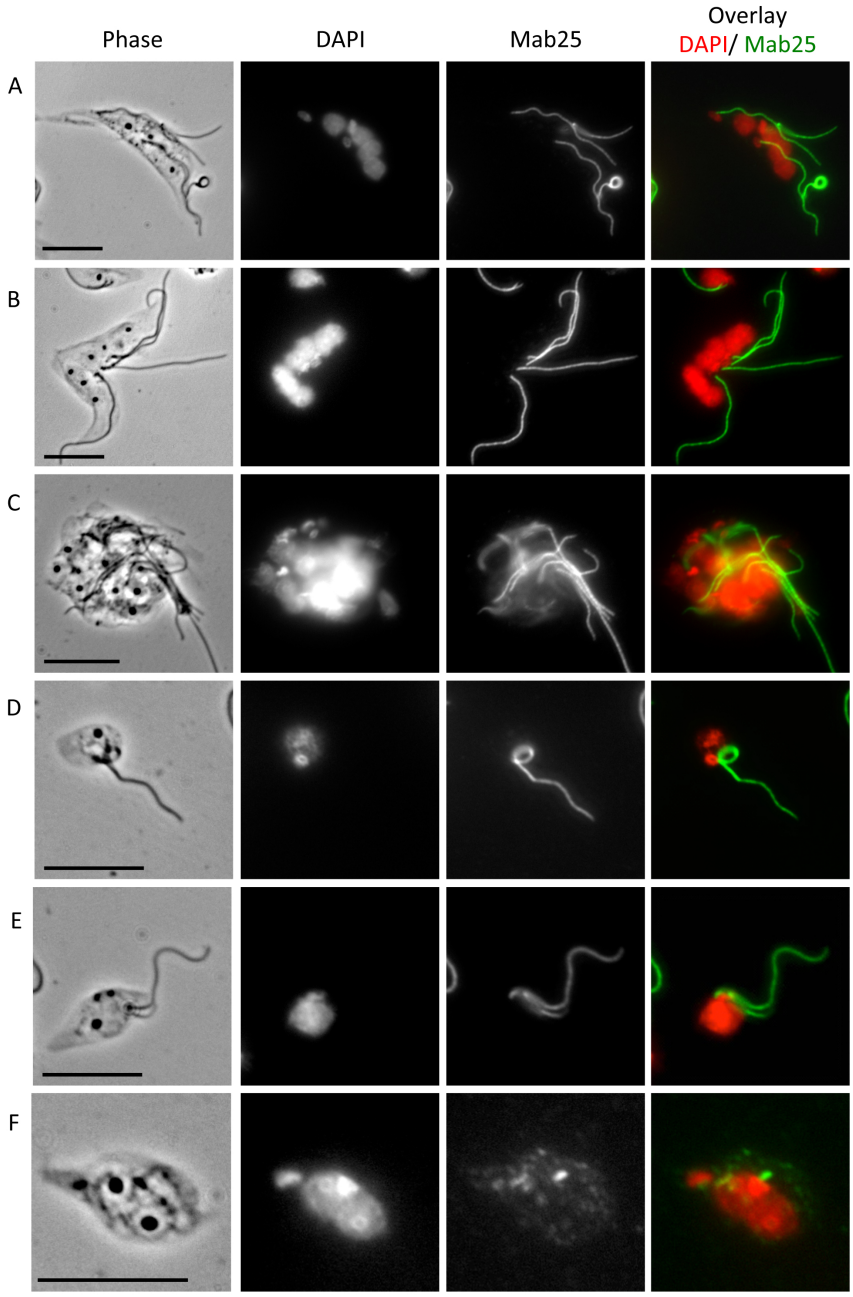


Figure 2.57: TbEB1 phenotypes stained with Mab25, an axonemal marker, in procyclic trypanosomes. A-**C**) An overall anterior-posterior orientation was still maintained even if cells were multi-nucleated or lost the typical trypanosomal shape. **D**-**E**) Small cells, which were found at the end of the 5 days induction period, still maintained a flagellum length similar to wild type cells. **F**) Aflagellated cells occurred at the end of TbEB1 depletion period. Detergent-extracted cells were probed. Scale bars represent 10µm.

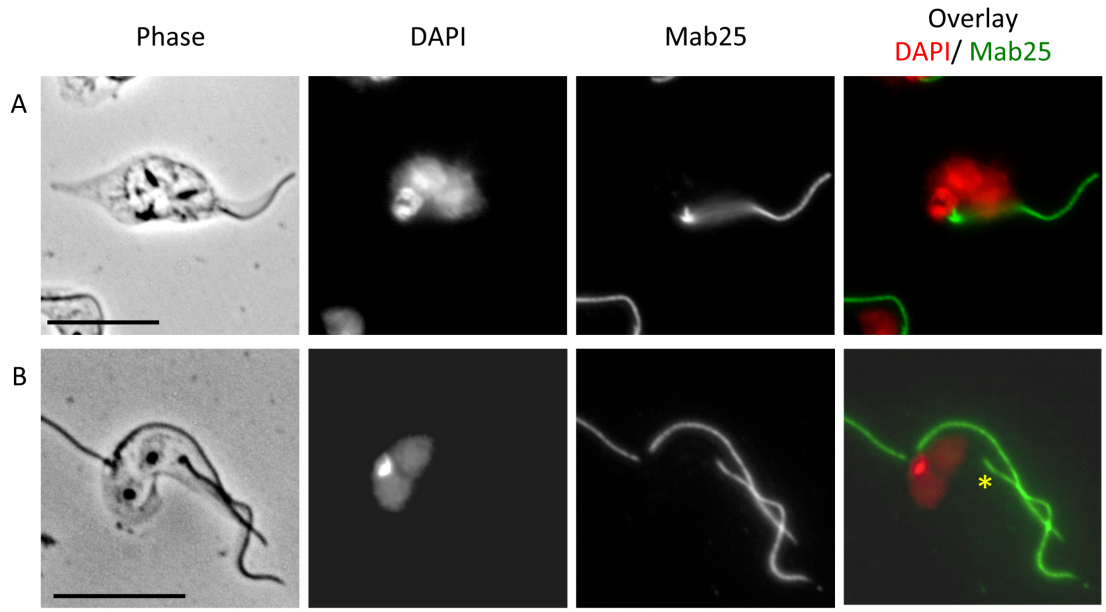


Figure 2.58: TbEB1 phenotypes detected by YL1/2 were confirmed by Mab25 staining in PCF. A) The cell possessed more kinetoplasts than flagella. **B**) A flagellum (star) occurred without any kinetoplast nearby. Cells were detergent-extracted with 1%NP-40. Scale bars represent 10µm.

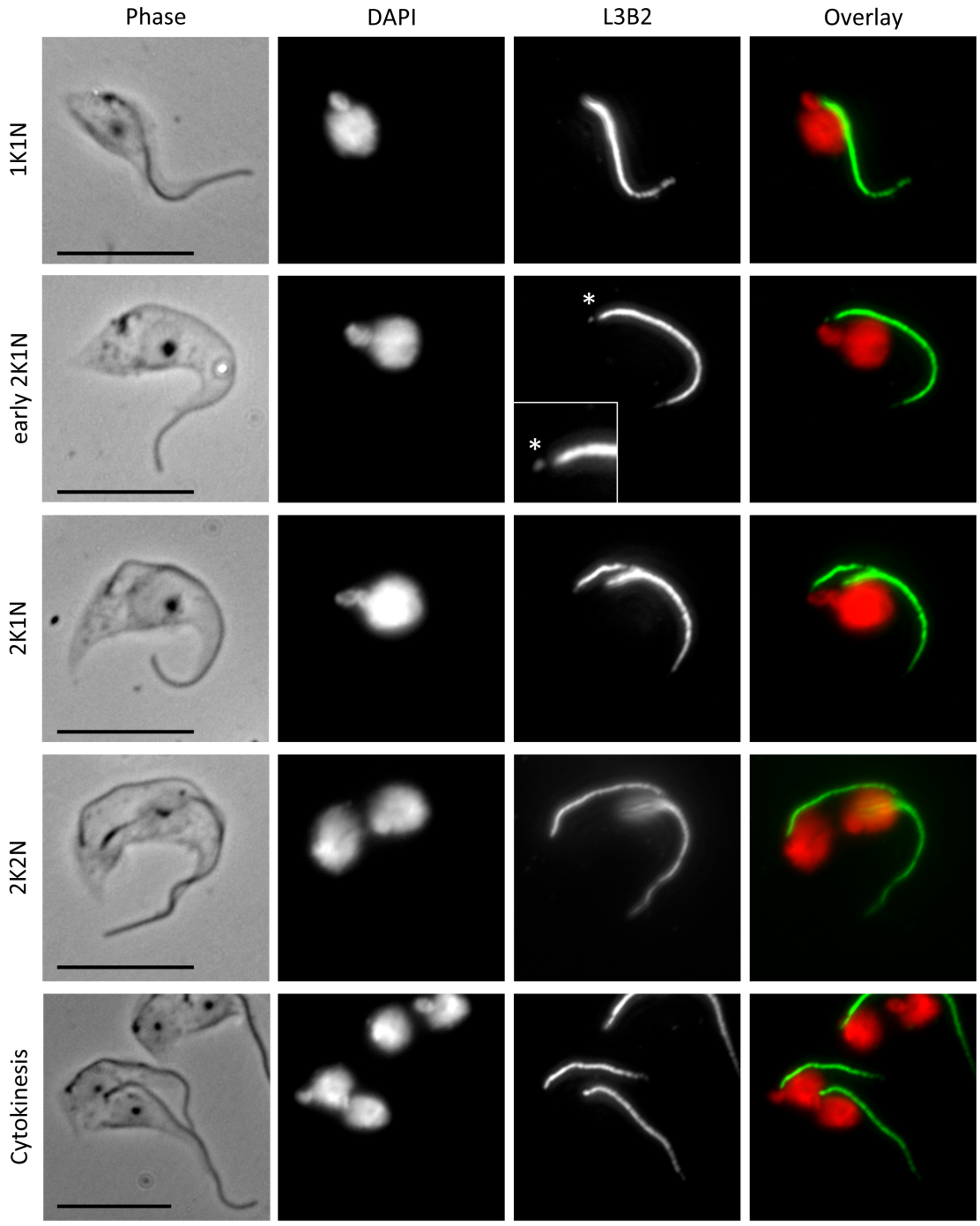


Figure 2.59: Labeling pattern of procyclic trypanosomes stained with L3B2-labeled FAZ1, a component of the FAZ filament, throughout the cell cycle in PCF. The star indicates the assembly start of the new FAZ during early G_2-phase, which is magnified in the insertion. L3B2 is a mouse monoclonal antibody and visualized by an anti-mouse secondary antibody conjugated to AlexaFluor488. Scale bars represent 10µm.

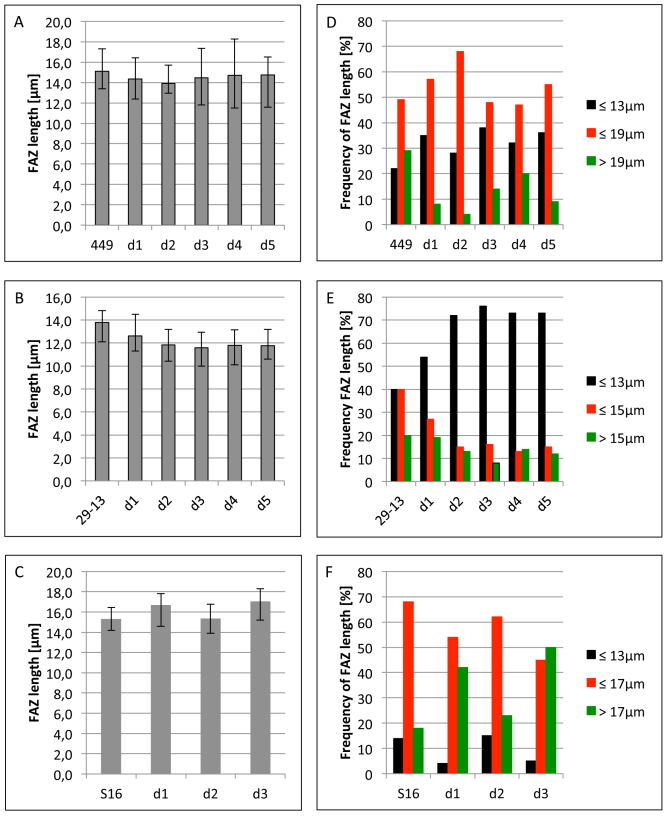


Figure 2.60: Depletion of TbEB1 resulted in an increase of small cells in procyclic trypanosomes. Wild-type (449, 29-13, S16) cells and knockdown samples of the corresponding RNAi cell lines were evaluated. The FAZ of the old flagellum of 100 cells per sample was measured, the average values were calculated (A-C) and cells were classified based on their FAZ length (D-F).

et al. , 2008). Figure 2.59 depicts trypanosomes in different cell cycle stages and probed with L3B2. FAZ1 fixates the flagellum to the cell body and is therefore detectable in both flagella. As the daughter flagella are characterized by continuous growth up to about 66% of old flagellum length during the cell cycle (Absalon *et al.* , 2007), only the mature FAZ with a fixed length over the cell cycle was investigated (Wheeler *et al.* , 2013; Langousis & Hill, 2014). In case of multinuclear cells, the FAZ which was positioned more anterior was measured as the new flagellum is always situated closer to the posterior cell pole and no evidence for a hampered basal body rotation was indicated. For procyclic and bloodstream RNAi cell lines and their corresponding wild type, 100 cells for each time point were evaluated independently of K/ N ratio. Procyclic wild type cell lines 449 and 29-13 demonstrated a median FAZ length of 15.1µm and 13.8µm, respectively (Fig. 2.60A, B). The median FAZ length for wild type BSF was 15.3µm

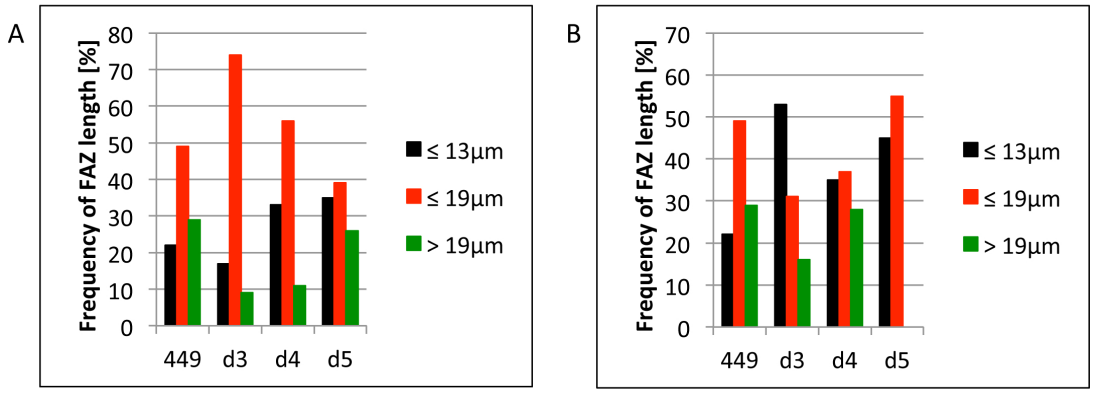


Figure 2.61: The reduced FAZ due to TbEB1 depletion was found in normal (1K1N, 2K1N, 2K2N) and abnormal (1K0N, 1K2N, xKxN) cell cycle stages of 449 TbEB1 RNAi cell line. **A**) Percentages of normal cell cycle stages and **B**) abnormal cell cycle stages of figure 47 were separated and assigned to groups according to their FAZ length. Obtained values were recalculated to 100%. Grouping of cellular FAZ length stated an increase in small cells at the end of the depletion period for normal and abnormal cell cycle stages.

(Fig. 2.60C). For RNAi cell lines, the median FAZ length did not vary, however, the distribution of different FAZ length changed particularly in TbEB1 depleted 29-13. Here from day 2 on, more than 70% of all cells demonstrated a FAZ length shorter or equal to 13µm. This was found to a lesser extent in TbEB1 depleted 449 cell line (Fig. 2.60 D, E).

For the BSF RNAi cell line (Fig. 2.60F), the amount of small cells decreased or was similar compared to wild type which is in strong contrast to the rising number of small cells observed in the procyclic cell lines. Also contrarily to PCF, the amount of large cells increased. The discrepancies to the procyclic RNAi cell lines might find their explanation in the different mode of cell division of both forms. As 449 TbEB1 RNAi demonstrated more abnormal cell cycle stages from day 3 on than 29-13 TbEB1 RNAi, only here normal and abnormal stages were differentiated (Fig. 2.61). Normal and abnormal cell cycle stages were affected. Figure 2.62A depicts a small cell with reduced FAZ length found during early time points of TbEB1 depletion. Later during TbEB1 knockdown, trypanosomes with a shortened FAZ but wild type flagellum were rarely detected (Fig. 2.62B). Those trypanosomes might be explained by a disordered cytokinesis due to the short FAZ. This is corroborated by aflagellated cells with only a tiny FAZ remaining (Fig. 2.62C). Notably, FAZ length seemed to lag behind flagella synthesis (Fig. 2.62D). Normal 2K2N cells possess two FAZ, with the new one being the starting point for the cleavage furrow. On day 3, most multi-nucleated cells demonstrated 1 or 2 FAZ. The number of the organelles duplicated over time indicated the assembly of new ones, though FAZ synthesis

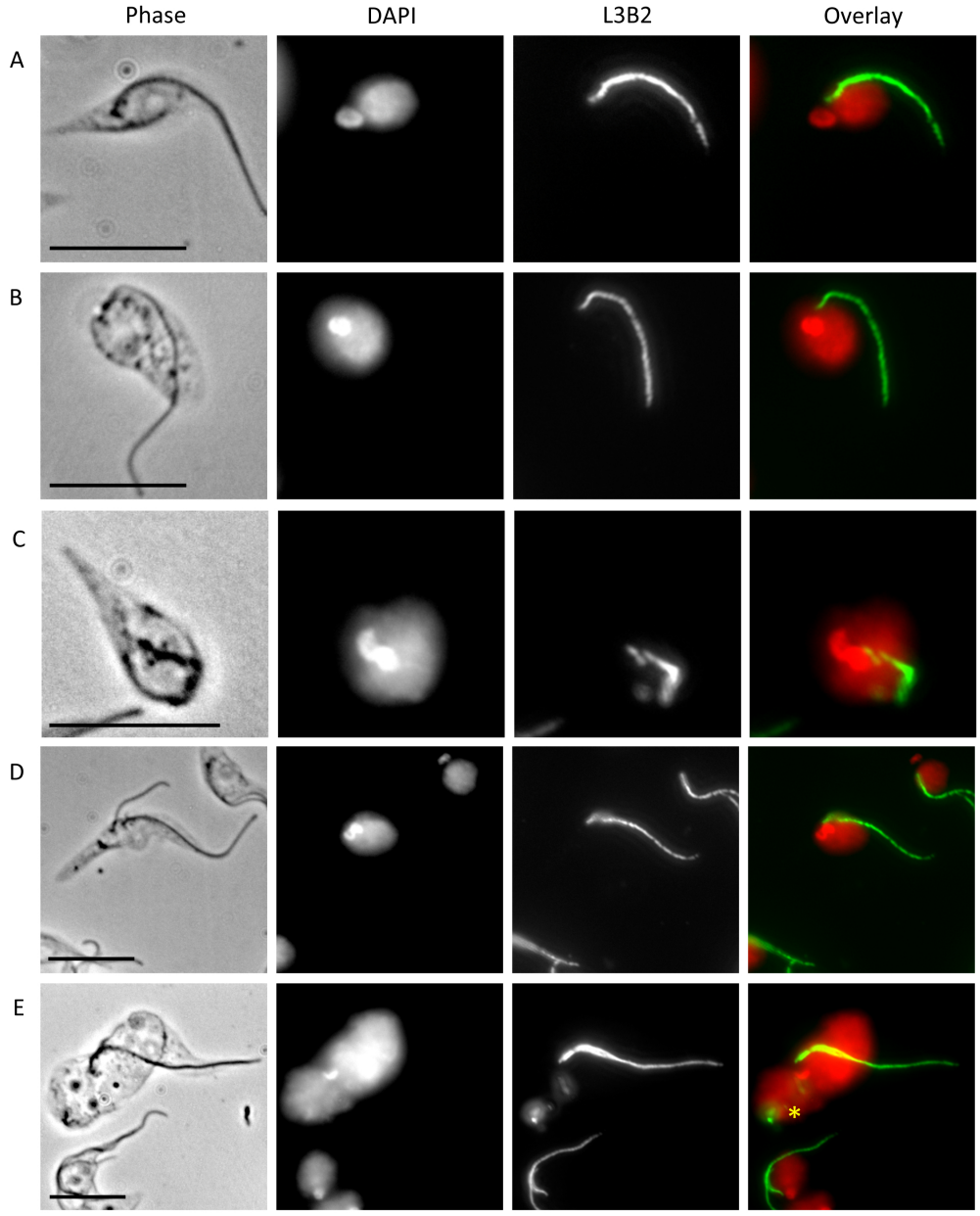


Figure 2.62: TbEB1 depletion resulted in aflagellated cells and shortened FAZ in procyclic trypanosomes. Example of **A**) a small cell with a reduced FAZ length (11.1µm), **B**) a deformed cell with a detached flagellum demonstrating also a shortened FAZ (11.4µm), **C**) an aflagellated cell with a short FAZ (4.1µm), and **D**) a cell with a new flagellum growing although the new FAZ length is dramatically reduced. **E**) The number of FAZ was smaller than the number of nuclei. The star indicates the starting point for new FAZ. The general FAZ length in 29-13 cells was about 14µm. Labeling of detergent-extracted cytoskeletons. Scale bars represent 10µm.

seemed to lag behind mitosis, as indicated by the presence of e. g. 2K4N cells with only 1 FAZ. Only even numbers were detected demonstrating a simultaneous replication in case of two or four FAZ per cell. However, just taking into account the number of nuclei especially during day 4 and day 5, more FAZ per cell would have been expected (Fig. 2.62E). But the low number of FAZ fits to the low number of kinetoplasts in that cells. Furthermore, as the developing FAZ uses the growing flagellum as template, a shortened FAZ due to a loose flagellum might explain the tiny cells with mostly wild type flagella length at the end of the 5-day depletion period in PCF.

Summing up, the increase in small cells was higher in the 29-13 TbEB1i than in 449 TbEB1i cell line, which is consistent with the higher percentage of detached flagella. Evaluation of the S16 TbEb1i cell line was hampered by the huge amount of lysed cells.

2.4.11 Depletion of TbEB1 does not affect the overall structure of the subpellicular microtubule array

Trypanosomal cell polarity and shape are defined by the subpellicular microtubule corset, and organelle distribution is mainly cytoskeleton-mediated by yet unknown mechanisms (Robinson *et al.* , 1995; Gull, 1999; He *et al.* , 2004; Selvapandiyan *et al.* , 2007). Since TbEB1 is attached to the subpellicular microtubules and depletion of TbEB1 interferes with cellular morphology combined with a reduced YL1/2 labeling and an impeded kinetoplast segregation, the assembly and organization of the microtubule array was questioned. Localization of TbEB1 was revealed by immunogold labeling via the specific antibody on detergent-extracted whole mount cytoskeletons. Analyzing the microtubule array composition, the microtubules still appeared evenly spaced and remained parallel when performing the typical left-handed helix twist. Similar to IFA, a decreased labeling density after TbEB1 depletion was only visible in some cells, independently of K/ N ratios (Fig. 2.63, 2.64). However, like in YL1/2 staining when cells were extremely rounded and a posterior cell pole was hardly distinguishable from the cell body, a strong decrease in TbEB1 labeling intensity was detected at the posterior end (Fig. 2.64) but labeling of the cell body was still detectable. As whole mount cytoskeletons of procyclics and TEM analysis of TbEB1 RNAi bloodstream cell line did not reveal a disturbed composition of the microtubule array. The subpellicular cytoskeleton of procyclic TbEB1 RNAi cell lines was not further investigated by TEM analysis.

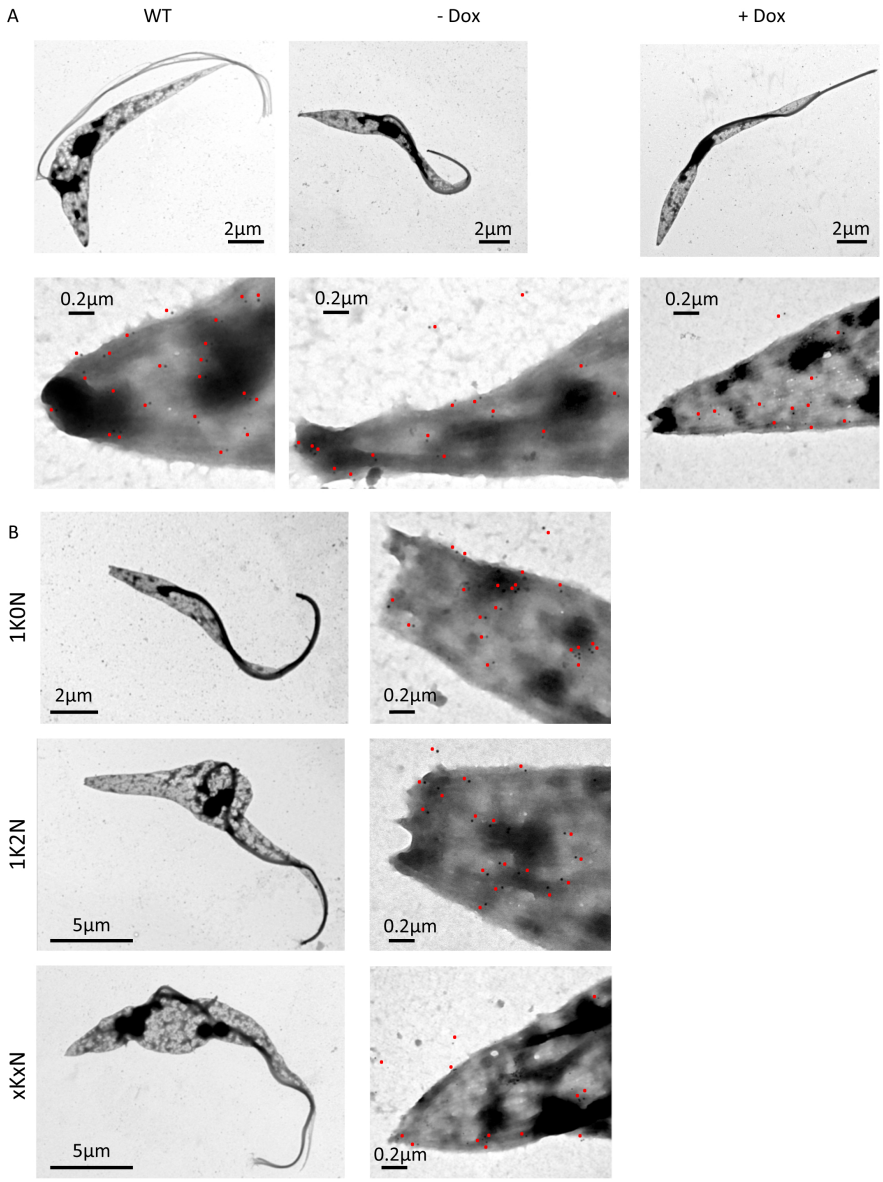


Figure 2.63: TbEB1 staining of procyclic RNAi cell lines of electron micrographs. **A**) TbEB1 labeling density is slightly reduced after depletion in some cells. **B**) Atypical cell cycle stages after TbEB1 RNAi knockdown (left) and TbEB1 labeling at their posterior cell pole (right). Whole mount cytoskeletons were produced by detergent-extraction of trypanosomes and visualized by electron microscopy. TbEB1 was detected by the anti-TbEB1 mouse monoclonal antibody and an anti-mouse antibody labeled with 10nm gold.

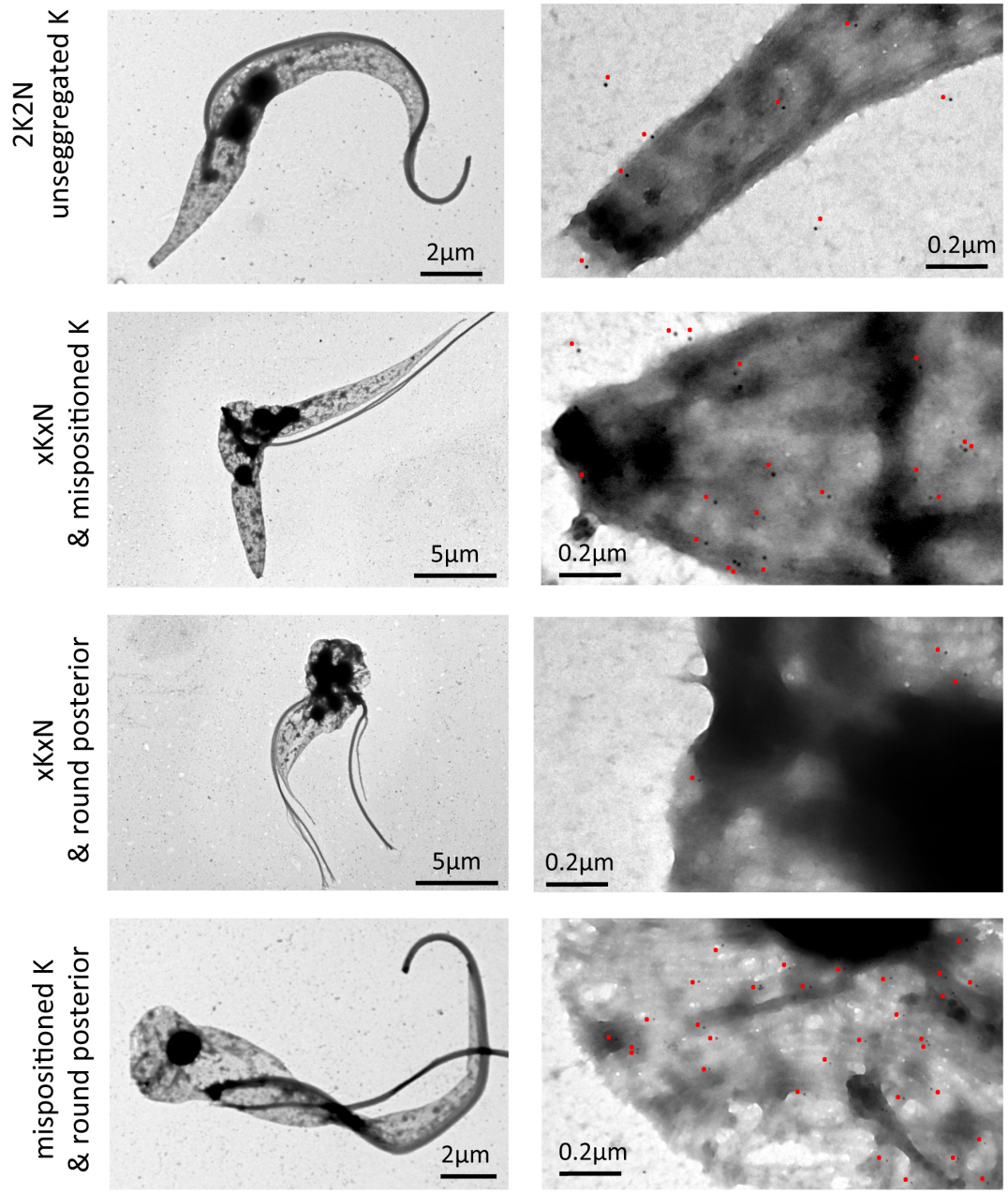


Figure 2.64: Comparison of atypical cell cycle stages with normal and rounded posterior cell end. As long as the cell morphology of TbEB1 depleted cells resembles the wild type (upper two panels), the anti-TbEB1 labeling density is comparable to wild type labeling. Cells with a rounded posterior (lower tow panels) frequently demonstrate a reduced TbEB1 labeling. Whole mount cytoskeletons were produced by detergent-extraction of trypanosomes and visualized by electron microscopy. TbEB1 was detected by the anti-TbEB1 mouse monoclonal antibody and an anti-mouse antibody labeled with 10nm gold.

2.4.12 Putative TbEB1 single gene knockout cell lines reflect some characteristics from RNAi phenotypes

To find a more distinct phenotype than observed by RNAi and to demonstrate essentiality of TbEB1, double gene knockout cell lines were planned to be for both, PCF and BSF. It was not possible to obtain null mutants (wild type background) for both forms. Even conditional double knockouts (TbEB1myc background) failed although here TbEB1 was ectopically expressed by doxycycline induction. However, TbEB1 single-allele knockout (sko) was achieved, whereby one wild type allele was exchanged by a drug resistance cassette (Fig. 2.65). Only TbEB1 sko based on wild type 427 and S16 background are described here, as possibly low amounts of tetracycline in cell culture media led to background induction in case of TbEB1myc cell lines, thereby weakening or covering effects due to the single gene knockout. Single gene knockout status of the obtained clones was verified by PCR and clones were named either 427 TbEB1 sko (Fig. 2.65 A) or S16 TbEB1 sko (Fig. 2.65 B). Two different PCR were performed: one used TbEB1 PCR for and rev as primer which bind to 5´and 3´UTR regions 100bp away from homologous recombination positions. Therefore, for the wild type allele a 2397bp fragment was expected, and for the allele with the drug resistance gene a 1388bp fragment. The second PCR contained TbEB1 PCR rev and Puro rev as primers. In the single-allele knockout cell lines, a PCR product of 994bp was expected. PCR results were positive for PCF although some unspecific bands of different size were detectable. For BSF, the first PCR gave a clear result. However, using the Puro rev primer resulted in an unspecific side product of almost identical size only in wild type bloodstream trypanosomes. But compared to wild type, the desired PCR fragment demonstrated a slightly different size and a stronger intensity.

However, only the monoclonal anti-TbEB1 antibody was available at that time. As it does not work on immuno blots, a reduction of the TbEB1 signal on immuno blots was not determinable. Microscopical analysis revealed atypical cell cycle stages: zoids, 1K2N, and xKxN cells for PCF (Fig. 2.67 A-D) and zoids and xKxN cells for BSF (Fig. 2.67 E-G). The amount of atypical stages was quite low in BSF, therefore, it was not further investigated. A census of the procyclic single gene knockout cell line revealed a relative amount of about 20% of atypical stages (Fig. 2.68 A). The quite even numbers of 1K0N, 1K2N, and xKxN cells again indicated an impeded cytokinesis (Fig. 2.68 B). Like for RNAi cell lines, sometimes an enlarged nucleus was found in 1K1N cells probably resulting in a 1K2N cell. This phenotype as well as one demonstrating a mispositioned kinetoplast were assigned to the category ‘others’. For both forms, the morphology of cells resembled the wild type. An extreme accumulation of nuclei as has been found in procyclic RNAi cell lines was not observed. Zoids in those cell lines were also not as slim and short as in RNAi cell lines and more comparable with those found in the pro-

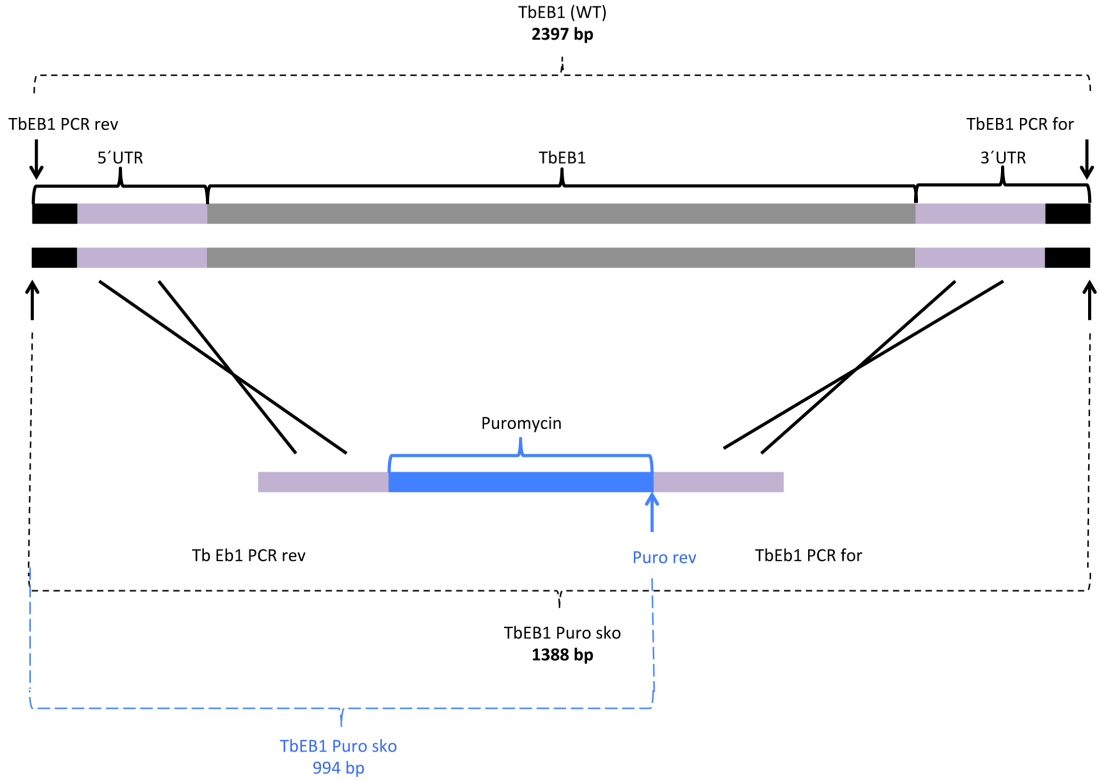


Figure 2.65: Schematic of single gene knockout strategy. One target allele (grey) was exchanged with a puromycin (blue) resistance by homologous recombination using flanking 5'and 3'UTR regions (purple). Black arrows mark positions of the TbEB1 PCR primer pair. The blue arrow marks the position for the puromycin reverse primer. Together with the TbEB1 PCR rev oligo, PCR only results in a gene product after successful target gene replacement.

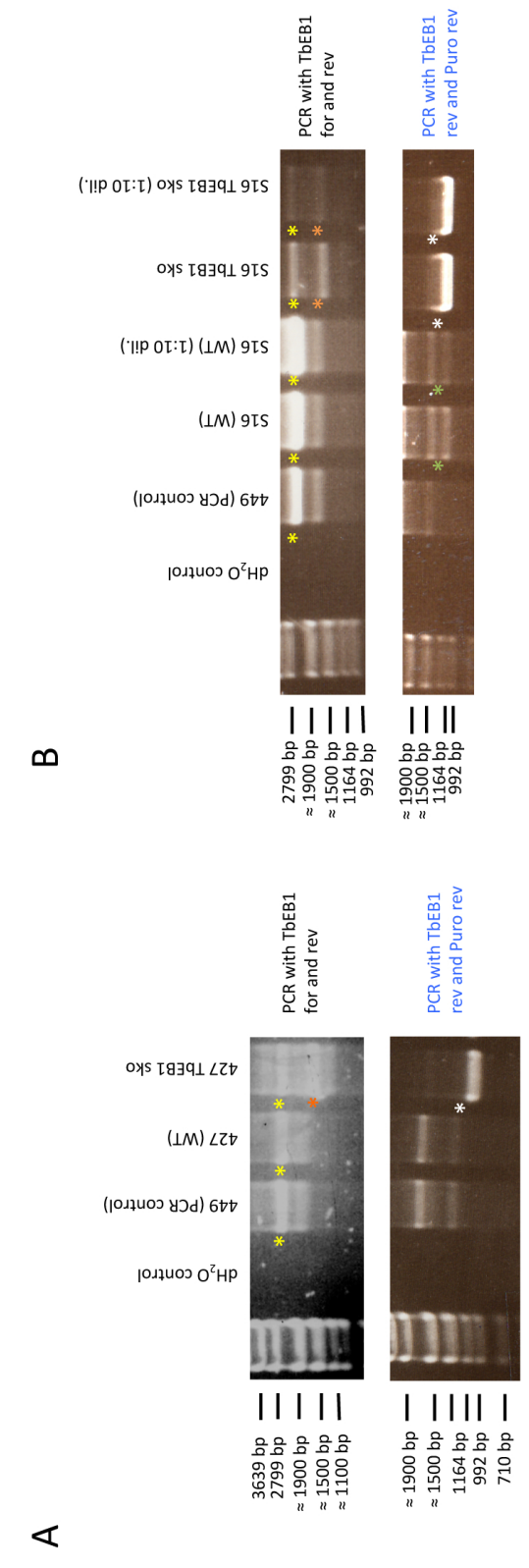


Figure 2.66: Single gene knockout cell lines of PCF and BSF trypanosomes were confirmed by PCR. A) PCR gels of PCF sko clones deriving from 427 (WT). A negative (dH_2O) and positive (genomic DNA of 449) sample were introduced as PCR controls. The upper panel shows the PCR result using TbEB1 PCR for and rev oligos. WT and single knock-out cell line possess a band of approx. 2400bp demonstrating the wild type allele (yellow star). Only the single knockout cell line 427 TbEB1 sko possesses an additional band of approx. 1400bp (orange star). The lower panel shows the PCR result using TbEB1 PCR rev and Puro rev oligos. Only the single knockout cell line demonstrates a band of approx. 1000bp size (white star). **B)** PCR gels of BSF sko clones deriving from S16 (WT). A negative (dH_2O) and a positive (genomic DNA of 449) sample were introduced as PCR controls. The upper panel shows the PCR result using TbEB1 PCR for and rev oligos. WT and single knockout cell line possess a band of approx. 2400bp demonstrating the wild type allele (yellow star). Only the single knockout cell line 427 TbEB1 sko possesses an additional band of approx. 1400bp (orange star) confirming the exchange of wild type allele with puromycin resistance cassette. The lower panel shows the PCR result using TbEB1 PCR rev and Puro rev oligos. Only the single knock-out cell line demonstrates a band of approx. 1000bp size (white star). Bands in wild type BSF samples marked with the green star have a slightly higher size and are unspecific side products only arising in BSF.

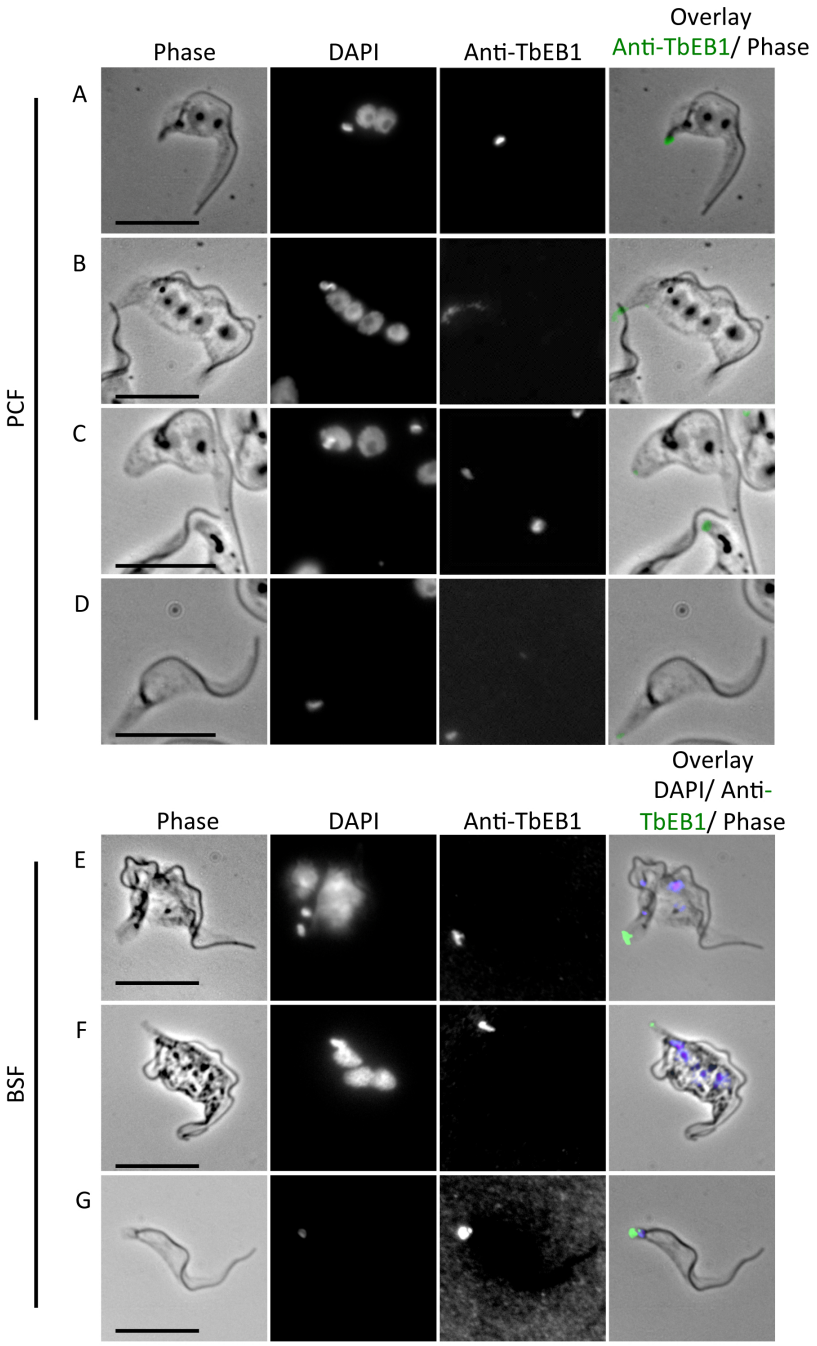


Figure 2.67: Putative TbEB1 single-allele knockouts reflect characteristics of the RNAi phenotype in procyclic and bloodstream trypanosomes. **A**-**D**) Typical abnormal cell cycle stages in procyclic trypanosomes: 1K2N, xKxN, mispositioned kinetoplast, and zoid. **E**-G) Typical abnormal cell cycle stages in bloodstream trypanosomes: xKxN and zoids. Cytoskeletons of PCF and BSF after detergent-extraction with NP-40. Scale bars represent 10µm.

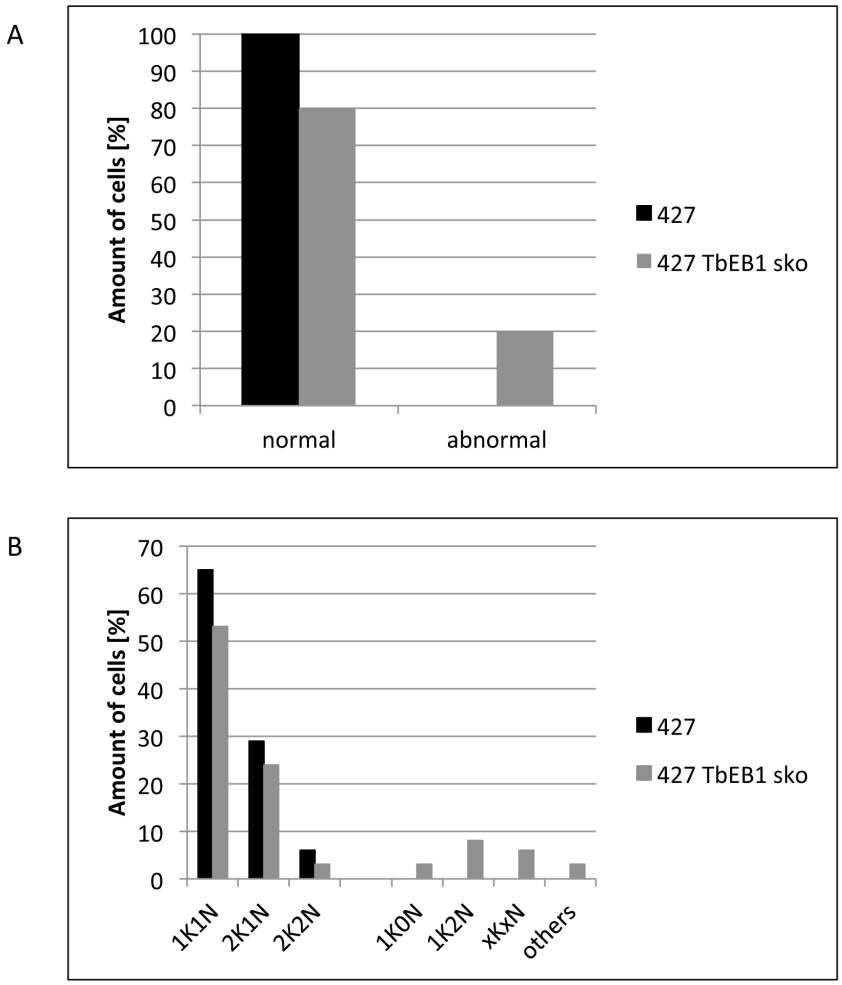


Figure 2.68: Accumulation of atypical cell cycle stages (1K0N, 1K2N, xKxN) in PCF due to TbEB1 single gene knockout indicating an impeded cytokinesis in PCF. A) Summary and **B**) detailed mapping of cell cycle stages occurring in 427 TbEB1 sko and corresponding wild type. 100 cells were categorized by DAPI-stained trypanosomal DNA and counted as multinuclear if the cell possessed more than two nuclei. Cells were classified as ‚others´ if the cell morphology was disturbed, e. g. demonstrated a mispositioned kinetoplast.

cyclic over-expression cell line TbEB1myc. Only few detached flagella were found, matching to the low occurrence of mispositioned kinetoplasts. TbEB1 was still localized to the posterior cell pole and to the posterior part of the division furrow (Fig. 2.67). Cultivation of single gene knockout cell lines was quite difficult as obtained cell lines either got extinct shortly after establishment or were outgrown in case of non-clonal cell lines. Both prevented further experiments with those cell lines.

Summing up, the observed phenotypes in PCF and BSF putative single gene knockouts resemble those for RNAi cell lines but are less pronounced suggesting a dosage effect of TbEB1. Together with the short cultivation period of the single-allele knockout, it supports the hypothesis that TbEB1 is an essential gene in *T. brucei*.

2.4.13 Evaluation of TbEB1 ectopic expression

2.4.13.1 Ectopically expressed TbEB1 localizes similar to endogenously tagged TbEB1 variants in PCF and BSF

Over-expression may aid localization in the cell if physiological levels are too low and conclusions on TbEB1 function can be drawn from the over-expression phenotype. Moreover, it is known, that over-expression of BIM1 in *S. cerevisiae,* the budding yeast homologue, leads to an abnormal budding index and cell cycle progression in G_2 (Sopko *et al.* , 2006). To over-express TbEB1, the complete open reading frame of TbEB1 was inserted into the pHD1800 vector enabling a high expression of the desired c-myc-tagged protein under control of a doxycycline-inducible TETrepressor-operator system. The construct was then stably integrated into the rRNA spacer region of 449 cell line by homologous recombination and correct translation of the c-myc tagged fusion protein confirmed by immuno blots. Obtained cell lines were referred to as TbEB1myc. The fusion proteins were detected at about 70kDa fitting to their calculated molecular mass of about 60kDa (Fig. 2.69). The additionally expressed c-myc-tagged TbEB1 proteins could interfere with proper localization, too. Therefore, first time course experiments were generated to monitor expression levels and localization of the protein within 24 hours of growth in the presence of doxycycline. Immuno fluorescence and blot samples from procyclic trypanosomes grown in the absence of doxycline often demonstrated a weak labeling or band indicating a slight leakiness of the expression system (Fig. 2.69A). The fusion protein was already detectable by both methods after 1 hour of induction (Fig. 2.69A, Fig. 2.70) and was strongest after 24 hours of induction for whole cell preparations. After 6 hours, the TbEB1$^{\text{C-2xmyc}}$ localized also at the posterior cell pole in most cells independently of cell cycle stage contrasting the results from the procyclic cell lines endogenously expressing the protein. Here, only the 12x c-myc tagged version of the protein was localized to the posterior cell pole of S-, G_2- and

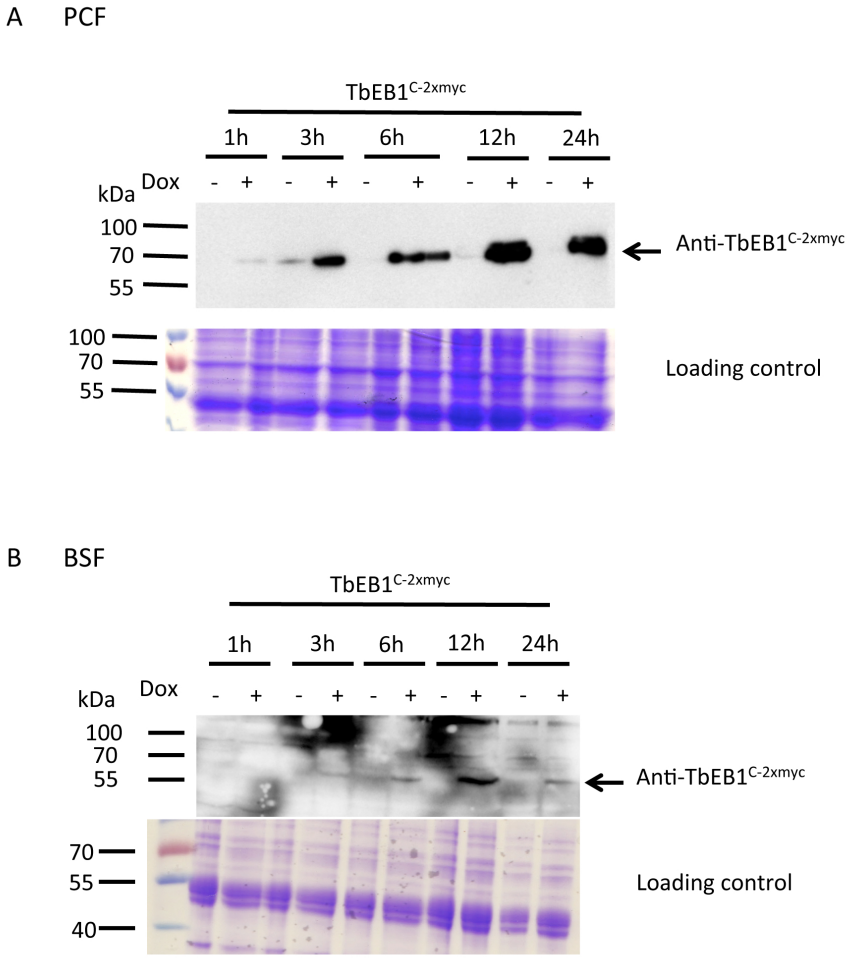


Figure 2.69: Confirmation of TbEB1$^{C\text{-}2xmyc}$ expression during a time course experiment by Western blot analysis of procyclic and bloodstream trypanosomes. Whole cell preparations of non-induced (-Dox) and induced (+Dox) trypanosomes were analyzed over time by the anti-c-myc antibody and an appropriate secondary antibody. The intensity of expression patterns were compared by immuno blotting and found strongest after 24 hours of induction for PCF and 12 hours of induction for BSF. **A**) In immuno blot analysis of PCF, a band of about 70kDa was detected in doxycycline-induced samples and correlating with the calculated mass for TbEB1$^{C\text{-}2xmyc}$. The light bands of about 70kDa detected in non-induced samples were due to background induction. **B**) In immuno blot analysis of BSF, a band of about 70kDa was detected in response to addition of doxycycline and correlating with the calculated mass for TbEB1$^{C\text{-}2xmyc}$. Additional bands detected on the immuno blot membrane are probably due to unspecific binding of the anti-c-myc primary antibody, which are intensified by the high exposure time. Coomassie-stained SDS gels were used as a loading control for whole cell lysates.

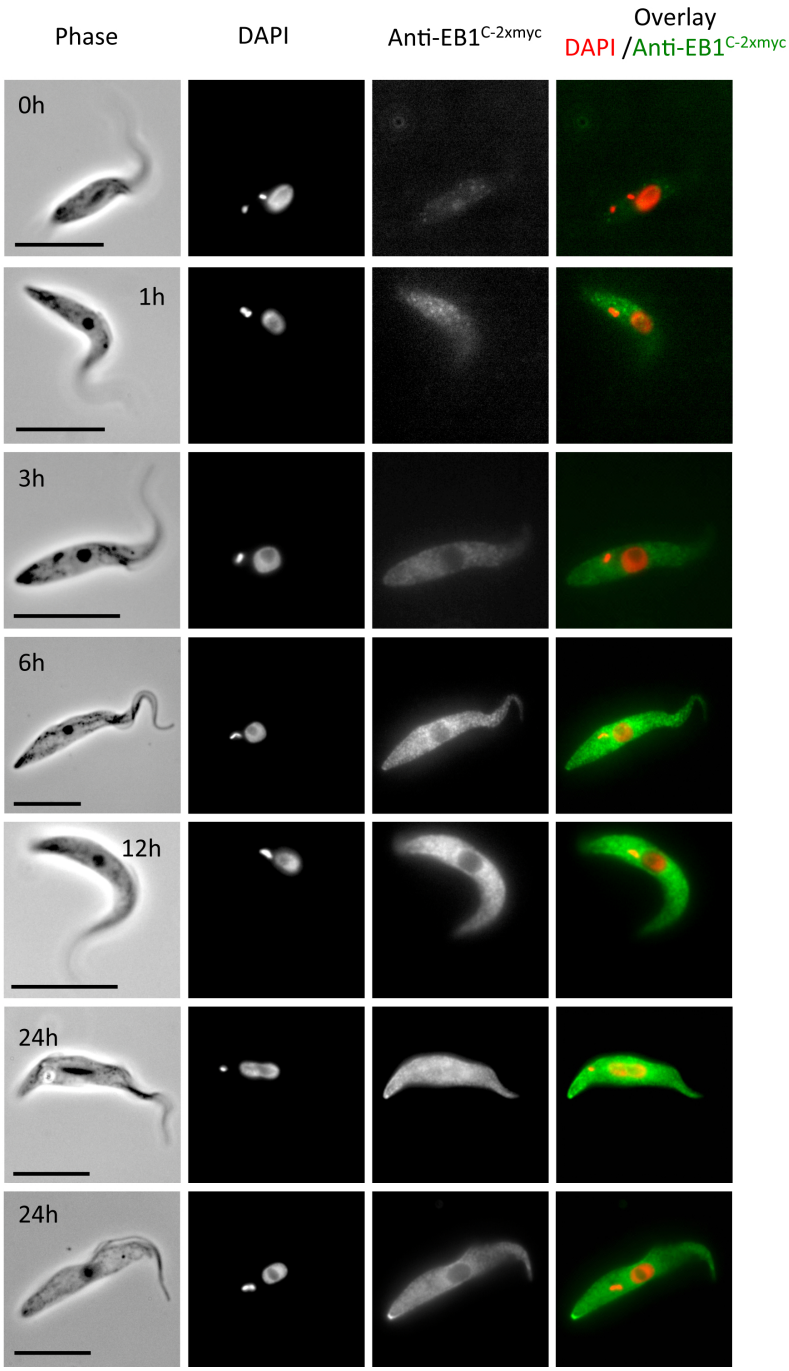


Figure 2.70: Labeling of a c-myc-tagged TbEB1 ectopically expressed in procyclic trypanosomes during a 24 hours time course. Whole cell preparations of non-induced (0h) and induced (1h-24h) trypanosomes were prepared and TbEB1$^{C\text{-}2xmyc}$ expression was observed over time by the anti-c-myc antibody and an appropriate secondary antibody. The intensity of expression patterns were compared and found strongest after 24 hours of induction. After 6 hours of induction, an accumulation of the ectopic TbEB1 at the posterior cell pole was detected in some cells. As the 24 hour panels demonstrate, not all cells were labeled with the same intensity. Scale bars of represent 10µm.

M-phase cells but never of G_1-phase cells (1K1N), the cell cycle stage with the lowest TbEB1 labeling signal at the posterior cell pole. Quite likely, the amount of exogenously tagged protein at the posterior cell pole was now high enough to be above the cell body labeling by cytoplasmic TbEB1$^{C\text{-}2xmyc}$. In cytoskeletons the subpellicular microtubule array, the FAZ, and the posterior cell pole were decorated with anti-c-myc antibody already 3 hours p. i. (Fig. 2.71). Here, the staining was more intense then in whole cells. This difference disappeared after 6 hours when the whole cytoplasm showed homogenous staining. Therefore, it is concluded that over-expression of TbEB1$^{C\text{-}2xmyc}$ leads to an unspecific accumulation of the protein in the cytoplasm. Except the mitotic spindle, the same sub-cellular compartments, including the cytoplasm, as for endogenous TbEB1 were identified. The number of epitope tags for both systems could be set equal which allows comparison of signal intensities. The comparison revealed that ectopic expression reached endogenous levels of tagged TbEB1 already after 3 hours on Western blots, which fits at large to the results obtained by IFA (Fig. 2.71). 24 hours samples were taken to describe the variation in labeling pattern during the cell cycle of over-expressed TbEB1$^{C\text{-}2xmyc}$ in PCF as here the highest levels were found (Fig. 2.72). TbEB1$^{C\text{-}2xmyc}$ was detected at the posterior cell pole throughout the whole cell cycle. In contrast to the antibody-mediated staining of endogenous TbEB1, the intensity of labeling at the posterior of 1K1N and 2K1N cells was not cell stage dependent. Nonetheless, when the kinetoplast was dividing a staining of the newly synthesized FAZ was frequently observed but no elongation of the posterior end labeling. An elongated signal was frequently found only on 2K2N cells resembling that obtained by the antibody. Up to cytokinesis, the signal intensity localized at the subpellicular microtubules enhanced suggesting an increased activity of microtubule generation and remodeling.

In BSF, first signals occurred in whole cell IFA and Western blot analysis after 3 hours p. i. and reached a maximum after 12 hours (Fig. 2.69 B, Fig 2.73). The signals included staining of the posterior cell pole and disperse loci formation on the subpellicular microtubule array. Again contrarily to endogenous tagging, not all cells demonstrated an intense posterior cell pole labeling, which might also be explained by a constant TbEB1 exchange. Similar to PCF, over-expression of TbEB1 resulted in an accumulation of the protein in the cytoplasm. On cytoskeletal preparations (Fig. 2.74), after 3 hours of induction only dividing cells (2K2N) demonstrated a posterior signal strong enough for detection by light microscopy. When 6 hours passed, in most cells a labeling of the posterior end, the subpellicular microtubule array, and sometimes a faint labeling of the FAZ were observed. Some cells in the 6 hours samples demonstrated a stronger labeling of the subpellicular microtubule array often coinciding with a dividing kinetoplast. As the strongest signals were obtained after 12 hours p. i., a variation in TbEB1 labeling pattern during the cell cycle was evaluated in those samples (Fig. 2.75). Again as in PCF, no differences in signal intensity were observed between 1K1N and 2K1N cells. However,

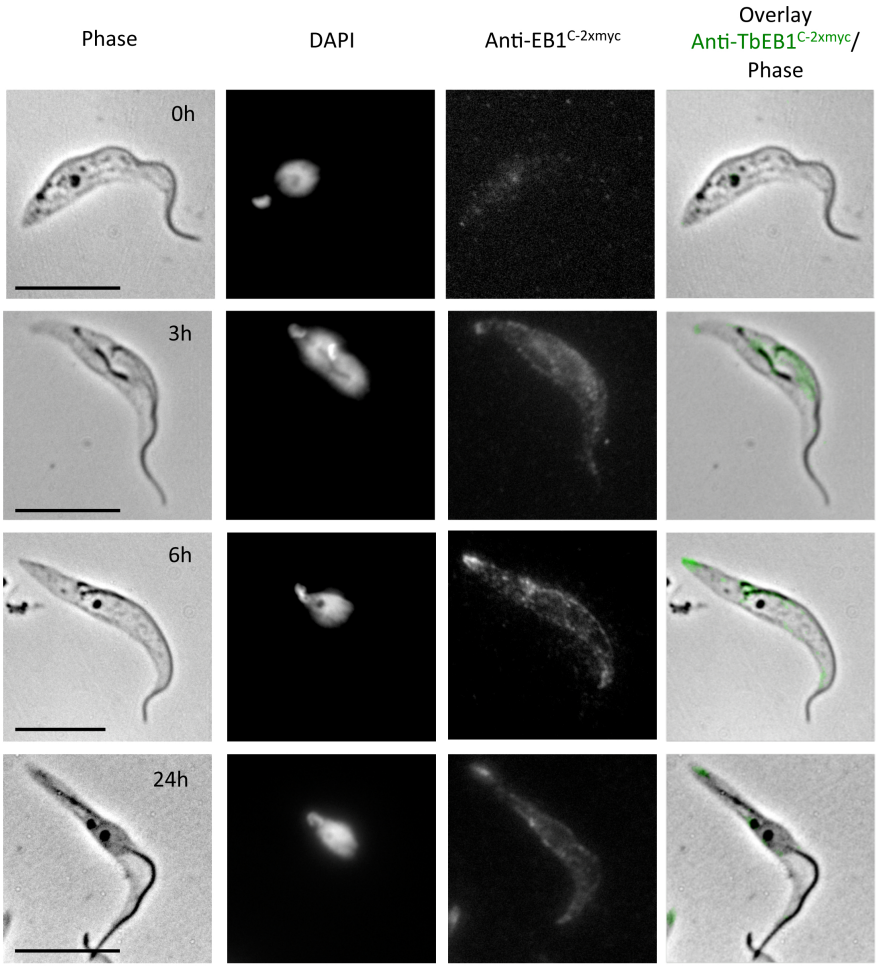


Figure 2.71: Labeling of c-myc-tagged TbEB1 ectopically expressed in procyclic trypanosomes during a 24 hours time course. Cytoskeletal preparations of non-induced (0h) and induced (3h, 6h, 24h) trypanosomes were performed and TbEB1$^{C\text{-}2xmyc}$ expression was observed over time by the anti-c-myc antibody and an appropriate secondary antibody. The intensity of expression patterns were compared and found strongest after 24 hours of induction. After 3 hours of induction, an accumulation of the ectopic TbEB1 at the posterior cell pole was detected in some cells as well as a localization to the cell body cytoskeleton. The signal intensity increased at these points after 6 and 24 hours. Compared to whole cell preparations most of ectopically expressed TbEB1 was localized in the cytoplasm. Scale bars represent 10µm.

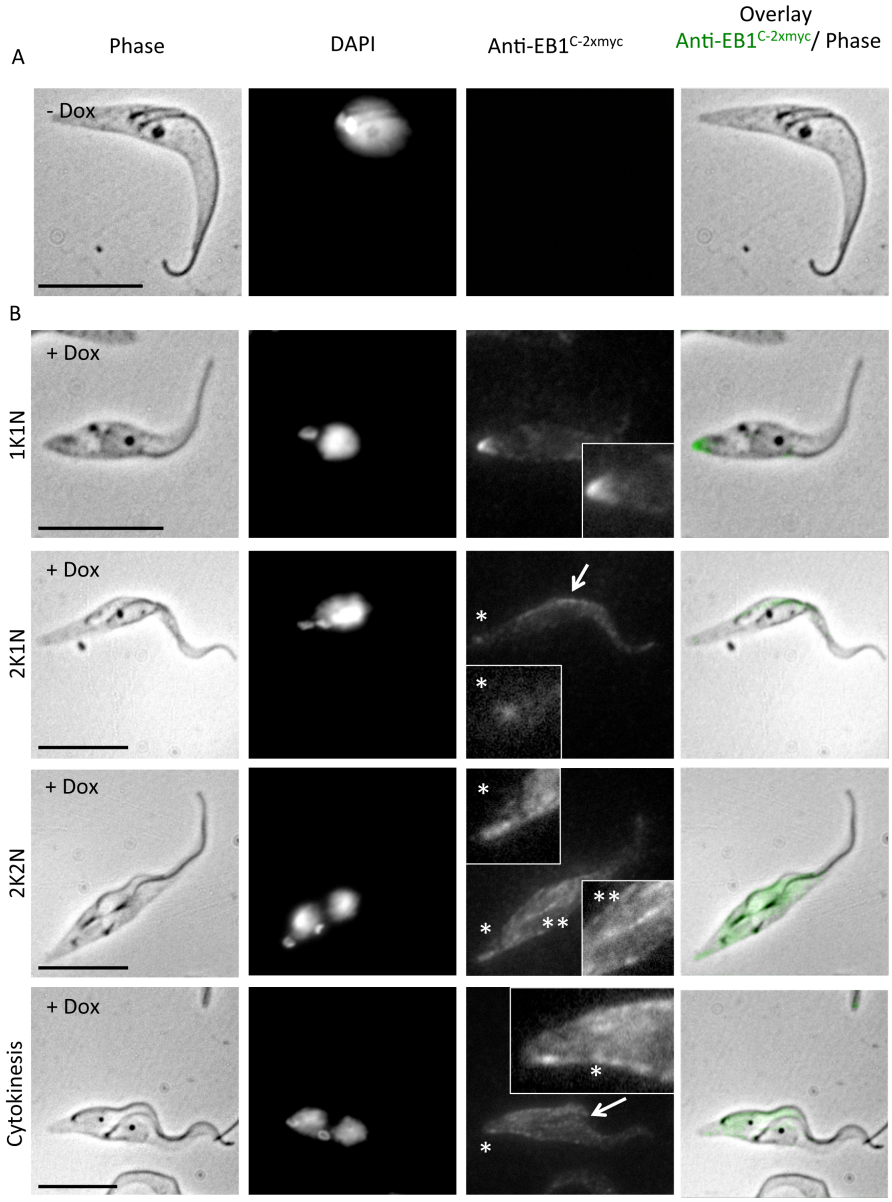


Figure 2.72: Labeling pattern of inducible ectopic expression of TbEB1 in procyclic trypanosomes after 24 hours concerning the cell cycle. Panel **A** demonstrates the non-induced control (-Dox), panel **B** (+Dox) the expression pattern of TbEB1$^{C\text{-}2xmyc}$ over the cell cycle. Detergent-extracted cytoskeletons revealed a TbEB1$^{C\text{-}2xmyc}$ labeling at the posterior cell pole (star) throughout the cell cycle. Cells with a dividing kinetoplast often demonstrated a stronger labeling of the FAZ (2K1N, arrow). Localization of ectopically expressed TbEB1 to the spindle is still questionable (2K2N, 2 stars). During cytokinesis, the newly formed posterior end of the old-daughter flagellum cell could be made out (star within insert) and the start of the ingression furrow (arrow). The ectopically expressed fusion protein was identified by a mouse monoclonal anti-c-myc antibody and an appropriate secondary antibody. Inserts are magnifications of TbEB1$^{C\text{-}2xmyc}$ labeling. CSK were fixed with ice-cold methanol. Scale bars represent 10µm.

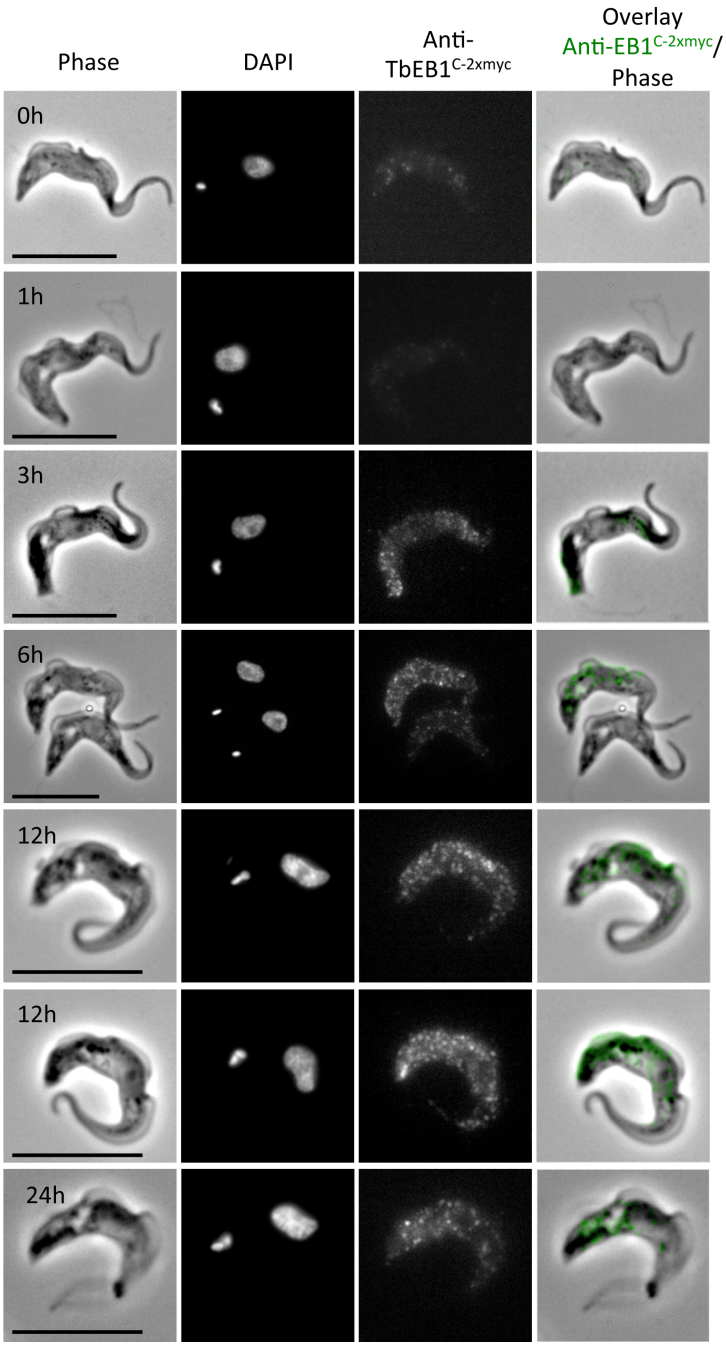


Figure 2.73: Labeling of a c-myc-tagged TbEB1 ectopically expressed in bloodstream trypanosomes during a 24 hours time course. Whole cell preparations of non-induced (0h) and induced (1h-24h) trypanosomes were prepared and TbEB1$^{C\text{-}2xmyc}$ expression was analyzed over time by the anti-c-myc antibody and an appropriate secondary antibody. The intensity of expression patterns were compared by IFA and found strongest after 12 hours of induction. After 3 hours of induction, an accumulation of the ectopic TbEB1 at the posterior cell pole was detected. As the 6 and 12 hour panels demonstrate, not all cells were labeled with the same intensity and an accumulation of the tagged protein was not always detected at the posterior end. The 24 hours labeling was less intensive than that for 12 hours. Scale bars represent 10µm.

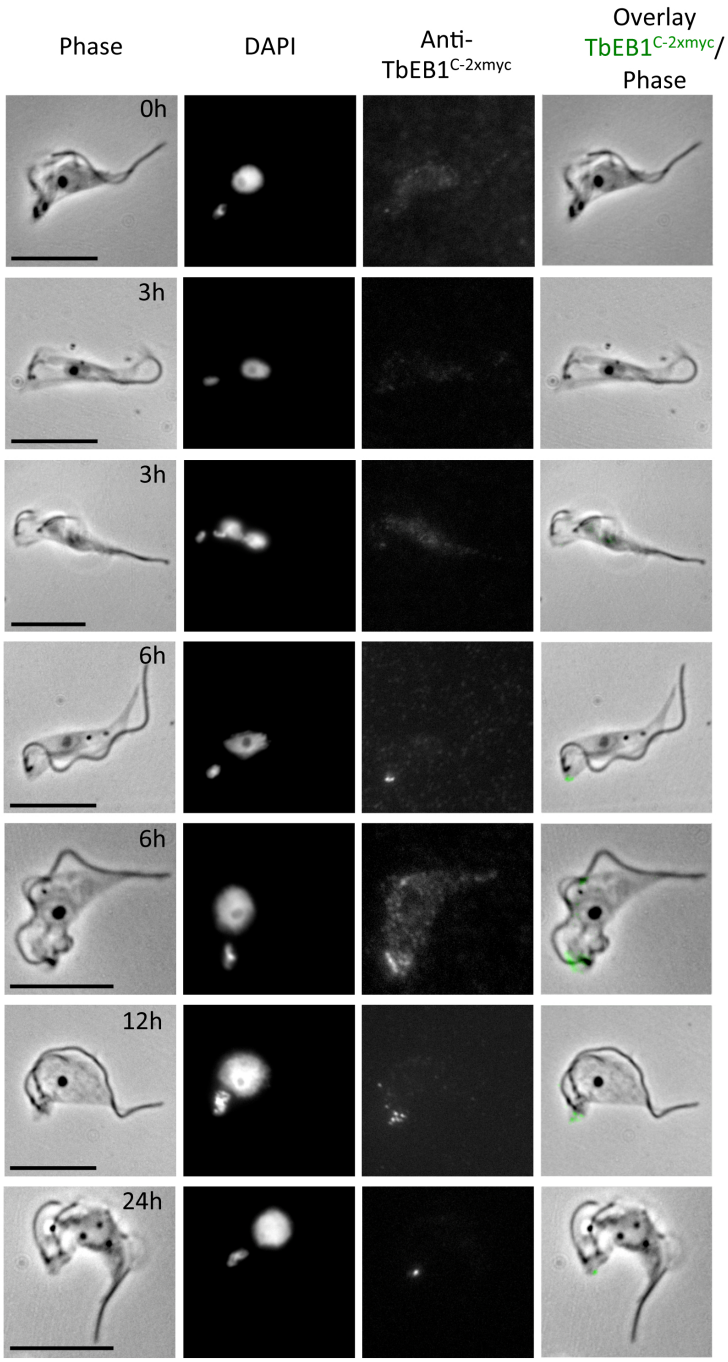


Figure 2.74: Labeling of a c-myc-tagged TbEB1 ectopically expressed in bloodstream trypanosomes during a 24 hours time course. Cytoskeletal preparations of non-induced (0h) and induced (3h, 6h, 12h, 24h) trypanosomes were performed and TbEB1$^{C\text{-}2xmyc}$ expression was followed over time by the anti-c-myc antibody and an appropriate secondary antibody. The intensity of expression patterns were compared by IFA and found strongest after 12 hours of induction. Only 2K2N cells demonstrated a beginning signal at the posterior cell pole after 3 hours p. i.. After 6 hours of induction, an accumulation of the ectopic TbEB1 at the posterior cell pole was detected in most cells. The 24 hours labeling was less intense than that for 12 hours. Scale bars represent 10µm.

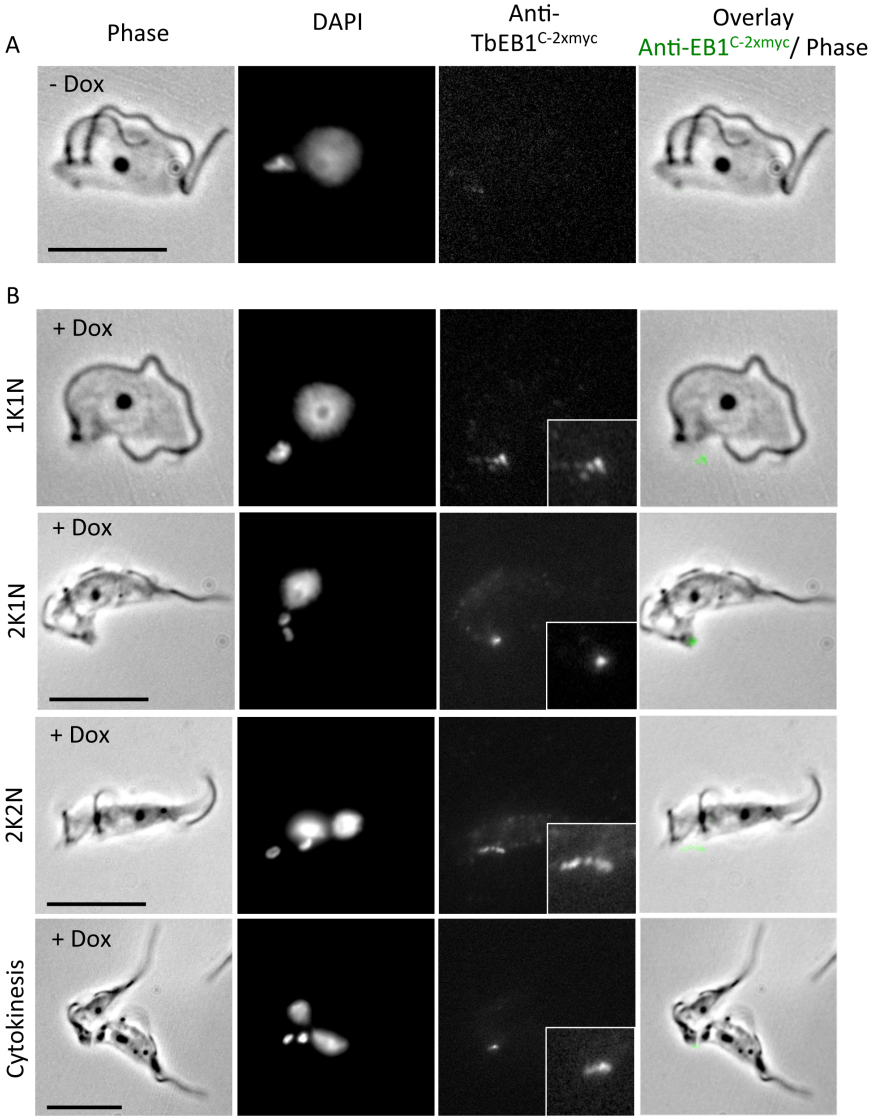


Figure 2.75: Labeling pattern of inducible ectopic expression of TbEB1 in bloodstream trypanosomes after 12 hours in cell cycle stages. Panel **A** demonstrates the non-induced control (-Dox), panel **B** (+Dox) the expression pattern of TbEB1$^{C\text{-}2xmyc}$ over the cell cycle. Detergent-extracted cytoskeletons revealed a TbEB1$^{C\text{-}2xmyc}$ labeling at the posterior cell pole. The ectopically expressed fusion protein was identified by a mouse monoclonal anti-c-myc antibody and an appropriate secondary antibody. Inserts are magnifications of TbEB1$^{C\text{-}2xmyc}$ labeling. CSK were fixed with 3.7% FA. Scale bars represent 10µm.

2K2N cells demonstrated the prolonged TbEB1 signal known from probing with the anti-TbEB1 antibody.

Summing up, ectopically expressed TbEB1$^{C\text{-}2xmyc}$ was localized to the posterior cell end, the FAZ, and the subpellicular microtubule array in PCF and BSF. However, a variation at the posterior cell pole during the cell cycle as for the mouse monoclonal antibody was not observed but 2K2N cells demonstrated a prolonged signal at the posterior cell end.

2.4.13.2 Over-expression of TbEB1 resulted in a mild growth delay and accumulation of abnormal K/ N- ratios in PCF

In general, cells are more adapted to an excess of protein than its partial or complete loss. Nonetheless, if phenotypes are obtained when the protein trespasses a certain threshold they provide a useful tool to obtain information about the function of a protein. To gain information if the over-expression of TbEB1 does influence trypanosomes, at first cell growth was analyzed over 10 days and trypanosomal morphology examined by light microscopy (Fig. 2.76 A, B). No aberrant growth or morphological phenotype were observed for bloodstream trypanosomes. Procyclic trypanosomes developed a modest growth defect, from day 6 on. Here, the amount of ectopically expressed TbEB1 was less than in 24h samples although the total amount of protein was higher (Fig. 2.76 C). This effect persisted until the end of the induction period. In addition, atypical cell cycle stages, especially zoids and 1K2N cells, accumulated in culture up to about 20% (Fig. 2.77 A). As for RNAi cell lines an impeded cytokinesis was supposed to be the underlying reason. The simultaneous emergence of 1K0N and 1K2N cells suggests that they are descendant of 2K2N cells. Some xKxN cells were found, too, but not with as many nuclei as in procyclic RNAi cell lines. However, compared to procyclic RNAi cell lines, the growth defect was a lot less severe. Therefore, it was not clear if the growth defect was due to extinction of affected cells as for RNAi cell lines or if the cell cycle was just slowed down. To distinguish between both possibilities a 'wash out' experiment was designed, which consists of three phases. Cells were first cultivated in presence of doxycycline for 10 days. Subsequently, the drug was removed by three washing steps with doxycycline-free culture medium after which the cells were cultivated in doxycycline-free media for another 9 days. Finally, a second 10 days growth period in presence of doxycycline followed. If affected cells died out, no growth effect or atypical K/ N ratios should be visible during the second induction period. If affected cells survived but just cell division would be decelerated, the same effects as during the first period should be observable. Growth curves of the first phase demonstrated the modest growth retardation (Fig. 2.78 A, compare Fig. 2.76). After the change to doxycycline-free media, growth of previously induced TbEB1myc cells lagged behind wild type and non-induced cells during the first days but recovered up to the end (Fig. 2.78 B). In the subsequent second induction period

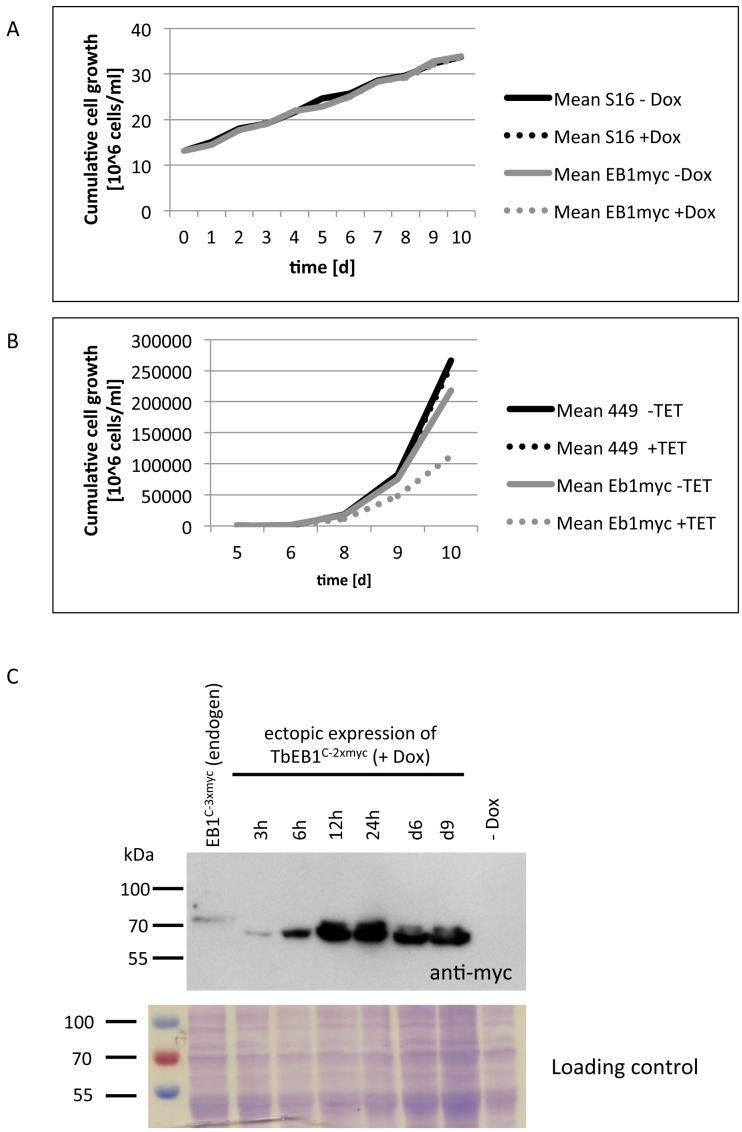


Figure 2.76: TbEB1 over-expression led to mild growth effects and an accumulation of atypical stages only in procyclic trypanosomes. Growth curves in the absence (-Dox) and presence (+Dox) of doxycycline of **A**) bloodstream and **B**) procyclic TbEB1myc cell lines and the corresponding wild type S16 (A) and 449 (B). The chart in B is presented in a non-logarithmical way to illustrate the mild growth retention of TbEB1myc cells over-expressing the protein. Both approaches started with $5*10^5$ cells per ml. Cultures were diluted at several time points to maintain a steadily growing culture. Dilution factors were taken into account and cumulative cell numbers stated. **C**) Immuno blot of PCF demonstrating the rise and fall of expression levels of TbEB1$^{C\text{-}2xmyc}$ of whole cell lysates in the presence of doxycycline during the first induction period of 10 days of the wash out experiment. Expression levels of the ectopic TbEB1$^{C\text{-}2xmyc}$ were compared to the endogenous level of TbEB1$^{C\text{-}3xmyc}$. The immuno blot was probed with anti-c-myc antibody and an appropriate secondary antibody. A Coomassie-stained SDS-gel was used as loading control.

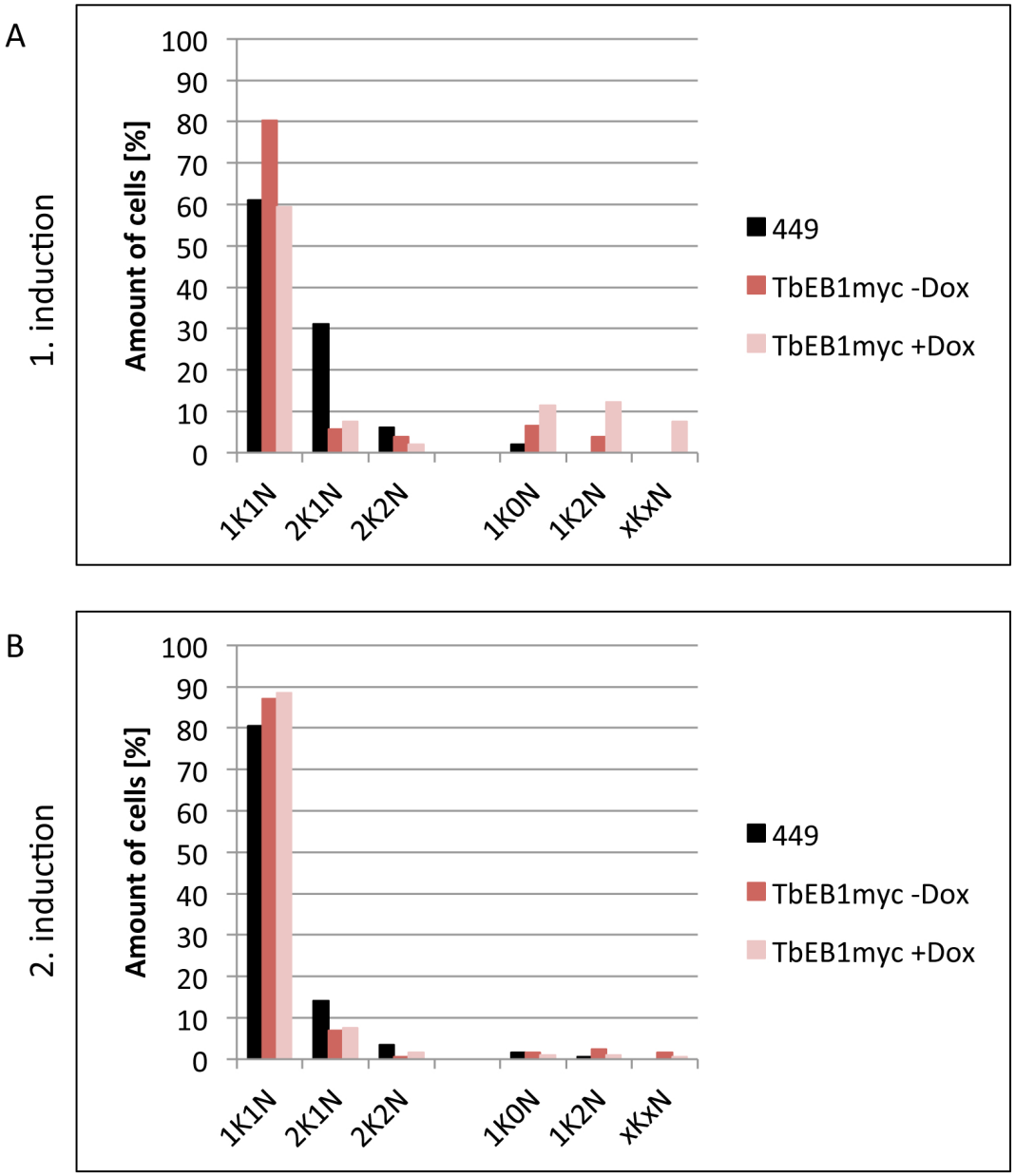


Figure 2.77: The mild growth defect was due to extinction of atypical cells. **A**) Procyclic trypanosomes were cultivated in the absence (-Dox) or presence (+Dox) of doxycycline for 9 days and over-expression of TbEB1 resulted in an accumulation of atypical stages (1K0N, 1K2N, xKxN) in the induced sample. Non-induced and induced TbEB1myc were compared to wild type 449 and 100 cells were evaluated per sample. **B**) During the 2. round of induction, cell cycle stages of non-induced (-Dox) and induced (+Dox) samples were again compared to wild type (449) on day 9. 200 cells were evaluated.

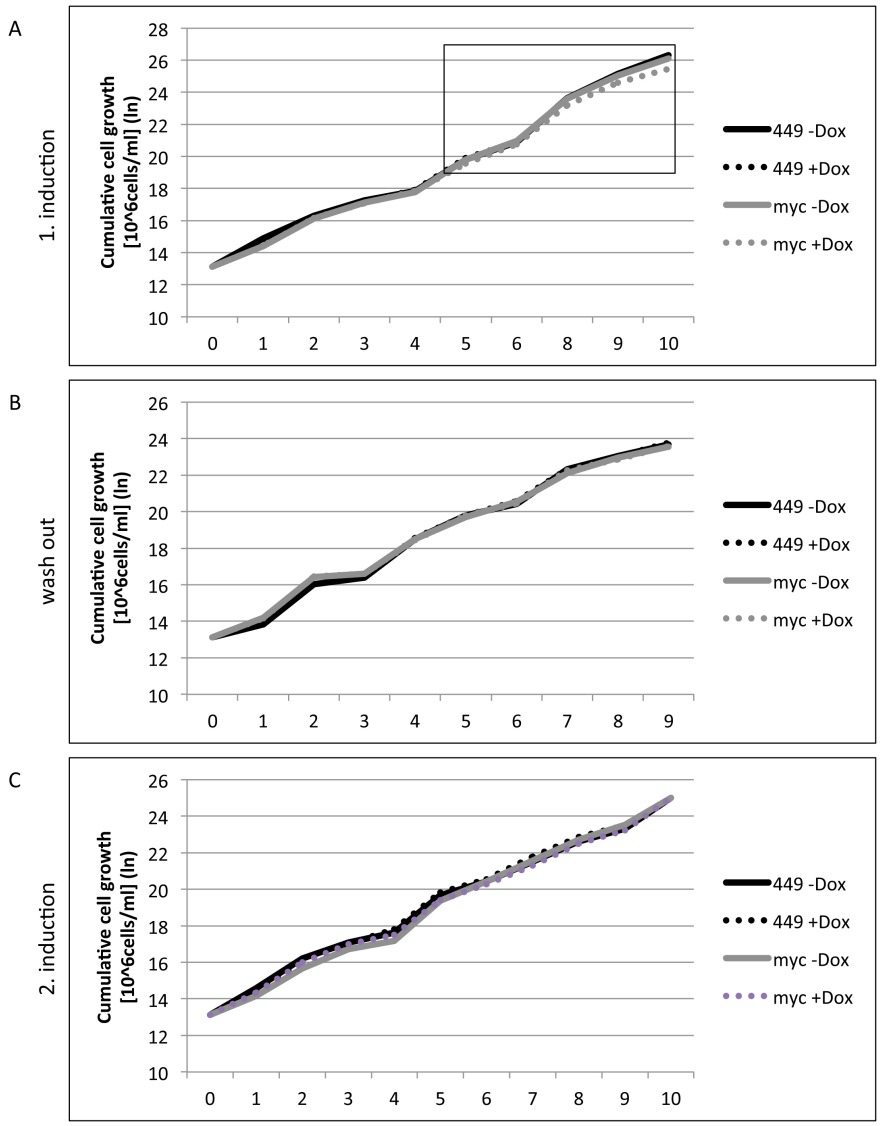


Figure 2.78: The mild growth retardation was only detectable during the first induction period. Wild type (449) and TbEB1$^{C\text{-}2xmyc}$ cells were grown in the absence (-Dox) and presence (+Dox) of 1µg/ml doxycycline. **A**) A mild growth retardation was observed after 8 days when cells were continuously growing in the presence of doxycycline. The square is separately presented in figure 2.76B on a linear scale to illustrate the mild growth retardation. **B**) Growth curves of the washout phase, when all cell lines were cultivated without doxycycline, demonstrated that cells recovered. **C**) A second round of doxycycline was added to the respective cultures and no growth retardation occurred again.

no growth retardation was observed compared to the controls (Fig. 2.78 C). Evaluation of cell cycle stages showed that their amount was similar to wild type and non-induced trypanosomes during the third phase (Fig. 2.77 B). Although overall TbEB1$^{C\text{-}2xmyc}$ was decreased, as shown in immuno blots (Fig. 2.76 C), at the end of the first period, the amount associated with the cytoskeleton after detergent-extraction stayed quite the same from day 1 to 10 (Fig. 2.79 A-D). Trypanosomes with atypical K/ N ratios demonstrated a labeling comparable to unaffected cells in pattern and intensity (Fig. 2.79 E). The successful washout of doxycycline was documented by the loss of detectable TbEB1myc in IFA (Fig. 2.79 F) although a faint signal corresponding to TbEB1myc was still detectable in more sensitive immuno blots (Fig. 2.79). Re-addition of doxycycline resulted again in a rise of TbEB1myc protein levels causing a similar labeling pattern which remained constant in signal intensity over the whole third period (Fig. 2.79 G). Notably, the signal intensities obtained in Western blots for samples of day 1, day 6, and day 9 during the second induction period were equal (Fig. 2.80). This indicates that probably those cells responding to doxycycline addition with high levels of TbEB1myc expression, developed the observed atypical K/ N-ratios and got extinct during the first induction period. Therefore, the modest discrepancy in growth dynamics was due to cell death and not due to retardation of cell cycle dynamics.

Over-expression of TbEB1$^{C\text{-}2xmyc}$ resulted in the accumulation of atypical cell cycle stages in PCF. However, the amount was lower than for procyclic RNAi cell lines.

2.4.13.3 The phenotypes obtained by an over-expression of TbEB1 resembled some observed during TbEB1 depletion

Light microscopic analysis of TbEB1 over-expression revealed the occurrence of atypical K/ N-ratios after several days of TbEB1 over-expression. About 20% of the trypanosomes were affected and those cells might give valuable insights in TbEB1 function. Probing of TbEB1myc samples with anti-TbEB1 antibody revealed an increase of anti-TbEB1 labeling at the posterior end in cells with elevated levels of TbEB1$^{C\text{-}2xmyc}$ when comparing cells of the same cell cycle stage (Fig. 2.81). Thus, under physiological conditions, microtubules are not saturated with TbEB1. However, the over-expression of TbEB1 did not yield in a stronger labeling of the cytoskeleton by mouse monoclonal anti-TbEB1. Indeed compared to the intense labeling of the cell pole, it was modest. However, sometimes a weak staining at the spindle occurred. Anti-TbEB1 staining of atypical cells demonstrated an intense staining pattern at the posterior cell pole (Fig. 2.82 A). 2K2N or 2KxN cells are supposed to be the main source of zoids (Fig. 2.82 B). The occurring 1K0N cells were more compact compared to those occurring during RNAi indicating the expansion of the subpellicular microtubule array (Fig. 2.82 C). Furthermore, xKxN cells were less deformed or crowded with nuclei as those occurring in RNAi cell lines. Indeed,

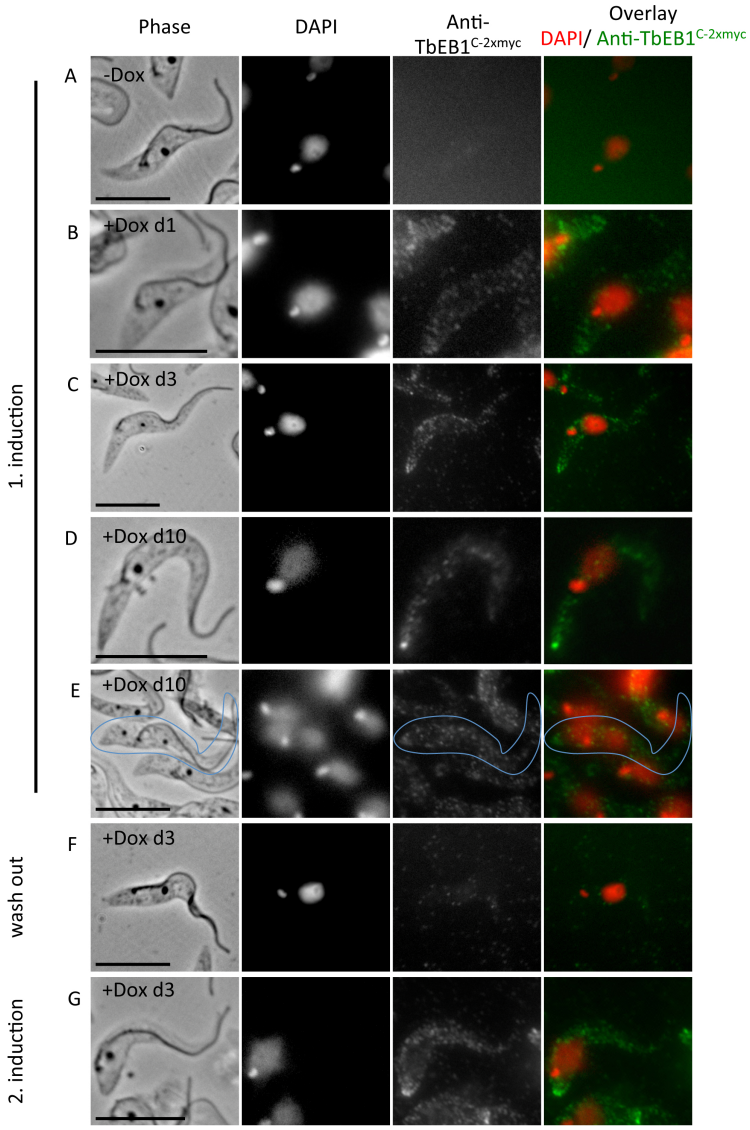


Figure 2.79: Surveillance of TbEB1$^{C\text{-}2xmyc}$ signal intensity during the washout experiment in PCF. The experiment comprised three phases: 1. induction, washout, and 2. induction. During the induction periods, cells were grown in the absence (-Dox) or presence (+Dox) of 1µg/ml doxycycline. **A)** No TbEB1$^{C\text{-}2xmyc}$ signal occurred in the absence of doxycycline. **B-D)** Examples of cells grown in the presence of doxycycline for 1, 3, and 10 days demonstrating the characteristic labeling pattern at the posterior cell pole and cell body. Probably due to a perpetual exchange of tagged protein, the signal intensity varies from cell to cell. **E)** Example of an atypical cell cycle stage occurring at the end of the 1. induction period. Those cells still demonstrate a similar TbEB1$^{C\text{-}2xmyc}$ labeling as regular cell cycle stages. **F)** After the washout of doxycycline on day 3, no signal was detectable in induced cells by IFA. **G)** Example of a regular cell cycle stage on day 3 of the 2. induction period. It demonstrates the typical TbEB1$^{C\text{-}2xmyc}$ labeling pattern of the posterior cell pole and the cell body. Cells were detergent-extracted and fixed in ice-cold methanol. Labeling was performed with anti-c-myc-antibody and an appropriate secondary antibody conjugated to AlexaFluor488. Scale bars represent 10µm.

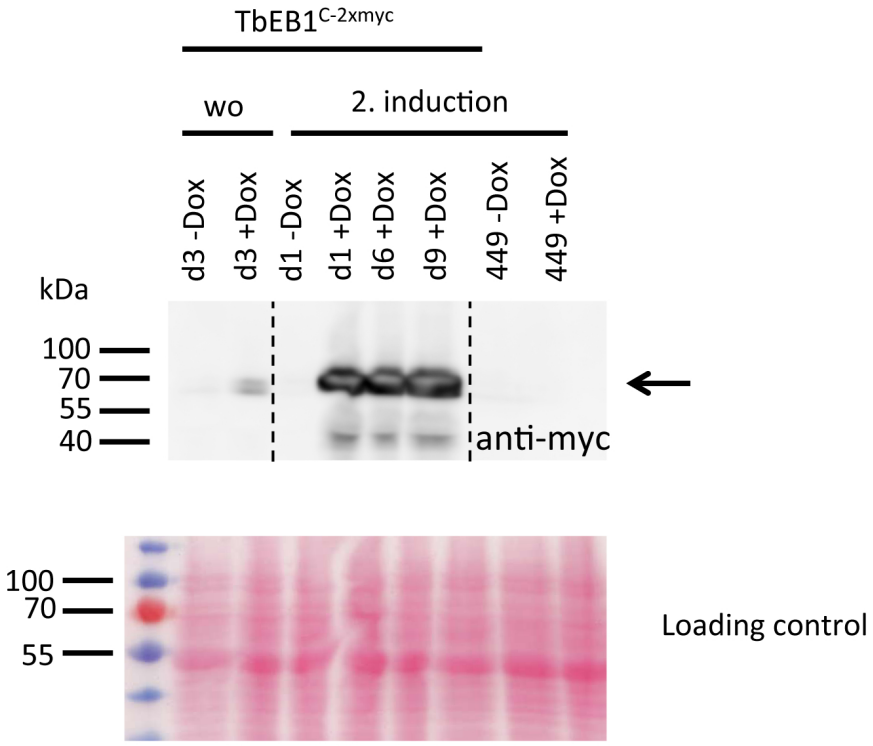


Figure 2.80: The TbEB1$^{C\text{-}2xmyc}$ signal intensity remained constant during the 2. induction period. Doxycycline was washed out (wo) in induced (+Dox) TbEB1$^{C\text{-}2xmyc}$ sample. The non-induced sample (-Dox) was treated the same way. Trypanosomes were then cultivated in the absence of doxycycline for 10 days. Samples were taken on day 3. Contrasting to IFA, a low signal was detected in the induced sample (TbEB1$^{C\text{-}2xmyc}$, wo, d3 +Dox). During the second induction period, representative samples of day 1, 6, and 9 demonstrated an equal signal intensity. Wild type cell line 449 cultivated in the absence (-) and presence (+) of doxycycline did not demonstrate anti-c-myc labeling. The immuno blot corresponding to the 1. induction period is presented in figure 2.76 C. The Ponceau S-stained immuno blot membrane was used as loading control.

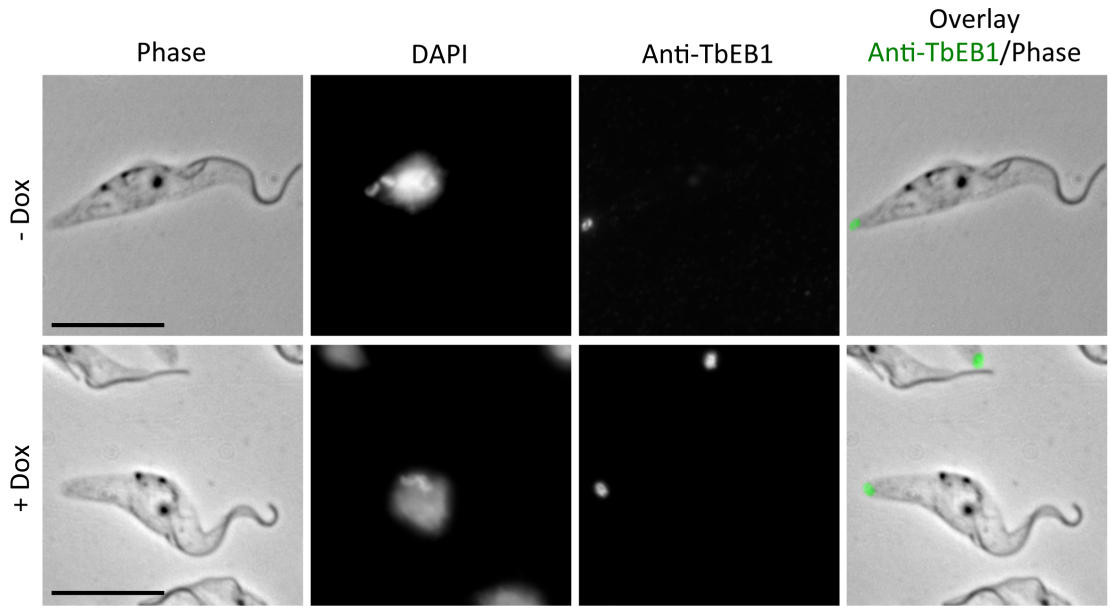


Figure 2.81: Expression of the ectopic TbEB1$^{C\text{-}2xmyc}$ led to an enhanced signal at the posterior end detected by the mouse monoclonal anti-TbEB1 antibody on procyclic trypanosomes. Cells were grown in the absence (-Dox) or presence (+Dox) of doxycycline for 8 days. Trypanosomes were detergent-extracted with 1% NP-40 and CSK were fixed with ice-cold methanol. Scale bars represent 10µm.

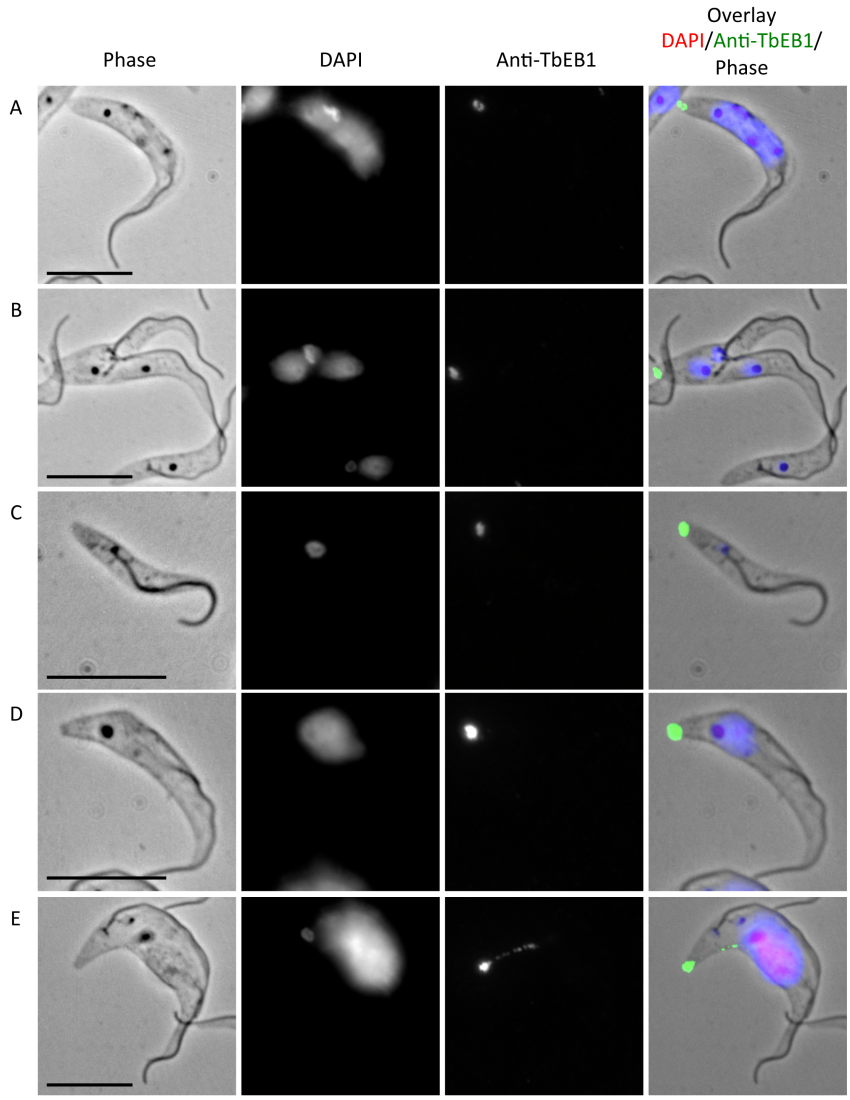


Figure 2.82: TbEB1 over-expression resulted in an impaired cytokinesis with an accumulation of 1K2N cells, zoids, and mispositioned kinetoplasts in PCF. A) A typical procyclic cell with divided kinetoplasts placed between nuclei, which frequently resulted in the impaired cytokinesis shown in **B**). **C**) Zoids were the frequently counted product from this event. **D**) More rarely, cells with a shortened posterior cell body were observed. **E**) A multi-nucleated cell, which probably resulted in a cell as shown in D after cytokinesis. TbEB1 labeling marked the newly defining posterior cell pole. Procyclic cells were cultivated in the presence of doxycycline for 8 days. Trypanosomes were detergent-extracted with 1% NP-40. Scale bars represent 10µm.

a maximum of four nuclei was found. And as for RNAi, the number of kinetoplasts frequently was too low for the number of nuclei. A mispositioned kinetoplast was a rare event but seemed to be inherited by daughter cells (Fig. 2.82 D). Depending on kinetoplast localization either zoids or 1K1N cells with mispositioned kinetoplast were produced by cell division. TbEB1 was localized to the posterior end of the division furrow, which was never displaced as it was the case for RNAi cell lines (Fig. 2.82 E). And no detached flagella were found, too. YL1/2 labeling to identify tyrosinated α-tubulin demonstrated the typical gradient distribution with its strongest intensity at the posterior cell body in all normal and abnormal cell cycle stages with elevated TbEB1 levels indicating that a surplus of TbEB1 did not cause grave changes in cellular morphology. Each kinetoplast was accompanied by one or two basal bodies according to its developmental state (Fig. 2.83 A-C). This was confirmed by Mab25 (axonemal marker) staining (Fig. 2.84). Therefore, basal body and kinetoplast segregation were still executed properly but are lagging behind mitosis. Identification of FAZ by L3B2 staining revealed that the assembly of the organelle was lagging behind that of nucleus synthesis but was still synchronously executed to the developmental cycle of the kinetoplast (Fig. 2.85 A-C). Furthermore, median FAZ length in procyclic TbEB1myc cell lines, grown in the presence of doxycycline for 8 days, was similar to wild type median FAZ length but a decrease of cells with a FAZ longer or equal to 19µm was detected (Fig. 2.86). The similarities to the phenotypes detected by TbEB1 RNAi and single gene knock out approaches may result from the fact, that TbEB1 putatively covers too many binding sites at the microtubule, thereby preventing interaction and/ or attachment of other (+TIP) proteins directly or sterically with the microtubule lattice and hence, mimicking some effects occurring at low levels of TbEB. An identical effect is described for other MAPs and Mal3p, the fission yeast homologue of TbEB1 (Beinhauer *et al.* , 1997).

Summing up, differences and similarities between procyclic RNAi and over-expression cell lines are presented in table 2.2.

2.4.14 A heterologous system: Expression of TbEB1$^{C\text{-}GFP}$ in HeLa cells

Mammalian cells provide a useful tool to express proteins of other eukaryotic organisms as correct protein folding and post-transcriptional modifications are provided and hence, ensure activity of the protein of interest (Khan, 2013). With this approach, the function and behavior of a heterologous protein can be studied and – due to known mechanisms and metabolic pathways of the host environment – interpreted (Yesilirmak & Sayers, 2009).

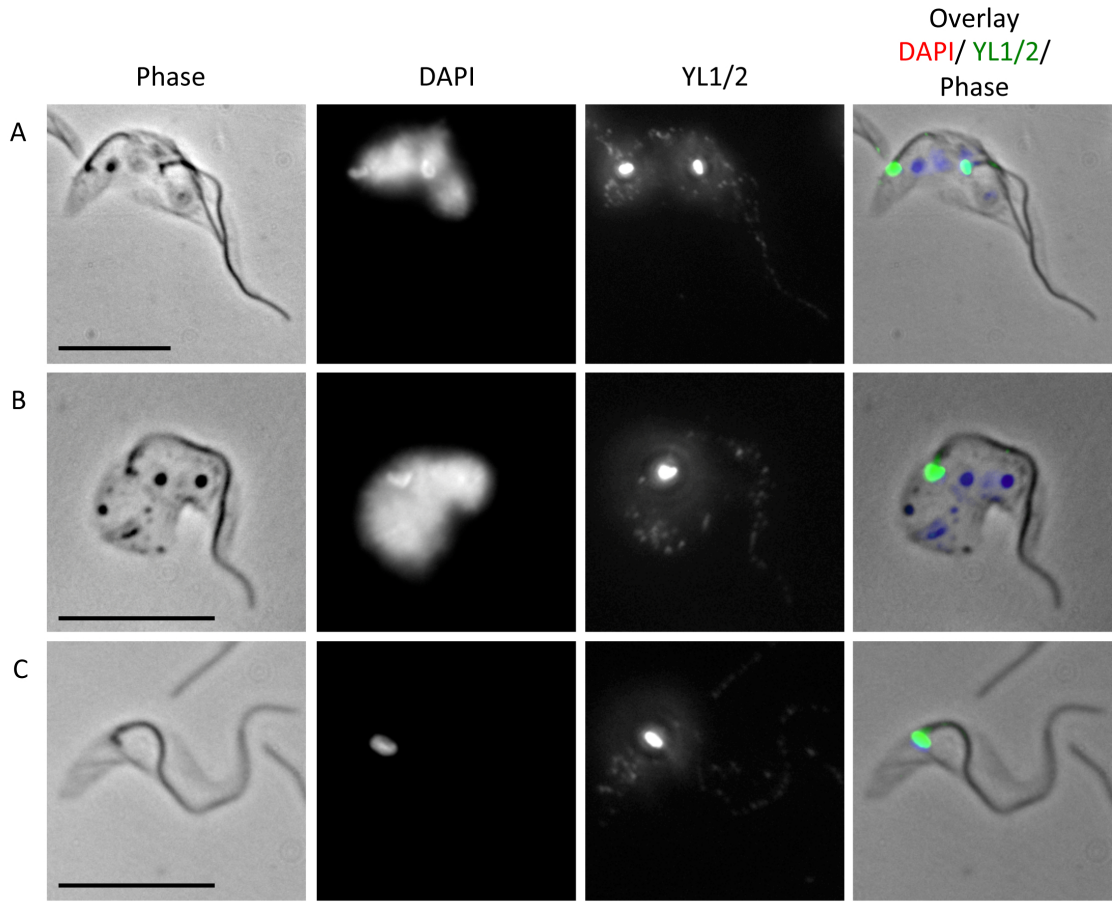


Figure 2.83: In procyclic TbEB1myc cell lines, examples of an adjoining basal body in cells with a mispositioned kinetoplast (A), with multiple nuclei (B), and zoids (C) demonstrated by YL1/2 labeling. Cells still possessed the typical gradient-distributed labeling of YL1/2 (tyrosinated α-tubulin). Procyclic cells were cultivated in the presence of doxycycline for 8 days. Trypanosomes were detergent-extracted with 1% NP-40. Scale bars represent 10µm.

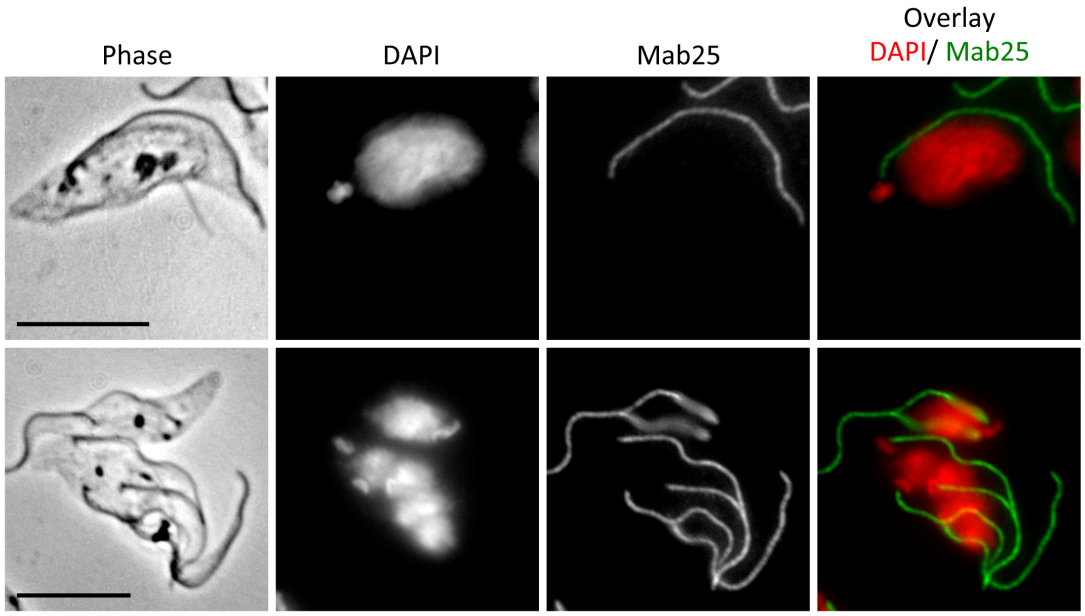


Figure 2.84: Labeling of the flagellum with Mab25 (axonemal marker) confirmed connection of basal bodies and kinetoplast in atypical cell cycle stages due to TbEB1 over-expression. Procyclic cells were cultivated in the presence of doxycycline for 8 days. Trypanosomes were detergent-extracted with 1% NP-40. Scale bars represent 10µm.

Table 2.2: Comparison of depletion and over-expression of TbEB1 in PCF.

	Overexpression	**RNAi**
Negative selection	Probably	Yes
Growth effect	mild	strong
Atypical cell cycle stages	20%	20% (29-13); 50% (449)
xKxN	low	moderate - high
Number of nuclei	a maximum of 4	often more than 4
Number of basal bodies	matching to number of kinetoplasts	frequently higher than number of kinetoplast
Number of FAZ	in general matching the number of nuclei, assembly probably retarded	frequently too low for the number of nuclei
FAZ length	normal	reduced
Zoids	broad	slim
Flagellum	attached	detached
Morphology	wild type - like	often distorted

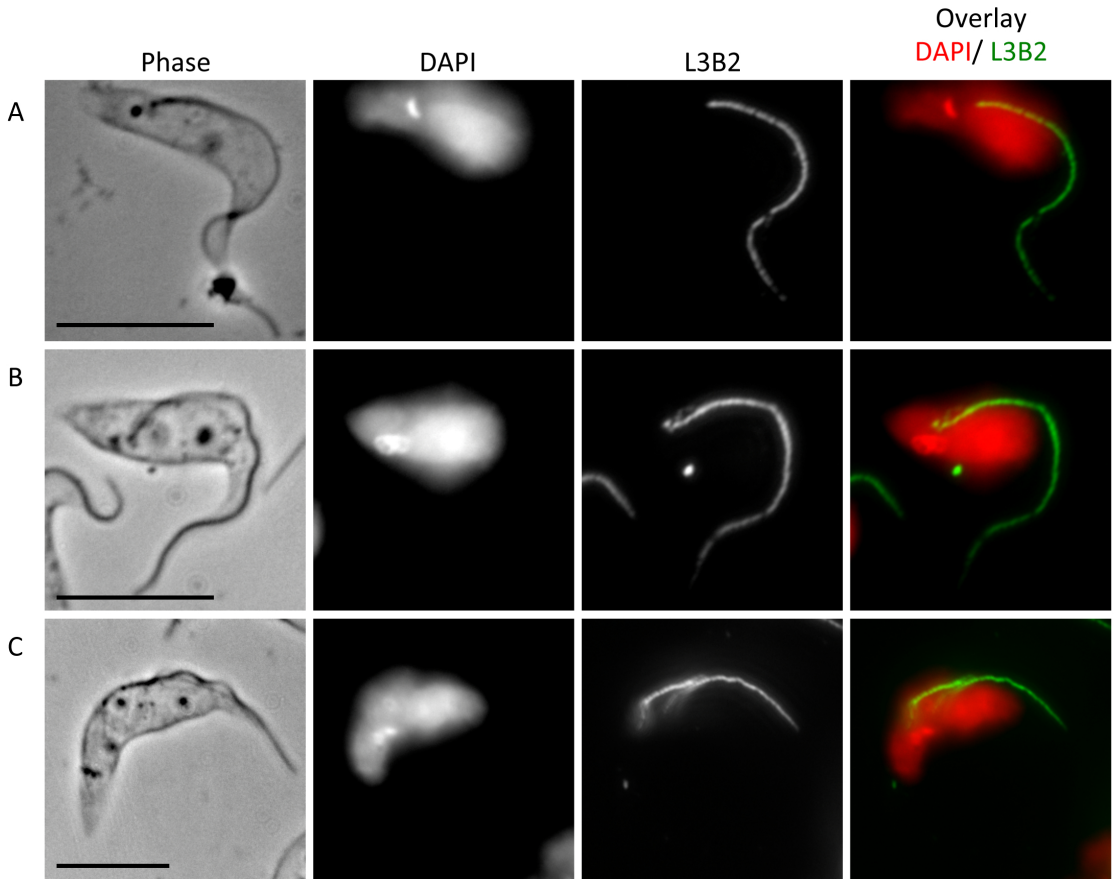


Figure 2.85: TbEB1 over-expression resulted in a delayed FAZ synthesis compared to number of nuclei. A) 1KxN cell containing one FAZ. **B**) The kinetoplast has segregated in the presence of multiple nuclei. The assembly of the second FAZ had just started. **C**) The number of FAZ and respective kinetoplasts approach the number of nuclei. Trypanosomes were cultivated in the presence of doxycycline for 8 days. Procyclic cells were detergent-extracted with 1% NP-40. Scale bars represent 10µm.

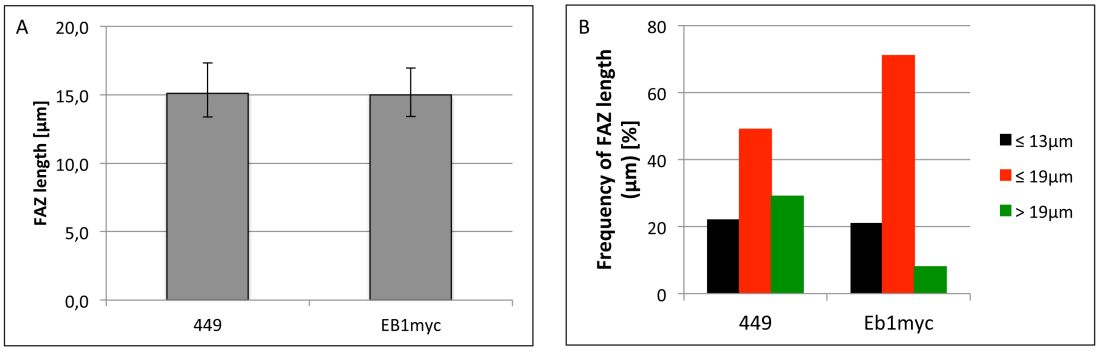


Figure 2.86: Overexpression of TbEB1myc had no effects on median FAZ length in procyclic trypanoxmes. **A**) Median FAZ length is equal in wild type and TbEB1myc cell lines, which grew in the presence of doxycycline for 8 days. **B**) Grouping of median FAZ length revealed a decrease in cells with a FAZ longer than 19µm. 100 cells was measured for each sample.

2.4.14.1 TbEB1 is localized at sub-cellular microtubules in mammalian cells

Even though TbEB1 has a similar domain architecture as vertebrate EB1, it shows great differences in its amino acid sequence length and in the lack of the EEY/F sequence, which is necessary for self-inhibition and interacting platform for many proteins (Komarova *et al.* , 2009). Additionally, there is only one end-binding protein encoded by the trypanosomal genome compared to the three variants (EB1-3) in human. Therefore, co-localization of TbEB1 with mammalian microtubule could also give some hints to a conserved operation mode of this protein. Also, it is easier to look at individual microtubules and to assess the effect of tags on EB1 proteins. The complete sequence of TbEB1 was cloned into the transient transfection vector pCS2 enabling expression of the protein with a C-terminal GFP-tag. Expression of the 100kDa transgene was verified by Western blot and IFA. In a first approach, samples were taken 1-3 days post transfection from an asynchronously growing culture (Fig. 2.87 A). Cells transfected with null vector also demonstrated barely detectable bands in immuno blot due to background expression of GFP in the empty vector (Fig. 2.87 B) and a weak cytoplasmic GFP staining around the nucleus (Fig. 2.88 A). However, TbEB1$^{C\text{-}GFP}$ demonstrated strong bands in immuno blots of appropriate size and also degradation products. Co-staining with an anti-tubulin antibody (TAT) revealed three distinct staining patterns: firstly, microtubules stained in alternating sections with TAT- or TbEB1$^{C\text{-}GFP}$- staining sections, secondly, individual microtubules were decorated with either TAT or TbEB1 and lastly, microtubules with overlapping patterns without clear co-localization signal (Fig. 2.88 B) Therefore, TbEB1 is able to localize to mammalian microtubules confirming the preserved N-terminal microtubule domain predicted by bioinformatical analysis. The alternating pattern indicates a competition between mammalian and trypanosomal end-binding pro-

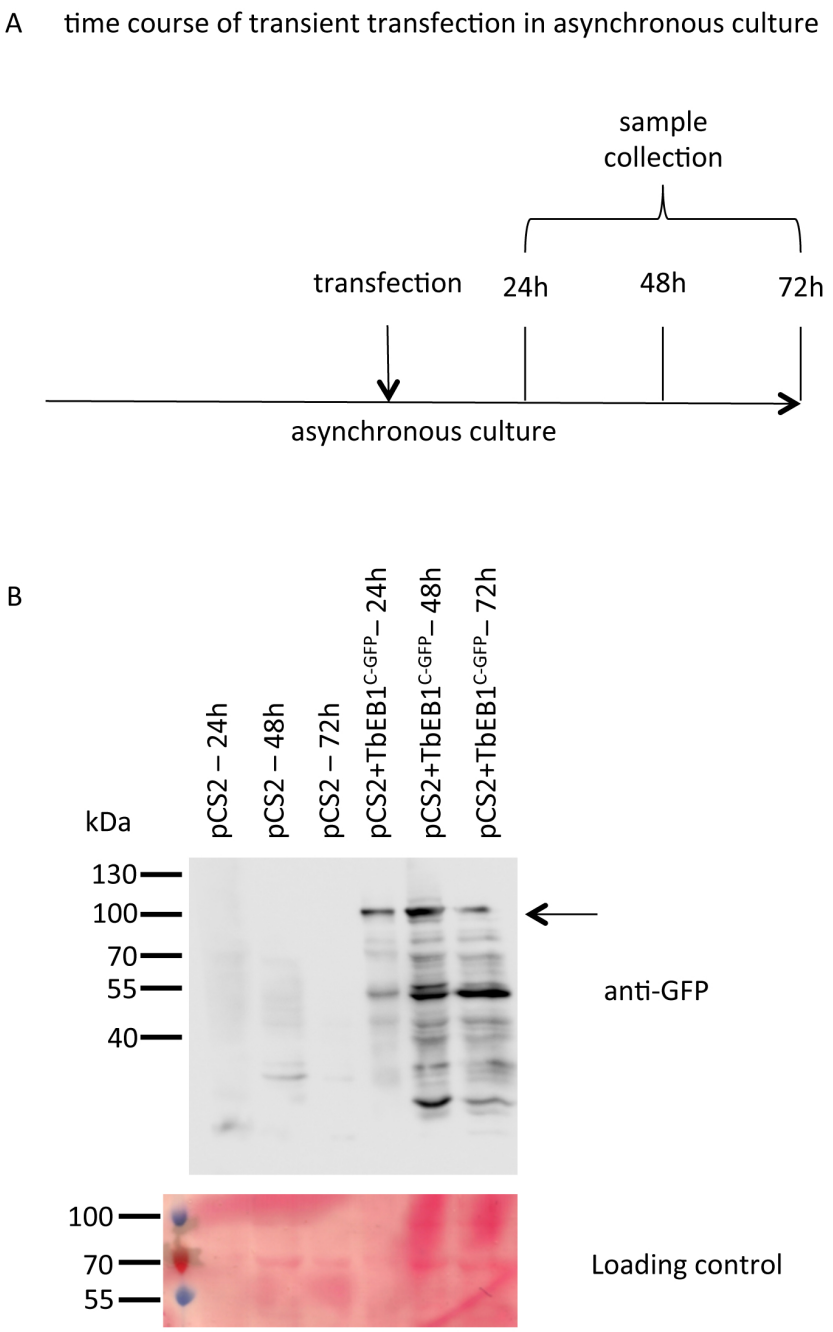


Figure 2.87: TbEB1$^{C\text{-}GFP}$ was transiently expressed in an asynchronous culture of HeLa cells. A) Schedule of transient transfection of the asynchronous culture of HeLa cells and time points of sample collection. **B**) HeLa cells were transfected either with the mock vector (pCS2) or TbEB1$^{C\text{-}GFP}$ (pCS2+TbEB1$^{C\text{-}GFP}$). The immuno blot was probed with an anti-GFP antibody and the appropriate secondary antibody. The Ponceau S-stained membrane was used as control for protein loading.

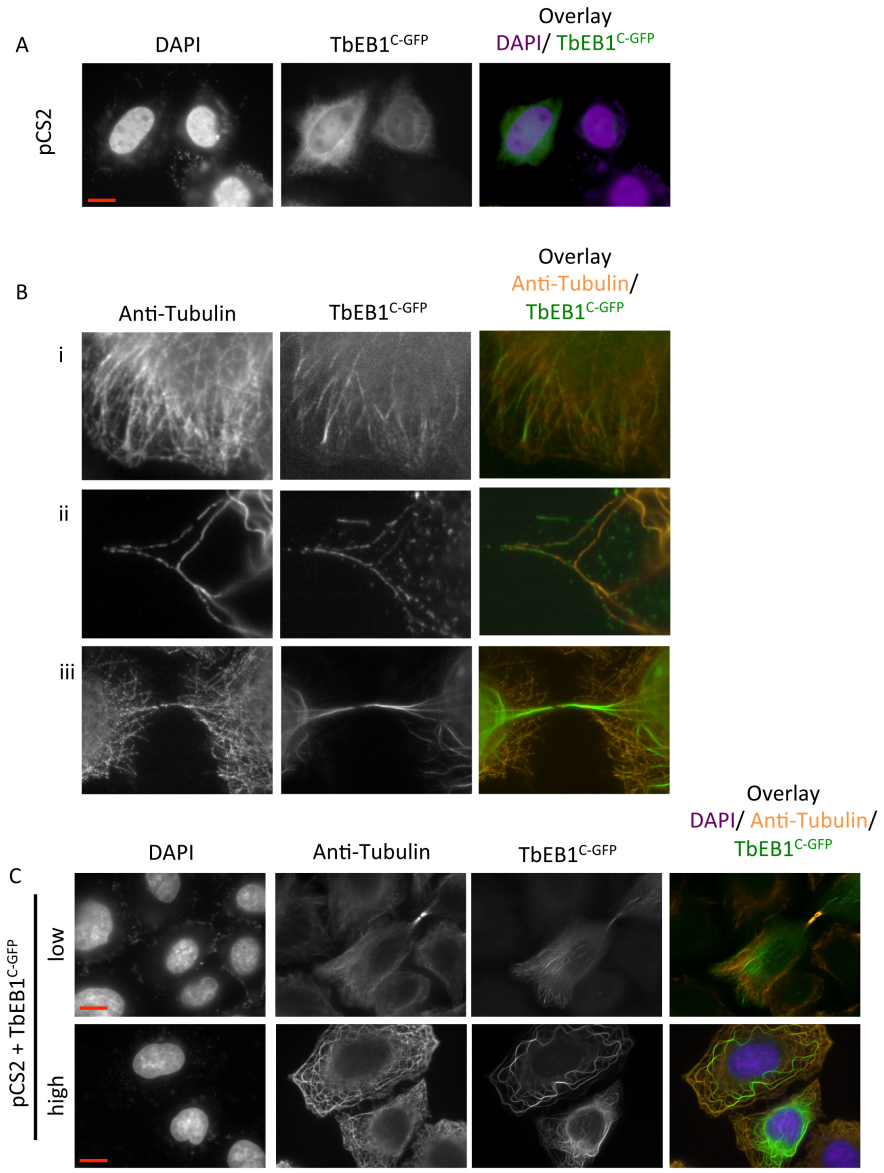


Figure 2.88: TbEB1$^{C\text{-}GFP}$ localizes to mammalian cytoplasmic microtubules. **A**) Mock (pCS2) transiently transfected HeLa cells demonstrated a faint cytoplasmic labeling around the nucleus. Scale bar represents 3µm. **B**) i-ii) Evaluation of TbEB1$^{C\text{-}GFP}$ labeling demonstrated alternating patterns with TAT staining, overlapping patterns without clear colocalization and microtubules decorated with either TAT labeling or TbEB1$^{C\text{-}GFP}$ labeling. iii) TbEB1$^{C\text{-}GFP}$ was accumulated at positions with increased microtubule turnover, e. g. at cytoplasmic protrusions. **C**) After transient transfection of HeLa cells with pCS2-TbEB1$^{C\text{-}GFP}$, low and high expression levels of TbEB1$^{C\text{-}GFP}$ are compared. Microtubules grew ordered at low levels of TbEB1$^{C\text{-}GFP}$ while the 'curly' phenotype was the result of high levels of TbEB1$^{C\text{-}GFP}$. Scale bars represent 3µm.

tein as those binding sites occupied with mammalian EBs lack a GFP-fluorescence signal. GFP-TbEB1 decorated microtubules overlapping with only TAT-labeled ones indicate that TbEB1 is able to promote growth of mammalian microtubules autonomously. Furthermore, TbEB1 is able to interact with other mammalian +TIP proteins in the network necessary for microtubule assembly, and finally to track the newly synthesizing microtubule along an already existing old one (Chen *et al.* , 2014a). The pCS2 vector contains the potent CMV promoter resulting in high expression levels of the target protein (Turner & Weintraub, 1994). Consistent with literature (Skube *et al.* , 2010), we found the deformation of the microtubule cytoskeleton in HeLa cells – generally referred to as 'curly' phenotype – correlating with high TbEB1$^{\text{C-GFP}}$ levels (Fig. 2.88C). That phenotype is characterized by bundled microtubules, which are extremely elongated and twisted in the cytoplasm (Tirnauer *et al.* , 2002b; Askham *et al.* , 2002; Ligon *et al.* , 2003). Expression of the transgene started as soon as the plasmid entered the nucleus after mitosis. In a follow-up experiment, cells were synchronized by a thymidine block, which arrests cells in S-phase. Washout of thymidine allows the cells to progress with cell cycle (Fig. 2.89 A). In a synchronous culture, cells with a similar expression level of TbEB1 are enriched and low expression levels are easier to investigate. Low levels of TbEB1 should demonstrate minor effects on microtubule morphology. Cells were transfected during the nucleotide block. After the release, the 0 hours sample was taken, when the majority of cells appeared to be mitotic. As the nuclear envelope breakdown is necessary for plasmids to enter the nucleus, first transcripts would be expected after mitosis and successful genome integration of the vector (P. Kahlen, personal communication). However, the 0 hours sample was stained positively for TbEB1$^{\text{C-GFP}}$ on a Western blot (Fig. 2.89 B). This putatively resulted from cells, which entered mitosis earlier than 12 hours. Nonetheless, cells with a lower expression of TbEB1$^{\text{C-GFP}}$ were now observed in the culture, their amount decreased over time. Notably, the microtubule pattern after short transient expression of TbEB1$^{\text{C-GFP}}$ resembled the wild type situation. However, a comet-like pattern as described in literature (Komarova *et al.* , 2009) had never been observed probably due to the still too high levels of the transgene compared to endogenous EB1 levels. The effect of low and high expression levels of TbEB1$^{\text{C-GFP}}$ was compared in IFAs and underlines the dose-dependent effect of TbEB1 on microtubule morphology (Fig. 2.90 C). Moreover, TbEB1$^{\text{C-GFP}}$ was found at positions with increased microtubule turn-over such as formation of cytoplasmic protrusions and during cytokinesis, but surprisingly not at mitotic spindles. However, this may be due to low transformation efficiencies and a too small population size of dividing cells.

Summing up, the action mode of TbEB1 resembles strongly that of mammalian EBs on cytoplasmic microtubules.

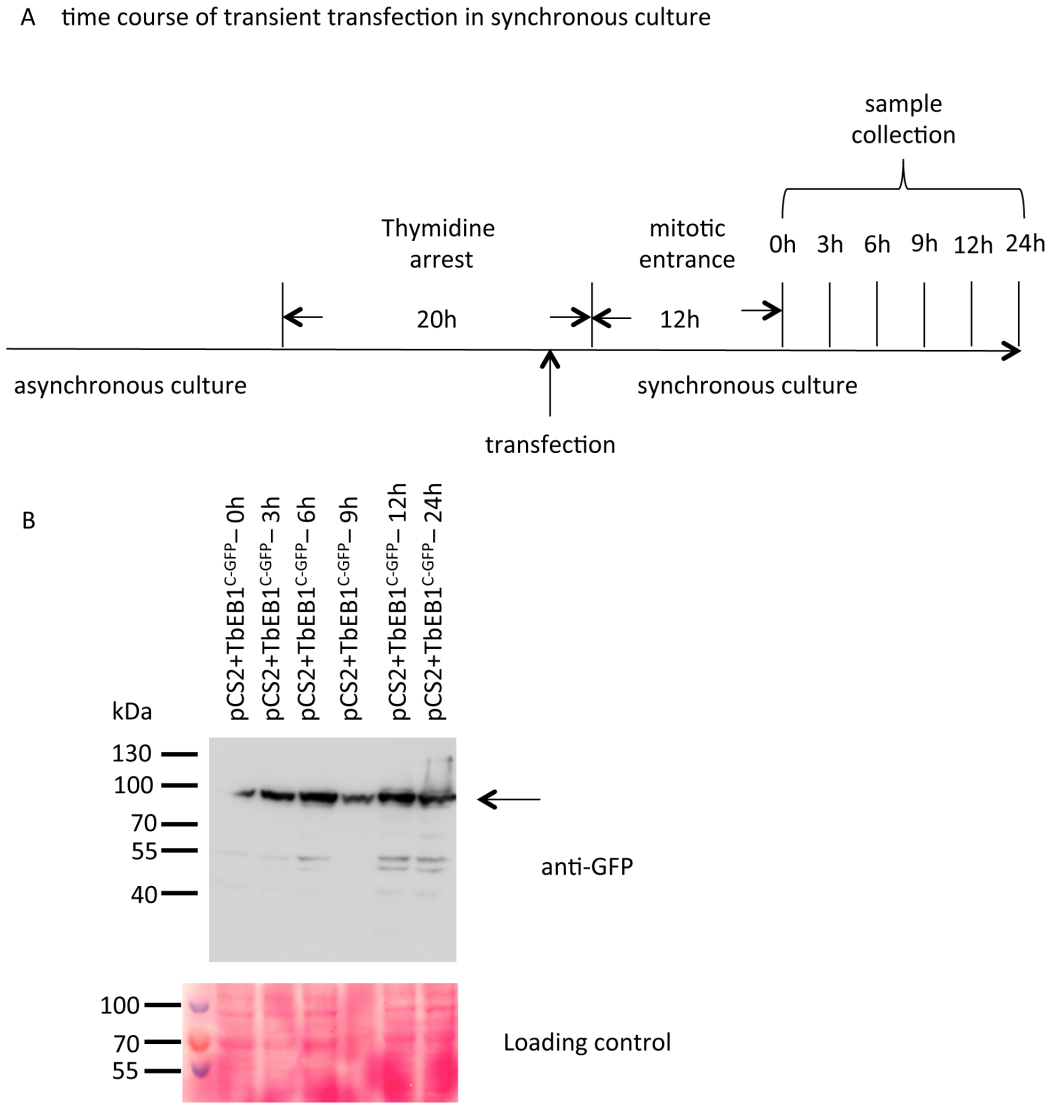


Figure 2.89: TbEB1$^{C\text{-}GFP}$ was transiently expressed in a synchronous culture of HeLa cells. **A**) Schedule of transient transfection of the synchronous culture in HeLa cells and time points of sample collection. The culture was synchronized by thymidine block within which transfection took place. The majority of cells entered mitosis after 12 hours when sample collection started. **B**) The corresponding immuno blot was probed with an anti-GFP antibody and the appropriate secondary antibody. The Ponceau S -tained membrane was used as control for protein loading.

2.4.14.2 Mouse monoclonal antibody anti-TbEB1 detects a putative mammalian end-binding protein on microtubule plus ends in HeLa cells and fibroblasts

Due to the sequence identity of domains in human and trypansoma end-binding proteins, the raised mouse monoclonal antibody anti-TbEB1 was tested on mammalian cells. TbEB1 recognized a protein, which accumulates at microtubule plus ends when probed on HeLa cells or fibroblasts. In HeLa cells a punctate or wedge-shaped signal was observed (Fig. 2.90 A, B) while fibroblasts frequently demonstrated a punctate pattern as well as some elongated signals (Fig. 2.90 C). Especially the latter one resembles the comet-like appearance of mammalian EBs described in literature (Komarova *et al.* , 2009). As the mouse monoclonal anti-TbEB1 was shown to specifically identify trypanosomal EB1 it is quite likely that a mammalian end-binding protein was stained. As all three mammalian end-binding proteins did not differ in their appearance at the end of cytoplasmic microtubules (Komarova *et al.* , 2009) and share sequence identity in parts as well, it is not possible to determine if only a single species or all were recognized. Commercial antibodies for mammalian EB variants are available. Therefore, identification of the detected protein by anti-TbEB1 would be easily obtained by co-localization experiments in IFA. Alternatively, mammalian EBs could be tagged endogenously, followed by an IP with TbEB1 and identification by a Western blot probed against the tags. Notably, a staining of the mammalian spindle was also not detectable with mouse monoclonal anti-TbEB1. Nonetheless, anti-TbEB1 might provide a tool to visualize microtubule ends and thus, cell dynamics also in mammalian cells.

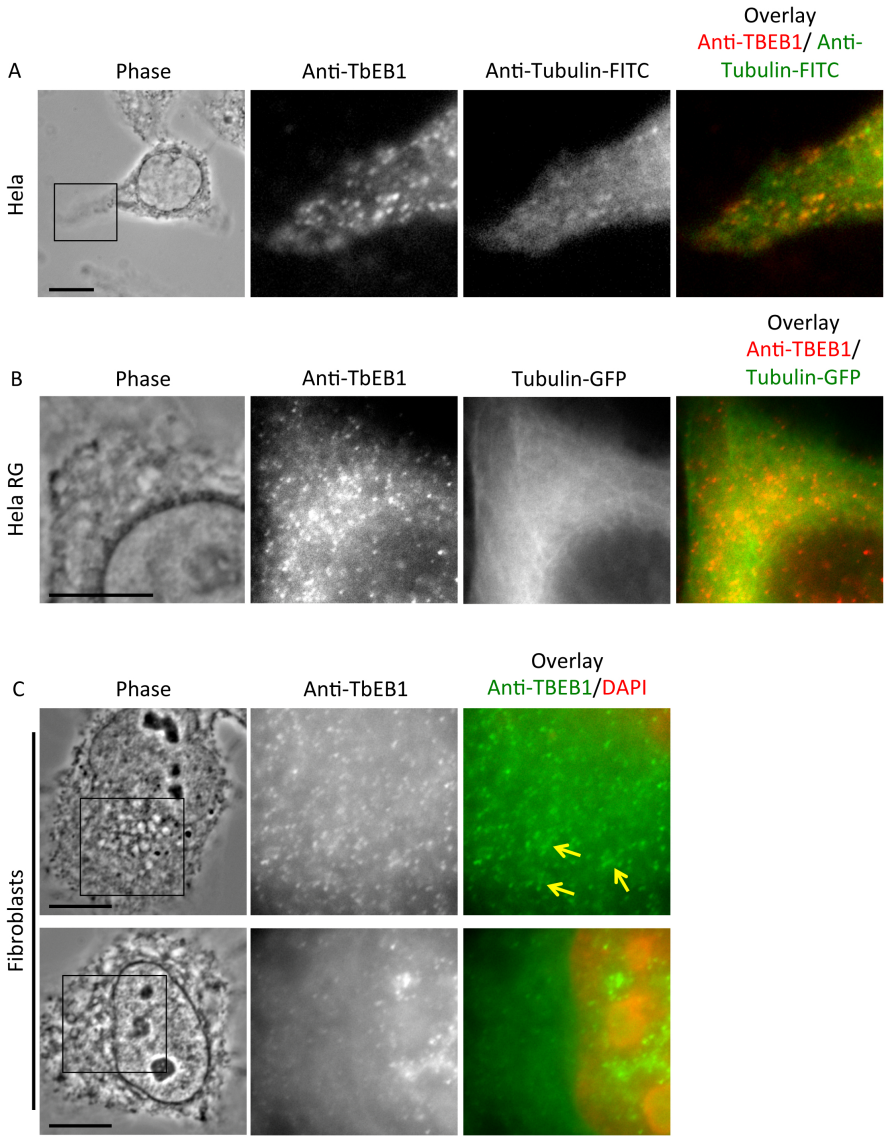


Figure 2.90: Mouse monoclonal anti-TbEB1 detects a cytoplasmic mammalian EB-protein. **A**) HeLa cells probed with anti-TbEB1 (red) and Anti-tubulin-FITC conjugated (green). **B**) Hela RG stably transfected with tubulin-GFP (green) and histon-mCherry probed with anti-TbEB1 (red). Hela cells frequently demonstrated a punctate pattern, occasionally in a comet-like pattern. **C**) Fibroblasts probed with anti-TbEB1 (green) demonstrated frequently a punctate pattern of EB1 labeling. Rarely an elongated labeling was detected (arrow). Sometimes a strong labeling in the nucleus occurred. Scale bars represent 10µm.

3 Discussion

The trypanosomal cytoskeleton is the key element to sustain the shape of the parasite cell during the cell cycle, to segregate organelles prior to cytokinesis, and to orchestrate the adaptions of the cell morphology when switching between host and vector environments. In this work the microtubule-associated protein TbEB1 was investigated. It was shown that TbEB1 is localized to the posterior cell pole, where the localization pattern varies during the cell cycle as well as to the subpellicular cytoskeleton and the flagellar attachment zone (FAZ). Reduction of TbEB1 caused an impeded cytokinesis and an accumulation of atypical cell cycle stages, mainly zoids (1K0N) and multinuclear cells, leading to a significant growth defect in procyclic (PCF) and bloodstream (BSF) trypanosomes. Over-expression of TbEB1 in PCF resulted in similar phenotypes, however, less severe. Additionally, ectopic expression of TbEB1 in mammalian cells hints to a conserved mode of action due to the localization on microtubules and microtubule-bundling upon high TbEB1 levels.

3.1 Amino acid sequence and domain architecture

Similarly to other described members of the EB1 protein family, TbEB1 is a microtubule-associated protein that localizes to the plus ends of microtubules (Fern, 2012; Sheriff *et al.* , 2014; Spindler, 2014). Consistent with those proteins, the characteristic highly conserved N-terminal CH domain as well as the less conserved C-terminal coiled-coil domain with the integrated EBH domain are present. The frequently C-terminally embedded EEY/F sequence motif is lacking in *T. brucei* (Fern, 2012). It mediates amongst others interaction with Cap-Gly proteins, like CLIP-170 or p150^{glued} (Goodson *et al.* , 2003; Hayashi *et al.* , 2005; Honnappa *et al.* , 2006; Weisbrich *et al.* , 2007). Although a trypanosomal CLIP-170 homologue might be present in the genome (Fern, 2012), Cap-Gly proteins are rare in *T. brucei (Fleming* et al. *, 2013)* and thus, interaction putatively mediated otherwise. The motif is a common feature of animal EB1 proteins as it is missing in plants (Komaki *et al.* , 2010). In animals, it is involved in the auto-inhibition mechanism of EB1 resulting in a shortening of microtubules (Hayashi *et al.* , 2005; Manna *et al.* , 2008; Kanaba *et al.* , 2013). The EEY/F motif is generally associated with evolutionary younger species while early branching single-cell organisms completely

lack the motif. Moving to higher phyla, an accumulation of acidic residues or single amino acids belonging to the motif evolved. Therefore, the use of the EEY/ F sequence to mediate interaction and intrinsically regulate activity may be an evolutionary young mechanism born by the necessity to overcome the increasing complexity in animals. Interestingly, plants developed EB1 auto-inhibition independently of the EEY/F sequence motif (Komaki *et al.* , 2010) and so may do trypanosomes. The parasite possesses an enormous number of kinesins reflecting the unchallenged supremacy of the tubulin-based cytoskeleton (Berriman *et al.* , 2005). Among the approximately 50 kinesins, 7 belong to the microtubule depolymerizing kinesin-13 family, whereby two of them are localized to the cell body (Berriman *et al.* , 2005; Chan, 2008; Wickstead *et al.* , 2010). Furthermore, besides their role in mitosis, some members of the family also demonstrate effects on interphase microtubules in other organisms (Mennella *et al.* , 2005; Dawson *et al.* , 2007). Additionally, two further trypanosomal kinesins, TbKinC and TbKinD, were reported to interfere with microtubule growth dynamics (Hu *et al.* , 2012b,a). Hence, a counter-regulation of EB1 promoted microtubule growth by a surplus of microtubule depolymerizing supporting kinesins could also be possible circumventing the need for auto-regulatory mechanisms. Due to the high sequence homology of CH and coiled-coil domains a modeling using the human EB3 as a template was possible. The additional unstructured insertion found in the amino-terminal region of trypanosomal species seemed to be a relict as it is not necessary for interaction with the microtubule surface and lost in evolutionary younger organisms. Notably, although TbEB1 possesses only a truncated version of the C-terminal region, the length of the coiled-coil domain was not constricted compared to other EB proteins. However, the linker region of TbEB1 is extraordinary long compared to other EB proteins. Up to the present, only one further TbEB1 homologue of a similar high molecular weight is known: DdEB1 (Rehberg & Gräf, 2002). Compared to TbEB1, the C-terminal region is extremely extended while the linker sequence is shorter.

3.2 TbEB1 is localized to hot spots of microtubule remodeling

In the course of this work, an article was published by Sheriff et al. (2014) describing the localization of TbEB1 throughout the cell cycle in PCF. The group used a polyclonal antibody (anti-EB1) and an N-terminal YFP- or Ty1-tagged fusion protein. Compared to the N-terminal fusion protein in this work ($TbEB1^{N\text{-}6xmyc}$), the group defined a clear variation of the labeling pattern of TbEB1 for both tags in procyclic trypanosomes throughout the cell cycle. A possible explanation to the obtained discrepancy in this study might be the c-myc tag on TbEB1, which resulted in a higher accumulation of the fusion protein in the cytoplasm and prevented a

clearly distinguishable signal of the posterior cell pole to the cell body in PCF trypanosomes. This is strengthened by the fact that only usage of the 12x-c-myc version of TbEB1 in PCF enabled a signal intensity at the cell pole above cytoplasmic labeling in whole cell preparations of 2K1N and 2K2N cells. Descriptions of endogenous TbEB1 localization in procyclic and bloodstream trypanosomes, visualized by poly- (Sheriff *et al.* , 2014) and monoclonal (Spindler, 2014) antibodies resembled observations obtained by mouse monoclonal anti-TbEB1 antibody in this work. However, using that anti-TbEB1 antibody on TbEB1 RNAi cell lines resulted only in about 50% of induced procyclic and 80% of induced bloodstream cells in a visible decrease of the signal at the posterior cell pole compared to wild type cells. In fact some, often multi-nucleated cells even demonstrated an intensified signal. Although the epitope binding site of monoclonal antibodies is just a few amino acids in length (Hebbes *et al.* , 1989), binding to another protein localizing in a similar pattern as TbEB1 at the posterior cell pole could not be fully excluded. By combination of different approaches, anti-TbEB1 monoclonal antibody, endogenous tagging of a TbEB1 allele and inducible expression of an ectopic TbEB1 fusion protein, three main parts of microtubule activity have been identified: the posterior cell pole, the subpellicular cytoskeleton, and the flagellar attachment zone.

3.2.1 Posterior cell pole

At the posterior cell pole, the TbEB1 labeling pattern monitors the microtubule remodeling during the cell cycle (Sheriff *et al.* , 2014). The high level of TbEB1 signal at that position was expected due to the high concentration of microtubule plus ends in that area (Sherwin & Gull, 1989b; Robinson *et al.* , 1995). EB1 proteins are highly conserved among eukaryotes and they preferentially localize to the plus ends of microtubules (Schuyler & Pellman, 2001; Akhmanova & Steinmetz, 2015). Both, endogenous and fusion protein, represented a dot-like signal at the posterior cell pole in G_1-phase cells for procyclic and bloodstream forms. The signal, which appeared often ring-shaped in detergent-extracted preparations, increased in intensity over the cell cycle. Consistent with literature (Sheriff *et al.* , 2014; Spindler, 2014), an elongation of the signal was found when progressing through the cell cycle. The elongation generally started with late S- or early G_2-phase, coinciding with nuclear division, and reached a maximum in 2K2N cells. Especially in PCF, the new-daughter posterior end was well visible at that cell cycle stage. The more condensed appearance of the signal in 2K2N bloodstream trypanosomes is attributed to a modulated division mechanism in that life cycle form (Wheeler *et al.* , 2013; Spindler, 2014). The pre-abscission bridge in PCF is situated laterally near the most posterior localized kinetoplast while in BSF the pre-abscission bridge is found at the posterior tip, where both kinetoplasts are found (Wheeler *et al.* , 2013). The immunofluorescence labeling pattern therefore appears smaller in BSF. Furthermore, remodeling processes of the posterior cell pole

consistent with progress in cell cycle have been observed. Notably, Wheeler et al. (2013) used TbXMAP215$^{\text{N-YFP}}$, the trypanosomal homologue to the *Xenopus* microtubule polymerase, to illustrate the remodeling processes at the posterior cell end. The N-terminally tagged version of the protein displayed the same variations of the labeling pattern at the posterior cell pole during the cell cycle as described for TbEB1 in this work and by others (Sheriff *et al.* , 2014; Spindler, 2014). This suggests a participation of TbEB1 in remodeling processes during the cell cycle at the posterior cell pole. A further microtubule plus-end binding protein was only described for trypanosomatids: TbGb4 (Rindisbacher *et al.* , 1993). That protein also localized exclusively to the posterior tip of the cell, which was well visible on whole cell preparations and detergent-extracted cells of PCF. Similar to labeling patterns obtained by the mouse monoclonal anti-TbEB1 antibody of this study, whole cell labeling only resulted in a dot-like staining at the posterior cell pole while detergent-extracted cytoskeletons often revealed the ring-like structure of the posterior cell pole. Although a variation of the TbGb4 signal throughout the cell cycle was not described by Rindisbacher et al. (1993), some 2K2N cells presented in that study demonstrated an elongated signal of the posterior tip similar to TbEB1.

3.2.2 Subpellicular cytoskeleton

A punctate TbEB1 distribution over the whole cell body was so far only described for whole cell preparations (Sheriff *et al.* , 2014; Spindler, 2014). In general, the endogenous TbEB1 labeling of the posterior cell end exceeded that of the microtubule array. However, a faint labeling of the whole cell body was detected for all cytoskeletal preparations of C-terminally tagged TbEB1 proteins and cells stained with the mouse polyclonal anti-TbEB1 antibody. Only high concentrations of monoclonal anti-TbEB1 antibody enabled the visualization of the pointed pattern of subpellicular microtubules by light microscopy (data not shown). Although the subpellicular microtubule corset demonstrated mostly a weak TbEB1 fluorescence signal, electron micrographs of cytoskeletal preparations labeled with monoclonal anti-TbEB1 antibody and whole cell immuno fluorescence assays of procyclic TbEB1$^{\text{C-12xmyc}}$ pointed towards a gradient distribution of the protein on the subpellicular microtubule array similar to the distribution of tyrosinated α-tubulin, which is a marker for newly synthesized microtubules (Sherwin *et al.* , 1987; Wheeler *et al.* , 2013). Therefore, the overlapping labeling patterns indicate a participation of TbEB1 in microtubule dynamics. The distribution of the punctate pattern did not change dramatically during the cell cycle as found for the posterior cell end, but when TbEB1$^{\text{C-12xmyc}}$ was labeled with an anti-myc antibody, especially in procyclic trypanosomes, the fluorescence signal at the posterior third of the cell increased throughout the cell cycle approaching cytokinesis. Electron micrographs of TbGb4 only demonstrated a surplus of TbGb4 at the posterior cell pole microtubules compared to the anterior one (Rindisbacher *et al.* , 1993). A localization of TbXMAP215

to subpellicular microtubules was not described by Wheeler et al. (2013). Furthermore, the punctate pattern of TbEB1 fluorescence resembled the pattern observed for another protein associated with the cytoskeleton: γ-tubulin, a marker for microtubule minus ends and component of microtubule organizing centers (MTOC) (Oakley & Oakley, 1989; Scott *et al.* , 1997; Zhou & Li, 2015). Up to the present, discrete MTOCs had not been localized to the subpellicular microtubules by detection of γ-tubulin or other components of the MTOCs in trypanosomes (Scott *et al.* , 1997; Zhou & Li, 2015). As Scott et al. (1997) specified, microtubules of the subpellicular cage do not proceed through the entire length of the cell. They vary in length but have the same polar orientation. Therefore, γ-tubulin was suggested to mark microtubule minus ends of single microtubules (Scott *et al.* , 1997). Single microtubules were distinguished in microtubule sheets analyzed by electron microscopy but a clear identification of a microtubule plus end decorated with TbEB1 was not possible. However, TbEB1 was definitely located along single microtubules. EB1 is known to decorate not only microtubule plus ends but also in lower abundance, the microtubule wall (Tirnauer *et al.* , 1999; Bieling *et al.* , 2007; Vitre *et al.* , 2008). As EB1 proteins are known to interact with other microtubule-associated proteins to control microtubule dynamics and to mediate cross-talk between components of the cytoskeleton and the cell (Alfaro-Aco & Petry, 2015), a localization of TbEB1 to the subpellicular microtubules might be associated with the re-organization of microtubule cross-links. That would be of importance during the cell cycle, when organelles have to be separated and re-arranged, but also for common transport activities and division of daughter cells in general. In addition, in the publication by Sherwin and Gull (1989b), electron micrographs of microtubule sheets were shown, showing short microtubules seemingly to sprout from longer, pre-existing ones. That 'branching' is a common feature of plant cortical microtubules (Wasteneys & Williamson, 1989; Fishel & Dixit, 2013) and is supposed to be an ancient process (Murata & Hasebe, 2007). It fits well to the *Trypanosoma* genus, which do not possess a centrosome or spindle pole body like in animals and yeast, respectively (Akiyoshi & Gull, 2014). Although this process deals with a centrosome-independent microtubule nucleation mechanism, γ-tubulin is present at the branch point of plants (Murata *et al.* , 2005). Furthermore, AtEB1a (an *A. thaliana* homologue of EB1) was shown to be located at those nucleation sites, too. Notably, AtEB1 binds to minus and plus ends, thereby mediating the anchoring of newly synthesized microtubules to the branching sites (Chan *et al.* , 2003). Furthermore, in *T. brucei* tyrosination of α-tubulin occurs in 1K1N cells not only at the plus end of microtubules but at the minus end as well (Sherwin & Gull, 1989b). Therefore, a connection of TbEB1 and γ-tubulin to growing microtubules at branching points in the subpellicular microtubule array of trypanosomes should not be excluded, although depletion of γ-TuSC subunits (Zhou & Li, 2015) and TbEB1 did not adversely affected the structure of the subpellicular microtubule array. However, the strong conservation of the polarity of the

subpellicular array by the semi-conservative inheritance pattern (Sherwin & Gull, 1989b) might prevent severe effects within the short time of RNAi activity post induction (mostly up to 5 days), and stronger effects would be visible only by complete eradication of the protein in double gene knockout cell lines. Thus, the composition of trypanosomal branching points, and the molecular mechanisms for their generation are still to be revealed as well as the definite role of TbEB1 in these processes.

3.2.3 The flagellar attachment zone (FAZ)

Previous anti-TbEB1 antibodies (Sheriff *et al.* , 2014; Spindler, 2014) were found to recognize the FAZ. However, TbEB1 RNAi approaches performed by Sheriff et al. (2014) could not confirm a reduced FAZ labeling and their YFP-labeled TbEB1 was not always localized to that region, too. Therefore until then, the labeling of the FAZ was considered to be unspecific, i. e. due to cross-reaction of the antibodies with other trypanosomal proteins (Sheriff *et al.* , 2014; Spindler, 2014). In this work in light microscopic approaches using the mouse monoclonal anti-TbEB1 antibody, the FAZ was only rarely detectable. However, on electron micrographs, using the same antibody a higher density of TbEB1 labeling at the FAZ was observed for procyclic trypanosomes. And endogenous 12xmyc C-terminal tagging as well as ectopic expression of TbEB1 also demonstrated a labeling of the FAZ region, which was detectable at new and old FAZ. Usually the newly synthesized one demonstrated a higher labeling density. Furthermore, in procyclic RNAi cell lines, the amount of small cells increased after TbEB1 depletion implying that the protein plays a role in cytoskeleton-dependent processes in that region. This is corroborated by the finding that indicators of microtubule synthesis and maturation, YFP-α-tubulin and tyrosinated α-tubulin, are also present at higher densities in the FAZ-region (Sherwin & Gull, 1989b; Wheeler *et al.* , 2013; Sheriff *et al.* , 2014) due to the duplication of the microtubule quartet and the integration of subpellicular microtubules between old and new FAZ (Wheeler *et al.* , 2013) which was also observed in TbEB1$^{\text{C-12xmyc}}$ 2K1N cells. Furthermore, FAZ synthesis has been shown to be a microtubule-driven process as its polymerization was adversely affected by knockdown of GCP2, a member of the γ-TuSC complex (Sheriff *et al.* , 2014). This connection was already suggest earlier by Zhou et al. (2011), when depletion of a FAZ component led to disordered microtubules between new and old FAZ resulting in small daughter cells.

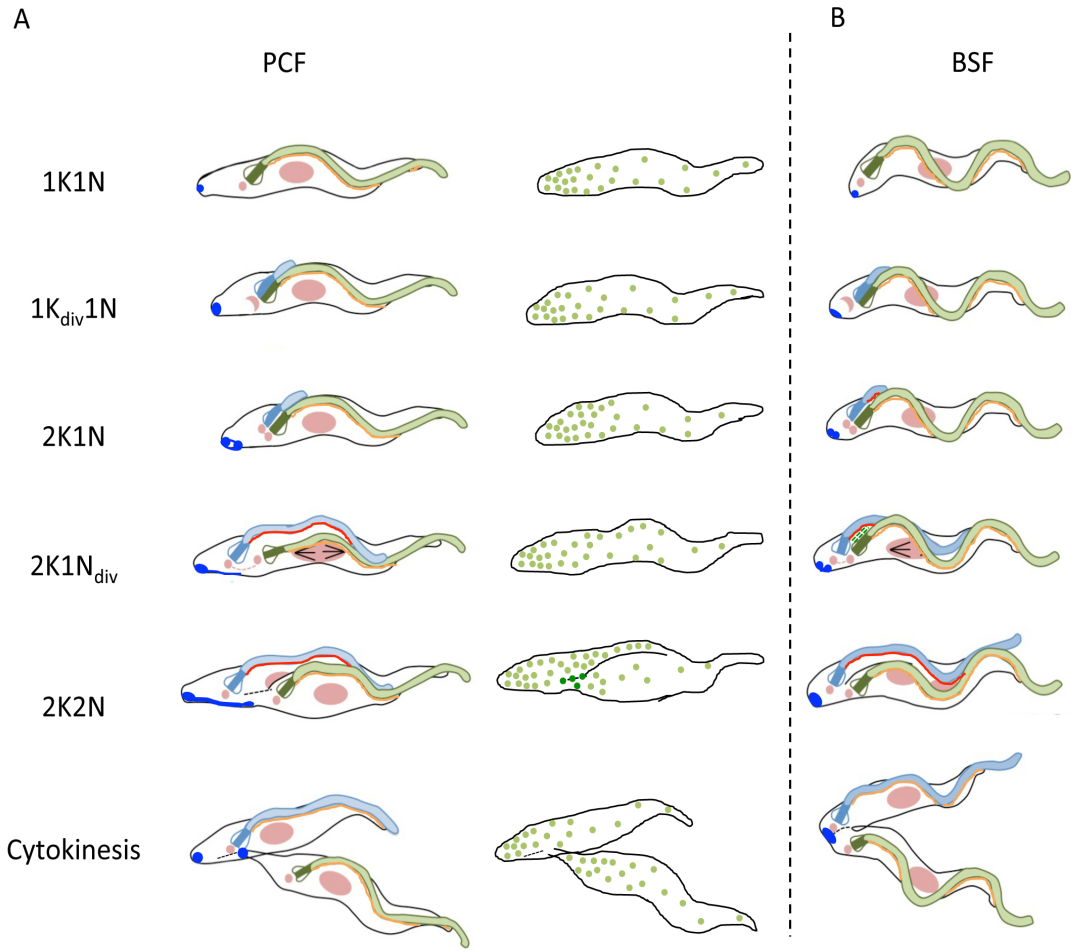


Figure 3.1: Model of TbEB1 distribution during the cell cycle in A) procyclic (PCF) and B) bloodstream (BSF) trypanosomes. The distribution of TbEB1 varies during the cell cycle. Especially, the signal at the posterior cell pole (blue) has a strong spatiotemporal correlation with single cell cycle stages. Labeling intesity of the newly assembled FAZ (red) is more intense than that of the old one (orange). Only in PCF, a varying labeling pattern of the subpellicular cytoskeleton was detectable during the cell cycle (light green). Especially at the posterior part of the division furrow a strong labeling was found (dark green). However, it is assumed that the subpellicular cytoskeleton labeling is quite similar in BSF.

3.3 TbEB1 labeling dynamics of the cytoskeletal components throughout the cell cycle

With the aid of a specific monoclonal antibody and various approaches of endogenous tagging of a TbEB1 allele, three main areas of a dynamic cytoskeleton were identified in both life cycle stages investigated: the posterior cell pole, the subpellicular microtubule array, and the FAZ or FAZ surroundings (Fig. 3.1). As the signal intensity for all regions seemed to vary with cell cycle position, the TbEB1 labeling during the trypanosomal cell cycle is described in more detail predominantly relying on the results obtained from PCF. During G_1-phase, 1K1N cells exhibit a weak labeling signal at the posterior cell pole and only a faint, distinct pattern over the cell body. A gradient distribution from posterior to anterior was assigned according to the decrease of microtubule plus end density in the same direction. The labeling of the FAZ was almost equally faint during that time. The low TbEB1 labeling intensity matches the low grade of α-tublin tyrosination at this point in the cell cycle indicating that the majority of microtubules have been synthesized in previous cell cycles (Sherwin & Gull, 1989b). Low levels of YFP-α-tubulin incorporation also point towards low microtubule assembly levels in these cells (Sheriff *et al.* , 2014). As soon as the new daughter flagellum arises from the basal body and exits the flagellar pocket, FAZ assembly starts (Sherwin & Gull, 1989a; Robinson *et al.* , 1995). The increased assembly activity of the FAZ is reflected by the simultaneously elongating signal pattern in immunofluorescence assays and elevated levels of TbEB1 staining at that organelle. An increased microtubule turnover at that region is also illustrated by integration of YFP-tubulin (Sheriff *et al.* , 2014). With approaching S-phase, the intensity of the posterior staining reached a maximum and was frequently assigned to two distinct dots at the posterior cell pole linked by a fine circle in 2K1N cells of G_2-phase. Similar to YFP-tubulin labeling and α-tublin tyrosination, the posterior third of the cell body increased in TbEB1 labeling intensity from G_1- to G_2-phase. At this point, the punctate labeling of the subpellicular corset covers more than two third of the cell body. The integration of new microtubules is asymmetric with the majority inserted in the new flagellum daughter cell (Wheeler *et al.* , 2013; Sheriff *et al.* , 2014). Prior to mitosis, in 2K1N cells, the amount of tyrosinated α-tubulin dropped remarkably despite the high occurrence of microtubule ends before it rose again (Sherwin *et al.* , 1987; Sherwin & Gull, 1989b). This contrasts TbEB1 labeling, which did not demonstrate such a wave-like labeling intensity. Instead, the labeling intensity of the subpellicular microtubules increased steadily up to mitosis, reaching a maximum in that cell cycle stage. However, this is in agreement with the hypothesis that subpellicular microtubule assembly usually proceeds quite slowly (Sherwin & Gull, 1989b) but a high amount of TbEB1 in combination with other factors present at microtubule plus ends, e. g. TbXMAP215, accelerate microtubule polymerization kinetics (Zanic *et al.* , 2013). In pre-

mitotic cells, the posterior signal apparently decreased because of the elongation of the labeled area synchronously to nuclear division. In general, near the most anterior kinetoplast, where the newly forming posterior end of the old flagellum daughter cell is assumed to be localized, an accumulation in the linear labeling pattern was frequently found. In mitotic cells, the highest TbEB1 labeling intensities were observed at the subpellicular cytoskeleton and at the newly assembled FAZ fitting to low tyrosination levels of α-tubulin, which increase only just after mitosis is finished (Sherwin & Gull, 1989b). Up to cytokinesis, the remodeled posterior thirds of the cell body, especially that of the old-flagellum daughter cell, are still strongly labeled by TbEB1 while other parts of the subpellicular cytoskeleton and the FAZ demonstrated diminished signal intensity, thereby indicating the end of remodeling processes.

Therefore, TbEB1 labeling is consistent with the tight spatial and temporal control of microtubule polymerization discovered for other markers of microtubule dynamics. The described dynamics of the subpellicular cytoskeleton labeling relying on results from PCF are assumed to be similar for BSF.

3.4 Functional analysis of TbEB1

3.4.1 TbEB1 is essential in procyclic and bloodstream trypanosomes

The function of TbEB1 was investigated in TbEB1 knockdown cell lines of procyclic and bloodstream trypanosomes. Only in cell line 449, TbEB1 was considerably reduced in qPCR analysis after induction of RNAi, however all analyzed cell lines demonstrated defects in cell growth and cytokinesis. TbEB1 protein levels were investigated by immunoblot and immunofluorescence analysis. Inconclusive results were obtained when detecting TbEB1 with a mouse monoclonal antibody. Only 50% (PCF) and 80% (BSF) of trypanosomal cell population demonstrated a reduced signal intensity at the posterior cell pole. Additionally, TbEB1 was detected during the whole depletion period. In some cases, protein levels seemingly increased as the detection signal intensified in immunofluorescence assays. Especially in PCF, the introduced tag interfered with normal cell growth. Observing protein depletion in tagged TbEB1 cell lines showed an almost complete reduction of tagged protein after RNAi induction. Still, reduction of tagged protein in these cell lines can be attributed to removal of dysfunctional proteins via the protein degradation pathways, as the introduced tag lead to a growth defect in PCF. Nonetheless, repeating the experiments with a mouse polyclonal antibody, resulted into a strong depletion of TbEB1 as shown in Western blots and immunofluorescence assays. Of course, off-target effects can never be ruled out completely. Specificity of RNAi is corroborated by single-allele gene knockouts which demonstrated similar phenotypes. Additionally, over-expression of TbEB1 also resulted

in similar, albeit weaker effects, which is common for microtubule-associated proteins (Beinhauer *et al.* , 1997).

A considerable retardation of cell cycle dynamics, and thus also of cell proliferation, was one of the key phenotypes upon lack of TbEB1. That severe loss of fitness in procyclic and bloodstream trypanosomes has been already predicted by a high-throughput phenotyping of RNAi targets (Alsford *et al.* , 2011, 2012b). Contrary to that study, the depletion of TbEB1 resulted in no growth defect and no detectable phenotypes in a master´s thesis (Fern, 2012). A similar result was found for first RNAi clones obtained during this work, which only demonstrated a modest growth retardation and few atypical cell cycle stages, e. g. a- and multinucleated cells. However, the answer might be found in the efficiency of RNAi silencing. RNAi knockdown levels of first TbEB1 RNAi clones obtained were considerably lower than those of final clones presented in this work. Furthermore, procyclic and bloodstream TbEB1 RNAi cell lines of this work demonstrated a stronger decrease of the TbEB1 signal on immuno blots compared to that of the master´s thesis. Altogether this suggests a strong selective pressure on RNAi cell lines, which is also illustrated by the low number of obtained clones. Especially bloodstream cell lines which escaped fast from RNAi-induced TbEB1 knockdown, too, demonstrated most severe phenotypes shortly after transformation and selection. Additionally, establishment of double gene knockouts failed. On this basis, it is quite likely that TbEB1 is an essential gene in *T. brucei.* Eventhough TbEB1 mRNA levels differ in the two different forms of the parasite, the lower transcription levels in BSF might be compensated by a higher translation rate as can be concluded from a higher recruitment of ribosomes to the mRNA (Vasquez *et al.* , 2014). This indicates a similar need for TbEB1 protein in both parasitic forms.

3.4.2 TbEB1 fulfills its main function in regulation of microtubule dynamics

The key phenotypes of TbEB1 deficient mutants - growth defects, accumulation of atypical cell cycle stages, and impeded cytokinesis - as well as continuous association with the subpellicular cytoskeleton indicated that TbEB1 fulfills its main function in regulation of microtubule dynamics throughout the cell cycle. Several lines of evidence support this assumption. Firstly, TbEB1 exhibits a conserved role in promoting microtubule dynamics. When TbEB1 was ectopically introduced into HeLa cells, thereby generating high cellular levels of TbEB1, alteration of microtubule size and form, e. g. extremely long and curved microtubules, was identical to phenotypes observed for over-expression of mammalian EB proteins. Additionally, cytoplasmic microtubules, which were solely decorated by TbEB1$^{\text{C-GFP}}$, indicated an autonomous microtubule polymerization activity by interaction with other members of the mammalian +TIP network. Finally, microtubules with overlapping anti-tubulin and TbEB1 signal but no clear co-localization

were found. As in *T. brucei* new microtubules are integrated between the pre-existing subpellicular microtubule cage (Sherwin & Gull, 1989b), this observation might be indicative for the ability of TbEB1 to track newly synthesizing microtubules along pre-existing ones similar to EB-influenced axon growth along actin bundles (Akhmanova & Steinmetz, 2015; Cammarata *et al.* , 2016).

Secondly, upon TbEB1 depletion, the TbEB1 signal at the subpellicular cytoskeleton was considerably reduced in procyclic trypanosomes. In line with this observation, the signal for tyrosinated α-tubulin, which is a hallmark of newly assembled microtubules (Sherwin *et al.* , 1987; Stephan *et al.* , 2007; Wheeler *et al.* , 2013), decreased after two days of TbEB1 depletion at the posterior third of the cell which was concomitant with a rounding of the posterior tip. Similar findings were found in single cases for bloodstream trypanosomes, albeit cellular morphology was not distorted. Therefore, without TbEB1 no further polymerization of new microtubules takes place. Remarkably, this finding is supported by the occurrence of of extremely slim zoids because the subpellicular cytoskeleton has not been enlarged by insertion of new microtubules. Quite frequently, those slim zoids demonstrated a decreased level of tyrosinated α-tubulin, indicating that their subpellicular cytoskeleton contains predominantly old microtubules. In over-expression experiments, the observed zoids were substantially broader, possibly because microtubule polymerization was still functional in these cells. This is also corroborated by the gradient distribution of tyrosinated α-tubulin.

Thirdly, at the end of the RNAi experiment, procyclic cells were extremely crowded with nuclei, lost their vermine shape, and often also the gradient labeling of tyrosinated α-tubulin. Albeit bigger than wild type cells, those cells were disproportionally smaller than would be expected from a multi-nucleated cell. This is similar to the phenotype observed in α-tubulin knockdown experiments (Ngô *et al.* , 1998). In both cases, cell growth is impaired due to a perturbed microtubule synthesis. However, in the latter case, α-tubulin is not present as a fundamental building block while an important tool for the construction of microtubules is missing if TbEB1 is depleted.

Finally, TbEB1 is also responsible for the elongation of pre-existing microtubules early in the cell cycle. Procyclic cells occurring within the first 48 hours of the RNAi knockdown, sometimes demonstrated an extensively elongated posterior cell end. As those cells are only part of the early RNAi population, pre-existing microtubules are initially still elongated at their plus ends as TbEB1 is still available. The following increase in microtubule number is no longer possible as TbEB1 levels drop beyond a certain concentration and thus, no assembly of new microtubules or severing of elongated microtubules take place.

In conclusion, TbEB1 is necessary for the elongation of pre-existing microtubules at the posterior cell end as well as for the insertion of new microtubules into the subpellicular micro-

tubule array. Further experiments are necessary to elucidate if the number of microtubules is augmented by *de novo* synthesis or severing of newly synthesized microtubules from branching points. Notably, the observed phenotypes caused by malfunctioning microtubule dynamics are less grave in single gene knockout cell lines and at the beginning of the RNAi experiment. This implies a dosage-dependent effect on microtubule dynamics according to the present TbEB1 concentration.

3.4.3 TbEB1 influences cytokinesis

TbEB1 plays an essential role in microtubule dynamics which also govern cytokinetic processes (Robinson *et al.* , 1995; Gull, 1999; Farr & Gull, 2012). Interestingly, a high frequency of atypical cell cycle stages has been found in all samples of TbEB1 knockdown cell lines which points to an involvement in cytokinesis. Similar phenotypes with defects in cytokinesis were observed for anti-microtubule agents such as vinblastine, vincristine or taxol (Gull, 1999; May, 2011). While the microtubule destabilizing drugs vinblastine and vincristine predominantly caused multi-nucleated cells, taxol as microtubule stabilizer also caused anucleated (1K0N) or akinetoplastid (0K1N) cells as well as organelle mispositioning. Notably, effects of taxol treatment also affected posterior end morphology (blunt end) either by directly interfering with growing microtubules or indirectly due to distorted cytokinesis (May, 2011). Effects of the microtubule-stabilizing cytotoxin taxol resemble more the phenotype of a TbEB1 knockdown than that of vinca alkaloids suggesting that a reduction of TbEB1 levels also decreases microtubule turn-over and thus, renders microtubules, especially at the dynamic posterior cell body, more stable.

Further evidence for the involvement of EB1 in cell division is given by depletion and over-expression phenotypes of microtubule severing enzymes. Although division fold generation is a simple in-folding of the plasma membrane between parallel subpellicular microtubules (Wheeler *et al.* , 2013), cross-links between microtubules at either side of the fold have to be released and re-organization takes place to maintain the cellular shape (Benz *et al.* , 2012). While spastin plays only a role in bloodstream trypanosomes, katanin was similarly important for both life cycle stages. Depletion or over-expression of KAT80 (katanin p80 regulatory subunit) resulted in growth retardation and an accumulation of atypical cell cycle stages, mainly zoids (1K0N) and multi-nucleated cells. Furthermore, knockdown of KAT80 also affected posterior end morphology, e. g. rounding and broadening, but did not interfere with microtubule spacing (Casanova *et al.* , 2009; Benz *et al.* , 2012). This is similar to effects observed for TbEB1 depletion. Furthermore, *Drosophila* KAT60 was shown to exhibit microtubule depolymerization activity and plays a crucial role in interphase to prevent uncontrolled microtubule growth at the cell cortex. It was suggested as a counterpart of EB1 by cutting microtubules behind the EB1 cap and/

or directly removing EB1-associated tubulin dimers from growing ends (Zhang *et al.* , 2011). A hypothesis, which is supported by Sharp and Ross (2012), who suggest that EB1-stabilized kinetochores are liberated by katanin. Thereby, an interplay of TbEB1 and katanins in *T. brucei* might be possible.

Further evidence for the putative role of EB1 in cytokinetic processes is provided by depletion phenotypes of other cytoskeleton-associated proteins. Knockdown of either CAP5.5/CAP5.5V or WCB resulted in a similar accumulation of atypical cell cycle stages, e. g. 1K0N, 1K2N, and xKxN. Remarkably, both proteins were immediately lost from the posterior part of the cell after RNAi onset reflecting the fast remodeling of the posterior subpellicular cytoskeleton in growing trypanosomes. As a consequence, the cytoskeleton stability, structure, and polarity had been adversely affected (Baines & Gull, 2008; Olego-Fernandez *et al.* , 2009). In contrast, during TbEB1 depletion, the integrity and polarity of the subpellicular microtubule array was not disturbed. Additionally, over-expression of anterior localized paralogues CAP15 and CAP17 also interferes with cytokinesis and hence, leads to abnormal cell cycle stages (Vedrenne *et al.* , 2002). Vedrenne et al. assumed that those CAPs stabilize microtubules at the less dynamic anterior. Due to over-expression, these proteins also localize to the posterior cell body, where they 'overstabilize' microtubules leading to aberrant cell divisions. This further supports the hypothesis that depletion of TbEB1 increases microtubule stability as phenotypes are highly similar. Identical to TbEB1 depletion in PCF, initially zoids (1K0N) and 1K2N were found as major atypical cell cycle stages due to poor coordination of kinetoplast duplication, mitotic events and cytokinesis. The 1K2N developed to multi-nucleated cells later on as kinetoplast segregation was also affected. Furthermore, single cases indicated a disconnection of the physical link between basal body and kinetoplast if cytokinesis is distorted (Ploubidou *et al.* , 1999; Vedrenne *et al.* , 2002). Strikingly, kinetoplast segregation was also impeded in PCF and BSF trypanosomes after TbEB1 knockdown and few cases were found where either the kinetoplast or the basal body were disconnected. That impediment in kinetoplast segregation might also explain the difference of nuclei number in BSF and PCF. In PCF, successful basal body segregation is not only crucial for kinetoplast segregation but also an indispensable checkpoint for cytokinesis (Robinson *et al.* , 1995; Ploubidou *et al.* , 1999). Furthermore, in TbEB1 knockdown cell lines, initial basal body segregation including rotation of the new basal body seems to be still functional while the following segregation was to be affected. Thereby, kinetoplast segregation was prevented. This supports the conclusion that cytokinesis is extremely decelerated but still performed, which is in agreement with findings by Ogbadoyi et al. (2003).

However, the hampered kinetoplast segregation may negatively affect cell division dynamics. Thus, multiple steps of organelle re-replication take place before aberrant cytokinesis follows resulting in procyclic trypanosomes heavily crowded with nuclei. Contrarily in BSF, no

such checkpoint exists and cytokinesis is inhibited if mitosis is impeded (Hammarton *et al.* , 2003; Tu & Wang, 2005). As mitosis is not perturbed due to TbEB1 down-regulation, aberrant cytokinesis results in zoids but it is not as much slowed down as in PCF. Additionally, usually a maximum of four nuclei was counted in BSF. This amount is also found in the naturally occurring tetrades (4K4N) suggesting that cytokinesis is probably inhibited to a lower degree.

At the beginning of the RNAi experiment, zoids and 1K2N cells were frequently found as siblings due to a defective cytokinesis. The division furrow runs between the new and old FAZ in an unilateral direction starting from the anterior. Additionally, all microtubules between the new and old FAZ are newly synthesized ones (Wheeler *et al.* , 2013). Therefore, if microtubules synthesis is perturbed, no integration of new microtubules occur and thus, the new FAZ is mis-positioned. Hence, in that case FAZ mis-positioning is a secondary effect due to a perturbed microtubule assembly.

Summing up, the accumulation of atypical cell cycle stages as well as similarities to depletion phenotypes of other cytoskeleton-associated proteins and anti-microtubule drugs suggest that TbEB1 is involved in proper execution of cytokinesis. However, in particular at the end of the RNAi experiment, cell morphology is heavily affected, and therefore unspecific effects on cytokinesis cannot be ruled out completely.

3.4.4 Is TbEB1 involved in proper FAZ synthesis?

Intriguingly, PCF and BSF trypanosomes demonstrated flagellar detachment after TbEB1 down-regulation. Analysis of flagellar localization at early time points after onset of RNAi indicated that generally the newly assembled daughter flagellum was detached. Flagellar attachment is mediated by the FAZ. Thus, flagellar detachment is a characteristic phenotype if FAZ formation or structure is perturbed and similar phenotypes were described for depletion of trypanosomal proteins FAZ1 (FAZ filament structure) or CC2D (coiled-coil and C2-domain containing protein) (Vaughan *et al.* , 2008; Zhou *et al.* , 2011; Rotureau *et al.* , 2014; Sunter *et al.* , 2015a). Furthermore, cell size is defined by the length of the FAZ in trypanosomes (Vaughan & Gull, 2008; Zhou *et al.* , 2011; Sunter & Gull, 2016). Small cells have been regularly observed at later stages of the RNAi experiments in procyclics. Together with the observed localization of TbEB1 to the FAZ, these phenotypes suggest an involvement of TbEB1 in processes that occur at the FAZ, possibly MtQ (microtubule quartet) formation or restructuring of adjacent subpellicular microtubules and their cross-links. The FAZ also defines the axis of cell division which could also contribute to some of the aforementioned defects in cytokinesis (see 3.4.3) (Kohl *et al.* , 2003; Li & Wang, 2008; Sunter & Gull, 2016).

Finally, CC2D inhibits FAZ assembly and depletion mutants show remarkable similarities to the TbEB1 depletion phenotype, i. e. reduced cell size coinciding with normal sized flag-

ellum, cytokinesis defects, impeded kinetoplast segregation, and cell growth deficiencies. If assembly of the new FAZ is inhibited by loss of CC2D, synthesis of subpellicular microtubules at the anterior cell body is impeded, too (Zhou *et al.* , 2011). Contrary to CC2D depletion, most short cells still demonstrated a FAZ labeling after TbEB1 depletion indicating that FAZ assembly still occurs. This is similar to GCP2 (γ-tubulin complex 2 protein) depletion which caused a delayed FAZ assembly due to impeded polymerization of new microtubules (Sheriff *et al.* , 2014) and might be true for TbEB1 as well. Robinson et al. (1995) and also other groups have linked assembly of the FAZ and the subpellicular microtubule array (Zhou *et al.* , 2011; Sheriff *et al.* , 2014; Sunter *et al.* , 2015a). Thus, TbEB1 depletion further corroborates this hypothesis.

Nonetheless, the precise localization of TbEB1 at the FAZ has to be elucidated in more detail to answer the question whether TbEB1 is involved in FAZ formation and to rule out secondary RNAi effects as the root cause of disturbed FAZ assembly. FAZ protein composition upon TbEB1 depletion has to be characterized and will also provide insights in putative interacting partners.

3.4.5 Individual phenotypes seem to rely on the time point when TbEB1 is depleted

During TbEB1 depletion a broad variation in cellular morphology occurred. The time point during which certain microtubule-driven processes are interrupted seem to lead to a different cellular morphology. Especially in PCF, the cell cycle stage, in which TbEB1 level dropped beyond a certain threshold, appeared to coincide with an individual phenotype and are further evidence for the influence of TbEB1 on miroctubule dynamics throughout the cell cycle. Phenotypes were evaluated predominantly during the beginning of the RNAi experiment (up to day 2) as here the combination of specific and unspecific phenotypes was expected to be quite low. Phenotypes can be assigned to three main intervals in the cell cycle: 1K1N to $1K_{div}1N$, $1K_{div}$ to $2KN_{div}$, and post-mitotic cells.

Cells in the early stage of the cell cycle (1K1N to $1K_{div}1N$) are generally most affected by TbEB1 depletion (Fig. 3.2 A). They keep their overall trypomastigote shape and tyrosinated α-tubulin indicates that microtubule polymerization occurred the cell cycle before (Sherwin & Gull, 1989b). DNA organelles are duplicated and as TbEB1 is not associated with mitotic microtubules, mitosis is executed. However, basal body segregation and positioning is impeded and thus, the duplicated kinetoplast is frequently localized between the two nuclei. Due to the localization of kinetoplasts the new FAZ is also mispositioned. The FAZ mispositioning is even more pronounced by the lack of new microtubules integrated between new and old flagellum. Due to a delayed FAZ assembly or defects in FAZ structure, detached flagella occur, too. Up to the present, it still remains enigmatic how the nuclei are kept at their position and if there

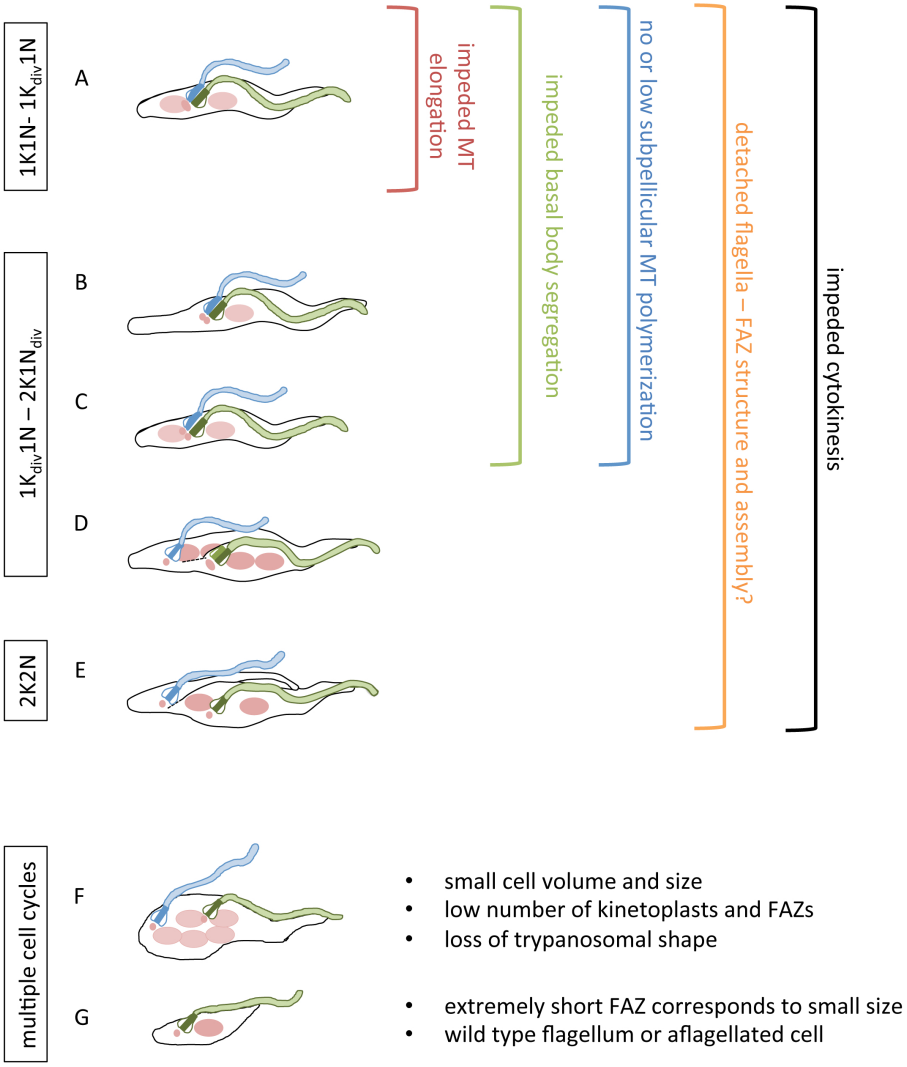


Figure 3.2: TbEB1 depletion and phenotype. The time point during which TbEB1 level fall beyond a certain threshold often interferes with a certain morphological manifestation. Example/s of a cell affected during **A)** 1K1N or 1K$_{div}$1N, **B-D)** 1K$_{div}$1N - 2K1N$_{div}$, and **E)** 2K2N. **F-G)** Phenotypes derived from several rounds of organelle re-replication combined with low levels of microtubule polymerization and a perturbed cytokinesis.

is a connection to the subpellicular cytoskeleton. Therefore, nuclear positioning might be also affected and thus, enforces the phenotype of a mispositioned kinetoplast. Further experiments determining the distance between the posterior cell end and the nuclei would be useful. It should kept in mind that a similar phenotype was also the division product of an impeded cytokinesis and may represent the higher portion.

Another phenotype demonstrating an extensively elongated posterior cell end falls between category one and two (Fig. 3.2 B). Here, elongation of pre-existing microtubules was executed but incorporation of new microtubules prior to mitosis was perturbed resulting in detached flagella, impaired kinetoplast segregation and cytokinesis.

The second category ($1K_{div}$ to $2KN_{div}$) contains amongst others cells with either a dividing kinetoplast or two kinetoplasts early after division, which are frequently mispositioned between the nuclei (Fig. 3.2 C). Here, the first step of basal body segregation occurred but the second step, during which the new basal body is pushed towards the posterior, is not executed. Frequently, flagella are also detached. Extension of cell diameter did not take place and occurring zoids are extremely slim concomitant to low levels of tyrosinated α-tubulin. Again, an additional mispositioning of the nuclei can not be ruled out.

2K4N cells also fall into this category (Fig. 3.2 D). Here, the TbEB1 level falls beyond the threshold after both steps of basal body segregation occurred. Therefore, basal bodies are properly positioned. However, cytokinesis is impeded and a second cell cycle performed. Additionally, there is no kinetoplast segregation during the second round and only low microtubule polymerization resulting in cells with a similar size as wild type 2K2N.

Quite likely, post-mitotic cells prior to cytokinesis belong to the least affected third group as microtubule polymerization, organelle segregation and positioning already took place. However, single cases of 2K2N cells possessing wild type morphology occurred which demonstrated an impeded cytokinesis resulting in 1K0N and 1K2N cells (Fig. 3.2 E). The latter frequently resembled the phenotype associated with G_1-phase and loss of TbEB1.

Two special cases were observed. The first one are multi-nucleated cells frequently combined with less pointed posterior cell end (Fig. 3.2F). Together with the low abundance of tyrosinated α-tubulin at the posterior cell body, the small size of the cell, and the low numbers of kinetoplast and FAZs, they point towards several rounds of organelle re-replication without microtubule polymerization and a perturbed cytokinesis. The second one are the small cells occurring late during the depletion period with a short FAZ due to impeded microtubule polymerization (Fig. 3.2 G).

Therefore, further experimental evidence is needed. Synchronisation of procyclic and bloodstream trypanosomes using either hydroxyurea, cell density, centrifugation or cell sorting (Chowdhury *et al.* , 2008; Kabani *et al.* , 2010; Archer *et al.* , 2011), may help to define the

role of TbEB1 at a certain cell cycle stage. Nonetheless, TbEB1 was not eradicated completely after RNAi expression and thus, microtubule polymerization is likely to be present, albeit at a very low degree. Even more, EB1 proteins have an extremely short dwell time on growing microtubule ends, which is beyond one second (Bieling *et al.* , 2008; Dixit *et al.* , 2009; Chen *et al.* , 2014b). Due to the rapid turn-over, even small amounts of TbEB1 can blur characteristic signs and thus, mix up phenotypes.

3.5 Differences and commonalities of TbEB1 to other members of the protein family

Most EB proteins accumulate at the distal tips of growing microtubules forming a comet-like gradient, which is a hallmark for +TIP proteins (Chan *et al.* , 2003; Komarova *et al.* , 2009; Tamura & Draviam, 2012). TbEB1 did neither demonstrate such a labeling pattern in *T. brucei* nor as ectopically expressed protein in HeLa cells. Nonetheless, in both organisms TbEB1 was localized to areas with an increased microtubule turn-over, such as the posterior cell end in trypanosomes or cytoplasmic protrusions in HeLa cells. In the mammalian system, high levels of TbEB1 also caused an extreme elongation and bundling of microtubules, known as 'curly' phenotype. In trypanosomes, microtubule bundling is executed prior to cell division to define the new and old posterior end (Wheeler *et al.* , 2013). Localization of TbEB1 to that cellular structures indicates that *T. brucei* EB1 not only participates in microtubule polymerization but is also involved in microtubule bundling.

Functional and localization studies on TbEB1 revealed that TbEB1 only interacts with microtubules of the subpellicular array but not with those of the axoneme or the spindle. This is in contrast to other organisms, e. g. mammalia or *G. lamblia*. Particularly, EB1 involvement in mitotic processes tends to be the rule rather than the exception (see also Tab. 1.2.3.4) and EB1 proteins mediate amongst others kinetochore-microtubule interactions (Akhmanova & Steinmetz, 2015). However, kinetochore proteins of kinetoplastids are different from all conventional kinetochore protein complexes (Akiyoshi & Gull, 2014). Thus, other proteins might participate in kinetochore-microtubule interactions rendering TbEB1 unimportant for this process.

EB1 localization to sub-cellular microtubules is ubiquitous and reported for a large variety of organisms. The loss of protein frequently resulted in short and less dynamic microtubules as well as altered cytoplasmic microtubule networks (see also Tab. 1.2.3.4). However, *T. brucei* did not possess cytoplasmic microtubules but instead a tightly cross-linked subpellicular microtubule array beneath the plasma membrane. Localization to a basically similarly constructed microtubule array is described for *A. thaliana*. There have been parallels observed between plant and trypanosomal microtubules in microtubule nucleation, cross-linking, positioning be-

neath the plasma membrane (May, 2011), the absence of centrosomes, and stability (Dixit & Cyr, 2004). Depletion of EB1 in roots of *A. thaliana* did not show a disturbed microtubule array (Bisgrove *et al.* , 2008). This is similar to findings for TbEB1 in this study as the trypanosomal subpellicular microtubule array is also very stable and is retained during the whole cell cycle. Thus, in *T. brucei* the semi-conservative mode of new microtubule integration putatively prevent stronger effects on that cellular substructure. Notably, EB1 single, double, and triple mutants in *A. thaliana* demonstrated only mild phenotypes and were fertile (Bisgrove *et al.* , 2008). This is in contrast to EB1 deletion and depletion phenotypes in *T. brucei,* where the gene appeared to be essential and already low knockdown levels interfered significantly with proliferation.

3.6 Conclusions

The variation of TbEB1 labeling pattern at the posterior cell pole of trypanosomes was confirmed. Additionally, a localization of TbEB1 to the subpellicular cytoskeleton and the FAZ/ FAZ region was observed. Depletion of TbEB1 caused aberrant K/ N ratios and cytokinesis resulting in a strong decrease in cell proliferation. This provided evidence that TbEB1, like homologous EB1 proteins in other organisms, is involved in microtubule polymerization and re-organization. Knockdown phenotypes indicate that TbEB1 also participates in cytokinesis. Furthermore, ectopic expression experiments in HeLa cells pointed towards a similar function of TbEB1 as mammalian EB proteins with a presumable similar regulation of dynamic microtubule networks. Additionally, there is a hint to a conserved mode of action, and thus to putative interacting partners of TbEB1 and regulatory mechanisms of microtubule polymerization and re-organization. One of the best candidates will be XMAP215, a conserved microtubule polymerase (Asbury, 2008). Zanic and colleagues (2013) reported a synergistic effect of EB1 and XMAP215 on microtubule growth rates *in vitro,* although there was no direct interaction between the two proteins necessary. TbXMAP displays a similar labeling pattern as TbEB1 in procyclic trypanosomes (Wheeler *et al.* , 2013) . Thus, the cooperation of both proteins in the regulation of microtubule dynamics, could be demonstrated in a similar experiment as performed by Zanic et al. using purified tubulin and recombinant proteins in TIRF microscopy (2013).

Further promising candidates will be the trypanosomal kinesins KinC and KinD, which occur in PCF and BSF as heterodimers (Hu *et al.* , 2012b,a; Wei *et al.* , 2013). RNAi phenotypes demonstrated an increased polymerization rate of subpellicular microtubules, contrary to the decreased microtubule assembly in TbEB1 knockdown cell lines. Therefore, further experiments should evaluate if these proteins act as counterparts in microtubule assembly and re-organization.

Finally, TbAUK1 might be identified as binding partner of TbEB1 during cytokinesis in co-immunoprecipitation assays. It is a component of the CPC in *T. brucei,* which moves towards the

distal tip of the new FAZ and migrates along the progressing cleavage furrow (Li *et al.* , 2008). The interaction between both proteins is documented for yeast, plant, and mammalian systems (Van Damme *et al.* , 2004; Zimniak *et al.* , 2009; Banerjee *et al.* , 2014). Notably, in mammalian and plant cells, EB proteins co-localize with Aurora kinase at areas important for cell division, e. g. the midbody in mammalia or the phragmoblast in plants (Van Damme *et al.* , 2004; Zimniak *et al.* , 2009). An interaction of TbEB1 with TbAUK1 might also support the presumable role of TbEB1 in cytokinesis and further underline the tight spatial and temporal control of microtubule dynamics, and thus reorganization of the subpellicular array including organelle positioning, to achieve a well co-ordinated and timed mitosis and cytokinesis in trypanosomes.

4 Material and Methods

4.1 Materials

4.1.1 Hard- and Software

This work was written on an „Apple MacBook Pro“ (Apple Inc., Cupertino, CA, USA) using “Microsoft Word 2011” (Microsoft Corporation, Redmond, WA, USA) and “LyX 2.1.4” (http://www.lyx.org//; the LyX Team). “Microsoft Excel 2011” (Microsoft Corporation, Redmond, WA, USA) was used for data analysis. Figures were created with “Adobe Photoshop CS4” and “Microsoft Power Point 2011” (Microsoft Corporation, Redmond, WA, USA).

Chemiluminescence signals were recorded using an “LAS-4000” system (Fuji Film, Europe, Düsseldorf) and the image analysis software “MultiGauge” (version 3.0; Fuji Film, Europe, Düsseldorf). Coomassie stained gels and Ponceau S stained immuno blot membranes were scanned on a “CanoScan LiDE 110” (Canon, Europe, Krefeld).

Electron microscopy was performed using a transmission electron microscope (EM 902A, Carl Zeiss GmbH, Oberkochen) equipped with a “Gatan Erlangshen ES 500, Model 782” camera (Gatan, Corporate Headquarters, Pleasanton, CA, USA) and “Gatan Digital Suite” (Gatan, Corporate Headquarters, Pleasanton, CA, USA). Image processing was performed with “Adobe Photoshop CS4” (Adobe Systems Inc., San Jose, CA, USA) and “ImageJ” (Rasband, 1997-2015; Abramoff et al., 2004; Scheider et al., 2012).

“Gene Construction Kit® 3.0” (Textco BioSoftware Incorporated, West Lebanon, NH, USA) was used for analysis of DNA and protein sequences. Bioinformatic analysis was performed using the online services of the University of Tübingen “Bioinformatics Toolkit” (http://www.toolkit.tuebingen.mpg.de). The EB1 phylogenetic tree figure was drawn in “FigTree 1.4.2” (http://tree.bio.ed.ac.uk/software/figtree/; Rambaut). Modeling of the trypanosomal EB1 bound to the microtubule was performed using “UCSF Chimera” (http://www.rbvi.ucsf.edu/chimera/).

The online services of the “National Center for Biotechnology Information” (http://www.ncbi.nlm.nih.gov/) were used for literature and database searches. Information on gene and protein sequences was obtained on “GeneDB” (http://genedb.org/) or “Uniprot” (UniProt Consortium, 2015).

4.1.2 Bioinformatic analysis

4.1.2.1 Blast analysis

For sequence comparison, TbEB1 homologous sequences were searched using BLAST (Altschul *et al.* , 1990). The search was performed using the algorithm blastp.

4.1.2.2 Phylogenetic tree of TbEB1

The sequence of TbEB1 was aligned to 21 EB1 homologues of 14 species. All sequences were taken from UniProt (UniProt Consortium, 2015). Alignment was performed using MAFFT (Katoh *et al.* , 2002; Katoh & Standley, 2013). The phylogenetic tree was produced with ClustalW using the nearest neighbor end joining method and exclusion of gaps (McWilliam *et al.* , 2013). The phylogenetic tree was drawn with FigTree (http://tree.bio.ed.ac.uk/software/figtree/).

4.1.2.3 TbEB1 homology model

Both N- and C-terminal domains of EB proteins are highly conserved and the respective models are based on the previously published models of human EB1 (Huang *et al.* , 2015) and yeast Bim1p (Hüls *et al.* , 2012), respectively. Homology models were produced in HHPred (Söding *et al.* , 2005; Hildebrand *et al.* , 2009). The model of TbEB1 N-terminal domain bound to α/β tubulin is derived from Zhang et al. (2015) by overlaying the homology model and the EB3 CH domain in the model 3JAK using UCSF Chimera (Pettersen *et al.* , 2004).

4.1.3 Protocols

The methods described in this section are based on standard techniques or follow the manufacturer´s protocol unless otherwise noted. If necessary, de-ionized water, solutions and flasks were sterilized.

4.1.4 Chemicals and reagents

If not otherwise noted, manufacturers are localized or have a subsidiary in Germany. Analytical grade chemical and reagent were used in the experiments. They were obtained from AppliChem (Darmstadt), BBInternational (BBI Solutions, Cardiff, UK), BIOZOL Diagnostica (Eching), Biorad (Munich), Fermentas (via Thermo Fisher Scientific, Erlangen), GE Healthcare (Munich), Invitrogen (via Thermo Fisher Scientific, Erlangen), Merck KGaA (Darmstadt), Merck Millipore (Darmstadt), New England Biolabs (NEB, Frankfurt a. M.), PJK GmbH (Kleinblittersdorf), Promega (Mannheim), Roche Diagnostics (Mannheim), Roth (Karlsruhe), Santa Cruz

Biotechnology Inc. (Heidelberg), Serva (Heidelberg), Sigma-Aldrich (Steinheim), and Thermo Fisher Scientific (Erlangen).

4.1.5 Buffers and solution

Blocking buffer	5% (w/v) skim milk in PBST
BSA-blocking solution	3% BSA (w/v) in PBS
Coomassie Staining solution	3mM Coomassie Brilliant blue R 250, 45.4% (v/v) methanol, 9.2% (v/v) acetic acid
Coomassie Destain solution	35% (v/v) methanol, 5% (v/v) acetic acid
DNA loading buffer (6x)	30% (w/v) glycerol, 0.25% (w/v) Bromphenol blue, 0.25% Xylene cyanol
ELISA substrate solution	24mM citric acid, 50mM Na_3PO_4, 3.7mM o-phenylenediamine, 0.006% H_2O_2
Extraction buffer	10mM Tris-HCl, pH 8.0, 0.1M EDTA, 0.5% SDS, 20µg/ml boiled RNaseA
GTE buffer	50mM glucose, 25mM Tris-HCl, pH 8.0, 10mM EDTA
Guanidinium chloride elution buffer	45mM NaH_2PO_4 x H_2O, 500mM NaCl, 6M guanidinium chloride, pH 7.8
Guanidinium chloride lysis buffer	20mM NaH_2PO_4 x H_2O, 270mM NaCl, 5.4M guanidinium chloride, pH 8.0
LB agar	1.5% (w/v) agar in LB medium
LB medium	1% (w/v) tryptone, 0.5% (w/v) yeast extract, 0,5% (w/v) $NaCl_2$ in dH_2O, adjusted to pH 7.2-7.4 with 1M NaOH, sterile
Lead citrate	130mM sodium citrate, 79mM lead nitrate in 1M NaOH
10% NaN_3	10% (w/v) NaN_3 in dH_2O
Native lysis buffer	500mM Tris, 200mM NaCl, 0.1% Triton X-100, pH 8.0
Native elution buffer	50mM Tris, 200mM NaCl, 250mM imidazole, pH 8.0
PBS	128mM NaCl, 2.7mM KCl, 10.1mM Na_2HPO_4, 1.7mM KH_2PO_4, adjust to pH 7.4 with 1M NaOH
PBST	0.1% (v/v) Tween20 in PBS
PM-buffer	100mM PIPES, 1mM $MgSO_4$, adjust to pH 6.9
Ponceau S Staining solution	33mM Ponceau S, 40% (v/v) methanol, 15% (v/v) acetic acid
RIPA buffer	150mM NaCl, 1mM $MgCl_2$, 1mM EGTA, 50mM Tris-HCl, pH 7.4, 1% (v/v) Triton X-100, 0.2% (w/v) SDS, 0.5% sodium deoxycholate

SDS-PAGE loading dye (2x)	124mM Tris-HCl, pH 8.8, 20% (w/v) glycerol, 4% (w/v) SDS, 5% (v/v) β-Mercaptoethanol
SDS-PAGE running buffer	25mM Tris, 19mM glycine, 1% (w/v) SDS
SDS-PAGE running gel	10% (v/v) acrylamide/ bisacrylamide solution, 375mM Tris-Hcl, pH 8.8, 0.1% (v/v) SDS, 0.05% (v/v) TEMED, 0.05% (v/v) APS
SDS-PAGE stacking gel	4% (v/v) acrylamide/ bisacrylamide solution, 108mM Tris-Hcl, pH 6.8, 0.1% (v/v) SDS, 0.1% (v/v) TEMED, 0.05% (v/v) APS
TAE	400mM Tris base, 1.1% acetic acid, 13mM EDTA, adjusted to pH 8.5
TE	10mM Tris-HCl, pH 7.4, 1mM EDTA
TELT	50mM Tris-HCl pH8, 62.5mM EDTA, 2.5M LiCl, 4% Triton X-100
TfBI	100mM RbCl, 50mM $MnCl_2$, 10mM $CaCl_2$, 30mM CH_3COOK, 15% (w/v) glycerol in dH_2O, adjust do pH 5.8 with 0.2M acetic acid, sterile
TfBII	10mM MOPS, 10mM RbCl, 75mM $CaCl_2$, 15% (w/v) in dH_2O, adjust to pH 7.0 with 1M NaOH, sterile
Transfection buffer (2x)	60mM Na_3PO_4, 3.33mM KCl, 0.1mM $CaCl_2$, 33.33mM HEPES, pH 7.3
Western Blot transfer buffer	25mM Tris, 19mM glycine, 10% (v/v) methanol

4.1.6 Antibodies

Table 4.2: Primary antibodies and TbEB1 anti-sera used in this work.

Primary Antibody	Application	Dilution Factor	Species	Source
Anti-GFP antibody	WB	1:500	Mouse	Kind gift of O. Stemmann (Dominik van Essen and Simona Saccani)
Anti-GFP antibody	IF	1:500	Rabbit	Santa Cruz Biotechnology
Anti-Tubulin FITC	IF	1:1.000	Mouse	Kind gift of O. Stemmann
Anti-TbEB1, monoclonal	IF, EM	1:50 - 1:200	Mouse	this work, clone 89, IgM ($\varkappa$)
Anti-TbEB1, polyclonal	IF, WB	1:50- 1:200	Mouse	this work, mice 1-4
His-Probe (H-3) HRP antibody	WB	1:2.000	Mouse	Santa Cruz Biotechnology
L3B2 (FAZ1)	IF	1:100	Mouse	Kohl *et al.* (1999)
Mab25 (axonemal marker)	IF	1:100	Mouse	Pradel *et al.* (2006)
MYC (anti-c-myc-tag)	IF, WB	1:200, 1:500	Mouse	DSHB, clone 9E10
TAT (α-tubulin)	IF	1:1.000	Mouse	Kind gift of K. Gull
YL1/2 (tyrosinated α-tubulin)	IF	1:50	Rat	Kilmartin *et al.* (1982)

EM = Electron microscopy, IF = Immunofluorescence assay, WB = Western blot

Table 4.3: Secondary antibodies used in this work.

Secondary Antibody	Application	Dilution Factor	Species	Source
Alexa Fluor 488 goat anti-mouse IgG, also recognizes IgM	IF	1:500	Goat	Invitrogen
Alexa Fluor 488 goat anti-rat IgG	IF	1:1.000	Goat	Invitrogen
Alexa Fluor 550 goat anti-mouse IgG, also recognizes IgM	IF	1:500	Goat	Invitrogen
Anti-rabbit IgG (whole molecule) F $(ab)_2$ fragment - FITC	IF	1:100	Goat	Sigma-Aldrich
EM goat anti-mouse IgG: 10nm colloidal gold, also recognizes IgM	EM	1:30	Goat	BBInternational
HRP-conjugated anti-mouse IgG (whole molecule), also recognizes IgM	WB, ELISA	1:80.000	Goat	Sigma-Aldrich

ELISA = enzyme-linked immunosorbent assay, EM = Electron microscopy, IF = Immunofluorescence assay, WB = Western blot

4.1.7 Plasmids

Table 4.4: Vectors

Vector	Tag	Source
pALC14		Kind gift of A. Schneider
pCS2	-GFP, C-terminal	Turner & Weintraub, 1994; MCS modified (FseI/ AscI sites inserted); kind gift of O. Stemmann
pEnG0P	-GFP, C-terminal	B. Wickstead, unpublished
pET28M-SUMO1-FA-revised	-6x-His-$SUMO_1$, N-terminal	Kind gift of O. Stemmann
pGEM® T-easy		Promega
pHD1800	-2x-c-myc, C-terminal	Derivate of pHD1700 (kindly provided by F. Voncken); MCS modified in this work (FseI/AscI)
pMOTag43M	-3x-c-myc, C-terminal	Oberholzer *et al.* , 2006
pNAT_BSD_6Myc_X	-6x-c-myc, N-terminal	Alsford & Horn, 2008
pNAT_BSD_X_12Myc	-12x-c-myc, C-terminal	Alsford & Horn (2008)
pTrcHisC	-6x-His, N-terminal	ThermoScientific
pZJMβ		Kind gift of J. E. Donelson

Table 4.5: Plasmids

Plasmid	Insert	Vector backbone	Resistance in *E. coli*/ *T. brucei*
N-terminal tagging			
pNAT$^{N\text{-}6xmyc}$	TbEB1$^{4\text{-}675bp}$	pNAT_BSD_6Myc_X	Amp/ BSD
C-terminal tagging			
pMOT$^{C\text{-}3xmyc}$	TbEB1$^{1260\text{-}1608bp}$, 3´UTR	pMOTag43M	Amp/ HYG
pNAT$^{C\text{-}12xmyc}$	TbEB1$^{1009\text{-}1608bp}$	pNAT_BSD_X_12Myc	Amp/ BSD
RNAi			
TbEB1 RNAi pALC14, construct 1	TbEB1$^{388\text{-}767bp}$	pALC14	Amp/ PU
TbEB1 RNAi pALC14, construct 2	TbEB1$^{1\text{-}333bp}$	pALC14	Amp/ PU
TbEB1 RNAi pALC14, construct 3	TbEB1$^{961\text{-}1216bp}$	pALC14	Amp/ PU
TbEB1 RNAi pZJMß, construct 2	TbEB1$^{1\text{-}333bp}$	pZJMβ	Amp/ BLE
TbEB1 RNAi pZJMß, construct 3	TbEB1$^{961\text{-}1216bp}$	pZJMβ	Amp/ BLE
Single-allele knockout			
TbEB1sko	Puromycin, 5´UTR and 3´UTR of TbEB1	pGEM® T-easy	Amp/ PU
Ectopic expression			
TbEB1$^{C\text{-}2xmyc}$	TbEB1$^{1\text{-}1608bp}$	pHD1800	Amp/ HYG
Transient expression in HeLa cells			
TbEB1$^{C\text{-}GFP}$	TbEB1$^{1\text{-}1608bp}$	pCS2	-
Expression of recombinant TbEB1 for monoclonal antibodies in mouse			
pET28-SUMO$_1$-TbEb1 (Spindler, 2014)	TbEB1$^{4\text{-}1611bp}$	pET28M-SUMO1-FA-revised	Kan/ -
Expression of recombinant TbEB1 for polyclonal antibodies in mouse			
pTrcC-His$_6$-TbEB1 full length	TbEB1$^{4\text{-}1611bp}$	pTrcHisC	Amp/ -
pTrcC-His$_6$-TbEB1 short	TbEB1$^{4\text{-}1167bp}$	pTrcHisC	Amp/ -

Amp = ampicillin, BLE = bleomycin D1, BSD = blasticidin S, HYG = hygromycin B, Kan = kanamycin, PU = puromycin

4.1.8 DNA oligonucleotides

DNA oligonucleotides were designed with Gene Construction and OligoCalc (Oligonucleotide Properties Calculator; Kibbe, 2007). Annealing temperatures were in a range 60 and 65°C.

Table 4.6: DNA nucleotides for qPCR, modification of vector pHD1800, sequencing, and confirmation of single-allele gene knockout

Primer	Sequence
Primer Normalization qPCR	
TERTqPCR f (MA Klaster)	5´-CTT GGA AAA ACG TGG CAA AT-3´
TERTqPCR r (MA Klaster)	5´-CAG TCA GCT CAC CAA CAG GA-3´
Primer for modification of pHD1800 (pHD1800ΔPaeI) and sequencing	
pHD1800dPaeIfor	5´-TTG CAA GGC CTT GCA GGC ATA TAA GCT AGC TTG TAT TCT-3´
pHD1800dPaeIrev	5´-AGA ATA CAA GCT AGC TTA TAT GCC TGC AAG GCC TTG CAA-3´
pHD1800dPaeIseq	5´-TTA TTT GCA ACA CAT TTA CGT ACA GCG-3´
Confirmation of single-allele knockout	
EB1ko PCR for	5´-TGA TAT GGA GGT CTT CCT CAT ATA TTC-3´
EB1ko PCR rev	5´-CGT TTT GTG TCC TCG CAT ACT CCG A-3´
Sequencing of pTrcC plasmids	
pTRCseqfor	5´-GCA CTC GAC CGG AAT TAT CG-3´

Table 4.7: DNA oligonucleotides for generation of plasmids

Primer	Sequence	Restriction enzyme
EB1pNAT for	5´-GAT CCT AGG GAC CAT CGC AAT ACC CAT GGG CT-3´	AvrII
EB1pNAT rev	5´-GAT GGA TCC AAT GAC GGG AGG CTC AGT GGA T-3´	BamHI
EB1MOT43tail for	5´-TGC GGT ACC AAT GTG AGG GAA CGG TGT GCG-3´	KpnI
EB1MOT43tail rev	5´-TCG CTC GAG CTC TGC AGC GTA CAA TAC ATC CA-3´	XhoI
EB1MOT43UTR for	5´-TGC GGA TCC ACA ATG GAT ATG CAT ATT CTT ATA TGC TG-3´	BamHI
EB1MOT43UTR rev	5´-ACG TCT AGA CGG TAA CGA TAA TAA CGG GGA CG-3´	XbaI
TbEB1pNAT12 for	5´-ATA GGC GCG CCA CCG ATG ACA AGG ATA TGA CTC CGA-3´	AscI
TbEB1pNAT12 rev	5´-ATA TCT AGA CTC TGC AGC GTA CAA TAC ATC CAA CA-3´	XbaI
EB1i for	5´-ATA GGA TCC AAG CTT GGC CTT GGT GAT GTG CTT ATG-3´	BamHI, HindIII
EB1i rev	5´-ATA CTC GAG TCT AGA GTG GAC GTC CGT CTG GAT AT-3´	XhoI, XbaI
EB1i 2 for	5´-ATA GGA TCC AAG CTT ATG GAC CAT CGC AAT ACC CAT GG-3´	BamHI, HindIII
EB1i 2 rev	5´-ATA CTC GAG TCT AGA ATC CAC ATC GTC CAC AAG CAC C-3´	XhoI, XbaI
EB1i 3 for	5´-ATA GGA TCC AAG CTT GCC GTA GAG GAC AAG CAG ACA-3´	BamHI, HindIII
EB1i 3 rev	5´-ATA CTC GAG TCT AGA CGG TCC TCA CAG GGG TCG A-3´	XhoI, XbaI
EB1ko5UTR for	5´-GGT GGG CTG AAA CGA GAG GGT-3´	-
EB1ko5UTR rev	5´-ATA GGC GCG CCT CCT ACT GTC CCT AGT GGT TCT AC-3´	AscI
EB1ko3UTR for	5´-ATA GGC CGG CCC GGT AAC GAT AAT AAC GGG GAC-3´	FseI
EB1ko3UTR rev	5´-ATG TTG CGA GTC TGA CGG CGG A-3´	-
Puro for	5´- ATA GGC GCG CCA TGA CCG AGT ACA AGC CCA CG-3´	AscI
Puro rev	5´- ATA GGC CGG CCG TTA GGC ACC GGG CTT GCG-3´	FseI
EB1myc for	5´-AGC TTG GCC GGC CAT GGA CCA TCG CAA TAC CCA TG-3´	FseI
EB1myc rev	5´-GAT CCG GCG CGC CTC TCT GCA GCG TAC AAT ACA TCC A-3´	AscI
EB1 pCS2 for	5´-ATA GGC CGG CCA TGG ACC ATC GCA ATA CCC ATG-3´	FseI
EB1 pCS2 rev	5´-TAT GGC GCG CCA CTC TGC AGC GTA CAA TAC ATC CA-3´	AscI
TbEB1pTrc for	5´-ATA CTC GAG ACG ACC ATC GCA ATA CCC ATG GG-3´	XhoI
TbEB1Trc rev	5´-ATA GAA TTC TTA CTC TGC AGC GTA CAA TAC ATC-3´	EcoRI
TbEB1Trcsh rev	5´-ATA GAA TTC TTA GAT GTC GCC GCT ACC ACT AAG-3´	EcoRI

4.2 Microbiological methods

If not noted otherwise, percentages of chemicals in solutions are stated as (v/v) and solutions were used at room temperature. Media for cultivation of organisms were sterilized either by filtration or autoclaving.

4.2.1 *Escherichia coli* strains

4.2.2 *E. coli* media, cultivation, and storage

E. coli strains were grown on LB agar (see 4.1.5) plates at 37°C or in LB medium (see 4.1.5) at 37°C, continuously shaking at 180rpm. Media were supplemented with 100µg/ml ampicillin or 30µg/ml kanamycin according to the resistance marker of the used plasmid. Bacterial growth was recorded by optical density measurement at 600nm (OD_{600}) using LB medium as blank value. Cultures in liquid medium were stored for a few hours while cultures on agar plates were stored up to one month. For long term storage, glycerin was added to a growing culture to a final concentration of 20% (v/v), and the culture subsequently flash frozen in liquid nitrogen and stored at -80°C.

4.2.3 Generation of chemically competent *E. coli*

600ml LB medium were inoculated with 3ml of an overnight culture and incubated at 37°C until an OD_{600} of 0.4-0.5 was reached. Bacterial cells were incubated on ice for 2min. Subsequently, bacterial suspensions were centrifuged at 7,500g, 4°C, 10min. The pellet was resuspended in a final volume of 90ml 1x TfBI (see 4.1.5) and stored on ice for 30-60min. Then, the suspension was centrifuged at 7,500g and 4°C for 10min. The pellet was resuspended in 18ml of ice-cold TfBII (see 4.1.5) and incubated for 15min on ice. Subsequently, 200µl aliquots of cell suspension were flash frozen in liquid nitrogen and stored at -80°C.

Table 4.8: *E. coli* strains used in this work.

Strain	Genotype	Use	Source
E. coli XL1 blue	*E. coli sup*E44, *hsd*R17, *rec*A1, *end*A1, *gyr*A46, *thi,* relA1, *lac*$^-$[F´*pro* AB *lacI*^{q}, *Lac* ZdM15, Tn10 (*Tet*^{r})]	molecular cloning, amplification of plasmids	Stratagene/Agilent Technologies (Santa Clara, CA, USA)
E. coli BL21 (DE3)	*E. coli* B F$^-$, *dcm, omp*T, *hsd*S(r_B^- m_B^-), *gal* λ (DE3)	protein expression	Kind gift of O. Stemmann

4.2.4 Transformation of plasmid DNA in *E. coli*

Competent *E. coli* were thawed slowly on ice. For transfection, 300ng plasmid DNA or 2µl of ligation mixture were added to 200µl of bacterial cell suspension. Subsequently, the preparation was incubated on ice for 30min followed by a heat shock at 42°C for 45s. Afterwards, 800µl of LB medium were added to the suspension. If ampicillin was used for clone selection, bacteria were directly plated onto agar plates. For protein expression and kanamycin selection, bacteria were incubated at 37°C on a shaking platform at 180rpm for 1h beforehand. In either case, the bacterial suspension was plated on LB agar undiluted and in 1:10 and 1:100 dilutions. Plates were incubated for at least 16h at 37°C.

4.2.5 Recombinant protein expression in *E. coli* BL21 (DE)

For expression of recombinant TbEB1 to generate mouse monoclonal antibodies, *E. coli* BL21 (DE) were transformed using the pET28-$SUMO_1$-TbEb1 plasmid (Spindler, 2014). 9ml of LB Medium supplemented with kanamycin [30µg/ml, final concentration] was inoculated with 1ml of transformed bacterial suspension and incubated at 37°C and 180rpm overnight. The obtained pre-culture was added to 500ml LB medium supplemented with kanamycin and incubated at 37°C and 180rpm. When an optical density of 0.6 was reached, recombinant protein expression was induced by addition of IPTG to a final concentration of 0.5mM. After 7h, cells were harvested by centrifugation at 3,300g and 4°C for 20min. The pellet was collected, weighed, flash frozen in liquid nitrogen, and stored at -80°C.

For expression of recombinant TbEB1 to generate mouse polyclonal antibodies, *E. coli* BL21 (DE) were transformed using either full length TbEB1 (pTrcC-His_6-TbEB1) or a truncated version of TbEB1 (pTrcC-His_6-TbEB1sh). The short fragment covered the first 1167bp which results in a His-tagged protein of about 45kDa in size. Transformation, pre-culture preparation, and bacterial pellet collection were similar to the pET28-$SUMO_1$-TbEb1 plasmid. However, ampicillin [100µg/ml, final concentration] was used for selection and recombinant protein expression was induced for 4h.

4.3 Molecular biology methods

4.3.1 Isolation of nucleic acids

4.3.1.1 Isolation of high molecular weight genomic DNA from *T. brucei*

The procedure was performed following a protocol obtained by G. Cross, Rockefeller University. 50ml of a late-log phase trypanosome culture (449) were harvested by centrifugation for 10min

at 3,000g. The supernatant was removed and cells resuspended in 10ml cold extraction buffer. The suspension was incubated at 37°C for 1h, continuously rotating in a hybridization oven (Hybaid Mini Oven, MWG Biotech, Ebersberg). Afterwards, proteinase K was added to a final concentration of 100µg/ml and the suspension incubated at 50°C for 3h. The suspension was cooled to room temperature, an equal volume of TE-saturated phenol was added, and slowly rotated at 15rpm (ELMI Intelli Mixer RM-2L, Progen Scientific Ltd, London, UK) for 10min. Phases were separated by centrifugation for 15min at 3,000g. The upper phase was discarded and the phenol extraction step repeated twice. 0.2 volumes of a 10M ammonium acetate solution as well as 2 volumes of 100% ethanol were added to the aqueous phase and mixed carefully. Precipitated genomic DNA was collected with a glass rod, washed with 5ml of 70% ethanol for 1-2min, and air-dried. Finally, 0.5ml of TE buffer were added. Genomic DNA was stored at 4°C.

4.3.1.2 Isolation of small amounts of genomic DNA from *T. brucei*

The method is adapted from Medina-Acosta & Cross (1993). 1.5ml of a trypanosomal culture at middle-log phase was centrifuged for 2min at 1,500g. The supernatant was discarded, the pellet resuspended in PBS, and again centrifuged for 1.5min at 1,500g. The pellet was mixed with 100µl TELT buffer (see 4.1.5) and incubated at room temperature for 5min. The same amount of a 1:1 phenol (pH 8.0) - chloroform solution was added. Phases were separated by centrifugation at 20,000g for 5min. To precipitate DNA, the upper phase was mixed with 200µl 100% ethanol and incubated at room temperature for 5min. Centrifugation was performed as before, the supernatant discarded and the DNA washed with 500µl of 70% ethanol. After a further centrifugation step, the ethanol was removed, DNA air-dried, and finally solved in 50µl TE buffer supplemented with 0.1µg/ml RNAse. Extracted DNA was either stored at 4°C or at -20°C.

4.3.1.3 Isolation of small amounts of plasmid DNA from *E. coli* ("Mini-Preparation")

The preparation follows the protocol of alkaline lysis mini-plasmid preparation (Birnboim & Doly, 1979). Single colonies were collected from agar plates after bacterial transformation and inoculated in 2ml LB medium supplemented with the appropriate antibiotic. Cultures were grown for a minimum of 8h at 37°C on a shaking platform at 140rpm. 1.5ml of the bacterial suspension were collected and pelleted. The pellet was dissolved in 150µl ice-cold GTE-buffer (see 4.1.5) supplemented with 100µg/ml RNase. To lyse bacteria, 200µl of 0.2N NaOH/1% SDS were added. The suspension was incubated for 5min on ice, then 150µl of a 3M potassium

acetate solution, pH 4.8, were added and samples again incubated on ice for 5min. Samples were centrifuged at 20,000g for 5min. Afterwards, up to 450µl of solution were transferred to a new micro-centrifuge tube. 2 volumes of 100% ethanol were added, samples mixed by inversion, and centrifuged at 20,000g for 15min. The supernatant was discarded and precipitated DNA washed with 0.2ml 70% ethanol. The DNA pellet was air-dried and finally resuspended in up to 50µl TE buffer (see 4.1.5). 5µl of DNA solution were analyzed via restriction digestion to screen for *E. coli* clones harboring the vector with the appropriate insert.

4.3.1.4 Isolation of high amounts of plasmid DNA from *E. coli*

50ml of LB medium supplemented with the respective antibiotic were inoculated with 1 bacterial colony and incubated over night at 37°C on a shaking platform at 180rpm. The bacterial suspension was pelleted by centrifugation at 3,000g for 10min. The pellet was further processed as recommended by the manufacturer (Qiagen Plasmid Plus Midi Kit, Qiagen, Venlo, Netherlands). Plasmid DNA was eluted from the column with 200µl elution buffer. 0.5-1.0 µg DNA were analyzed by restriction digestion.

4.3.1.5 Isolation of RNA from *T. brucei*

1.5ml of a trypanosomal culture at middle-log phase were harvested and RNA was isolated following the instructions of the manufacturer´s manual (Qiagen RNeasy Mini Kit). RNA was eluted in 40µl of dH_2O (RNase-free). Samples were stored at -20°C or at -80°C for longer time periods.

4.3.1.6 Determination of nucleic acid concentration in solutions

For determination of DNA or RNA concentrations, the absorbance at a wavelength of 260nm (OD_{260}) was measured using a ND-1000 Spectrophotometer (Peqlab, Erlangen). The buffer, in which the DNA was solved, was used to obtain a blank value. An OD_{260}value of 1 corresponds to 50µg/ml dsDNA or 40µg/ml RNA, respectively.

4.3.2 PCR techniques

4.3.2.1 Polymerase chain reaction (PCR) using genomic DNA as template

The method was either used to amplify a certain DNA-sequence for subsequent cloning (preparative approach) or to verify knockout mutants (analytical approach). All PCR approaches were performed with *Phusion* polymerase (2U/µl, Finnzymes, Espoo, Finland) except amplification of sequences used for RNAi and gene knock out, which was done with *Taq* polymerase (5U/µl,

Table 4.9: PCR cycle protocol for *Phusion* polymerase

Step	Temperature, time	Number of cycles
Initial denaturation	98°C, 60s	1
Denaturation	98°C, 30s	30-40
Annealing	55°C, 30s	
Elongation	72°C, 1kbp/30s	
Final elongation	72°C, 5min	1
Final hold	4°C, ∞	1

Table 4.10: PCR cycle protocol for *Taq* polymerase

Step	Temperature, time	Number of cycles
Initial denaturation	95°C, 60s	1
Denaturation	95°C, 30s	30-40
Annealing	55°C, 30s	
Elongation	68°C, 1kbp/ 60s	
Final elongation	68°C, 10min	1
Final hold	4°C, ∞	1

NEB). PCR reactions were performed in a volume of 50µl, which was supplemented with the appropriate buffer, 2µl of deoxyribonucleotide mix (each 10mM, Fermentas), 1µl of each forward and reverse oligonucleotide primer (each 10µM), and 0.3µl of DNA polymerase. As template, they contained either 1µl of a high genomic DNA solution (50ng/µl, 449) or 1µl of DNA solutions (1:10 diluted in dH_2O; analysis of single knockout cell lines). For each DNA polymerases, an individual PCR approaches was established based on the manufacturers manuals (Tab. 4.9 and Tab. 4.10). The elongation period was adapted to the length of the amplified gene sequence. PCR cycles were carried out in a temperature cycler (MyCycler Thermal Cycler System, Biorad). Samples were checked by agarose gel electrophoresis and stored at 4°C or -20°C.

4.3.2.2 RT-PCR (Reverse transcription PCR)

1µl of total RNA solution was reverse-transcribed to complementary DNA (cDNA) in a volume of 20µl using an RT-PCR Kit (RevertAid First Strand cDNA synthesis kit, Thermo Fisher Scientific). The reaction mix was composed of 4µl 5x reaction buffer, 1µl random hexamers (0.2µg/µl), 2µl deoxynucleotide mix (each 10mM), 1µl RiboLock RNase Inhibitor (20U/µl) and 1µl of reverse transcriptase (200U/µl). To control that genomic DNA was eliminated sufficiently during the RNA isolation process, a reaction lacking reverse transcriptase was included for each sample (Klaster, 2013). RT-PCR cycles were carried out in a temperature cycler (MyCycler Thermal Cycler System, Biorad). The program is denoted in Tab. 4.11. cDNA samples were

Table 4.11: PCR cycle protocol for RT-PCR

Step	Temperature, time	Number of cycles
RT	25°C, 5min	1
RT	42°C, 60min	1
RT	70°C, 5min	1
Final hold	4°C, ∞	1

Table 4.12: PCR cycle protocol for qPCR

Step	Temperature, time	Number of cycles
Initial denaturation	95°C, 10min	1
Denaturation	95°C, 10min	40
Annealing	60°C, 30s	
Elongation	72°C, 1min	
Dissociation	95°C, 15s	1
	60°C, 20s	1
	95°C, 15s	1

stored at -20°C.

4.3.2.3 Real-time qPCR (RT-qPCR)

To quantify the relative knockdown of a gene of interest in RNAi cell lines, qPCR analysis in 48 well-format on a Step One real time PCR system (Applied Biosystems/ Life Technologies) was performed. The procedure follows the protocol described by Klaster (2013). qPCR reactions were carried out in a final volume of 20µl. The reaction mix contained 10µl of SYBR GreenI (SYBR Green/ ROX qPCR Mastermix, Thermo Fisher Scientific), 0.6µl of forward and reverse oligonucleotides (each 10µM), and 1µl of transcribed RT-PCR sample. The oligonucleotides used for qPCR analysis were the same as used for generation of RNAi plasmids. Due to the length of the amplicons (>200bp) an elongation step was included as indicated in the protocol (Tab. 4.12).

The included fluorescence dye SYBR GreenI intercalates with double-strand DNA after each cycle and the amount of PCR product can be determined. The obtained value is compared to a threshold, which is defined by the time point when the signal intensity exceeds the background noise for the first time. That value is referred to as C_T (threshold cycle) and decreases if high amounts of cDNA are present. The C_T value is in general defined within the log phase. Furthermore, as the amplification efficiency depends on used oligonucleotides and template, a standard curve was included using the RNAi oligonucleotides and the RNAi plasmid with the corresponding gene sequence as template. The amplification efficiency is represented by the

slope of the linear regression, which is 100% if equal to -3.32. The fluorescent dye associates with all kind of double-stranded DNA independently of sequence. Hence, a differentiation between product and unspecific side products is not possible. Therefore, after all qPCR runs, a melt curve was established. With increasing temperature, the dsDNA separates and the dye is liberated. Depending on several factors such as amplicon length or GC content, each product has a specific melting point (T_m) and thereby, the nature of qPCR amplicons can be verified (Raymaekers *et al.* , 2009) .

All analyses were relative quantifications. RNAi samples were calculated with the $\Delta\Delta C_T$-method, which delivers the fold change in gene expression after normalization to an endogenous house keeping (reference) gene and calibration to an untreated control (Livak & Schmittgen, 2001; Schmittgen & Livak, 2008). To normalize obtained values by RT-qPCR, amplification of a part of the TERT (telomerase reverse transcriptase) gene was used as a reference (Brenndörfer & Boshart, 2010). Non-induced and induced samples of RNAi cell lines were compared to the corresponding wild type cell line, which was set as untreated control ("calibrator"). For the calibrator, $\Delta\Delta C_T$ is set as 0, thereby the solution of the equation $2^{-\Delta\Delta C_T}$ is 1. Hence, in wild type cell lines the mRNA levels of the gene of interest are presented as 100%. To obtain the fold change relative to the wild type, the following equation is solved:

$2^{-\Delta\Delta C_T}$= [C_T gene of interest - C_T TERT]$_A$ - [C_T gene of interest - C_T TERT]$_B$

If non-induced and induced samples are set in relation to the wild type, they represent A, the wild type then represents B. If the induced sample is set in relation to the non-induced sample, it represents A while the non-induced sample is stated as B.

Calculation of n-fold expression of wild type bloodstream and procyclic cell lines relative to reference gene was performed similarly. However, here only the ΔC_Tvalues were calculated to determine relative mRNA levels of wild type cell lines as there are only untreated control samples. The formula to calculate n-fold expression levels was modified as stated below.

ΔC_T= C_T gene of interest - C_T TERT

$2^{-(\Delta C_T)}$ = n-fold expression level relative to reference gene

(see also www6.appliedbiosystems.com/support/tutorials/pdf/performing_rq_gene_exp_rtpcr.pdf; www.sigmaaldrich.com/content/dam/sigma-aldrich/docs/Sigma/General_Information/qpcr_technical_guide.pdf)

4.3.2.4 Generation of A-overhang by PCR

The pGEM® T-easy vector is a linearized vector and has T-sticky ends. Therefore, to insert DNA sequences A-overhangs were added to them by PCR. PCR reactions at a final volume of 10µl were supplemented with 1µl of the appropriate buffer, 1µl of 10mM ATP, 1µl of taq polymerase,

and 5µl of purified PCR product. Samples were incubated at 72°C for 10min in a temperature cycler (MyCycler Thermal Cycler System, BioRad). They were stored at 4°C.

4.3.3 Agarose gel electrophoresis

For preparative or analytical analysis, agarose gels contained 1-2% (w/v) agarose in 1x TAE buffer and were placed in an electrophoresis tank filled with 1x TAE buffer (see 4.1.5). DNA samples were mixed with 6x DNA loading dye (see 4.1.5), loaded onto the gel, and electrophoretically separated at 80-120V for 30-45min. Afterwards, agarose gels were stained with ethidium bromide (0.5µg/ml final concentration) to visualize DNA fragments under a UV transilluminator (324nm). 5µl of standard DNA size marker, Spp1 (High molecular weight marker; 100ng/µl ; K. Angermann) and pJH3468 (low molecular weight marker; 50ng/µl; K. Angermann), were used to estimate the size and amount of DNA fragments.

4.3.4 Purification of PCR products

DNA fragments were purified from PCR reactions before restriction digestion. 45-90µl of PCR reaction mix were purified according to the manufacturers protocol (NucleoSpin Gel and PCR Clean up, Macherey and Nagel, Düren) and analyzed by agarose gel electrophoresis (see 4.3.3).

4.3.5 Restriction digestion of DNA

Digestion reaction were set up according to the manufacturer´s protocol (NEB or Fermentas) and standard protocols (Sambrook & Russel, 2001). 5µl of DNA solution obtained by mini preparation or up to 1µg of vector DNA were mixed with 2-10 units of the respective restriction enzyme(s). Corresponding reaction buffers were adjusted to a final concentration of 1x or 2x. Reactions were incubated for at least 1h at the recommended temperature. Afterwards, the reactions were stopped by addition of DNA loading buffer.

4.3.6 Linearization of plasmid DNA for transfection of trypanosomes

To linearize 30µg of plasmid DNA, 2µl of the respective restriction enzyme was added. The appropriate buffer was adjusted to a final concentration of 1x and the mixture incubated at 37°C for at least 12h. The next day, the suspension was mixed with 2 volumes of ice-cold, absolute ethanol and 1/10 volume of 3M sodium acetate solution, pH 5.2, followed by a centrifugation step at 20,000g and room temperature for 10min. The supernatant was discarded and the pellet washed with 500µl 70% ethanol followed by a centrifugation step at 20,000g and room temperature for 10min. All following steps were carried out under a laminar air flow. The supernatant

was discarded and DNA pellets air-dried for 15min. Finally, DNA was resuspended in 50µl of sterile distilled water. To control for proper linearization, 2µl of DNA solution was analyzed by agarose gel electrophoresis (see 4.3.3). DNA solutions were stored at 4°C.

4.3.7 DNA extraction from agarose gels

If necessary, agarose gel pieces containing single DNA fragments were excised after gel electrophoresis using X-Tracta Generation II (Biozym Scientific GmbH, Oldendorf). DNA extraction from agarose gels was performed according to the manufacturer´s manual (NucleoSpin Gel und PCR Clean up, Macherey und Nagel, Düren). DNA was eluted in 30µl elution buffer as supplied by the manufacturer.

4.3.8 Ligation of DNA fragments

Restriction digested DNA fragments and vectors were ligated in a molar ratio of 2.5:1. 1µl of T4 DNA Ligase (Fermentas) and the appropriate ligation buffer were added to the DNA solution to obtain a final volume of 10µl. Ligation reaction was incubated at room temperature for 2h or at 18°C overnight. The obtained ligation mixture was used for transformation of *E. coli*.

If the pGEM® T-easy vector system was used, the procedure was performed according to the manufacturer´s protocol (Promega). 10µl of reaction mix were supplemented with 5µl of 2x rapid ligation buffer, 1µl of pGEM® T-easy vector, 1µl of T4 ligase, and 3µl of A-overhang PCR product. The ligation mixture was incubated at 4ºC for 16h prior to transformation of *E. coli*.

4.3.9 Site-directed mutagenesis of DNA

The pHD1800 plasmid was modified by site-directed mutagenesis to remove a PaeI restriction site that was not compatible with the cloning strategy. PCR reactions were set up using single mismatch oligonucleotides as primer (Tab. 4.6) and *PfuUltra* HF DNA polymerase. Thereby, a mutated plasmid containing staggered nicks is produced. Afterwards, the parental template is digested by DpnI because it is methylated and hemimethylated. The obtained mutated vector was amplified by transformation in *E. coli* XL1 blue. The procedure was performed according to the manufacturer´s protocol (QuikChange II XL Site-directed mutagenesis kit, Agilent technologies, Böblingen).

4.3.10 DNA sequencing

0.5µg plasmid DNA were supplemented with 20pmol sequencing oligonucleotid to obtain a final volume of 10µl. Sequencing services were performed by Macrogen (Macrogen Europe,

Amsterdam, the Netherlands).

4.4 Protein biochemical methods

4.4.1 Preparation of trypanosomes for SDS-PAGE

At least 30x10^6 PCF or BSF trypanosomes were harvested by centrifugation at 20,000g for 30s. For whole cell extracts, trypanosomes were washed once in PBS. The supernatant was discarded and the cell pellet dissolved in 50µl of 1x SDS-PAGE loading dye (see 4.1.5) and heated at 99°C for 5min. For SDS-PAGE, 10µl of the solution were loaded per lane.

To analyze sub-cellular distribution of endogenous and fusion proteins, trypanosomal pellets obtained by centrifugation were washed once in PM buffer (see 4.1.5). The cell pellet was resuspended in PM buffer supplemented with 1% (v/v) NP-40 and incubated for 2min on ice. Cell lysates were separated in pellet and supernatant fractions by centrifugation at 20,000g and 4°C for 1min. Supernatants were concentrated by methanol-chloroform precipitation (see 4.4.2) and resulting pellets resuspended in 1x SDS-PAGE loading dye. The pellet fraction was washed 3-6 times with 1% NP-40 containing PM-buffer prior to resuspension in 1x SDS-PAGE loading dye. Pellet and supernatant fractions were heated at 99°C for 5min and 10µl suspension loaded per lane.

4.4.2 Methanol-chloroform precipitation

Protein solutions were supplemented with 4 volumes of methanol and 1 volume of chloroform. After excessive shaking, 3 volumes of distilled water were added. Samples were mixed and centrifuged at 20,000g for 1min. The supernatant was discarded and 3 volumes of methanol added. Samples were mixed and centrifuged at 20,000g for 1min. The remaining liquid was discarded and precipitates were air-dried for several minutes at room temperature. Subsequently, 1x SDS loading dye was added and samples were heated for 10min at 99°C.

4.4.3 Denaturing SDS polyacrylamide gel electrophoresis (SDS-PAGE)

To separate protein samples by molecular weight a discontinuous gel electrophoresis was performed as described by Laemmli (1970). If samples were cell pellets, they were mixed with 1x SDS-PAGE loading dye (Laemmli buffer), otherwise 2x SDS-PAGE loading dye was used. Afterwards, samples were heated at 99°C for 10min prior to loading onto SDS polyacrylamide gels. SDS gels were composed of a separating gel (10% polyacrylamide) and a stacking gel (4% polyacrylamide) (see 4.1.5). Samples run at 130V for about 2h in a wet chamber containing 1x SDS PAGE running buffer (see 4.1.5). Sample molecular weight was estimated by comparison

with PageRuler Pre-stained Protein Ladder (ThermoScientific) or PageRuler Unstained Protein Ladder (ThermoScientific).

4.4.4 Staining of SDS gels with Coomassie

Coomassie stained SDS gels were used as loading control of immuno blots or to monitor protein purification from *E. coli*. SDS gels were incubated in Coomassie Staining solution for 10min at room temperature after SDS-PAGE on a shaking platform. To remove excessive staining, SDS gels were incubated several hours in Coomassie Destaining solution (see 4.1.5)

4.4.5 Transfer of proteins on nitrocellulose or PVDF membranes

Separated proteins of SDS-PAGE were transferred on a nitrocellulose or PVDF (polyvinylidene fluoride) membrane using the tank blot method (Towbin *et al.* , 1979; Gültekin & Heermann, 1988). PVDF membranes were incubated with pure methanol for 15min. Afterwards, tap water was added gradually to equilibrate the membrane to the methanol concentration of the blotting buffer. Blotting on PVDF membranes was performed at 250mA for 2h, on nitrocellulose membranes at 100V for 1h using 1x Western blot transfer buffer (see 4.1.5).

4.4.6 Staining of immuno blot membranes with Ponceau S

To monitor protein transfer, immuno blot membranes were incubated with Ponceau S (see 4.1.5) for 3min at room temperature. Excessive Ponceau S staining was removed by several washes of the membrane with tap water. Ponceau S stained membranes were also used as loading controls for immuno blots.

4.4.7 Immuno blotting

All incubation steps were performed on a shaking platform. Membranes were incubated two times in blocking buffer (see 4.1.5) for 15min at room temperature to block unspecific binding, followed by an incubation step with primary antibodies for 1h at room temperature. Subsequently, the membrane was washed 3 times with PBST (see 4.1.5) for 10min. A 1h incubation step with the appropriate HRP-labeled secondary antibody followed. Primary and secondary antibodies were diluted in blocking buffer with the dilution factor indicated in Tab. 4.2 and Tab. 4.3, respectively. Subsequently, the membrane was washed 3 times with PBST for 10min, followed by a final wash in PBS for 5min. The membrane was placed in a transparent bag. The secondary antibody was visualized enzymatically by adding 'HRP juice component A and B' (Pjk, Kleinblittersdorf) or 'Lumigen TMA-6 solution A and B' (Lumigen, Southfield, MI, USA)

according to the manufacturer´s manual to the membrane. The chemiluminescent signal was recorded with an LAS-4000 detection system.

4.4.8 Immunoprecipitation (IP) using the mouse monoclonal anti-TbEB1 antibody

All buffers, centrifuges, and samples were cooled during the procedure and RIPA buffer (see 4.1.5) was supplemented with protease inhibitor cocktail (Complete^{TM}, EDTA-free protease inhibitor cocktail, Roche). Expression of TbEB1$^{C\text{-}2xmyc}$in the procyclic cell line TbEB1myc was induced for 24h by supplementation of the medium with 1µg/ml doxycycline, a non-induced sample was taken as control. For input, controls, and IP-experiment, 30*10^6 trypanosomes were harvested by centrifugation at 4,000g for 1min and washed once with PBS.

For pre-experiments, whole cell extracts (input) were prepared as described in 4.4.1. To elevate free TbEB1$^{C\text{-}2xmyc}$ levels for IP, trypanosomes were resuspended in a) PM buffer supplemented with 1% (v/v) NP-40, b) PM buffer supplemented with 1% (v/v) NP-40 and 300mM NaCl, c) RIPA buffer, and d) RIPA buffer supplemented with 1% (w/v) SDS. All samples were incubated on ice for 5min. Cell lysates were separated in pellet (P) and supernatant fractions (S) by centrifugation at 20,000g and 4°C for 1min. Pellets were washed six times with the corresponding buffer prior to resuspension in 1x SDS-PAGE loading dye. Supernatants were methanol-chloroform precipitated (see 4.4.2) followed by resuspension in 1x SDS-PAGE loading dye.

For the IP experiment, the cell pellet was resuspended in RIPA buffer and incubated on ice for 5min. The suspension was centrifuged at 20,000g and 4°C for 5min. The obtained pellet was washed 6 times with RIPA buffer prior to resuspension in 1x SDS-PAGE loading dye. 50µl of anti-TbEB1antibody (ammonium sulfate precipitated hybridoma cell culture supernatant, see 4.6.10) were added to the resulting cell lysate supernatant and incubated on a rotator for 1 hour at 4°C. 10µl Protein L beads (kindly provided by M. Hermann) were equilibrated by washing three times with RIPA buffer at 300g and 4°C for 2min. Subsequently, beads were added to the supernatant and incubated for another 1h at 4°C on a rotating mixer. Beads were harvested by centrifugation at 300g and 4°C for 1min. The supernatant (IP S) was concentrated by methanol-chloroform precipitation (see 4.4.2) and resuspended in 1x SDS-PAGE loading dye. Beads (IP P) were mixed with an equal volume of 2x SDS-PAGE loading dye. The input sample (input) was prepared as described for whole cell extracts (see 4.4.1). To visualize the amount of cytoplasmic TbEB1$^{C\text{-}2xmyc}$ available for binding by anti-TbEB1 antibody, trypanosomes were resuspended in RIPA-buffer and incubated on ice for 5min. Subsequent centrifugation at 20,000g and 4°C for 1min resulted in a pellet and a supernatant fraction, which contained free TbEB1$^{C\text{-}2xmyc}$. The pellet (Control RIPA P) was washed 6 times with RIPA buffer then resuspended in 1x SDS-PAGE

loading dye. The supernatant (Control RIPA S) was precipitated with methanol-chloroform (see 4.4.2) prior to resuspension in 1x SDS-PAGE loading dye.

4.4.9 His-tag purification of TbEB1 for mouse polyclonal antibody generation under native conditions

All buffers, samples, and centrifuges were cooled. Equilibration of His-Pur^{TM} Ni-NTA resin beads (ThermoScientific) was performed by washing three times with a 10-fold volume of native lysis buffer at 300g and 4°C for 2min. pTrcC-His$_6$-TbEB1 and pTrcC-His$_6$-TbEB1sh were expressed bacterially and cell pellets collected as described in section 4.2.5. 10ml of native lysis buffer (see 4.1.5) were added per 1g of bacterial pellet. Additionally the suspension was supplemented with 0.2mM PMSF (final concentration), lysozyme, and protease inhibitor cocktail for purification of histidine-tagged proteins (Sigma-Aldrich). The suspension was chilled while stirring in a beaker for 30min prior to cell disruption using a high pressure homogenizer (EmulsiFlex-C5, Avestine Europe GmbH, Mannheim) for 20min and ice-cooling. Bacterial lysates were centrifuged at 15,000g and 4°C for 20min. Supernatants were collected, mixed with previously equilibrated His-Pur^{TM} Ni-NTA resin beads (ThermoFisher), and incubated on a rotating mixer (ELMI Intelli Mixer RM-2L, Progen Scientific Ltd, London, UK) at 30rpm and 4°C for 1h. Beads were harvested by centrifugation at 300g and 4°C for 2min. The supernatant (flow-through) was stored at 4°C for further purification steps. Beads were washed with a 10-fold volume of native lysis buffer. Subsequently, beads were loaded onto a column and the flow-through (FT) was collected. Proteins were eluted in 2ml native elution buffer (see 4.1.5) and collected in 100µl fractions. Samples were stored at -20°C.

Protein expression and purification was analyzed on Coomassie stained SDS polyacrylamide gels and immuno blots (see 4.4.4, 4.4.7). Samples referred to as b.I. (before induction) and a.I. (after induction) were normalized by their OD_{200}value. Samples taken after cell disruption are referred to as P^L (pellet after bacterial lysis) and S^L (supernatant after bacterial lysis) and normalized to 0.04% of volume. Samples drawn from flow-through (FT) and wash (W) were also normed to 0.04% of volume. 1/10 -1/20 volume of elution fractions were loaded onto gels.

4.4.10 His-tag purification of TbEB1 for mouse monoclonal antibody generation under denaturing conditions

If the antigen purification was performed under denaturing conditions, all steps were performed at room temperature if not stated otherwise. Expression and purification of pET28-SUMO$_1$-TbEb1 was performed as described by Spindler (2014). In brief, bacteria were harvested at

3,300g and 4°C for 20min. The obtained pellet was directly dissolved in guanidinium chloride lysis buffer (see 4.1.5) followed by stirring in a beaker at room temperature for 30min. Subsequently, bacterial cells were homogenized (EmulsiFlex-C5, Avestine Europe GmbH, Mannheim) and centrifuged at 25,000g for 15min. The supernatant was mixed with previously equilibrated His-Pur^{TM} Ni-NTA resin beads (see 4.4.9) and incubated on a rotating mixer at 30rpm (ELMI Intelli Mixer RM-2L, Progen Scientific Ltd, London, UK) for 1h at room temperature. Beads were harvested by centrifugation at 300g and 4°C for 2min followed by a wash with a 10-fold volume of guanidinium chloride lysis buffer. Proteins bound to the beads were eluted with a final volume of 2ml guanidinium chloride elution buffer (see 4.1.5) and collected in 100µl fractions. Elution fractions were dialyzed against PBS at 4°C over night using visking dialysis tubes with a molecular weight cut off value of 12 - 14 kDa (Medicell International Ltd, London, UK).

His-tagged TbEB1 for the second round of monoclonal antibody generation was provided by M. Spindler and X. Chelius.

4.5 Cell culture

All media, buffer, flasks, and vessels were sterilized either by filtration or autoclaving. Cells were handled in sterile conditions using a laminar air flow (Scanlaf Mars Safety Class 2, Weiss Labortechnik GmbH, Heroldsberg).

4.5.1 Trypanosomal cell lines

4.5.1.1 Cultivation of procyclic trypanosoma cell lines

Procyclic cell lines 427, 449, 29-13, and their derivatives were kept in air incubation at 27°C and cultures diluted into fresh media three times a week with a split ratio of 1:20 - 1:50. Cells were cultivated in SDM-79 medium (PAA, Pasching, Austria) supplemented with 2g/l $NaHCO_3$, 10% (v/v) heat-inactivated (56°C, 30min) fetal calf sera (Sigma-Aldrich), and 7.5mg/ml hemin (Brun

Table 4.13: Final concentrations of antibiotics used for maintenance and selection of procyclic trypanosomes. BLE = bleomycin D1, BSD = blasticidin S, HYG = hygromycin B, NEO = neomycin / G418, PU = puromycin

Antibiotic	Concentration
BLE	0.5-5µg/ml
BSD	10-50µg/ml
HYG	50µg/ml
NEO	15µg/ml
PU	1µg/ml

Table 4.14: Basic procyclic trypanosomal strains and their derivates used in this work, their application, and their culture media. BLE = bleomycin D1, HYG = hygromycin B, NEO = neomycin / G418

Cell line	Antibiotic/s	Application
427	none	endogenous tagging, gene knockout
449	BLE	over-expression, RNAi
29-13	HYG, NEO	RNAi, endogenous tagging

Table 4.15: Cell lines derived from strain 427, antibiotics for selection, and their application.

Cell line	Antibiotic/s	Application
427 EB1pMOT$^{C\text{-}3xmyc}$	HYG	C-terminal endogenous tagging
427 TbEB1 so	PU	single allele knockout

& Schönenberger, 1979) referred to as SDM-79. The basic procyclic cell line 427 was kept in standard medium SDM-79. Cell line 449 harbors an ectopic TETrepressor gene in its genome therefore, bleomycin is necessary for maintenance (Tab. 4.13) (Biebinger *et al.* , 1997). Cell line 29-13 contains the ectopic TETrepressor gene as well as the gene for the T7 RNA polymerase and was kept in SDM-79 supplemented with neomycin and hygromycin (Tab. 4.13) (Wirtz *et al.* , 1999). Additionally, applications of procyclic host cell lines are indicated in table 4.14. Depending on the host strain and introduced plasmid, derivative cell lines were supplemented with antibiotics as indicated in tables 4.15 - 4.17.

4.5.1.2 Cultivation of bloodstream trypanosoma cell lines

Bloodstream cell line S16 and its derivatives were kept at 37°C in a 5% CO_2 humid atmosphere. Cells were split in a ratio of 1:50 - 1:100 three times a week. BSF were cultivated in HMI-9 medium (PAA) supplemented with 10% (v/v) heat-inactivated (56°C, 30min) fetal calf serum (Sigma-Aldrich), 5% (v/v) serum plus (Sigma-Aldrich), and 0.0014% (v/v) 2-mercaptoethanol (Hirumi & Hirumi, 1989) referred to as HMI-9. The S16 cell line stably expresses the TETre-

Table 4.16: Cell lines derived from strain 449, antibiotics for selection, and their application.

Cell line	Antibiotic/s	Application
449 pNAT$^{C\text{-}12xmyc}$	BLE, BSD	C-terminal endogenous tagging
449 TbEB1i	BLE, PU	RNAi
449 TbEB1i pNAT$^{C\text{-}12xmyc}$	BLE, PU, BSD	C-terminal endogenous tagging, RNAi
TbEB1myc	BLE, HYG	over-expression

Table 4.17: Cell lines derived from strain 29-13, antibiotics for selection, and their application.

Cell line	Antibiotic/s	Application
29-13 EB1pNAT$^{N\text{-}6xmyc}$	HYG, NEO, BSD	N-terminal endogenous tagging
29-13 pNAT$^{C\text{-}12xmyc}$	HYG, NEO, BSD	C-terminal endogenous tagging
29-13 TbEB1i	HYG, NEO, PU	RNAi
29-13 TbEB1i pNAT$^{C\text{-}12xmyc}$	HYG, NEO, PU, BSD	C-terminal endogenous tagging, RNAi

Table 4.18: Cell lines derived from strain S16, antibiotics for selection, and their application.

Cell line	Antibiotic/s	Application
S16 EB1pNAT$^{N\text{-}6xmyc}$	NEO, BSD	N-terminal endogenous tagging
S16 EB1pMOT$^{C\text{-}3xmyc}$	HYG	C-terminal endogenous tagging
S16 pNAT$^{C\text{-}12xmyc}$	NEO, BSD	C-terminal endogenous tagging
S16 TbEB1 so	NEO, PU	single allele knockout
TbEB1myc	NEO, HYG	over-expression

pressor and the T7 RNA polymerase under control of the single marker neomycin (2.5µg/ml) (Wirtz *et al.* , 1999). The S16 cell lines was used for N- and C-terminal tagging, RNAi experiments, single allele knockout, and over-expression. Depending on the introduced plasmid, derivatives were maintained with antibiotics as indicated in table 4.18. Final concentrations of antibiotics are indicated in table 4.19.

4.5.1.3 Cryopreservation of trypanosomal cell lines and resuscitation

All solutions and equipment were at room temperature prior to freezing. Antibiotic-free standard medium for procyclic or bloodstream trypanosomes was supplemented with 7% (v/v) glycerol (freezing medium). 10-20ml of a mid-log phase culture were centrifuged at 500g for 5min,

Table 4.19: Final concentrations of antibiotics used for maintenance and selection of bloodstream trypanosomes. BLE = bleomycin D1, BSD = blasticidin S, HYG = hygromycin B, NEO = neomycin / G418, PU = puromycin

Antibiotic	Concentration
BLE	2.5µg/ml
BSD	10µg/ml
HYG	2.5µg/ml
NEO	2.5µg/ml
PU	0.5µg/ml

the pellet resuspended in 2ml respective freezing medium, and distributed to three cryo tubes (Nunc CryoTubes, Sigma-Aldrich). Cryotubes were frozen at -80°C using a Nalgene® Frosty™ Cryo 1°C freezing container (Sigma-Aldrich). The container allows a continues decrease of temperature at a rate of 1°C per minute. After a minimum of 3h at -80°C, cells were transferred into the liquid nitrogen tank for long-term storage.

To enable a fast resuscitation, vials were thawed in a water bath at 37°C for a few minutes and immediately transferred into culture flasks containing pre-warmed medium.

4.5.1.4 Determination of cell density and growth curves

To determine cell density, 12.5µl of cell suspension were added to 5ml CASYton solution prior to measurement using a CASY® cell counter (Schärfe System, Reutlingen). The device evaluates cell density by resistance measurement combined with pulse area analysis and determines viable and whole cell numbers.

For growth curves of PCF and BSF, 10^5cells per ml were seeded in 6-well plates containing 5ml of respective culture medium. If cells were induced, culture media were supplemented with 1µg/ml doxycycline. Cells were maintained in log-phase growth by appropriate dilution, which was taken into account in data analysis. For RNAi experiments, procyclic and bloodstream trypanosomes were maintained for 5 days. For ectopic expression experiments, cells were cultivated for 8-10 days. If samples were drawn to determine cell density, wells were mixed properly by pipetting and collected every 24h during the time course.

4.5.1.5 Transfection of trypanosomes

Transfection of bloodstream and procyclic trypanosomes was performed following the instructions published by the Roditi group (Burkard *et al.* , 2007; Schumann Burkard *et al.* , 2011). For transfection, $2*10^7$ procyclic or $6*10^7$ bloodstream trypanosomes were centrifuged at 500g for 5min and the supernatant completely discarded by pipetting. Subsequently, the cell pellet was resuspended in 50µl of DNA solution (see 4.3.6) diluted with an equal volume of 2x transfection buffer (see 4.1.5). The volume of the final suspension should not exceed 108µl. The suspension was transferred into an electroporation cuvette (2mm, VWR, Bruchsal). For the transfection of PCF, the program X-014 on an Amaxa™ Nucleofector™ II (Lonza, Köln) was used. The program was changed to X-001 for BSF. After transfection, the cell suspension was pipetted into 10ml of pre-warmed media if necessary supplemented with antibiotics. To recuperate from transfection, cells were incubated overnight at their optimum temperature. Afterwards, cells were mixed with 40ml of medium supplemented with the appropriate antibiotics for maintenance and selection. From this stock, 50ml of a 1:10 dilution were prepared additionally. Both

cell suspensions were plated on 24-well plates with 1 - 2ml of cell suspension per well. For PCF, 24-well plates were sealed with parafilm. Cells were cultivated at their optimum temperature until cell growth was detectable in single wells. For further analysis, transfectants were transferred to 6-well plates.

4.5.1.6 N-terminal in situ tagging of trypanosomes

For N-terminal tagging of TbEB1, the first 4 - 675bp of the open reading frame (ORF) of TbEB1 without the start codon were amplified from *T. brucei* strain 449 genomic DNA by PCR using the oligonucleotides presented in table 4.7. The PCR product was enzymatically digested with BamHI and AvrII and finally ligated into the vector pNAT_BSD_6Myc_X (Alsford & Horn, 2008). The final construct (pNAT$^{N\text{-}6xmyc}$) was linearized with EcoRV in the ORF region and transfected into 29-13 (PCF) and S16 (BSF) trypanosomes generating the cell lines 29-13 EB1pNAT$^{N\text{-}6xmyc}$ and S16 EB1pNAT$^{N\text{-}6xmyc}$by homologous recombination. Transfectants were selected by medium supplementation with BSD to a final concentration of 10µg/ml. The correct integration of the tagging cassette was verified by immuno blot analysis.

4.5.1.7 C-terminal in situ tagging of trypanosomes

For C-terminal tagging of TbEB1 using the pMOT43M vector (Oberholzer *et al.* , 2006), the last 348bp of the ORF of TbEB1 without the stop codon and 339bp of the corresponding 3´UTR were amplified from *T. brucei* strain 449 genomic DNA by PCR using the oligonucleotides presented in table 4.7. The ORF PCR product was digested with KpnI and XhoI and the 3´UTR PCR product was digested with BamHI and XbaI. Subsequently, both PCR products were ligated into the pMOT43M vector. Prior to transfection, the construct (pMOT$^{C\text{-}3xmyc}$) was digested with KpnI and XbaI resulting in a DNA fragment containing a C-terminally tagged end of the ORF, which was integrated into the trypanosomal genome of 427 (PCF) and S16 (BSF) trypanosomes by homologous recombination. Transfectants were selected by medium supplementation with HYG to a final concentration of 50µg/ml. The correct integration of the tagging cassette was verified by immuno blot analysis. Established cell lines were referred to as 427 EB1 pMOT$^{C\text{-}3xmyc}$ and S16 EB1 pMOT$^{C\text{-}3xmyc}$.

For C-terminal tagging using the pNAT_BSD_X_12Myc vector (Alsford & Horn, 2008), the last 600bp of the ORF of TbEB1, without the stop codon, were amplified from *T. brucei* strain 449 genomic DNA by PCR using the oligonucleotides presented in table 4.7. The PCR product was enzymatically digested with AscI and XbaI and finally ligated into the pNAT_BSD_X_12Myc vector. The final construct (pNAT$^{C\text{-}12xmyc}$) was linearized with HindIII in the ORF region and introduced into 449, 29-13 (PCF) and S16 (BSF) cell lines by homologous recombina-

tion. Established cell lines were referred to as 449 pNAT$^{C\text{-}12xmyc}$, 29-13 pNAT$^{C\text{-}12xmyc}$, and S16 pNAT$^{C\text{-}12xmyc}$. Additionally, the construct was introduced into the TbEB1 RNAi cell lines 449 TbEB1i and 29-13 TbEB1i (both construct1) generating the cell lines 449 TbEB1i pNAT$^{C\text{-}12xmyc}$ and 29-13 TbEB1i pNAT$^{C\text{-}12xmyc}$. Transfectants were selected by medium supplementation with BSD to a final concentration of 50µg/ml for 449 derived cell lines and 10µg/ml for 29-13 and S16 derived cell lines. The correct integration of the tagging cassette was verified by immuno blot analysis.

4.5.1.8 Generation of cell lines ectopically expressing TbEB1 in trypanosomes

The complete ORF of TbEB1 except the stop codon was amplified from *T. brucei* strain 449 genomic DNA by PCR using the oligonucleotides presented in table 4.7. The PCR product was enzymatically digested with AscI and FseI followed by ligation into the pHD1800 vector. The vector is a derivative of pHD1700, which contains the TET operon for inducible expression of the ectopic fusion protein by addition of tetracycline or its analogs. The final construct (TbEB1$^{C\text{-}2xmyc}$) was linearized with NotI in the rDNA spacer region and introduced into 449 (PCF) and S16 (BSF) cell lines by homologous recombination. Transfectants were selected by medium supplementation with HYG to a final concentration of 50µg/ml in PCF and 2.5µg/ml in BSF. The protein was ectopically expressed after medium supplementation with 1µg/ml doxycycline. Established cell lines were referred to as TbEB1myc. The correct integration of the tagging cassette was verified by immuno blot analysis.

4.5.1.9 Generation of RNAi cell lines

Three sequence parts of TbEB1 ORF were identified with trypanoFAN (Redmond *et al.* , 2003). They were between 200 and 400bp long and covered most of TbEB1 DNA sequence. They were referred to as construct 1 (388-767bp), construct 2 (1-333bp), and construct 3 (961-1216bp). Non-homology to other trypanosomal proteins was confirmed by BLAST analysis (Altschul *et al.* , 1990). Constructs 1-3 were cloned into the pALC14 vector in a first round via HindIII and XbaI restriction sites followed by a second cloning round with restriction enzymes BamHI and XhoI. RNA transcribed from those sites forms a stem-loop fragment (Wirtz *et al.* , 1999). Constructs 2 and 3 were additionally introduced in the pZJMß vector via restriction sites XhoI and HindIII. The vector contains a dual promotor system and hence, dsRNA formation happens in the cytoplasm after transcription (Wang *et al.* , 2000). All constructs were linearized with NotI and introduced into the rDNA region of 449 and 29-13 (PCF) and S16 (BSF) cell lines by homologous recombination after transfection. Transfectants were selected by medium supplementation with PU in case of pALC14 vector to a final concentration of 1µg/ml for procyclic

cell lines and 0.5µg/ml for bloodstream cell lines. If the pZJMß vector was used, procyclic trypanosomes were cultivated in the presence of 5µg/ml BLE and bloodstream ones with 2.5µg/ml BLE. Expression of dsRNA was induced by medium supplementation with 1µg/ml doxycycline. The cell morphology of induced and non-induced cultures was compared by light microscopy. Combined with relative TbEB1 mRNA levels determined by qPCR analysis, appropriate clones were identified and one was used for further experiments. Three cell lines containing a pALC14 vector - construct 1 combination were used for experiments in this work. They are referred to as 449 TbEB1 RNAi, 29-13 TbEB1 RNAi, and S16 TbEB1 RNAi.

4.5.1.10 Generation of single gene knockout cell lines

294bp of the 5´UTR sequence and 295bp of 3´UTR sequence of TbEB1 were amplified from 449 genomic DNA by PCR using the oligonucleotides denoted in table 4.7. The ORF sequence for PU was amplified from the vector pEnG0P. The 5´UTR PCR product was enzymatically digested with AscI, the 3´UTR PCR product with FseI. The ORF sequence of PU was digested with AscI and FseI. Subsequently, products were ligated and ligation products loaded onto 1% agarose gels. The band of approximately 1200bp was excised from the gel and an A-overhang added by PCR prior to ligation into pGEM® T-easy for plasmid amplification. Prior to transfection, the insert was excised by Eco RI restriction digest. Subsequently, transfection of 427 (PCF) and S16 (BSF) cell lines was performed. Transfectants were selected by medium supplementation with 1µg/ml PU in case of PCF and 0.5µl/ml in case of BSF. Established cell lines were referred to as 427 TbEB1 so and S16 TbEB1 so. Correct exchange of the TbEB1 allele by the drug resistance cassette via homologous recombination was verified by PCR.

4.5.1.11 Washout experiment

The procyclic cell line TbEB1$^{C\text{-}2xmyc}$ was used for this experiment to analyze the underlying reason for the observed growth retardation. The experiment comprised three phases: 1. induction, wash-out, 2. induction. TbEB1$^{C\text{-}2xmyc}$cells were cultivated in two flasks, whereby in one flask the medium was supplemented with 1µg/ml doxycycline and referred to as 'induced' culture. Both cultures were maintained for 10 days. Afterwards, both cultures were washed three times with SDM-79 by centrifugation at 500g for 5min. The non-induced culture was treated the same way to exclude experimental artifacts. Both cultures were grown without doxycycline for another 9 days. Finally, the culture grown in the presence of doxycycline during the first period was cultivated again in the presence of 1µg/ml of the drug. Both cultures were maintained for 10 further days. During the whole experiment, samples for immunofluorescence and Western blot analysis were drawn. Cell cycle stages of 200 cells were counted from day 9 of the first and

second induction period, respectively.

4.5.2 Mammalian cell lines

4.5.2.1 Cultivation of myeloma and hybridoma cell lines and determination of cell density

The mouse myeloma cell line Ag8x63 was cultivated in Opti-MEM® I (1x) + GlutaMAX™ -I reduced serum medium (Gibco® by Life Technologies, Karlsbad, CA, USA) supplemented with 10% (v/v) heat-inactivated (56°C, 30min) FCS (Biochrom, Berlin). The medium is referred to as complete Opti-MEM. Cells were kept at 37°C in a 5% CO_2 humid atmosphere. Cells were patted off from culture dishes and diluted in a ratio of 1:5 - 1:20 twice a week. Established mouse hybridoma cell lines were cultivated under identical conditions as myeloma cell lines.

To determine cell density, the cell suspension was 1:10 diluted with PBS and cell numbers were determined by the trypan blue exclusion method via a Vi-cell cell viability analyzer (Beckman Coulter, Krefeld).

4.5.2.2 Cultivation of HeLa cell lines and mouse fibroblast cell line

HeLa cells (HeLa K, human cervix adenocarcinoma cell line, sub-clone K), the HeLa RG cell line, and the mouse fibroblast (NIH/ 3T3) cell line were cultivated at 37°C in a 5% CO_2 humid atmosphere. The HeLa RG cell line is stably transfected with tubulin-GFP and histone-mCherry (kindly provided by O. Stemmann). Cells were maintained in Dulbeccos´s Modified Eagle Medium high glucose (DMEM high glucose; PAA, Pasching, Austria) supplemented with 10% (v/v) heat-inactivated (56°C, 30min) FCS (Biochrom, Berlin). It is referred to as DMEM complete. To split mammalian cell lines, the culture medium was removed and replaced by an appropriate amount of 1x trypsin/EDTA (Sigma-Aldrich). Subsequently, culture dishes were incubated for a few minutes at 37°C until cells detached from the surface. The enzyme solution was immediately inactivated by addition of DMEM complete and the cell suspension centrifuged at 200g for 2min. Cell pellets were resuspended in complete medium and transferred to new dishes.

4.5.2.3 Cryopreservation and resuscitation of mammalian cell lines

All solutions and equipment were at room temperature prior to freezing. Myeloma and hybridoma cells were collected by patting them off the dishes, HeLa, Hela RG, and fibroblast cells lines were harvested by trypsinization. Cell suspensions were pelleted by centrifugation at 200g for 2min. The supernatant was discarded and the cell pellet resuspended in cryo medium con-

sisting of 10% (v/v) DMSO in heat-inactivated (56°C, 30min) FCS (Biochrom, Berlin). Cell suspensions were distributed to cryotubes (Nunc CryoTubes, SigmaAldrich). Cryotubes were frozen at -80°C using a Nalgene® Frosty™ Cryo 1°C freezing container (Sigma-Aldrich). After a minimum of 3h at -80°C, cryotubes were transferred into the liquid nitrogen tank for long-term storage.

Cryotubes were thawed rapidly in a 37°C water bath followed by centrifugation at 200g for 2min to remove DMSO containing freezing medium. The supernatants were discarded and pellets resuspended in corresponding culture medium followed by transfer to culture dishes.

4.5.2.4 Transient transfection of HeLa K cell lines

The complete ORF of TbEB1, except the stop codon, was amplified from 449 genomic DNA by PCR using the oligonucleotides denoted in table 4.7. The PCR product was enzymatically digested with FseI and AscI and ligated into the vector pCS2. HeLa K cells were seeded onto 6-Well plates and maintained until 70% confluence was reached for transient transfection based on the polyethylenimine (PEI, Polysciences Inc., Warrington, PA, USA) method. In three wells, 480µl Opti-MEM® I (1x) + GlutaMAX™ -I reduced serum medium (Life Technologies, Karlsbad, CA, USA) were mixed with 7.5µg plasmid DNA, either pCS2 (mock) or TbEB1$^{C\text{-}GFP}$, and incubated at room temperature for 5min. Afterwards, PEI was added to a final concentration of 1mg/ml followed by a second incubation period of 15min. Subsequently, the transfection mixture was distributed to the wells. Cells were incubated for 16-24h. Then, the transfection medium was discarded and new complete medium added. In a first experiment, an asynchronous culture was transfected and samples for immunofluorescence and blot were collected after 24h, 48h, and 72h. In the second set up, the culture was synchronized as described below.

4.5.2.5 Synchronization of mammalian cell lines

As the expression of transgene TbEB1$^{C\text{-}GFP}$ started as soon as the plasmid enters the nucleus, cells were arrested in S-phase with a surplus of thymidine to gain more control about transgene expression (Ma & Poon, 2011). Therefore, thymidine was added to the complete medium in a final concentration of 2mM and cells incubated for 20h. Transient transfection of HeLa cells was carried out after 18h, thus, cells were still under thymidine arrest. Finally, the cells were released from thymidine block by washing the culture twice with PBS and a final addition of complete medium. This marked the 0h time point during the time course experiment. Cells were cultivated for 24h and samples for immunofluorescence and blot collected every 3h.

4.6 Generation of mouse poly- and monoclonal antibodies

4.6.1 Immunization of mice

4.6.1.1 Anti-TbEB1 polyclonal antibodies

For generation of polyclonal antibodies, four fancy mice (*Mus musculus*, Hagebaumarkt, Bayreuth) were used. Two mice, mouse 1 and 2, were immunized with purified TbEB1 full length protein (64kDa), the remaining two, mouse 3 and 4, with the truncated TbEB1 protein (45kDa). In total, a number of three subcutaneous antigen injections into the peritoneum was performed and injection volume did not exceed 150µl per mouse and injection. For each injection, 50µg of TbEB1 full length and 100µg of TbEB1 truncated recombinant protein were used per mouse. For the first injection, Freund´s Complete Adjuvant (CFA, Sigma-Aldrich) was used, which contains mycobacterial components to enhance immune system stimulation. Equal volumes of CFA and antigene were mixed up to 30 times with two syringes and a connector. The obtained water-in-oil emulsion persisted if dropped onto a water surface. For further injections, the CFA was replaced by Freund´s Incomplete Adjuvant (IFA, Sigma-Aldrich), which lacks the mycobacterial components (Leenaars & Hendriksen, 2005). Injections were settled in two-week intervals. First blood sample collection (pre-sera) by tail bleed was done prior to initial immunization, the second one (anti-TbEB1 serum) one week after the second immunization. Third blood sample collection was done one week after the third immunization followed by euthanasia of animals.

Mouse 3 was taken out of the experiment after 3 weeks due to unspecific reactions of the pre-serum in immunofluorescence analysis.

4.6.1.2 Anti-TbEB1 monoclonal antibodies

For generation of monoclonal antibodies, two BALB/c mice (Janvier Labs, Saint-Berthevin Cedex, France) were used for one approach. For the first injections, mice were immunized with 100µg of TbEB1 recombinant protein (purified by M. Spindler and X. Chelius) per mouse. Preparation of antigen emulsion with CFA was done as described (see 4.6.1.1). The second injection was 14 days later with IFA (see 4.6.1.1). As serum samples did not indicate a strong immune response against TbEB1 a week later, a third injection was performed followed by another blood sample collection. Only mouse 2 demonstrated a satisfying immune response and hence, was used when continuing the experiment with a forth injection of antigen one week after the second serum collection by tail bleed. Finally, 50µg of TbEB1 recombinant protein were mixed with IFA (see 4.6.1.1) and subcutaneously injected into the peritoneum four days before euthanasia and collection of spleen lymphocytes.

4.6.2 Test serum collection and analysis

To control if immunization against TbEB1 was successful, blood from the tail vein was taken. To do so, mice were settled under an infrared lamp for several minutes to increase blood circulation. Afterwards, a tiny piece of the tail end was cut with a razor blade, the blood collected in a tube, and lesions covered with spray-on bandage. Obtained samples were left at room temperature for at least 15min to enable clotting. Blood samples were centrifuged at 20,000g for 10min and the serum pipetted into new tubes. Subsequently, 10% NaN_3 (see 4.1.5)was added to a final concentration of 0.02% and sera stored at 4°C. For long-term storage, sera were transferred to -80°C.

In case of polyclonal antibodies, pre-sera and anti-TbEB1 sera were compared in Western blot and immunofluorescence analysis. For Western blots, pre-sera and anti-TbEB1 sera were diluted 1:200 in blocking buffer (see 4.1.5). For immunofluorescence assays, pre-sera and sera were used at dilutions 1:50 and 1:200 in PBST (see 4.1.5).

In case of monoclonal antibodies, sera derived by tail bleed were tested in Western Blot and immunofluorescence assays using identical concentrations as described for polyclonal antibodies. Test serum of mouse 2 was also used to establish the ELISA (see 4.6.3) for screening of hybridoma cells.

4.6.3 Enzyme-linked immunosorbent assay (ELISA)

The technique provides a rapid and easy-applicable tool to screen the huge amount of supernatants derived from hybridoma cells for putative anti-TbEB1 secreting hybridoma cells (Greenfield, 2014). A pre-test using serum of mouse 2 was performed to evaluate the optimal concentration of coated antigen enabling a clearly detectable immune reaction. As the antigen for coating of ELISA plates has to be soluble and recombinant TbEB1 (pET28-$SUMO_1$-TbEb1) is only soluble in presence of guanidinium chloride, dilution of recombinant TbEB1 was performed in guanidinium chloride elution buffer (see 4.1.5). Duplicates of wells of a 96-well plate were coated with a two-fold serial dilution of recombinant TbEB1 from 10µg to 1.25µg. The coating volume per well was 100µl of the corresponding dilution. The plate was sealed and incubated at 37°C for 2h. Afterwards, three washing steps with 200µl PBS per well followed. Subsequently, 250µl BSA-blocking solution (see 4.1.5) was added per well and incubated at 37°C for 30min or at 4°C overnight. The blocking solution was removed and the plate washed three times with PBS. Mouse serum 2 was diluted 1:500 in PBS, 100µl applied per well, and the plate incubated at 37°C for 1h. The plate was washed 3 times with PBS. The secondary antibody, HRP-conjugated anti-mouse IgG, was diluted 1:40.000 in PBS, 50µl per well were added, and the plate was incubated at 37°C for 30min. Subsequently, the plate was washed three

times with PBS and 200µl freshly prepared ELISA substrate solution were added to each well. The plate was incubated in the dark at room temperature until a color change from colorless to yellow occurred. The reaction was stopped by addition of 50µl per well 2.5M sulfuric acid solution. The absorption was measured at 492nm using a fluorescence reader (FLOUstar Omega, BMG Labtech, Ortenberg) and corresponding Omega software. A curve was plotted in Excel to determine the optimal amount of recombinant protein, which was 7.5µg per well.

4.6.4 Conditioned medium derived from macrophages

For selection and sub-cloning of hybridoma cells, medium supplementation with conditioned medium is necessary. Therefore, peritoneal macrophages were collected. A mouse (fancy mouse or BALB/c) was euthanized by cervical dislocation, dipped in 70% ethanol, pinned onto a polystyrene plate under a laminar air flow, and the peritoneal cavity was opened. Subsequently, the abdominal wall was elevated with a forceps and 5ml ice-cold complete Opti-MEM injected. Macrophages were released from tissue by gently massaging the abdomen with a moistened finger for several minutes. A tiny opening is cut into the abdominal wall and the liquid collected with a pipette. The cell suspension was mixed with 40ml of pre-warmed complete Opti-MEM and depending on the purpose, distributed either to two 96-well plates or a 50ml cell culture flask. Macrophages were maintained at 37°C and 5% CO_2 humid atmosphere for at least 2 days. Conditioned medium was either used immediately or stored at -20°C.

4.6.5 Harvesting myeloma cells and conditioned medium for fusion

Prior to fusion, 4-6 cell culture flasks (75cm^2) of Ag8x63 myeloma cells were raised in 50ml complete Opti-MEM per flask until a modest cell density was reached. Cells were centrifuged at 400g for 5min and the supernatants collected and used as conditioned medium for fusion. The pellets were resuspended with 10ml DMEM high glucose each, pooled, and stored at 37°C and 5% CO_2 humid atmosphere. The tube cap was loosened to allow gas exchange.

4.6.6 Isolation of lymphocytes derived from spleen

A mouse was euthanized by cervical dislocation, dipped in 70% ethanol, pinned onto a polystyrene plate under a laminar air flow, and the peritoneal cavity was opened. The abdominal wall was opened and the spleen removed. The spleen was washed once in PBS, then in DMEM high glucose. Afterwards, the spleen was transferred to a petri dish with 10ml fresh DMEM high glucose. Most of the connective tissue was removed, and the spleen was cut in several small pieces, from which the spleen tissue was scraped out with a 90° bent needle. The cell suspen-

sion was transferred to a 50ml tube via a 100µm cell strainer to homogenize cell suspension and to remove pieces of residual tissue. DMEM high glucose was added to a final volume of 40ml.

4.6.7 Fusion of lymphocytes and myeloma cells

To establish immortal antibody-secreting hybridoma cell lines, myeloma cells and B-lymphocytes derived from mouse spleen had to be fused (Köhler & Milstein, 1975). To do so, both cell suspensions (see 4.6.5, 4.6.6) were centrifuged at 400g for 5min. The pellet of myeloma cells should be 1.5-2 times the size of the pellet derived from spleen. The pellets were washed with 30ml of DMEM high glucose by a second centrifugation step. 90% of the supernatants were discarded and the myeloma cell pellet added to the pellet derived from spleen. DMEM high glucose was added to a final volume of 40ml followed by another centrifugation step. The supernatant was removed completely and the pellet loosened by gentle flicking against the tube. The pellet was incubated in a 37°C water bath for 3min. Subsequently, while the cell suspension was gently rotated, 0.25% (w/v) PEG 4000 was stepwise added. First, 1ml of PEG 4000 solution was added drop-wise within 30s followed by a 1min incubation period at 37°C. Secondly, 3ml of PEG 4000 solution were added drop-wise within 30s followed by a 1min incubation period at 37°C. Thirdly, 16ml of PEG 4000 solution were added within 60s followed by a 5min incubation period at 37°C. Subsequently, the cell suspension was centrifuged at 250g for 5min and the pellet resuspended in 40ml selection medium. For selection medium, complete Opti-MEM was supplemented with 10% conditioned medium (either derived from macrophages or myeloma culture supernatant), 1% penicillin/ streptomycin, 50µM 2-mercaptoethanol, and 1x HAT. 2ml of cell suspension were mixed with 48ml of pre-warmed selection medium prior to distribution onto a 24-well plate. In total, 20 plates were obtained and incubated at 37°C and 5% CO_2 humid atmosphere until cell clusters were visible. The plates were checked daily for contamination. If contamination occurred, the affected well was emptied, refilled with 1M $CuSO_4$ solution, and the lid of the 24-well plate was exchanged.

4.6.8 Screening of hybridoma cells

When single cell clusters were visible, 200µl supernatant per well were collected. 100µl were used for a first screening by ELISA (see 4.6.3). Additionally, a blank sample was added comprising 100µl of selection medium instead of supernatant. Obtained ELISA data for supernatants were blank corrected. Depending on the obtained values, about 40 wells were selected reaching a high value in ELISA (OD_{492nm} higher than 0.8) and 24 wells demonstrating a moderate ELISA signal (OD_{492nm} between 0.6 and 0.8). 50µl of the supernatant of those wells was used undiluted in immunofluorescence assay on cytoskeletal preparations fixed with methanol. Because only

few wells demonstrated the characteristic posterior labeling signal of TbEB1, a further 200 wells were screened by immunofluorescence assay. In total, 13 wells had been identified demonstrating the characteristic TbEB1 labeling. Corresponding supernatants were also tested on immuno blots using procyclic TbEB1$^{C\text{-}2myc}$ (grown in the presence of 1µg/ml doxycycline) as antigens. Supernatants were diluted 1:4 in blocking buffer. Anti-TbEB1 positive wells were transferred to 6-well plates. After confirmation of antibody-secreting status, 2 wells were used for sub-cloning.

4.6.9 Sub-cloning of hybridoma cells

During the selection process, in general more than one cell cluster occurs per well. Therefore, more than one fusion event has occurred and the mixed population has to be separated by sub-cloning. The cell density was determined (see 4.5.2.1) and cells diluted in complete Opti-MEM supplemented with 2x HAT to a final concentration of 50, 20, 10 and 5 cells per ml. 100µl of each dilution was distributed to 48 wells of a 96-well plate containing macrophages (see 4.6.4) thus, two 96-well plates are necessary. Plates were maintained for at least 14 days until cell clusters were visible and grown to the size of a pinhead. Supernatants were tested in immunofluorescence assays and immuno blots as described above. Anti-TbEB1 positive clones were transferred to 24-well plates, then to 6-well plates, and finally to cell culture flasks. During the whole process, immune status of hybridoma cells was supervised by immunofluorescence assay.

4.6.10 Fractional precipitation with ammonium sulfate

Anti-TbEB1 hybridoma cells were cultivated in up to 10 cell culture flasks (75cm^2) containing 50ml of complete Opti-MEM. Initial FCS concentration was 10%. The FCS content was reduced to 2% and below in subsequent cultivation steps. Cultures were maintained until cells started to die off. Cell suspensions were pooled and centrifuged at 4.400g for 5min to remove cell fragments. The supernatant was cooled to 4°C and the exact volume determined. 313g of ammonium sulfate are used per 1l cell culture supernatant. To extract and hence, also to concentrate the anti-TbEB1 antibody, the cell culture supernatant of the anti-TbEB1 hybridoma cell line was supplemented in three steps with ammonium sulfate to a final concentration of 50% over 15min while stirring in a beaker at 4°C. The suspension was stirred for further 45min at 4°C. Finally, the suspension was centrifuged at 12.000g and 4°C for 20min. The supernatant was discarded and the pellet resuspended in 5-10ml PBS containing 0.02% (v/v) NaN_3. The obtained anti-TbEB1 antibody solution was tested by IFA and the dilution factor for working solutions was determined as 1:50-1:200.

4.6.11 Determination of isotypes of hybridoma cell lines

Antibodies are isotyped by the Isostrip mouse monoclonal antibody isotyping kit (Roche, Mannheim). The kit allows the classification by identification of heavy and light chains of the immunoglobulin. The procedure was performed after the manufacturer´s protocol. Supernatants derived from anti-TbEB1 hybridoma cell lines were 1:10 diluted in PBS containing 1% (w/v) BSA.

4.7 Microscopy

4.7.1 Light microscopy

4.7.1.1 Whole cell preparations of trypanosomes for immunofluorescence assay

For whole cell preparations of procyclic and bloodstream trypanosomes, 0.5-1.5ml of a cell suspension of a mid-log phase culture were collected and centrifuged at 3.300g for 1min. PCF were washed with 500µl PBS. In case of BSF, the PBS was supplemented with 2% (w/v) dextrose (PBS-Glc). PCF and BSF were resuspended in 500µl of PBS and PBS-Glc, respectively. Subsequently, 7.4% (v/v) formaldehyde in PBS were added and the cell suspension mixed. Cells were fixed for 5-10min at room temperature followed by centrifugation at 3.300g for 1min. The supernatant was discarded and the pellet of PCF and BSF resuspended in 100-500µl of PBS depending on cell density of the used culture. At this point, samples can be stored at 4°C for up to one week. Afterwards, cell suspensions were distributed onto poly-L-lysine coated slides, and allowed to attach for 5-10min. Subsequently, trypanosomes were permeabilized with 0.1% Triton X-100 in PBS for 3-5min at room temperature and slides washed once with PBS prior to immunofluorescence assay.

If cells were fixed with ice-cold methanol, the procedure was slightly different. Trypanosomes were collected and washed as described above. After the washing step, PCF and BSF were resuspended in PBS or PBS-Glc, respectively, followed by distribution onto poly-L-lysine coated slides. Cells were allowed to attach in a wet chamber for 10min. Unattached cells were removed by washing slides with PBS. Subsequently, slides were transferred to ice-cold methanol and fixed at -20°C for 30min. Samples could be left in ice-cold methanol for two weeks. After fixation, cells were rehydrated twice in PBS for 5min before continuing with immunofluorescence assay.

4.7.1.2 Cytoskeletal preparations of trypanosomes for immunofluorescence assay

For PCF, 100-300µl of cell suspension in mid-log phase were centrifuged at 3.300g for 1min. The pellet was washed with 500µl PM buffer (see 4.1.5). The pellet was resuspended in 500µl PM buffer and the cell suspension was distributed onto poly-L-lysine coated slides. Slides were incubated in a wet chamber for 5min to allow cells to settle. The slides were washed once with PBS to remove unattached cells. Cells were extracted with 1% (v/v) NP-40 in PM buffer for 5min on ice. Afterwards, slides were washed immediately with PM buffer prior to fixation.

For BSF, 500-1500µl of cell suspension in mid-log phase were centrifuged at 3.300g for 1min. Trypanosomes were washed once with PM-buffer. Cell pellets were resuspended in 0.5% (v/v) NP-40 in PM buffer and extracted at room temperature for 1min. Afterwards, slides were washed immediately with PM buffer prior to fixation.

For fixation of PCF and BSF, slides were either placed in a goblin jar with ice-cold methanol and fixed at -20°C for 30min or treated with 3.7% (v/v) formaldehyde in PM buffer and incubated for 5-10min in a wet chamber followed by a PBS washing step. If methanol fixation was used, samples could be left in ice-cold methanol for two weeks. If samples were fixed with formaldehyde, slides could be covered with PBS and stored at 4°C overnight. If samples were fixed in ice-cold methanol, they were rehydrated twice in PBS for 5min before immuno fluorescence assay.

4.7.1.3 Whole cell preparations of mammalian cells for immunofluorescence assay

Round coverslips (13mm, Marienfeld, Lauda-Königshofen) were sterilized with 70% ethanol. Three of them were placed in an empty well of a 6-well plate before DMEM complete and cells were were added. The cells grew on the coverslips and therefore, liquid displacement and addition was done carefully. The cells were washed once with PBS followed by fixation with 3.7% formaldehyde in PBS for 10min at room temperature. Subsequently, cells were washed twice with 100mM glycine in PBS followed by another washing step with PBS. Afterwards, cells were permeabilized with 0.5% (v/v) Triton X-100 in PBS for 5min. The coverslips were settled onto parafilm in a wet chamber prior to blocking with 1% (w/v) BSA in PBS for 20min. After blocking, the immunofluorescence assay was performed.

Except figure 2.88Bii, all figures of mammalian cells were derived from whole cell preparations.

4.7.1.4 Pre-extraction of mammalian cells for immunofluorescence assay

Only figure 2.88Bii was derived from pre-extracted mammalian cell samples. Cells were grown on coverslips as described above. Cells were pre-extracted with 0.1% Triton X-100 in PBS for 3min prior to fixation in 3.7% (v/v) formaldehyde in PBS for 10min. Samples were washed twice with 100mM glycine in PBS followed by another washing step with PBS. Coverslips were settled onto a parafilm in a wet chamber prior to blocking with 1% (w/v) BSA in PBS for 20min. After blocking, the IFA was performed.

4.7.1.5 Immunofluorescence assay (IFA)

All incubation steps were carried out in a wet chamber at room temperature. The primary antibodies were diluted in PBST as established in pre-tests and samples were incubated for 1h. Slides were washed three times in PBST for 5min. The appropriate secondary antibodies were diluted according to the manufacturer´s protocol and samples were incubated for 45-60min. Slides were washed three times in PBST for 5min. Finally, slides were rinsed with distilled water to remove salt components. Samples were embedded with Vectashield mounting medium containing 1.5µg/ml DAPI (4´6-diamidino-2-phenylidole), covered with a glass coverslip, and sealed with nail polish. Preparations were stored at 4°C. Images were acquired using the fluorescence microscope Axio Imager.M2 (Carl Zeiss GmbH, Oberkochen) equipped with a SPOT Pursuit camera (Diagnostic Instruments Inc., Sterling Heights, MI, USA) and the VisiView Imaging software (version 2.0.8; Visitron Software GmbH, Puchheim).

For double-labeling experiments, the treatment of samples was the same except that a second primary or secondary antibody was added to the first one and hence, incubated simultaneously.

4.7.1.6 Quantification of cell cycle stages

To quantify the distinct cell cycle stages in *T. brucei,* whole cell preparations, fixed with 3.7% (v/v) formaldehyde in PBS, were prepared and stained with DAPI (see 4.7.1.1, 4.7.1.5). The number of DAPI-stained nuclei and kinetoplasts can be used to categorize the different cell cycle stages of *T. brucei* (Woodward & Gull, 1990). 100-200 cells per sample were examined and assigned to normal (1K1N, 2K1N, and 2K2N) and abnormal (1K0N, 1K2N, xKxN) stages of cell cycle. Quantification was performed using the fluorescence microscope Axio Imager.M2 equipped with a SPOT Pursuit camera and the VisiView Imaging software.

4.7.1.7 Measurement of FAZ length

Cytoskeletal preparations were prepared and fixed in ice-cold methanol as described (see 4.7.1.2). An IFA was performed (see 4.7.1.5) using L3B2 antibody as primary antibody. The antibody recognizes FAZ1, which is a component of old and new FAZ. Only the old FAZ was measured as its length is considered to be constant over the cell cycle. 100 cells were analyzed independently of K/ N ratio and images acquired as described above. For determination of FAZ length, overlays of phase contrast and L3B2 labeled images were performed and FAZ length measured using ImageJ. Data analysis was done in Excel.

4.7.2 Electron microscopy

4.7.2.1 Coating of grids for electron microscopy

Glass slides were cleaned with a fibre-free tissue and placed into a crucible adapter filled with 1% (w/v) pioloform in chloroform or 1% (w/v) formvar in chloroform. The stopcock was opened to remove the liquid. A moderate, steady flow was favored to produce the appropriate thickness of the pioloform or formvar film. Solutions were stored in brown flasks at 4°C and be re-used multiple times. Glass slides were dried on air for several minutes. The film on the glass slide was scribed with a scalpel along the long sides near the rim and on one short side. It was breathed on the scribed film before it was introduced into a glass dish filled with dH_2O with the scribed surface up and 45° angle. The dust was removed from the water surface with a glass rod before. The film detached and floated on the water surface. It possessed the appropriate thickness if its color appeared silver. Square mesh copper (400 mesh, Plano, Wetzlar) or copper slot (1.2mm, Plano, Wetzlar) TEM support grids were placed onto the film. The grid-filled film was picked up from the water surface with parafilm, air-dried, and stored in petri dishes up to eight weeks.

4.7.2.2 Whole mount cytoskeletons

The method was modified after Sherwin and Gull (1989a). All buffers and solutions were sterile-filtrated through a 0.2µm filter unit prior to usage. For whole mount cytoskeletons, square mesh grids were used. Uranyl acetate was centrifuged prior to usage at 20.000g and room temperature for 8min. 3 - $5x10^7$ trypanosomes was used per experiment. Cells were centrifuged at 3.300g for 5min. The pellet was washed three times with PM-buffer (see 4.1.5) prior to resuspension in 300-500µl PM-buffer. 20µl of cell suspension was dropped onto parafilm. If immuno electron microscopy was performed, grids were coated with formvar or with pioloform. Grids were placed onto the drops for 10min to allow cell attachment. Subsequently, the grids were transferred to 1ml of freshly prepared 1% (v/v) NP-40 in PM buffer, which is sufficient for 5 grids.

Grids were incubated for 2.5min under continuous motion. The step was repeated once. Afterwards, grids were washed for 5min with PM buffer and fixed in 2.5% (v/v) glutaraldehyde in PM buffer (Plano GmbH, Wetzlar) for 1min. Grids were washed twice for 1min in dH_2O. For negative staining, samples were incubated with 2% (w/v) uranyl acetate in the dark for 20min. Grids were washed two times for 1min with dH_2O followed to two washes for 2min in dH_2O. Grids were air-dried and excessive fluids removed by filter paper. Grids were stored on filter paper in petri dishes. Images were acquired at an accelerating voltage of 80kV using the transmission electron microscope Zeiss EM 902A (Carl Zeiss GmbH, Oberkochen) equipped with a Erlangshen ES500W CCD camera (Gatan Pleasanton, CA, USA) and the Gatan digital micrograph software.

4.7.2.3 Immuno electron microscopy of whole mount cytoskeletons

The method was modified after Hemphil et al. (1991b) and Dacheux et al. (2012). All buffers and solutions were sterile-filtrated through a 0.2µm filter unit prior to usage. Antibodies were centrifuged at 20.000g and 4°C for 10min, uranyl acetate at 20.000g and room temperature for 8min. Incubation steps were performed in a wet chamber. Cells were collected, attached to grids, and extracted as described above. The extracted and washed samples were fixed in PM buffer supplemented with 2% (v/v) formaldehyde (Plano GmbH, Wetzlar) and 0.025% glutaraldehyde for 30min. Grids were washed twice with 100mM glycine for 10min and blocked with 1% BSA (w/v) in PBS for 30min. Anti-TbEB1 antibody was diluted 1:50 in PBS and samples incubated for 1h at room temperature. Three wash steps with PBS for 10min followed. The 10nm colloidal gold anti-mouse antibody was diluted 1:30 in PBS and samples incubated for 1h at room temperature. Antibodies were fixed with 2.5% glutaraldehyde in dH_2O for 30min. Afterwards, grids were washed four times in dH_2O for 5min prior to negative staining with 2% (w/v) uranyl acetate for 20min. Grids were washed and stored as described above. Images were acquired as described above.

4.7.2.4 Fixation of samples for transmission electron microscopy (whole cells)

50ml of a trypanosome culture growing at mid-log phase were harvested by centrifugation at 500g and room temperature for 5min. The supernatant was discarded until about 0.5ml of culture medium was left. The cell pellet was resuspended and distributed to two 1.5ml tubes. Subsequently, 500µl of a 2.5% glutaraldehyde solution in 0.1M sodium phosphate buffer, pH. 7.0 were added slowly to avoid disturbance of the pellet and incubated for 15min at room temperature. The pellet was detached from the bottom with a toothpick, broken into 3-5mm pieces, about 1ml fresh fixative added, and incubated for another 45min. The first fixative was dis-

carded and a second fixative used. That solution contained 4% (v/v) formaldehyde, 2% (v/v) glutaraldehyde, and 0.1% (w/v) picric acid in 0.1M sodium phosphate buffer, pH 7.0 (Sabatini *et al.* , 1963). Samples were left in the second fixative for 1h. Afterwards, the liquid was discarded and 1% (v/v) osmium tetroxide was added and cells were fixed for 1h (Palade, 1952). Cell pellets were washed twice with dH_2O prior to staining with 2% (w/v) uranyl acetate for 16h at 4°C. Dehydration of samples was done in a descending acetone series (30%, 50%, 70%, 90%, 100%) in 30min intervals. The 100% step was repeated. Finally, samples were incubated in a 1:1mixture of acetone and epon/araldite resin for 90min (kindly provided by Rita Grotjahn) (Glauert & Glauert, 1958; Luft, 1961). Afterwards, the liquid was discarded, the tube filled with fresh resin and samples incubated for 3h, which was repeated once. Finally, samples were transferred to BEEM capsules (Plano, Wetzlar), which were completely filled with resin. The resin was hardened at 50°C for 2-3 days.

4.7.2.5 Preparation and post-staining of ultra-thin sections

Specimen were removed from BEEM capsules and the surplus of resin removed with a trimming device (Leica, Bensheim) and a diamond milling cutter. 50-70nm thick ultra-thin sections were prepared using a diamond knife (Diatom, Biel, Switzerland) and a ultramicrotome (Leica Microsystems, Heerbrugg, Switzerland). Ribbons were mounted onto slot grids and dried on a filter paper overnight. Specimen were post-stained with 2% (w/v) uranyl acetate for 30min in the dark followed by 4 washes with dH_2O (Watson, 1958). Subsequently, specimen were incubated with lead citrate (4.1.5) in the presence of some sodium hydroxide pellets for 3min to minimize lead citrate precipitation (Reynolds, 1963). Subsequently, grids were washed four times with dH_2O and stored as described above.

5 Bibliography

Absalon, Sabrina, Kohl, Linda, Branche, Carole, Blisnick, Thierry, Toutirais, Géraldine, Rusconi, Filippo, Cosson, Jacky, Bonhivers, Mélanie, Robinson, Derrick, & Bastin, Philippe. 2007. Basal body positioning is controlled by flagellum formation in Trypanosoma brucei. *PLoS One*, **2**(5), e437.

Absalon, Sabrina, Blisnick, Thierry, Kohl, Linda, Toutirais, Géraldine, Doré, Gwénola, Julkowska, Daria, Tavenet, Arounie, & Bastin, Philippe. 2008. Intraflagellar transport and functional analysis of genes required for flagellum formation in trypanosomes. *Mol Biol Cell*, **19**(3), 929–44.

Akhmanova, Anna, & Hoogenraad, Casper C. 2005. Microtubule plus-end-tracking proteins: mechanisms and functions. *Curr Opin Cell Biol*, **17**(1), 47–54.

Akhmanova, Anna, & Hoogenraad, Casper C. 2015. Microtubule minus-end-targeting proteins. *Curr Biol*, **25**(4), R162–71.

Akhmanova, Anna, & Steinmetz, Michel O. 2008. Tracking the ends: a dynamic protein network controls the fate of microtubule tips. *Nat Rev Mol Cell Biol*, **9**(4), 309–22.

Akhmanova, Anna, & Steinmetz, Michel O. 2010. Microtubule +TIPs at a glance. *J Cell Sci*, **123**(Pt 20), 3415–9.

Akhmanova, Anna, & Steinmetz, Michel O. 2015. Control of microtubule organization and dynamics: two ends in the limelight. *Nat Rev Mol Cell Biol*, **16**(12), 711–26.

Akiyoshi, Bungo, & Gull, Keith. 2014. Discovery of unconventional kinetochores in kinetoplastids. *Cell*, **156**(6), 1247–58.

Alberico, Emily O, Lyons, Daniel F, Murphy, Ryan J, Philip, Julia T, Duan, Aranda R, Correia, John J, & Goodson, Holly V. 2013. Biochemical evidence that human EB1 does not bind preferentially to the microtubule seam. *Cytoskeleton (Hoboken)*, **70**(6), 317–27.

Alberico, Emily O, Zhu, Zhiqing C, Wu, Yueh-Fu O, Gardner, Melissa K, Kovar, Dave R, & Goodson, Holly V. 2016. Interactions between the Microtubule Binding Protein EB1 and F-Actin. *J Mol Biol*, **428**(6), 1304–14.

Alfaro-Aco, Ray, & Petry, Sabine. 2015. Building the Microtubule Cytoskeleton Piece by Piece. *J Biol Chem*, **290**(28), 17154–62.

Alsford, Sam, & Horn, David. 2008. Single-locus targeting constructs for reliable regulated RNAi and transgene expression in Trypanosoma brucei. *Mol Biochem Parasitol*, **161**(1), 76–9.

Alsford, Sam, Turner, Daniel J, Obado, Samson O, Sanchez-Flores, Alejandro, Glover, Lucy, Berriman, Matthew, Hertz-Fowler, Christiane, & Horn, David. 2011. High-throughput phenotyping using parallel sequencing of RNA interference targets in the African trypanosome. *Genome Res*, **21**(6), 915–24.

Alsford, Sam, duBois, Kelly, Horn, David, & Field, Mark C. 2012a. Epigenetic mechanisms, nuclear architecture and the control of gene expression in trypanosomes. *Expert Rev Mol Med*, **14**, e13.

Alsford, Sam, Eckert, Sabine, Baker, Nicola, Glover, Lucy, Sanchez-Flores, Alejandro, Leung, Ka Fai, Turner, Daniel J, Field, Mark C, Berriman, Matthew, & Horn, David. 2012b. High-throughput decoding of antitrypanosomal drug efficacy and resistance. *Nature*, **482**(7384), 232–6.

Altschul, S F, Gish, W, Miller, W, Myers, E W, & Lipman, D J. 1990. Basic local alignment search tool. *J Mol Biol*, **215**(3), 403–10.

Amos, Linda A, & Schlieper, Daniel. 2005. Microtubules and maps. *Adv Protein Chem*, **71**, 257–98.

Angelopoulos, E. 1970. Pellicular microtubules in the family Trypanosomatidae. *J Protozool*, **17**(1), 39–51.

Archer, Stuart K, Inchaustegui, Diana, Queiroz, Rafael, & Clayton, Christine. 2011. The cell cycle regulated transcriptome of Trypanosoma brucei. *PLoS One*, **6**(3), e18425.

Armstrong, D J, & Roman, A. 1993. The anomalous electrophoretic behavior of the human papillomavirus type 16 E7 protein is due to the high content of acidic amino acid residues. *Biochem Biophys Res Commun*, **192**(3), 1380–7.

Asbury, Charles L. 2008. XMAP215: a tip tracker that really moves. *Cell*, **132**(1), 19–20.

Askham, J M, Vaughan, K T, Goodson, H V, & Morrison, E E. 2002. Evidence that an interaction between EB1 and p150(Glued) is required for the formation and maintenance of a radial microtubule array anchored at the centrosome. *Mol Biol Cell*, **13**(10), 3627–45.

Baines, Andrea, & Gull, Keith. 2008. WCB is a C2 domain protein defining the plasma membrane - sub-pellicular microtubule corset of kinetoplastid parasites. *Protist*, **159**(1), 115–25.

Banerjee, Budhaditya, Kestner, Cortney A, & Stukenberg, P Todd. 2014. EB1 enables spindle microtubules to regulate centromeric recruitment of Aurora B. *J Cell Biol*, **204**(6), 947–63.

Bartolini, Francesca, & Gundersen, Gregg G. 2006. Generation of noncentrosomal microtubule arrays. *J Cell Sci*, **119**(Pt 20), 4155–63.

Bastin, P, Sherwin, T, & Gull, K. 1998. Paraflagellar rod is vital for trypanosome motility. *Nature*, **391**(6667), 548.

Bastin, P, MacRae, T H, Francis, S B, Matthews, K R, & Gull, K. 1999. Flagellar morphogenesis: protein targeting and assembly in the paraflagellar rod of trypanosomes. *Mol Cell Biol*, **19**(12), 8191–200.

Beinhauer, J D, Hagan, I M, Hegemann, J H, & Fleig, U. 1997. Mal3, the fission yeast homologue of the human APC-interacting protein EB-1 is required for microtubule integrity and the maintenance of cell form. *J Cell Biol*, **139**(3), 717–28.

Benz, Corinna, Clucas, Caroline, Mottram, Jeremy C, & Hammarton, Tansy C. 2012. Cytokinesis in bloodstream stage Trypanosoma brucei requires a family of katanins and spastin. *PLoS One*, **7**(1), e30367.

Berriman, Matthew, Ghedin, Elodie, Hertz-Fowler, Christiane, Blandin, Gaëlle, Renauld, Hubert, Bartholomeu, Daniella C, Lennard, Nicola J, Caler, Elisabet, Hamlin, Nancy E, Haas, Brian, Böhme, Ulrike, Hannick, Linda, Aslett, Martin A, Shallom, Joshua, Marcello, Lucio, Hou, Lihua, Wickstead, Bill, Alsmark, U Cecilia M, Arrowsmith, Claire, Atkin, Rebecca J, Barron, Andrew J, Bringaud, Frederic, Brooks, Karen, Carrington, Mark, Cherevach, Inna, Chillingworth, Tracey-Jane, Churcher, Carol, Clark, Louise N, Corton, Craig H, Cronin, Ann, Davies, Rob M, Doggett, Jonathon, Djikeng, Appolinaire, Feldblyum, Tamara, Field, Mark C, Fraser, Audrey, Goodhead, Ian, Hance, Zahra, Harper, David, Harris, Barbara R, Hauser, Heidi, Hostetler, Jessica, Ivens, Al, Jagels, Kay, Johnson, David, Johnson, Justin, Jones, Kristine, Kerhornou, Arnaud X, Koo, Hean, Larke, Natasha, Landfear, Scott, Larkin, Christopher, Leech, Vanessa, Line, Alexandra, Lord, Angela, Macleod, Annette, Mooney, Paul J, Moule, Sharon, Martin, David M A, Morgan, Gareth W, Mungall, Karen, Norbertczak,

Halina, Ormond, Doug, Pai, Grace, Peacock, Chris S, Peterson, Jeremy, Quail, Michael A, Rabbinowitsch, Ester, Rajandream, Marie-Adele, Reitter, Chris, Salzberg, Steven L, Sanders, Mandy, Schobel, Seth, Sharp, Sarah, Simmonds, Mark, Simpson, Anjana J, Tallon, Luke, Turner, C Michael R, Tait, Andrew, Tivey, Adrian R, Van Aken, Susan, Walker, Danielle, Wanless, David, Wang, Shiliang, White, Brian, White, Owen, Whitehead, Sally, Woodward, John, Wortman, Jennifer, Adams, Mark D, Embley, T Martin, Gull, Keith, Ullu, Elisabetta, Barry, J David, Fairlamb, Alan H, Opperdoes, Fred, Barrell, Barclay G, Donelson, John E, Hall, Neil, Fraser, Claire M, Melville, Sara E, & El-Sayed, Najib M. 2005. The genome of the African trypanosome Trypanosoma brucei. *Science*, **309**(5733), 416–22.

Berrueta, L, Kraeft, S K, Tirnauer, J S, Schuyler, S C, Chen, L B, Hill, D E, Pellman, D, & Bierer, B E. 1998. The adenomatous polyposis coli-binding protein EB1 is associated with cytoplasmic and spindle microtubules. *Proc Natl Acad Sci U S A*, **95**(18), 10596–601.

Biebinger, S, Wirtz, L E, Lorenz, P, & Clayton, C. 1997. Vectors for inducible expression of toxic gene products in bloodstream and procyclic Trypanosoma brucei. *Mol Biochem Parasitol*, **85**(1), 99–112.

Bieling, Peter, Laan, Liedewij, Schek, Henry, Munteanu, E Laura, Sandblad, Linda, Dogterom, Marileen, Brunner, Damian, & Surrey, Thomas. 2007. Reconstitution of a microtubule plus-end tracking system in vitro. *Nature*, **450**(7172), 1100–5.

Bieling, Peter, Kandels-Lewis, Stefanie, Telley, Ivo A, van Dijk, Juliette, Janke, Carsten, & Surrey, Thomas. 2008. CLIP-170 tracks growing microtubule ends by dynamically recognizing composite EB1/tubulin-binding sites. *J Cell Biol*, **183**(7), 1223–33.

Birnboim, H C, & Doly, J. 1979. A rapid alkaline extraction procedure for screening recombinant plasmid DNA. *Nucleic Acids Res*, **7**(6), 1513–23.

Bisgrove, Sherryl R, Hable, Whitney E, & Kropf, Darryl L. 2004. +TIPs and microtubule regulation. The beginning of the plus end in plants. *Plant Physiol*, **136**(4), 3855–63.

Bisgrove, Sherryl R, Lee, Yuh-Ru Julie, Liu, Bo, Peters, Nick T, & Kropf, Darryl L. 2008. The microtubule plus-end binding protein EB1 functions in root responses to touch and gravity signals in Arabidopsis. *Plant Cell*, **20**(2), 396–410.

Bochud-Allemann, N, & Schneider, A. 2002. Mitochondrial substrate level phosphorylation is essential for growth of procyclic Trypanosoma brucei. *J Biol Chem*, **277**(36), 32849–54.

Bonhivers, Mélanie, Nowacki, Sophie, Landrein, Nicolas, & Robinson, Derrick R. 2008. Biogenesis of the trypanosome endo-exocytotic organelle is cytoskeleton mediated. *PLoS Biol*, **6**(5), e105.

Brecht, M, & Parsons, M. 1998. Changes in polysome profiles accompany trypanosome development. *Mol Biochem Parasitol*, **97**(1-2), 189–98.

Brenndörfer, Martin, & Boshart, Michael. 2010. Selection of reference genes for mRNA quantification in Trypanosoma brucei. *Mol Biochem Parasitol*, **172**(1), 52–5.

Briggs, Laura J, McKean, Paul G, Baines, Andrea, Moreira-Leite, Flavia, Davidge, Jacqueline, Vaughan, Sue, & Gull, Keith. 2004. The flagella connector of Trypanosoma brucei: an unusual mobile transmembrane junction. *J Cell Sci*, **117**(Pt 9), 1641–51.

Bringaud, Frédéric, Rivière, Loïc, & Coustou, Virginie. 2006. Energy metabolism of trypanosomatids: adaptation to available carbon sources. *Mol Biochem Parasitol*, **149**(1), 1–9.

Broadhead, Richard, Dawe, Helen R, Farr, Helen, Griffiths, Samantha, Hart, Sarah R, Portman, Neil, Shaw, Michael K, Ginger, Michael L, Gaskell, Simon J, McKean, Paul G, & Gull, Keith. 2006. Flagellar motility is required for the viability of the bloodstream trypanosome. *Nature*, **440**(7081), 224–7.

Brun, R, & Schönenberger. 1979. Cultivation and in vitro cloning or procyclic culture forms of Trypanosoma brucei in a semi-defined medium. Short communication. *Acta Trop*, **36**(3), 289–92.

Brun, Reto, Blum, Johannes, Chappuis, Francois, & Burri, Christian. 2010. Human African trypanosomiasis. *Lancet*, **375**(9709), 148–59.

Brüning-Richardson, Anke, Langford, Kelly J, Ruane, Peter, Lee, Tracy, Askham, Jon M, & Morrison, Ewan E. 2011. EB1 is required for spindle symmetry in mammalian mitosis. *PLoS One*, **6**(12), e28884.

Bu, W, & Su, L K. 2001. Regulation of microtubule assembly by human EB1 family proteins. *Oncogene*, **20**(25), 3185–92.

Bu, Wen, & Su, Li-Kuo. 2003. Characterization of functional domains of human EB1 family proteins. *J Biol Chem*, **278**(50), 49721–31.

Burkard, Gabriela, Fragoso, Cristina M, & Roditi, Isabel. 2007. Highly efficient stable transformation of bloodstream forms of Trypanosoma brucei. *Mol Biochem Parasitol*, **153**(2), 220–3.

Cammarata, Garrett M, Bearce, Elizabeth A, & Lowery, Laura Anne. 2016. Cytoskeletal social networking in the growth cone: How +TIPs mediate microtubule-actin cross-linking to drive axon outgrowth and guidance. *Cytoskeleton (Hoboken)*, Jan.

Casanova, Magali, Crobu, Lucien, Blaineau, Christine, Bourgeois, Nathalie, Bastien, Patrick, & Pagès, Michel. 2009. Microtubule-severing proteins are involved in flagellar length control and mitosis in Trypanosomatids. *Mol Microbiol*, **71**(6), 1353–70.

Casarégola, S, Jacq, A, Laoudj, D, McGurk, G, Margarson, S, Tempête, M, Norris, V, & Holland, I B. 1992. Cloning and analysis of the entire Escherichia coli ams gene. ams is identical to hmp1 and encodes a 114 kDa protein that migrates as a 180 kDa protein. *J Mol Biol*, **228**(1), 30–40.

Chan, Jordi, Calder, Grant M, Doonan, John H, & Lloyd, Clive W. 2003. EB1 reveals mobile microtubule nucleation sites in Arabidopsis. *Nat Cell Biol*, **5**(11), 967–71.

Chan, Kuan Yoow. 2008. *The Characterisation of Family-13 Kinesins in Trypanosoma brucei*. Ph.D. thesis, University of Hull.

Chan, Kuan Yoow, & Ersfeld, Klaus. 2010. The role of the Kinesin-13 family protein TbKif13-2 in flagellar length control of Trypanosoma brucei. *Mol Biochem Parasitol*, **174**(2), 137–40.

Chan, Kuan Yoow, Matthews, Keith R, & Ersfeld, Klaus. 2010. Functional characterisation and drug target validation of a mitotic kinesin-13 in Trypanosoma brucei. *PLoS Pathog*, **6**(8), e1001050.

Checchi, Francesco, Filipe, João A N, Barrett, Michael P, & Chandramohan, Daniel. 2008. The natural progression of Gambiense sleeping sickness: what is the evidence? *PLoS Negl Trop Dis*, **2**(12), e303.

Checchi, Francesco, Funk, Sebastian, Chandramohan, Daniel, Haydon, Daniel T, & Chappuis, François. 2015. Updated estimate of the duration of the meningo-encephalitic stage in gambiense human African trypanosomiasis. *BMC Res Notes*, **8**, 292.

Cheeseman, Iain M, & Desai, Arshad. 2008. Molecular architecture of the kinetochore-microtubule interface. *Nat Rev Mol Cell Biol*, **9**(1), 33–46.

Chen, Chun-Ti, Kelly, Megan, Leon, Jessica de, Nwagbara, Belinda, Ebbert, Patrick, Ferguson, David J P, Lowery, Laura Anne, Morrissette, Naomi, & Gubbels, Marc-Jan. 2015. Compartmentalized Toxoplasma EB1 bundles spindle microtubules to secure accurate chromosome segregation. *Mol Biol Cell*, **26**(25), 4562–76.

Chen, Jie, Luo, Youguang, Li, Lixin, Ran, Jie, Wang, Xincheng, Gao, Siqi, Liu, Min, Li, Dengwen, Shui, Wenqing, & Zhou, Jun. 2014a. Phosphoregulation of the dimerization and functions of end-binding protein 1. *Protein Cell*, **5**(10), 795–9.

Chen, Yalei, Rolls, Melissa M, & Hancock, William O. 2014b. An EB1-kinesin complex is sufficient to steer microtubule growth in vitro. *Curr Biol*, **24**(3), 316–21.

Chowdhury, Arnab Roy, Zhao, Zhixing, & Englund, Paul T. 2008. Effect of hydroxyurea on procyclic Trypanosoma brucei: an unconventional mechanism for achieving synchronous growth. *Eukaryot Cell*, **7**(2), 425–8.

Chrétien, D, Fuller, S D, & Karsenti, E. 1995. Structure of growing microtubule ends: two-dimensional sheets close into tubes at variable rates. *J Cell Biol*, **129**(5), 1311–28.

Colasante, Claudia, Ellis, Margrit, Ruppert, Thomas, & Voncken, Frank. 2006. Comparative proteomics of glycosomes from bloodstream form and procyclic culture form Trypanosoma brucei brucei [Abstract]. *Proteomics*, **6**(11), 3275–93.

Connor, R J. 1994. The impact of nagana. *Onderstepoort J Vet Res*, **61**(4), 379–83.

Corell, R A, Feagin, J E, Riley, G R, Strickland, T, Guderian, J A, Myler, P J, & Stuart, K. 1993. Trypanosoma brucei minicircles encode multiple guide RNAs which can direct editing of extensively overlapping sequences. *Nucleic Acids Res*, **21**(18), 4313–20.

Dacheux, Denis, Landrein, Nicolas, Thonnus, Magali, Gilbert, Guillaume, Sahin, Annelise, Wodrich, Harald, Robinson, Derrick R, & Bonhivers, Mélanie. 2012. A MAP6-related protein is present in protozoa and is involved in flagellum motility. *PLoS One*, **7**(2), e31344.

Davidge, Jacqueline A, Chambers, Emma, Dickinson, Harriet A, Towers, Katie, Ginger, Michael L, McKean, Paul G, & Gull, Keith. 2006. Trypanosome IFT mutants provide insight into the motor location for mobility of the flagella connector and flagellar membrane formation. *J Cell Sci*, **119**(Pt 19), 3935–43.

Dawson, Scott C, Sagolla, Meredith S, Mancuso, Joel J, Woessner, David J, House, Susan A, Fritz-Laylin, Lillian, & Cande, W Zacheus. 2007. Kinesin-13 regulates flagellar, interphase, and mitotic microtubule dynamics in Giardia intestinalis. *Eukaryot Cell*, **6**(12), 2354–64.

de Forges, Hélène, Bouissou, Anaïs, & Perez, Franck. 2012. Interplay between microtubule dynamics and intracellular organization. *Int J Biochem Cell Biol*, **44**(2), 266–74.

De Groot, Christian O, Jelesarov, Ilian, Damberger, Fred F, Bjelić, Sasa, Schärer, Martin A, Bhavesh, Neel S, Grigoriev, Ilia, Buey, Ruben M, Wüthrich, Kurt, Capitani, Guido, Akhmanova, Anna, & Steinmetz, Michel O. 2010. Molecular insights into mammalian end-binding protein heterodimerization. *J Biol Chem*, **285**(8), 5802–14.

de Souza, Wanderley. 2008. Electron microscopy of trypanosomes–a historical view. *Mem Inst Oswaldo Cruz*, **103**(4), 313–25.

de Souza, Wanderley. 2010. *Structures and organelles in pathogenic protists*. 2010 edition edn. Microbiology Monographs, vol. 17. Springer, Heidelberg: Springer.

Deflorin, J, Rudolf, M, & Seebeck, T. 1994. The major components of the paraflagellar rod of Trypanosoma brucei are two similar, but distinct proteins which are encoded by two different gene loci. *J Biol Chem*, **269**(46), 28745–51.

Desai, A, & Mitchison, T J. 1997. Microtubule polymerization dynamics. *Annu Rev Cell Dev Biol*, **13**, 83–117.

Dilbeck, V, Berberof, M, Van Cauwenberge, A, Alexandre, H, & Pays, E. 1999. Characterization of a coiled coil protein present in the basal body of Trypanosoma brucei. *J Cell Sci*, **112 (Pt 24)**(Dec), 4687–94.

Dixit, Ram, & Cyr, Richard. 2004. The cortical microtubule array: from dynamics to organization. *Plant Cell*, **16**(10), 2546–52.

Dixit, Ram, Barnett, Brian, Lazarus, Jacob E, Tokito, Mariko, Goldman, Yale E, & Holzbaur, Erika L F. 2009. Microtubule plus-end tracking by CLIP-170 requires EB1. *Proc Natl Acad Sci U S A*, **106**(2), 492–7.

Dogterom, Marileen, Kerssemakers, Jacob W J, Romet-Lemonne, Guillaume, & Janson, Marcel E. 2005. Force generation by dynamic microtubules. *Curr Opin Cell Biol*, **17**(1), 67–74.

Dong, Xin, Liu, Fangfang, Sun, Lei, Liu, Min, Li, Dengwen, Su, Dan, Zhu, Zhengmao, Dong, Jin-Tang, Fu, Li, & Zhou, Jun. 2010. Oncogenic function of microtubule end-binding protein 1 in breast cancer. *J Pathol*, **220**(3), 361–9.

Drewes, G, Ebneth, A, & Mandelkow, E M. 1998. MAPs, MARKs and microtubule dynamics. *Trends Biochem Sci*, **23**(8), 307–11.

Dutoya, S, Gibert, S, Lemercier, G, Santarelli, X, Baltz, D, Baltz, T, & Bakalara, N. 2001. A novel C-terminal kinesin is essential for maintaining functional acidocalcisomes in Trypanosoma brucei. *J Biol Chem*, **276**(52), 49117–24.

Dyer, Naomi A, Rose, Clair, Ejeh, Nicholas O, & Acosta-Serrano, Alvaro. 2013. Flying tryps: survival and maturation of trypanosomes in tsetse flies. *Trends Parasitol*, **29**(4), 188–96.

Eckert, Thomas, Le, Doan Tuong-Van, Link, Susanne, Friedmann, Lena, & Woehlke, Günther. 2012. Spastin's microtubule-binding properties and comparison to katanin. *PLoS One*, **7**(12), e50161.

Elliott, Sarah L, Cullen, C Fiona, Wrobel, Nicola, Kernan, Maurice J, & Ohkura, Hiroyuki. 2005. EB1 is essential during Drosophila development and plays a crucial role in the integrity of chordotonal mechanosensory organs. *Mol Biol Cell*, **16**(2), 891–901.

Engstler, Markus, Thilo, Lutz, Weise, Frank, Grünfelder, Christoph G, Schwarz, Heinz, Boshart, Michael, & Overath, Peter. 2004. Kinetics of endocytosis and recycling of the GPI-anchored variant surface glycoprotein in Trypanosoma brucei. *J Cell Sci*, **117**(Pt 7), 1105–15.

Ersfeld, Klaus. 2011. Nuclear architecture, genome and chromatin organisation in Trypanosoma brucei. *Res Microbiol*, **162**(6), 626–36.

Fairlamb, A H, Weislogel, P O, Hoeijmakers, J H, & Borst, P. 1978. Isolation and characterization of kinetoplast DNA from bloodstream form of Trypanosoma brucei. *J Cell Biol*, **76**(2), 293–309.

Farr, Helen, & Gull, Keith. 2012. Cytokinesis in trypanosomes. *Cytoskeleton (Hoboken)*, **69**(11), 931–41.

Fenn, Katelyn, & Matthews, Keith R. 2007. The cell biology of Trypanosoma brucei differentiation. *Curr Opin Microbiol*, **10**(6), 539–46.

Fern, Lim Li. 2012. *End-binding protein 1 (EB1): Characterization of an EB1 homologue in Trypanosoma brucei*. M.Phil. thesis, National University of Singapore.

Field, Mark C, & Carrington, Mark. 2009. The trypanosome flagellar pocket. *Nat Rev Microbiol*, **7**(11), 775–86.

Fishel, Erica A, & Dixit, Ram. 2013. Role of nucleation in cortical microtubule array organization: variations on a theme. *Plant J*, **75**(2), 270–7.

Fleming, Jennifer R, Morgan, Rachel E, Fyfe, Paul K, Kelly, Sharon M, & Hunter, William N. 2013. The architecture of Trypanosoma brucei tubulin-binding cofactor B and implications for function. *FEBS J*, **280**(14), 3270–80.

Fletcher, Daniel A, & Mullins, R Dyche. 2010. Cell mechanics and the cytoskeleton. *Nature*, **463**(7280), 485–92.

Florimond, Célia, Sahin, Annelise, Vidilaseris, Keni, Dong, Gang, Landrein, Nicolas, Dacheux, Denis, Albisetti, Anna, Byard, Edward H, Bonhivers, Mélanie, & Robinson, Derrick R. 2015. BILBO1 is a scaffold protein of the flagellar pocket collar in the pathogen Trypanosoma brucei. *PLoS Pathog*, **11**(3), e1004654.

Franco, Jose R, Simarro, Pere P, Diarra, Abdoulaye, & Jannin, Jean G. 2014. Epidemiology of human African trypanosomiasis. *Clin Epidemiol*, **6**, 257–75.

Galjart, Niels. 2005. CLIPs and CLASPs and cellular dynamics. *Nat Rev Mol Cell Biol*, **6**(6), 487–98.

Galjart, Niels. 2010. Plus-end-tracking proteins and their interactions at microtubule ends. *Curr Biol*, **20**(12), R528–37.

Gallo, J M, Précigout, E, & Schrével, J. 1988. Subcellular sequestration of an antigenically unique beta-tubulin. *Cell Motil Cytoskeleton*, **9**(2), 175–83.

García-Salcedo, José A, Pérez-Morga, David, Gijón, Purificación, Dilbeck, Vincent, Pays, Etienne, & Nolan, Derek P. 2004. A differential role for actin during the life cycle of Trypanosoma brucei. *EMBO J*, **23**(4), 780–9.

Gheiratmand, Ladan, Brasseur, Anais, Zhou, Qing, & He, Cynthia Y. 2013. Biochemical characterization of the bi-lobe reveals a continuous structural network linking the bi-lobe to other single-copied organelles in Trypanosoma brucei. *J Biol Chem*, **288**(5), 3489–99.

Glauert, A M, & Glauert, R H. 1958. Araldite as an embedding medium for electron microscopy. *J Biophys Biochem Cytol*, **4**(2), 191–4.

Gluenz, Eva, Povelones, Megan L, Englund, Paul T, & Gull, Keith. 2011. The kinetoplast duplication cycle in Trypanosoma brucei is orchestrated by cytoskeleton-mediated cell morphogenesis. *Mol Cell Biol*, **31**(5), 1012–21.

Goldspink, Deborah A, Gadsby, Jonathan R, Bellett, Gemma, Keynton, Jennifer, Tyrrell, Benjamin J, Lund, Elizabeth K, Powell, Penny P, Thomas, Paul, & Mogensen, Mette M. 2013. The microtubule end-binding protein EB2 is a central regulator of microtubule reorganisation in apico-basal epithelial differentiation. *J Cell Sci*, **126**(Pt 17), 4000–14.

Goodson, Holly V, Skube, Susan B, Stalder, Romaine, Valetti, Caterina, Kreis, Thomas E, Morrison, Ewan E, & Schroer, Trina A. 2003. CLIP-170 interacts with dynactin complex and the APC-binding protein EB1 by different mechanisms. *Cell Motil Cytoskeleton*, **55**(3), 156–73.

Greenfield, E A. 2014. *Antibodies: A Laboratory Manual, Second edition*. second edn. Cold Spring Harbor, N. Y., USA: Inglis, John.

Grigoriev, Ilya, Gouveia, Susana Montenegro, van der Vaart, Babet, Demmers, Jeroen, Smyth, Jeremy T, Honnappa, Srinivas, Splinter, Daniël, Steinmetz, Michel O, Putney, Jr, James W, Hoogenraad, Casper C, & Akhmanova, Anna. 2008. STIM1 is a MT-plus-end-tracking protein involved in remodeling of the ER. *Curr Biol*, **18**(3), 177–82.

Gull, K. 1999. The cytoskeleton of trypanosomatid parasites. *Annu Rev Microbiol*, **53**, 629–55.

Gull, K, Birkett, C, Gerke-Bonet, R, Parma, A, Robinson, D, Sherwin, T, & Woodward, R. 1990. The cell cycle and cytoskeletal morphogenesis in Trypanosoma brucei. *Biochem Soc Trans*, **18**(5), 720–2.

Gültekin, H, & Heermann, K H. 1988. The use of polyvinylidenedifluoride membranes as a general blotting matrix. *Anal Biochem*, **172**(2), 320–9.

Halpain, Shelley, & Dehmelt, Leif. 2006. The MAP1 family of microtubule-associated proteins. *Genome Biol*, **7**(6), 224.

Hamilton, Patrick B, Stevens, Jamie R, Gaunt, Michael W, Gidley, Jennifer, & Gibson, Wendy C. 2004. Trypanosomes are monophyletic: evidence from genes for glyceraldehyde phosphate dehydrogenase and small subunit ribosomal RNA. *Int J Parasitol*, **34**(12), 1393–404.

Hamilton, Patrick B, Gibson, Wendy C, & Stevens, Jamie R. 2007. Patterns of co-evolution between trypanosomes and their hosts deduced from ribosomal RNA and protein-coding gene phylogenies. *Mol Phylogenet Evol*, **44**(1), 15–25.

Hammarton, Tansy C. 2007. Cell cycle regulation in Trypanosoma brucei. *Mol Biochem Parasitol*, **153**(1), 1–8.

Hammarton, Tansy C, Clark, Jade, Douglas, Fiona, Boshart, Michael, & Mottram, Jeremy C. 2003. Stage-specific differences in cell cycle control in Trypanosoma brucei revealed by RNA interference of a mitotic cyclin. *J Biol Chem*, **278**(25), 22877–86.

Hammarton, Tansy C, Monnerat, Séverine, & Mottram, Jeremy C. 2007a. Cytokinesis in trypanosomatids. *Curr Opin Microbiol*, **10**(6), 520–7.

Hammarton, Tansy C, Kramer, Susanne, Tetley, Laurence, Boshart, Michael, & Mottram, Jeremy C. 2007b. Trypanosoma brucei Polo-like kinase is essential for basal body duplication, kDNA segregation and cytokinesis. *Mol Microbiol*, **65**(5), 1229–48.

Hayashi, Ikuko, & Ikura, Mitsuhiko. 2003. Crystal structure of the amino-terminal microtubule-binding domain of end-binding protein 1 (EB1). *J Biol Chem*, **278**(38), 36430–4.

Hayashi, Ikuko, Wilde, Andrew, Mal, Tapas Kumar, & Ikura, Mitsuhiko. 2005. Structural basis for the activation of microtubule assembly by the EB1 and p150Glued complex. *Mol Cell*, **19**(4), 449–60.

He, Cynthia Y, Ho, Helen H, Malsam, Joerg, Chalouni, Cecile, West, Christopher M, Ullu, Elisabetta, Toomre, Derek, & Warren, Graham. 2004. Golgi duplication in Trypanosoma brucei. *J Cell Biol*, **165**(3), 313–21.

He, Cynthia Y, Pypaert, Marc, & Warren, Graham. 2005. Golgi duplication in Trypanosoma brucei requires Centrin2. *Science*, **310**(5751), 1196–8.

Hebbes, T R, Turner, C H, Thorne, A W, & Crane-Robinson, C. 1989. A "minimal epitope" anti-protein antibody that recognises a single modified amino acid. *Mol Immunol*, **26**(9), 865–73.

Hemphill, A, Lawson, D, & Seebeck, T. 1991a. The cytoskeletal architecture of Trypanosoma brucei. *J Parasitol*, **77**(4), 603–12.

Hemphill, A, Seebeck, T, & Lawson, D. 1991b. The Trypanosoma brucei cytoskeleton: ultrastructure and localization of microtubule-associated and spectrin-like proteins using quick-freeze, deep-etch, immunogold electron microscopy. *J Struct Biol*, **107**(3), 211–20.

Hendriks, E, van Deursen, F J, Wilson, J, Sarkar, M, Timms, M, & Matthews, K R. 2000. Life-cycle differentiation in Trypanosoma brucei: molecules and mutants. *Biochem Soc Trans*, **28**(5), 531–6.

Hertz-Fowler, C, Ersfeld, K, & Gull, K. 2001. CAP5.5, a life-cycle-regulated, cytoskeleton-associated protein is a member of a novel family of calpain-related proteins in Trypanosoma brucei. *Mol Biochem Parasitol*, **116**(1), 25–34.

Hildebrand, Andrea, Remmert, Michael, Biegert, Andreas, & Söding, Johannes. 2009. Fast and accurate automatic structure prediction with HHpred. *Proteins*, **77 Suppl 9**, 128–32.

Hirumi, H, & Hirumi, K. 1989. Continuous cultivation of Trypanosoma brucei blood stream forms in a medium containing a low concentration of serum protein without feeder cell layers. *J Parasitol*, **75**(6), 985–9.

Hoare, C A. 1964. MORPHOLOGICAL AND TAXONOMIC STUDIES ON MAMMALIAN TRYPANOSOMES. X. REVISION OF THE SYSTEMATICS. *J Protozool*, **11**(May), 200–7.

Hoare, C A, & Wallace, F G. 1966. Developmental stages of trypanosomatid flagellates: a new terminology. *Nature*, **212**(5068), 1385 – 1386.

Honnappa, Srinivas, Okhrimenko, Oksana, Jaussi, Rolf, Jawhari, Hatim, Jelesarov, Ilian, Winkler, Fritz K, & Steinmetz, Michel O. 2006. Key interaction modes of dynamic +TIP networks. *Mol Cell*, **23**(5), 663–71.

Honnappa, Srinivas, Gouveia, Susana Montenegro, Weisbrich, Anke, Damberger, Fred F, Bhavesh, Neel S, Jawhari, Hatim, Grigoriev, Ilya, van Rijssel, Frederik J A, Buey, Ruben M, Lawera, Aleksandra, Jelesarov, Ilian, Winkler, Fritz K, Wüthrich, Kurt, Akhmanova, Anna, & Steinmetz, Michel O. 2009. An EB1-binding motif acts as a microtubule tip localization signal. *Cell*, **138**(2), 366–76.

Horio, T, & Hotani, H. 1986. Visualization of the dynamic instability of individual microtubules by dark-field microscopy. *Nature*, **321**(6070), 605–7.

Horn, David. 2014. Antigenic variation in African trypanosomes. *Mol Biochem Parasitol*, **195**(2), 123–9.

Howard, Joe, & Hyman, Anthony A. 2003. Dynamics and mechanics of the microtubule plus end. *Nature*, **422**(6933), 753–8.

Hu, Huiqing, Hu, Liu, Yu, Zhonglian, Chasse, Amanda E, Chu, Feixia, & Li, Ziyin. 2012a. An orphan kinesin in trypanosomes cooperates with a kinetoplastid-specific kinesin to maintain cell morphology by regulating subpellicular microtubules. *J Cell Sci*, **125**(Pt 17), 4126–36.

Hu, Huiqing, Liu, Yi, Zhou, Qing, Siegel, Sara, & Li, Ziyin. 2015a. The Centriole Cartwheel Protein SAS-6 in Trypanosoma brucei Is Required for Probasal Body Biogenesis and Flagellum Assembly. *Eukaryot Cell*, **14**(9), 898–907.

Hu, Huiqing, Zhou, Qing, & Li, Ziyin. 2015b. A Novel Basal Body Protein That Is a Polo-like Kinase Substrate Is Required for Basal Body Segregation and Flagellum Adhesion in Trypanosoma brucei [Abstract]. *J Biol Chem*, **290**(41), 25012–22.

Hu, Liu, Hu, Huiqing, & Li, Ziyin. 2012b. A kinetoplastid-specific kinesin is required for cytokinesis and for maintenance of cell morphology in Trypanosoma brucei. *Mol Microbiol*, **83**(3), 565–78.

Huang, X, Lovelace, L. L., Smith, D., & Lebioda, L. 2015. Structure of a fragment of human end-binding protein 1 (EB1) containing the N-terminal domain at 1.35 A resolution. *to be published.*

Hughes, Louise, Towers, Katie, Starborg, Tobias, Gull, Keith, & Vaughan, Sue. 2013. A cell-body groove housing the new flagellum tip suggests an adaptation of cellular morphogenesis for parasitism in the bloodstream form of Trypanosoma brucei. *J Cell Sci*, **126**(Pt 24), 5748–57.

Hüls, Daniela, Storchova, Zuzana, & Niessing, Dierk. 2012. Post-translational modifications regulate assembly of early spindle orientation complex in yeast. *J Biol Chem*, **287**(20), 16238–45.

Ikeda, Kyojiro N, & de Graffenried, Christopher L. 2012. Polo-like kinase is necessary for flagellum inheritance in Trypanosoma brucei. *J Cell Sci*, **125**(Pt 13), 3173–84.

Imboden, M A, Laird, P W, Affolter, M, & Seebeck, T. 1987. Transcription of the intergenic regions of the tubulin gene cluster of Trypanosoma brucei: evidence for a polycistronic transcription unit in a eukaryote. *Nucleic Acids Res*, **15**(18), 7357–68.

Kabani, Sarah, Waterfall, Martin, & Matthews, Keith R. 2010. Cell-cycle synchronisation of bloodstream forms of Trypanosoma brucei using Vybrant DyeCycle Violet-based sorting. *Mol Biochem Parasitol*, **169**(1), 59–62.

Kanaba, Teppei, Maesaki, Ryoko, Mori, Tomoyuki, Ito, Yutaka, Hakoshima, Toshio, & Mishima, Masaki. 2013. Microtubule-binding sites of the CH domain of EB1 and its autoinhibition revealed by NMR. *Biochim Biophys Acta*, **1834**(2), 499–507.

Katoh, Kazutaka, & Standley, Daron M. 2013. MAFFT multiple sequence alignment software version 7: improvements in performance and usability. *Mol Biol Evol*, **30**(4), 772–80.

Katoh, Kazutaka, Misawa, Kazuharu, Kuma, Kei-ichi, & Miyata, Takashi. 2002. MAFFT: a novel method for rapid multiple sequence alignment based on fast Fourier transform. *Nucleic Acids Res*, **30**(14), 3059–66.

Kennedy, Peter Ge. 2013. Clinical features, diagnosis, and treatment of human African trypanosomiasis (sleeping sickness). *Lancet Neurol*, **12**(2), 186–94.

Khan, K H. 2013. Gene expression in mammalian cells and its applications. *Adv Pharm Bull*, **3**(2), 257–63.

Kilmartin, J V, Wright, B, & Milstein, C. 1982. Rat monoclonal antitubulin antibodies derived by using a new nonsecreting rat cell line. *J Cell Biol*, **93**(3), 576–82.

Kim, Juri, Nagami, Sara, Lee, Kyu-Ho, & Park, Soon-Jung. 2014. Characterization of microtubule-binding and dimerization activity of Giardia lamblia end-binding 1 protein. *PLoS One*, **9**(5), e97850.

Kinunel, B E, Samson, S, Wu, J, Hirschberg, R, & Yarbrough, L R. 1985. Tubulin genes of the African trypanosome Trypanosoma brucei rhodesiense:nucleotide sequence of a 3.7-kb fragment containing genes for alpha and beta tubulins. *Gene*, **35**(3), 237–48.

Klaster, Sabrina. 2013. *Die Bedeutung eines Kinesin-Motorproteins bei der Pentamidinresistenz in Trypanosoma brucei*. M.Phil. thesis, University of Bayreuth.

Klingbeil, Michele M, & Englund, Paul T. 2004. Closing the gaps in kinetoplast DNA network replication. *Proc Natl Acad Sci U S A*, **101**(13), 4333–4.

Kohl, L, & Gull, K. 1998. Molecular architecture of the trypanosome cytoskeleton. *Mol Biochem Parasitol*, **93**(1), 1–9.

Kohl, L, Sherwin, T, & Gull, K. 1999. Assembly of the paraflagellar rod and the flagellum attachment zone complex during the Trypanosoma brucei cell cycle. *J Eukaryot Microbiol*, **46**(2), 105–9.

Kohl, Linda, & Bastin, Philippe. 2005. The flagellum of trypanosomes. *Int Rev Cytol*, **244**, 227–85.

Kohl, Linda, Robinson, Derrick, & Bastin, Philippe. 2003. Novel roles for the flagellum in cell morphogenesis and cytokinesis of trypanosomes. *EMBO J*, **22**(20), 5336–46.

Köhler, G, & Milstein, C. 1975. Continuous cultures of fused cells secreting antibody of predefined specificity. *Nature*, **256**(5517), 495–7.

Kollman, Justin M, Merdes, Andreas, Mourey, Lionel, & Agard, David A. 2011. Microtubule nucleation by gamma-tubulin complexes. *Nat Rev Mol Cell Biol*, **12**(11), 709–21.

Komaki, Shinichiro, Abe, Tatsuya, Coutuer, Silvie, Inzé, Dirk, Russinova, Eugenia, & Hashimoto, Takashi. 2010. Nuclear-localized subtype of end-binding 1 protein regulates spindle organization in Arabidopsis. *J Cell Sci*, **123**(Pt 3), 451–9.

Komarova, Yulia, Lansbergen, Gideon, Galjart, Niels, Grosveld, Frank, Borisy, Gary G, & Akhmanova, Anna. 2005. EB1 and EB3 control CLIP dissociation from the ends of growing microtubules. *Mol Biol Cell*, **16**(11), 5334–45.

Komarova, Yulia, De Groot, Christian O, Grigoriev, Ilya, Gouveia, Susana Montenegro, Munteanu, E Laura, Schober, Joseph M, Honnappa, Srinivas, Buey, Rubén M, Hoogenraad, Casper C, Dogterom, Marileen, Borisy, Gary G, Steinmetz, Michel O, & Akhmanova, Anna. 2009. Mammalian end binding proteins control persistent microtubule growth. *J Cell Biol*, **184**(5), 691–706.

Korenbaum, Elena, & Rivero, Francisco. 2002. Calponin homology domains at a glance. *J Cell Sci*, **115**(Pt 18), 3543–5.

Kronja, Iva, Kruljac-Letunic, Anamarija, Caudron-Herger, Maïwen, Bieling, Peter, & Karsenti, Eric. 2009. XMAP215-EB1 interaction is required for proper spindle assembly and chromosome segregation in Xenopus egg extract. *Mol Biol Cell*, **20**(11), 2684–96.

Kumar, Manish, Mehra, Siddharth, Thakar, Alok, Shukla, Nootan Kumar, Roychoudhary, Ajoy, Sharma, Mehar Chand, Ralhan, Ranju, & Chauhan, Shyam Singh. 2016. End Binding 1 (EB1) overexpression in oral lesions and cancer: A biomarker of tumor progression and poor prognosis. *Clin Chim Acta*, May.

Kumar, Praveen, & Wittmann, Torsten. 2012. +TIPs: SxIPping along microtubule ends. *Trends Cell Biol*, **22**(8), 418–28.

Lacomble, Sylvain, Vaughan, Sue, Gadelha, Catarina, Morphew, Mary K, Shaw, Michael K, McIntosh, J Richard, & Gull, Keith. 2009. Three-dimensional cellular architecture of the flagellar pocket and associated cytoskeleton in trypanosomes revealed by electron microscope tomography. *J Cell Sci*, **122**(Pt 8), 1081–90.

Lacomble, Sylvain, Vaughan, Sue, Gadelha, Catarina, Morphew, Mary K, Shaw, Michael K, McIntosh, J Richard, & Gull, Keith. 2010. Basal body movements orchestrate membrane organelle division and cell morphogenesis in Trypanosoma brucei. *J Cell Sci*, **123**(Pt 17), 2884–91.

LaCount, Douglas J, Barrett, Brian, & Donelson, John E. 2002. Trypanosoma brucei FLA1 is required for flagellum attachment and cytokinesis. *J Biol Chem*, **277**(20), 17580–8.

Laemmli, U K. 1970. Cleavage of structural proteins during the assembly of the head of bacteriophage T4. *Nature*, **227**(5259), 680–5.

Langousis, Gerasimos, & Hill, Kent L. 2014. Motility and more: the flagellum of Trypanosoma brucei. *Nat Rev Microbiol*, **12**(7), 505–18.

Lansbergen, Gideon, & Akhmanova, Anna. 2006. Microtubule plus end: a hub of cellular activities. *Traffic*, **7**(5), 499–507.

Larsen, Jesper, Grigoriev, Ilya, Akhmanova, Anna, & Pedersen, Lotte B. 2013. Analysis of microtubule plus-end-tracking proteins in cilia. *Methods Enzymol*, **524**, 105–22.

Leenaars, Marlies, & Hendriksen, Coenraad F M. 2005. Critical steps in the production of polyclonal and monoclonal antibodies: evaluation and recommendations. *ILAR J*, **46**(3), 269–79.

Leterrier, Christophe, Vacher, Hélène, Fache, Marie-Pierre, d'Ortoli, Stéphanie Angles, Castets, Francis, Autillo-Touati, Amapola, & Dargent, Bénédicte. 2011. End-binding proteins EB3 and EB1 link microtubules to ankyrin G in the axon initial segment. *Proc Natl Acad Sci U S A*, **108**(21), 8826–31.

Li, Ziyin, & Wang, Ching C. 2008. KMP-11, a basal body and flagellar protein, is required for cell division in Trypanosoma brucei. *Eukaryot Cell*, **7**(11), 1941–50.

Li, Ziyin, Lee, Ju Huck, Chu, Feixia, Burlingame, Alma L, Günzl, Arthur, & Wang, Ching C. 2008. Identification of a novel chromosomal passenger complex and its unique localization during cytokinesis in Trypanosoma brucei. *PLoS One*, **3**(6), e2354.

Ligon, Lee A, Shelly, Spencer S, Tokito, Mariko, & Holzbaur, Erika L F. 2003. The microtubule plus-end proteins EB1 and dynactin have differential effects on microtubule polymerization. *Mol Biol Cell*, **14**(4), 1405–17.

Lin, Ruo-Hong, Lai, De-Hua, Zheng, Ling-Ling, Wu, Jie, Lukeš, Julius, Hide, Geoff, & Lun, Zhao-Rong. 2015. Analysis of the mitochondrial maxicircle of Trypanosoma lewisi, a neglected human pathogen. *Parasit Vectors*, **8**(1), 665.

Liu, Jiayu, & Han, Rong. 2015. The evolution of microtubule end-binding protein 1 (EB1) and roles in regulating microtubule behavior. *AJPS*, **6**(13), 2114–2121.

Livak, K J, & Schmittgen, T D. 2001. Analysis of relative gene expression data using real-time quantitative PCR and the 2(-Delta Delta C(T)) Method. *Methods*, **25**(4), 402–8.

Logan-Klumpler, Flora J, De Silva, Nishadi, Boehme, Ulrike, Rogers, Matthew B, Velarde, Giles, McQuillan, Jacqueline A, Carver, Tim, Aslett, Martin, Olsen, Christian, Subramanian, Sandhya, Phan, Isabelle, Farris, Carol, Mitra, Siddhartha, Ramasamy, Gowthaman, Wang, Haiming, Tivey, Adrian, Jackson, Andrew, Houston, Robin, Parkhill, Julian, Holden, Matthew, Harb, Omar S, Brunk, Brian P, Myler, Peter J, Roos, David, Carrington, Mark,

Smith, Deborah F, Hertz-Fowler, Christiane, & Berriman, Matthew. 2012. GeneDB–an annotation database for pathogens. *Nucleic Acids Res*, **40**(Database issue), D98–108.

Lopez, Benjamin J, & Valentine, Megan T. 2016. The +TIP coordinating protein EB1 is highly dynamic and diffusive on microtubules, sensitive to GTP analog, ionic strength, and EB1 concentration. *Cytoskeleton (Hoboken)*, **73**(1), 23–34.

Louie, Ryan K, Bahmanyar, Shirin, Siemers, Kathleen A, Votin, Violet, Chang, Paul, Stearns, Tim, Nelson, W James, & Barth, Angela I M. 2004. Adenomatous polyposis coli and EB1 localize in close proximity of the mother centriole and EB1 is a functional component of centrosomes. *J Cell Sci*, **117**(Pt 7), 1117–28.

Luft, J H. 1961. Improvements in epoxy resin embedding methods. *J Biophys Biochem Cytol*, **9**(Feb), 409–14.

Lukes, J, Jirkû, M, Dolezel, D, Kral'ová, I, Hollar, L, & Maslov, D A. 1997. Analysis of ribosomal RNA genes suggests that trypanosomes are monophyletic. *J Mol Evol*, **44**(5), 521–7.

Lukeš, Julius, Skalický, Tomáš, Týč, Jiří, Votýpka, Jan, & Yurchenko, Vyacheslav. 2014. Evolution of parasitism in kinetoplastid flagellates. *Mol Biochem Parasitol*, **195**(2), 115–22.

Ma, Hoi Tang, & Poon, Randy Y C. 2011. Synchronization of HeLa cells. *Methods Mol Biol*, **761**, 151–61.

Malvy, D, & Chappuis, F. 2011. Sleeping sickness. *Clin Microbiol Infect*, **17**(7), 986–95.

Mandelkow, E M, Mandelkow, E, & Milligan, R A. 1991. Microtubule dynamics and microtubule caps: a time-resolved cryo-electron microscopy study. *J Cell Biol*, **114**(5), 977–91.

Manna, Tapas, Honnappa, Srinivas, Steinmetz, Michel O, & Wilson, Leslie. 2008. Suppression of microtubule dynamic instability by the +TIP protein EB1 and its modulation by the CAP-Gly domain of p150glued. *Biochemistry*, **47**(2), 779–86.

Marx, Alexander, Hoenger, Andreas, & Mandelkow, Eckhard. 2009. Structures of kinesin motor proteins. *Cell Motil Cytoskeleton*, **66**(11), 958–66.

Maslov, Dmitri A, Votýpka, Jan, Yurchenko, Vyacheslav, & Lukeš, Julius. 2013. Diversity and phylogeny of insect trypanosomatids: all that is hidden shall be revealed. *Trends Parasitol*, **29**(1), 43–52.

Mathur, Jaideep, Mathur, Neeta, Kernebeck, Birgit, Srinivas, Bhylahalli P, & Hülskamp, Martin. 2003. A novel localization pattern for an EB1-like protein links microtubule dynamics to endomembrane organization. *Curr Biol*, **13**(22), 1991–7.

Matovu, E, Seebeck, T, Enyaru, J C, & Kaminsky, R. 2001. Drug resistance in Trypanosoma brucei spp., the causative agents of sleeping sickness in man and nagana in cattle. *Microbes Infect*, **3**(9), 763–70.

Matthews, K R, & Gull, K. 1994. Cycles within cycles: the interplay between differentiation and cell division in Trypanosoma brucei. *Parasitol Today*, **10**(12), 473–6.

Matthews, Keith R. 2005. The developmental cell biology of Trypanosoma brucei. *J Cell Sci*, **118**(Pt 2), 283–90.

Matthews, Keith R. 2015. 25 years of African trypanosome research: From description to molecular dissection and new drug discovery. *Mol Biochem Parasitol*, **200**(1-2), 30–40.

Maurer, Sebastian P, Fourniol, Franck J, Bohner, Gergő, Moores, Carolyn A, & Surrey, Thomas. 2012. EBs recognize a nucleotide-dependent structural cap at growing microtubule ends. *Cell*, **149**(2), 371–82.

Maurer, Sebastian P, Cade, Nicholas I, Bohner, Gergő, Gustafsson, Nils, Boutant, Emmanuel, & Surrey, Thomas. 2014. EB1 accelerates two conformational transitions important for microtubule maturation and dynamics. *Curr Biol*, **24**(4), 372–84.

May, Sophie F. 2011. *Research on regulation of cytokinesis in T. brucei*. Ph.D. thesis, University of Glasgow.

McKean, Paul G. 2003. Coordination of cell cycle and cytokinesis in Trypanosoma brucei. *Curr Opin Microbiol*, **6**(6), 600–7.

McWilliam, Hamish, Li, Weizhong, Uludag, Mahmut, Squizzato, Silvano, Park, Young Mi, Buso, Nicola, Cowley, Andrew Peter, & Lopez, Rodrigo. 2013. Analysis Tool Web Services from the EMBL-EBI. *Nucleic Acids Res*, **41**(Web Server issue), W597–600.

Medina-Acosta, E, & Cross, G A. 1993. Rapid isolation of DNA from trypanosomatid protozoa using a simple 'mini-prep' procedure. *Mol Biochem Parasitol*, **59**(2), 327–9.

Mennella, Vito, Rogers, Gregory C, Rogers, Stephen L, Buster, Daniel W, Vale, Ronald D, & Sharp, David J. 2005. Functionally distinct kinesin-13 family members cooperate to regulate microtubule dynamics during interphase. *Nat Cell Biol*, **7**(3), 235–45.

Michels, Paul A M, Bringaud, Frédéric, Herman, Murielle, & Hannaert, Véronique. 2006. Metabolic functions of glycosomes in trypanosomatids. *Biochim Biophys Acta*, **1763**(12), 1463–77.

Mimori-Kiyosue, Yuko, & Tsukita, Shoichiro. 2003. "Search-and-capture" of microtubules through plus-end-binding proteins (+TIPs). *J Biochem*, **134**(3), 321–6.

Mitchison, T, & Kirschner, M. 1984. Dynamic instability of microtubule growth. *Nature*, **312**(5991), 237–42.

Moreira-Leite, F F, Sherwin, T, Kohl, L, & Gull, K. 2001. A trypanosome structure involved in transmitting cytoplasmic information during cell division. *Science*, **294**(5542), 610–2.

Morgan, Gareth W, Hall, Belinda S, Denny, Paul W, Carrington, Mark, & Field, Mark C. 2002. The kinetoplastida endocytic apparatus. Part I: a dynamic system for nutrition and evasion of host defences. *Trends Parasitol*, **18**(11), 491–6.

Morrison, E E, Wardleworth, B N, Askham, J M, Markham, A F, & Meredith, D M. 1998. EB1, a protein which interacts with the APC tumour suppressor, is associated with the microtubule cytoskeleton throughout the cell cycle. *Oncogene*, **17**(26), 3471–7.

Morriswood, Brooke. 2015. Form, Fabric, and Function of a Flagellum-Associated Cytoskeletal Structure. *Cells*, **4**(4), 726–47.

Morriswood, Brooke, & Schmidt, Katy. 2015. A MORN Repeat Protein Facilitates Protein Entry into the Flagellar Pocket of Trypanosoma brucei. *Eukaryot Cell*, **14**(11), 1081–93.

Morriswood, Brooke, He, Cynthia Y, Sealey-Cardona, Marco, Yelinek, Jordan, Pypaert, Marc, & Warren, Graham. 2009. The bilobe structure of Trypanosoma brucei contains a MORN-repeat protein. *Mol Biochem Parasitol*, **167**(2), 95–103.

Morriswood, Brooke, Havlicek, Katharina, Demmel, Lars, Yavuz, Sevil, Sealey-Cardona, Marco, Vidilaseris, Keni, Anrather, Dorothea, Kostan, Julius, Djinovic-Carugo, Kristina, Roux, Kyle J, & Warren, Graham. 2013. Novel bilobe components in Trypanosoma brucei identified using proximity-dependent biotinylation. *Eukaryot Cell*, **12**(2), 356–67.

Mouriño-Pérez, Rosa R, Linacre-Rojas, Lorena P, Román-Gavilanes, Ariana I, Lew, Thomas K, Callejas-Negrete, Olga A, Roberson, Robert W, & Freitag, Michael. 2013. MTB-3, a microtubule plus-end tracking protein (+TIP) of Neurospora crassa. *PLoS One*, **8**(8), e70655.

Murata, Takashi, & Hasebe, Mitsuyasu. 2007. Microtubule-dependent microtubule nucleation in plant cells. *J Plant Res*, **120**(1), 73–8.

Murata, Takashi, Sonobe, Seiji, Baskin, Tobias I, Hyodo, Susumu, Hasezawa, Seiichiro, Nagata, Toshiyuki, Horio, Tetsuya, & Hasebe, Mitsuyasu. 2005. Microtubule-dependent microtubule nucleation based on recruitment of gamma-tubulin in higher plants. *Nat Cell Biol*, **7**(10), 961–8.

Nakamura, Masayoshi, Ehrhardt, David W, & Hashimoto, Takashi. 2010. Microtubule and katanin-dependent dynamics of microtubule nucleation complexes in the acentrosomal Arabidopsis cortical array. *Nat Cell Biol*, **12**(11), 1064–70.

Ngô, H, Tschudi, C, Gull, K, & Ullu, E. 1998. Double-stranded RNA induces mRNA degradation in Trypanosoma brucei. *Proc Natl Acad Sci U S A*, **95**(25), 14687–92.

Nozaki, T, Haynes, P A, & Cross, G A. 1996. Characterization of the Trypanosoma brucei homologue of a Trypanosoma cruzi flagellum-adhesion glycoprotein. *Mol Biochem Parasitol*, **82**(2), 245–55.

Oakley, C E, & Oakley, B R. 1989. Identification of gamma-tubulin, a new member of the tubulin superfamily encoded by mipA gene of Aspergillus nidulans. *Nature*, **338**(6217), 662–4.

Oberholzer, Michael, Morand, Sabine, Kunz, Stefan, & Seebeck, Thomas. 2006. A vector series for rapid PCR-mediated C-terminal in situ tagging of Trypanosoma brucei genes. *Mol Biochem Parasitol*, **145**(1), 117–20.

Ochsenreiter, Torsten, Anderson, Sedrick, Wood, Zachary A, & Hajduk, Stephen L. 2008. Alternative RNA editing produces a novel protein involved in mitochondrial DNA maintenance in trypanosomes. *Mol Cell Biol*, **28**(18), 5595–604.

Ogbadoyi, E, Ersfeld, K, Robinson, D, Sherwin, T, & Gull, K. 2000. Architecture of the Trypanosoma brucei nucleus during interphase and mitosis. *Chromosoma*, **108**(8), 501–13.

Ogbadoyi, Emmanuel O, Robinson, Derrick R, & Gull, Keith. 2003. A high-order transmembrane structural linkage is responsible for mitochondrial genome positioning and segregation by flagellar basal bodies in trypanosomes. *Mol Biol Cell*, **14**(5), 1769–79.

Olego-Fernandez, Sofia, Vaughan, Sue, Shaw, Michael K, Gull, Keith, & Ginger, Michael L. 2009. Cell morphogenesis of Trypanosoma brucei requires the paralogous, differentially expressed calpain-related proteins CAP5.5 and CAP5.5V. *Protist*, **160**(4), 576–90.

Ooi, Cher-Pheng, & Bastin, Philippe. 2013. More than meets the eye: understanding Trypanosoma brucei morphology in the tsetse. *Front Cell Infect Microbiol*, **3**, 71.

Opperdoes, F R, & Borst, P. 1977. Localization of nine glycolytic enzymes in a microbody-like organelle in Trypanosoma brucei: the glycosome. *FEBS Lett*, **80**(2), 360–4.

Overath, Peter, & Engstler, Markus. 2004. Endocytosis, membrane recycling and sorting of GPI-anchored proteins: Trypanosoma brucei as a model system. *Mol Microbiol*, **53**(3), 735–44.

Palade, G E. 1952. A study of fixation for electron microscopy. *J Exp Med*, **95**(3), 285–98.

Peacock, Lori, Ferris, Vanessa, Sharma, Reuben, Sunter, Jack, Bailey, Mick, Carrington, Mark, & Gibson, Wendy. 2011. Identification of the meiotic life cycle stage of Trypanosoma brucei in the tsetse fly. *Proc Natl Acad Sci U S A*, **108**(9), 3671–6.

Pedersen, Lotte B, Geimer, Stefan, Sloboda, Roger D, & Rosenbaum, Joel L. 2003. The Microtubule plus end-tracking protein EB1 is localized to the flagellar tip and basal bodies in Chlamydomonas reinhardtii. *Curr Biol*, **13**(22), 1969–74.

Perdomo, Doranda, Bonhivers, Mélanie, & Robinson, Derrick R. 2016. The Trypanosome Flagellar Pocket Collar and Its Ring Forming Protein-TbBILBO1. *Cells*, **5**(1).

Petry, Sabine, & Vale, Ronald D. 2015. Microtubule nucleation at the centrosome and beyond. *Nat Cell Biol*, **17**(9), 1089–93.

Pettersen, Eric F, Goddard, Thomas D, Huang, Conrad C, Couch, Gregory S, Greenblatt, Daniel M, Meng, Elaine C, & Ferrin, Thomas E. 2004. UCSF Chimera–a visualization system for exploratory research and analysis. *J Comput Chem*, **25**(13), 1605–12.

Ploubidou, A, Robinson, D R, Docherty, R C, Ogbadoyi, E O, & Gull, K. 1999. Evidence for novel cell cycle checkpoints in trypanosomes: kinetoplast segregation and cytokinesis in the absence of mitosis. *J Cell Sci*, **112 (Pt 24)**(Dec), 4641–50.

Portman, Neil, & Gull, Keith. 2010. The paraflagellar rod of kinetoplastid parasites: from structure to components and function. *Int J Parasitol*, **40**(2), 135–48.

Portman, Neil, & Gull, Keith. 2012. Proteomics and the Trypanosoma brucei cytoskeleton: advances and opportunities. *Parasitology*, **139**(9), 1168–77.

Portman, Neil, & Gull, Keith. 2014. Identification of paralogous life-cycle stage specific cytoskeletal proteins in the parasite Trypanosoma brucei. *PLoS One*, **9**(9), e106777.

Povelones, Megan L. 2014. Beyond replication: division and segregation of mitochondrial DNA in kinetoplastids. *Mol Biochem Parasitol*, **196**(1), 53–60.

Pradel, Lydie C, Bonhivers, Mélanie, Landrein, Nicolas, & Robinson, Derrick R. 2006. NIMA-related kinase TbNRKC is involved in basal body separation in Trypanosoma brucei. *J Cell Sci*, **119**(Pt 9), 1852–63.

Prokop, Andreas, Beaven, Robin, Qu, Yue, & Sánchez-Soriano, Natalia. 2013. Using fly genetics to dissect the cytoskeletal machinery of neurons during axonal growth and maintenance. *J Cell Sci*, **126**(Pt 11), 2331–41.

Ralston, Katherine S, & Hill, Kent L. 2008. The flagellum of Trypanosoma brucei: new tricks from an old dog. *Int J Parasitol*, **38**(8-9), 869–84.

Ralston, Katherine S, Kabututu, Zakayi P, Melehani, Jason H, Oberholzer, Michael, & Hill, Kent L. 2009. The Trypanosoma brucei flagellum: moving parasites in new directions. *Annu Rev Microbiol*, **63**, 335–62.

Raymaekers, Marijke, Smets, Rita, Maes, Brigitte, & Cartuyvels, Reinoud. 2009. Checklist for optimization and validation of real-time PCR assays. *J Clin Lab Anal*, **23**(3), 145–51.

Redmond, Seth, Vadivelu, Jamuna, & Field, Mark C. 2003. RNAit: an automated web-based tool for the selection of RNAi targets in Trypanosoma brucei. *Mol Biochem Parasitol*, **128**(1), 115–8.

Rehberg, Markus, & Gräf, Ralph. 2002. Dictyostelium EB1 is a genuine centrosomal component required for proper spindle formation. *Mol Biol Cell*, **13**(7), 2301–10.

Reuner, B, Vassella, E, Yutzy, B, & Boshart, M. 1997. Cell density triggers slender to stumpy differentiation of Trypanosoma brucei bloodstream forms in culture. *Mol Biochem Parasitol*, **90**(1), 269–80.

Reynolds, E S. 1963. The use of lead citrate at high pH as an electron-opaque stain in electron microscopy. *J Cell Biol*, **17**(Apr), 208–12.

Rico, Eva, Rojas, Federico, Mony, Binny M, Szoor, Balazs, Macgregor, Paula, & Matthews, Keith R. 2013. Bloodstream form pre-adaptation to the tsetse fly in Trypanosoma brucei. *Front Cell Infect Microbiol*, **3**, 78.

Rindisbacher, L, Hemphill, A, & Seebeck, T. 1993. A repetitive protein from Trypanosoma brucei which caps the microtubules at the posterior end of the cytoskeleton. *Mol Biochem Parasitol*, **58**(1), 83–96.

Robinson, D R, & Gull, K. 1991. Basal body movements as a mechanism for mitochondrial genome segregation in the trypanosome cell cycle. *Nature*, **352**(6337), 731–3.

Robinson, D R, Sherwin, T, Ploubidou, A, Byard, E H, & Gull, K. 1995. Microtubule polarity and dynamics in the control of organelle positioning, segregation, and cytokinesis in the trypanosome cell cycle. *J Cell Biol*, **128**(6), 1163–72.

Rogers, Stephen L, Rogers, Gregory C, Sharp, David J, & Vale, Ronald D. 2002. Drosophila EB1 is important for proper assembly, dynamics, and positioning of the mitotic spindle. *J Cell Biol*, **158**(5), 873–84.

Rotureau, Brice, Subota, Ines, & Bastin, Philippe. 2011. Molecular bases of cytoskeleton plasticity during the Trypanosoma brucei parasite cycle. *Cell Microbiol*, **13**(5), 705–16.

Rotureau, Brice, Subota, Ines, Buisson, Johanna, & Bastin, Philippe. 2012. A new asymmetric division contributes to the continuous production of infective trypanosomes in the tsetse fly. *Development*, **139**(10), 1842–50.

Rotureau, Brice, Blisnick, Thierry, Subota, Ines, Julkowska, Daria, Cayet, Nadège, Perrot, Sylvie, & Bastin, Philippe. 2014. Flagellar adhesion in Trypanosoma brucei relies on interactions between different skeletal structures in the flagellum and cell body. *J Cell Sci*, **127**(Pt 1), 204–15.

Sabatini, D D, Bensch, K, & Barrnett, R J. 1963. Cytochemistry and electron microscopy. The preservation of cellular ultrastructure and enzymatic activity by aldehyde fixation. *J Cell Biol*, **17**(Apr), 19–58.

Sambrook, J, & Russel, D. W. 2001. *Molecular cloning: a laboratory manual*. 3 edn. Cold Spring Harbor, N. Y., USA: Cold Spring Harbor Laboratory Press.

Sandblad, Linda, Busch, Karl Emanuel, Tittmann, Peter, Gross, Heinz, Brunner, Damian, & Hoenger, Andreas. 2006. The Schizosaccharomyces pombe EB1 homolog Mal3p binds and stabilizes the microtubule lattice seam. *Cell*, **127**(7), 1415–24.

Sasse, R, & Gull, K. 1988. Tubulin post-translational modifications and the construction of microtubular organelles in Trypanosoma brucei. *J Cell Sci*, **90 (Pt 4)**(Aug), 577–89.

Schlaeppi, K, Deflorin, J, & Seebeck, T. 1989. The major component of the paraflagellar rod of Trypanosoma brucei is a helical protein that is encoded by two identical, tandemly linked genes. *J Cell Biol*, **109**(4 Pt 1), 1695–709.

Schmittgen, Thomas D, & Livak, Kenneth J. 2008. Analyzing real-time PCR data by the comparative C(T) method. *Nat Protoc*, **3**(6), 1101–8.

Schneider, A, Plessmann, U, & Weber, K. 1997. Subpellicular and flagellar microtubules of Trypanosoma brucei are extensively glutamylated. *J Cell Sci*, **110 (Pt 4)**(Feb), 431–7.

Schrøder, Jacob M, Larsen, Jesper, Komarova, Yulia, Akhmanova, Anna, Thorsteinsson, Rikke I, Grigoriev, Ilya, Manguso, Robert, Christensen, Søren T, Pedersen, Stine F, Geimer, Stefan, & Pedersen, Lotte B. 2011. EB1 and EB3 promote cilia biogenesis by several centrosome-related mechanisms. *J Cell Sci*, **124**(Pt 15), 2539–51.

Schumann Burkard, Gabriela, Jutzi, Pascal, & Roditi, Isabel. 2011. Genome-wide RNAi screens in bloodstream form trypanosomes identify drug transporters. *Mol Biochem Parasitol*, **175**(1), 91–4.

Schuyler, S C, & Pellman, D. 2001. Microtubule "plus-end-tracking proteins": The end is just the beginning. *Cell*, **105**(4), 421–4.

Schwartz, K, Richards, K, & Botstein, D. 1997. BIM1 encodes a microtubule-binding protein in yeast. *Mol Biol Cell*, **8**(12), 2677–91.

Scott, V, Sherwin, T, & Gull, K. 1997. gamma-tubulin in trypanosomes: molecular characterisation and localisation to multiple and diverse microtubule organising centres. *J Cell Sci*, **110 (Pt 2)**(Jan), 157–68.

Seebeck, T, Hemphill, A, & Lawson, D. 1990. The Cytoskeleton of trypanosomes. *Parasitol Today*, **6**(2), 49–52.

Seebeck, T, T, Schneider, A, Kueng, V, Schlaeppi, K, & Hemphill, A. 1988. The cytoskeleton of Trypanosoma brucei - the beauty of simplicity. *Protoplasma*, 188–194.

Selvapandiyan, Angamuthu, Kumar, Praveen, Morris, James C, Salisbury, Jeffrey L, Wang, Ching C, & Nakhasi, Hira L. 2007. Centrin1 is required for organelle segregation and cytokinesis in Trypanosoma brucei. *Mol Biol Cell*, **18**(9), 3290–301.

Sen, Indrani, Veprintsev, Dmitry, Akhmanova, Anna, & Steinmetz, Michel O. 2013. End binding proteins are obligatory dimers. *PLoS One*, **8**(9), e74448.

Sharma, Reuben, Peacock, Lori, Gluenz, Eva, Gull, Keith, Gibson, Wendy, & Carrington, Mark. 2008. Asymmetric cell division as a route to reduction in cell length and change in cell morphology in trypanosomes. *Protist*, **159**(1), 137–51.

Sharma, Reuben, Gluenz, Eva, Peacock, Lori, Gibson, Wendy, Gull, Keith, & Carrington, Mark. 2009. The heart of darkness: growth and form of Trypanosoma brucei in the tsetse fly. *Trends Parasitol*, **25**(11), 517–24.

Sharp, David J, & Ross, Jennifer L. 2012. Microtubule-severing enzymes at the cutting edge. *J Cell Sci*, **125**(Pt 11), 2561–9.

Sheriff, Omar, Lim, Li-Fern, & He, Cynthia Y. 2014. Tracking the biogenesis and inheritance of subpellicular microtubule in Trypanosoma brucei with inducible YFP-alpha-tubulin. *Biomed Res Int*, **2014**, 893272.

Sherwin, T, & Gull, K. 1989a. The cell division cycle of Trypanosoma brucei brucei: timing of event markers and cytoskeletal modulations. *Philos Trans R Soc Lond B Biol Sci*, **323**(1218), 573–88.

Sherwin, T, & Gull, K. 1989b. Visualization of detyrosination along single microtubules reveals novel mechanisms of assembly during cytoskeletal duplication in trypanosomes. *Cell*, **57**(2), 211–21.

Sherwin, T, Schneider, A, Sasse, R, Seebeck, T, & Gull, K. 1987. Distinct localization and cell cycle dependence of COOH terminally tyrosinolated alpha-tubulin in the microtubules of Trypanosoma brucei brucei. *J Cell Biol*, **104**(3), 439–46.

Shi, Jie, Franklin, Joseph B, Yelinek, Jordan T, Ebersberger, Ingo, Warren, Graham, & He, Cynthia Y. 2008. Centrin4 coordinates cell and nuclear division in T. brucei. *J Cell Sci*, **121**(Pt 18), 3062–70.

Siegel, T Nicolai, Hekstra, Doeke R, & Cross, George A M. 2008. Analysis of the Trypanosoma brucei cell cycle by quantitative DAPI imaging. *Mol Biochem Parasitol*, **160**(2), 171–4.

Simpson, Alastair G B, Stevens, Jamie R, & Lukes, Julius. 2006. The evolution and diversity of kinetoplastid flagellates. *Trends Parasitol*, **22**(4), 168–74.

Skube, Susan B, Chaverri, José M, & Goodson, Holly V. 2010. Effect of GFP tags on the localization of EB1 and EB1 fragments in vivo. *Cytoskeleton (Hoboken)*, **67**(1), 1–12.

Slep, Kevin C. 2010. Structural and mechanistic insights into microtubule end-binding proteins. *Curr Opin Cell Biol*, **22**(1), 88–95.

Söding, Johannes, Biegert, Andreas, & Lupas, Andrei N. 2005. The HHpred interactive server for protein homology detection and structure prediction. *Nucleic Acids Res*, **33**(Web Server issue), W244–8.

Sopko, Richelle, Huang, Dongqing, Preston, Nicolle, Chua, Gordon, Papp, Balázs, Kafadar, Kimberly, Snyder, Mike, Oliver, Stephen G, Cyert, Martha, Hughes, Timothy R, Boone,

Charles, & Andrews, Brenda. 2006. Mapping pathways and phenotypes by systematic gene overexpression. *Mol Cell*, **21**(3), 319–30.

Spindler, Marcus. 2014. *Herstellung von monoklonalen Antikörpern gegen strukturelle Komponenten des Zytoskeletts und Chromatins in Trypanosoma brucei brucei*. M.Phil. thesis, University of Bayreuth.

Staudt, Mark W, Kruzel, Emilia K, Shimizu, Kiminori, & Hull, Christina M. 2010. Characterizing the role of the microtubule binding protein Bim1 in Cryptococcus neoformans. *Fungal Genet Biol*, **47**(4), 310–7.

Stephan, Angela, Vaughan, Sue, Shaw, Michael K, Gull, Keith, & McKean, Paul G. 2007. An essential quality control mechanism at the eukaryotic basal body prior to intraflagellar transport. *Traffic*, **8**(10), 1323–30.

Steverding, Dietmar. 2008. The history of African trypanosomiasis. *Parasit Vectors*, **1**(1), 3.

Stypula-Cyrus, Yolanda, Mutyal, Nikhil N, Dela Cruz, Mart, Kunte, Dhananjay P, Radosevich, Andrew J, Wali, Ramesh, Roy, Hemant K, & Backman, Vadim. 2014. End-binding protein 1 (EB1) up-regulation is an early event in colorectal carcinogenesis. *FEBS Lett*, **588**(5), 829–35.

Su, L K, & Qi, Y. 2001. Characterization of human MAPRE genes and their proteins. *Genomics*, **71**(2), 142–9.

Su, L K, Burrell, M, Hill, D E, Gyuris, J, Brent, R, Wiltshire, R, Trent, J, Vogelstein, B, & Kinzler, K W. 1995. APC binds to the novel protein EB1. *Cancer Res*, **55**(14), 2972–7.

Su, Xiaolei, Ohi, Ryoma, & Pellman, David. 2012. Moving in for the kill: motile microtubule regulators. *Trends Cell Biol*, **22**(11), 567–75.

Sunter, Jack D, & Gull, Keith. 2016. The Flagellum Attachment Zone: 'The Cellular Ruler' of Trypanosome Morphology. *Trends Parasitol*, Jan.

Sunter, Jack D, Varga, Vladimir, Dean, Samuel, & Gull, Keith. 2015a. A dynamic coordination of flagellum and cytoplasmic cytoskeleton assembly specifies cell morphogenesis in trypanosomes. *J Cell Sci*, **128**(8), 1580–94.

Sunter, Jack D, Benz, Corinna, Andre, Jane, Whipple, Sarah, McKean, Paul G, Gull, Keith, Ginger, Michael L, & Lukeš, Julius. 2015b. Modulation of flagellum attachment zone protein FLAM3 and regulation of the cell shape in Trypanosoma brucei life cycle transitions. *J Cell Sci*, **128**(16), 3117–30.

Tait, Andy, Macleod, Annette, Tweedie, Alison, Masiga, Dan, & Turner, C Michael R. 2007. Genetic exchange in Trypanosoma brucei: evidence for mating prior to metacyclic stage development. *Mol Biochem Parasitol*, **151**(1), 133–6.

Tamura, Naoka, & Draviam, Viji M. 2012. Microtubule plus-ends within a mitotic cell are 'moving platforms' with anchoring, signalling and force-coupling roles. *Open Biol*, **2**(11), 120132.

Taylor, A E, & Godfrey, D G. 1969. A new organelle of bloodstream salivarian trypanosomes. *J Protozool*, **16**(3), 466–70.

Tirnauer, J S, & Bierer, B E. 2000. EB1 proteins regulate microtubule dynamics, cell polarity, and chromosome stability. *J Cell Biol*, **149**(4), 761–6.

Tirnauer, J S, O'Toole, E, Berrueta, L, Bierer, B E, & Pellman, D. 1999. Yeast Bim1p promotes the G1-specific dynamics of microtubules. *J Cell Biol*, **145**(5), 993–1007.

Tirnauer, Jennifer S, Grego, Sonia, Salmon, E D, & Mitchison, Timothy J. 2002a. EB1-microtubule interactions in Xenopus egg extracts: role of EB1 in microtubule stabilization and mechanisms of targeting to microtubules. *Mol Biol Cell*, **13**(10), 3614–26.

Tirnauer, Jennifer S, Canman, Julie C, Salmon, E D, & Mitchison, Timothy J. 2002b. EB1 targets to kinetochores with attached, polymerizing microtubules. *Mol Biol Cell*, **13**(12), 4308–16.

Towbin, H, Staehelin, T, & Gordon, J. 1979. Electrophoretic transfer of proteins from polyacrylamide gels to nitrocellulose sheets: procedure and some applications. *Proc Natl Acad Sci U S A*, **76**(9), 4350–4.

Tu, Xiaoming, & Wang, Ching C. 2004. The involvement of two cdc2-related kinases (CRKs) in Trypanosoma brucei cell cycle regulation and the distinctive stage-specific phenotypes caused by CRK3 depletion. *J Biol Chem*, **279**(19), 20519–28.

Tu, Xiaoming, & Wang, Ching C. 2005. Pairwise knockdowns of cdc2-related kinases (CRKs) in Trypanosoma brucei identified the CRKs for G1/S and G2/M transitions and demonstrated distinctive cytokinetic regulations between two developmental stages of the organism. *Eukaryot Cell*, **4**(4), 755–64.

Turner, D L, & Weintraub, H. 1994. Expression of achaete-scute homolog 3 in Xenopus embryos converts ectodermal cells to a neural fate. *Genes Dev*, **8**(12), 1434–47.

UniProt Consortium. 2015. UniProt: a hub for protein information. *Nucleic Acids Res*, **43**(Database issue), D204–12.

Urwyler, Simon, Studer, Erwin, Renggli, Christina Kunz, & Roditi, Isabel. 2007. A family of stage-specific alanine-rich proteins on the surface of epimastigote forms of Trypanosoma brucei. *Mol Microbiol*, **63**(1), 218–28.

Van Damme, Daniël, Bouget, François-Yves, Van Poucke, Kris, Inzé, Dirk, & Geelen, Danny. 2004. Molecular dissection of plant cytokinesis and phragmoplast structure: a survey of GFP-tagged proteins. *Plant J*, **40**(3), 386–98.

Van der Ploeg, L H, Smith, C L, Polvere, R I, & Gottesdiener, K M. 1989. Improved separation of chromosome-sized DNA from Trypanosoma brucei, stock 427-60. *Nucleic Acids Res*, **17**(8), 3217–27.

van der Vaart, Babet, Akhmanova, Anna, & Straube, Anne. 2009. Regulation of microtubule dynamic instability. *Biochem Soc Trans*, **37**(Pt 5), 1007–13.

Vasquez, Juan-José, Hon, Chung-Chau, Vanselow, Jens T, Schlosser, Andreas, & Siegel, T Nicolai. 2014. Comparative ribosome profiling reveals extensive translational complexity in different Trypanosoma brucei life cycle stages. *Nucleic Acids Res*, **42**(6), 3623–37.

Vassella, E, Reuner, B, Yutzy, B, & Boshart, M. 1997. Differentiation of African trypanosomes is controlled by a density sensing mechanism which signals cell cycle arrest via the cAMP pathway. *J Cell Sci*, **110 (Pt 21)**(Nov), 2661–71.

Vaughan, Kevin T. 2005. Microtubule plus ends, motors, and traffic of Golgi membranes. *Biochim Biophys Acta*, **1744**(3), 316–24.

Vaughan, Sue, & Gull, Keith. 2008. The structural mechanics of cell division in Trypanosoma brucei. *Biochem Soc Trans*, **36**(Pt 3), 421–4.

Vaughan, Sue, & Gull, Keith. 2015. Basal body structure and cell cycle-dependent biogenesis in Trypanosoma brucei. *Cilia*, **5**, 5.

Vaughan, Sue, Kohl, Linda, Ngai, Ian, Wheeler, Richard J, & Gull, Keith. 2008. A repetitive protein essential for the flagellum attachment zone filament structure and function in Trypanosoma brucei. *Protist*, **159**(1), 127–36.

Vedrenne, Cécile, Giroud, Christiane, Robinson, Derrick R, Besteiro, Sébastien, Bosc, Christophe, Bringaud, Frédéric, & Baltz, Théo. 2002. Two related subpellicular cytoskeleton-associated proteins in Trypanosoma brucei stabilize microtubules. *Mol Biol Cell*, **13**(3), 1058–70.

Vicente, Juan Jesus, & Wordeman, Linda. 2015. Mitosis, microtubule dynamics and the evolution of kinesins. *Exp Cell Res*, **334**(1), 61–9.

Vickerman, K. 1962. The mechanism of cyclical development in trypanosomes of the Trypanosoma brucei sub-group: an hypothesis based on ultrastructural observations. *Trans R Soc Trop Med Hyg*, **56**(Nov), 487–95.

Vickerman, K. 1965. Polymorphism and mitochondrial activity in sleeping sickness trypanosomes. *Nature*, **208**(5012), 762–6.

Vickerman, K. 1969. On the surface coat and flagellar adhesion in trypanosomes. *J Cell Sci*, **5**(1), 163–93.

Vickerman, K. 1985. Developmental cycles and biology of pathogenic trypanosomes. *Br Med Bull*, **41**(2), 105–14.

Vitre, Benjamin, Coquelle, Frédéric M, Heichette, Claire, Garnier, Cyrille, Chrétien, Denis, & Arnal, Isabelle. 2008. EB1 regulates microtubule dynamics and tubulin sheet closure in vitro. *Nat Cell Biol*, **10**(4), 415–21.

Wang, Z, Morris, J C, Drew, M E, & Englund, P T. 2000. Inhibition of Trypanosoma brucei gene expression by RNA interference using an integratable vector with opposing T7 promoters. *J Biol Chem*, **275**(51), 40174–9.

Wasteneys, Geoffrey O, & Ambrose, J Christian. 2009. Spatial organization of plant cortical microtubules: close encounters of the 2D kind. *Trends Cell Biol*, **19**(2), 62–71.

Wasteneys, Geoffrey O, & Williamson, Richard E. 1989. Reassembly of microtubules in Nitella tasmanica: assembly of cortical microtubules in branching clusters and its relevance to steady-state microtubule assembly. *J Cell Sci*, **93**, 705–714.

Watson, M L. 1958. Staining of tissue sections for electron microscopy with heavy metals. *J Biophys Biochem Cytol*, **4**(4), 475–8.

Wei, Ying, Hu, Huiqing, Lun, Zhao-Rong, & Li, Ziyin. 2013. The cooperative roles of two kinetoplastid-specific kinesins in cytokinesis and in maintaining cell morphology in bloodstream trypanosomes. *PLoS One*, **8**(9), e73869.

Weisbrich, Anke, Honnappa, Srinivas, Jaussi, Rolf, Okhrimenko, Oksana, Frey, Daniel, Jelesarov, Ilian, Akhmanova, Anna, & Steinmetz, Michel O. 2007. Structure-function relationship of CAP-Gly domains. *Nat Struct Mol Biol*, **14**(10), 959–67.

Wheeler, Richard J, Scheumann, Nicole, Wickstead, Bill, Gull, Keith, & Vaughan, Sue. 2013. Cytokinesis in Trypanosoma brucei differs between bloodstream and tsetse trypomastigote forms: implications for microtubule-based morphogenesis and mutant analysis. *Mol Microbiol*, **90**(6), 1339–55.

Wickstead, Bill, & Gull, Keith. 2006. A "holistic" kinesin phylogeny reveals new kinesin families and predicts protein functions. *Mol Biol Cell*, **17**(4), 1734–43.

Wickstead, Bill, Carrington, Jamie T, Gluenz, Eva, & Gull, Keith. 2010. The expanded Kinesin-13 repertoire of trypanosomes contains only one mitotic Kinesin indicating multiple extranuclear roles. *PLoS One*, **5**(11), e15020.

Wieczorek, Michal, Bechstedt, Susanne, Chaaban, Sami, & Brouhard, Gary J. 2015. Microtubule-associated proteins control the kinetics of microtubule nucleation. *Nat Cell Biol*, **17**(7), 907–16.

Wiese, C, & Zheng, Y. 2000. A new function for the gamma-tubulin ring complex as a microtubule minus-end cap. *Nat Cell Biol*, **2**(6), 358–64.

Wirtz, E, Leal, S, Ochatt, C, & Cross, G A. 1999. A tightly regulated inducible expression system for conditional gene knock-outs and dominant-negative genetics in Trypanosoma brucei. *Mol Biochem Parasitol*, **99**(1), 89–101.

Woods, Katherine, Nic a'Bhaird, Noirin, Dooley, Clodagh, Perez-Morga, David, & Nolan, Derek P. 2013a. Identification and characterization of a stage specific membrane protein involved in flagellar attachment in Trypanosoma brucei. *PLoS One*, **8**(1), e52846.

Woods, Kerry L, Theiler, Romina, Mühlemann, Marcus, Segiser, Adrian, Huber, Sandra, Ansari, Hifzur R, Pain, Arnab, & Dobbelaere, Dirk A E. 2013b. Recruitment of EB1, a master regulator of microtubule dynamics, to the surface of the Theileria annulata schizont. *PLoS Pathog*, **9**(5), e1003346.

Woodward, R, & Gull, K. 1990. Timing of nuclear and kinetoplast DNA replication and early morphological events in the cell cycle of Trypanosoma brucei. *J Cell Sci*, **95 (Pt 1)**(Jan), 49–57.

Wu, Xufeng, Xiang, Xin, & Hammer, 3rd, John A. 2006. Motor proteins at the microtubule plus-end. *Trends Cell Biol*, **16**(3), 135–43.

Yan, Xiumin, Habedanck, Robert, & Nigg, Erich A. 2006. A complex of two centrosomal proteins, CAP350 and FOP, cooperates with EB1 in microtubule anchoring. *Mol Biol Cell*, **17**(2), 634–44.

Yau, Kah Wai, van Beuningen, Sam F B, Cunha-Ferreira, Inês, Cloin, Bas M C, van Battum, Eljo Y, Will, Lena, Schätzle, Philipp, Tas, Roderick P, van Krugten, Jaap, Katrukha, Eugene A, Jiang, Kai, Wulf, Phebe S, Mikhaylova, Marina, Harterink, Martin, Pasterkamp, R Jeroen, Akhmanova, Anna, Kapitein, Lukas C, & Hoogenraad, Casper C. 2014. Microtubule minus-end binding protein CAMSAP2 controls axon specification and dendrite development. *Neuron*, **82**(5), 1058–73.

Yesilirmak, Filiz, & Sayers, Zehra. 2009. Heterelogous expression of plant genes. *Int J Plant Genomics*, **2009**, 296482.

Zanic, Marija, Stear, Jeffrey H, Hyman, Anthony A, & Howard, Jonathon. 2009. EB1 recognizes the nucleotide state of tubulin in the microtubule lattice. *PLoS One*, **4**(10), e7585.

Zanic, Marija, Widlund, Per O, Hyman, Anthony A, & Howard, Jonathon. 2013. Synergy between XMAP215 and EB1 increases microtubule growth rates to physiological levels. *Nat Cell Biol*, **15**(6), 688–93.

Zhang, Dong, Grode, Kyle D, Stewman, Shannon F, Diaz-Valencia, Juan Daniel, Liebling, Emily, Rath, Uttama, Riera, Tania, Currie, Joshua D, Buster, Daniel W, Asenjo, Ana B, Sosa, Hernando J, Ross, Jennifer L, Ma, Ao, Rogers, Stephen L, & Sharp, David J. 2011. Drosophila katanin is a microtubule depolymerase that regulates cortical-microtubule plus-end interactions and cell migration. *Nat Cell Biol*, **13**(4), 361–70.

Zhang, Rui, Alushin, Gregory M, Brown, Alan, & Nogales, Eva. 2015. Mechanistic Origin of Microtubule Dynamic Instability and Its Modulation by EB Proteins. *Cell*, **162**(4), 849–59.

Zhao, Zhixing, Lindsay, Megan E, Roy Chowdhury, Arnab, Robinson, Derrick R, & Englund, Paul T. 2008. p166, a link between the trypanosome mitochondrial DNA and flagellum, mediates genome segregation. *EMBO J*, **27**(1), 143–54.

Zhou, Qing, & Li, Ziyin. 2015. Gamma-Tubulin complex in Trypanosoma brucei: molecular composition, subunit interdependence and requirement for axonemal central pair protein assembly. *Mol Microbiol*, **98**(4), 667–80.

Zhou, Qing, & Li, Ziyin. 2016. A backup cytokinesis pathway in Trypanosoma brucei. *Cell Cycle*, **15**(18), 2379–80.

Zhou, Qing, Liu, Binghai, Sun, Ying, & He, Cynthia Y. 2011. A coiled-coil- and C2-domain-containing protein is required for FAZ assembly and cell morphology in Trypanosoma brucei. *J Cell Sci*, **124**(Pt 22), 3848–58.

Zhou, Qing, Hu, Huiqing, & Li, Ziyin. 2014. New insights into the molecular mechanisms of mitosis and cytokinesis in trypanosomes. *Int Rev Cell Mol Biol*, **308**, 127–66.

Zhou, Qing, Hu, Huiqing, He, Cynthia Y, & Li, Ziyin. 2015. Assembly and maintenance of the flagellum attachment zone filament in Trypanosoma brucei. *J Cell Sci*, **128**(13), 2361–72.

Zhou, Qing, Gu, Jianhua, Lun, Zhao-Rong, Ayala, Francisco J, & Li, Ziyin. 2016. Two distinct cytokinesis pathways drive trypanosome cell division initiation from opposite cell ends. *Proc Natl Acad Sci U S A*, Feb.

Zhu, Zhiqing C, Gupta, Kamlesh K, Slabbekoorn, Aranda R, Paulson, Benjamin A, Folker, Eric S, & Goodson, Holly V. 2009. Interactions between EB1 and microtubules: dramatic effect of affinity tags and evidence for cooperative behavior. *J Biol Chem*, **284**(47), 32651–61.

Zimniak, Tomasz, Stengl, Katharina, Mechtler, Karl, & Westermann, Stefan. 2009. Phospho-regulation of the budding yeast EB1 homologue Bim1p by Aurora/Ipl1p. *J Cell Biol*, **186**(3), 379–91.

6 Appendix

6.1 Abbreviations

Amp ampicillin

BLAST basic local alignment search tool

BLE bleomycin D1

BSD blasticidin S

BSF bloodstream form

cAMP cyclic adenosine monophosphate

CAP cytoskeleton-associated protein

cDNA complementary DNA

CH calponin homology

CSK cytoskeleton

DAPI 4´,6-diamidino-2-phenylindole

div dividing

DNA deoxyribonucleic acid

EB end-binding protein

EBH end-binding protein homology

F flagellum

FA formaldehyde

FAZ flagellar attachment zone

FER FAZ endoplasmic reticulum

IFA immunofluorescence analysis

GPI glycosylphosphatidylinositol

HAT human African trypanosomiasis

HYG hygromycin B

K kinetoplast

Kan kanamycin

MAP microtubule-associated protein

MT microtubule

MTOC MT organizing center

MtQ microtubule quartet

N Nucleus

NEO neomycin / G418

NP-40 Tergitol-type NP (Nonyl phenoxypolyethoxylethanol) -40

PCF procyclic form

PCR polymerase chain reaction

qPCR quantitative PCR

PFR paraflagellar rod

p. i. post induction

PU puromycin

RIPA buffer radioimmunoprecipitation assay buffer

RNA ribonucleic acid

RNAi RNA interference

mRNA messenger RNA

SDS PAGE sodium dodecyl sulfate polyacrylamide gel electrophoresis

SIF stumpy induction factor

siRNA small interfering RNA

TAC tripartite attachment complex

TERT telomerase reverse transcriptase

+TIP plus-end tracking proteins

VSG variant surface glycoprotein

6.2 (Eidesstattliche) Versicherungen und Erklärungen

Hiermit erkläre ich mich damit einverstanden, dass die elektronische Fassung meiner Dissertation unter Wahrung meiner Urheberrechte und des Datenschutzes einer gesonderten Überprüfung hinsichtlich der eigenständigen Anfertigung der Dissertation unterzogen werden kann. (§ 8 S. 2 Nr. 6 PromO)

Hiermit erkläre ich eidesstattlich, dass ich die Dissertation selbständig verfasst und keine anderen als die von mir angegebenen Quellen und Hilfsmittel benutzt habe. (§ 8 S. 2 Nr. 8 PromO)

Ich habe die Dissertation nicht bereits zur Erlangung eines akademischen Grades anderweitig eingereicht und habe auch nicht bereits diese oder eine andere gleichartige Doktorprüfung endgültig nicht bestanden. (§ 8 S. 2 Nr. 9 PromO)

Hiermit erkläre ich, dass ich keine Hilfe von gewerblichen Promotionsberatern bzw. -vermittlern in Anspruch genommen habe und auch künftig nicht nehmen werde. (§ 8 s. 2 Nr. 10 PromO)

Warthausen, den 27. September 2016

Gertrud Lallinger-Kube